# Investigation of Alternative Rotorcraft Powerplant Configurations for Improving Airframe Performance

by

Austin James Ritz

B.S. Mechanical Engineering, University of Wisconsin-Madison, 2015

Submitted to the Department of Mechanical Engineering
in partial fulfillment of the requirements for the degree of

Master of Science in Mechanical Engineering

at the

MASSACHUSETTS INSTITUTE OF TECHNOLOGY

June 2017



Signature redacted

Author .....
Department of Mechanical Engineering
May 12, 2017

Signature redacted

Certified by .....
John Brisson
Professor of Mechanical Engineering
Thesis Supervisor

Signature redacted

Accepted by .....
Professor Rohan Abeyarante
Chairman, Committee on Graduate Students

# Investigation of Alternative Rotorcraft Powerplant Configurations for Improving Airframe Performance

by

Austin James Ritz

Submitted to the Department of Mechanical Engineering
on May 12, 2017, in partial fulfillment of the
requirements for the degree of
Master of Science in Mechanical Engineering

## Abstract

Alternative rotorcraft powerplant configurations were analyzed to determine their improvements to airframe performance capabilities, with the main goal of increasing an aircraft's range. The helicopter's engine was the focus of this thesis, with emphasis on improving its specific power (power vs weight ratio), efficiency, performance in high altitude and temperature, or capabilities during engine failure. Gas turbines, used in the majority of applications, were characterized through turboshaft databases, industry trends, and identifying changes to their operation and architecture at varying sizes. These results indicated that gas turbine performance capabilities are limited in low power class operation (i.e. small airframe sizes), providing the niche region where alternative engines have the potential for improvements. Standard gasoline and diesel piston engines, operating in both four- and two- stroke modes, were considered as alternative configurations and were evaluated using industry trends and example engine data. Additionally, the two/four-stroke switching gasoline engine (changing operation mode between two- and four-stroke) was used to achieve higher specific powers, with simulations suggesting substantial improvements. Flight profile modeling was conducted using a variety of airframes, created using industry standard practices. The identified engines were conceptually implemented in the aircraft through standard engine swaps replacing the gas turbines with piston engines, hybrid designs incorporating both a gas turbine and piston engine, and auxiliary engine configurations that include a small gas turbine in addition to the main gas turbine or piston engine(s). Equipped with each design, the aircraft were simulated as conducting a characteristic flight path, providing a comparison in performance. Based on these results, the standard, hybrid, and auxiliary two/four-stroke engine, auxiliary diesel two-stroke design, and auxiliary gas turbine configuration provided significant improvements in range at various airframe sizes, with a maximum increase of 49%.

Thesis Supervisor: John Brisson
Title: Professor of Mechanical Engineering

# Contents

# List of Figures

# List of Tables

# Chapter 1

# Project Direction

This investigation was executed with the goal of finding and analyzing alternative engine technologies to improve rotorcraft performance in the future. As part of this analysis, the current state of rotorcraft technologies was evaluated to provide a baseline for their capabilities. This information determined the airframe features that the project would focus on improving, as well as the anticipated aircraft operation characteristics and conditions that must be considered when evaluating helicopter performance. Finally, using these inputs, the project goals were established to assist in directing this analysis, with the resulting discussions provided.

## 1.1 Current State of Rotorcraft

A wide variety of applications utilize modern rotorcrafts, including servicing of offshore oil platforms, providing corporate transit, and carrying out search-and-rescue missions. Helicopters range in size from smaller than the Airbus H120, operating at a maximum gross takeoff mass of 1,800 kilograms, up to the Bell Boeing V-22 Osprey, with a maximum gross takeoff mass of 27,443 kilograms, and beyond [1, 2]. Within this range of sizes, rotorcraft flight speeds can vary between stationary hovering and record setting speeds in excess of 229 miles per hour [3]. Despite the continued push for researching improvements for fixed wing and alternative aircraft, the rotorcraft remains an essential vehicle used to carry out the many missions they service on a

daily basis.

To generate the power required for flight, the rotorcraft's engine converts the chemical energy stored in the aircraft's fuel into the mechanical energy that drives the rotor of the helicopter. The airfoils that encompass the moving rotor accelerate ambient air to provide the airframe's lift and forward propulsion forces, as well as control over attitude and position in three-dimensional space [3]. As the performance of this system is crucial to the operation of the helicopter, Chapter 5 evaluates the basic functionality of these airfoils, in addition to the parameters that are crucial to their success.

Furthermore, the powerplant configuration predominately used to drive the rotor(s) is the turboshaft; a gas turbine equipped with an output shaft that produces mechanical power. These engines have been in development for over half a century and were largely responsible for enabling the commercial success of early helicopters [3]. In addition to turboshafts, reciprocating piston engine configurations power a select number of lightweight helicopters. These engines most commonly use gasoline for fuel, including the Robinson Raven II, which operates with the six-cylinder Lycoming IO-540 gasoline engine. Alternatively, a handful of aircraft engines run on diesel or jet fuel, such as the experimental configuration of the Airbus H120 that was retrofitted with an eight-cylinder turbocharged piston engine running on aviation-grade kerosene fuel [4, 5]. While the majority of modern helicopters utilize gas turbines, gasoline engines were instrumental in the development of early rotorcraft, and are still of interest in many lightweight applications [3].

## 1.2 Essential Rotorcraft Parameters

The process of designing a rotorcraft begins with specifying the parameters that are essential to the airframe's operation. The following factors provide an example of representative requirements that determine the development of a helicopter [6]:

- Desired flight missions, such as the required payloads and ranges of operation, patrol/loiter durations, and hover roles for rescues. These missions determine

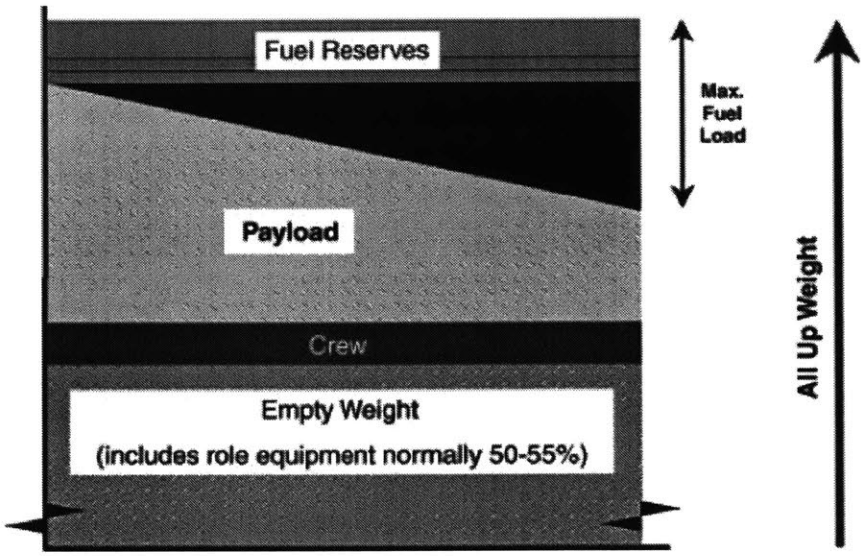


Figure 1-1: The rotorcraft's weight is allocated among multiple categories, including the fuel, payload, crew, and remaining weight, known as the "empty weight" [6].

the airframe's weight, which encompasses the helicopter's empty, payload, crew, and fuel weights, resulting in the gross maximum takeoff weight, or "All Up" weight. Figure 1-1 illustrates this breakdown.

- Specific requirements for operation in various atmospheric conditions (i.e. mission capabilities in adverse temperatures and pressure altitudes).
- Safety requirements regarding engine failure.
- Environment of operation (i.e. oil rig, airfield, etc.).
- Dimensional limitations for storage and transportation.

Once an airframe's design is completed, the rotorcraft's performance can be broken down into a variety of essential parameters, including the installed engine power required for the anticipated flight conditions, suggested flight speed, ceiling of operation, and the estimated airframe range [3]. Specifically, based on discussions with industry professionals, this latter parameter was considered the highest priority for

evaluation, as the helicopter's range heavily influences its mission capabilities and attractiveness to operators. Furthermore, the suggested flight speed (i.e. maximum range speed) also received specific attention, albeit to a lesser extent, due to this parameter impacting a mission's completion time. Thus, these aircraft features will serve as the tools for measuring the impact of changes to an airframe's design and will be essential for comparing the feasibility of the various avenues for improvement identified by this project.

## 1.3 Project Goals

After initial evaluation of a rotorcraft' operation, an airframe's powerplant was identified as heavily influencing the essential helicopter performance characteristics listed in Section 1.2. Using this insight, along with input from industry professionals, it is clear that engine performance is of major concern to the advancement of rotorcraft capabilities. Verifying this observation, substantial effort has been devoted to the development of turboshafts for standard airframe sizes, as evident by simple-cycle gas turbine thermal efficiencies tripling from roughly 15% to upwards of 45% in the past 20 years [7]. However, engine performance is still a major restriction on the improvement of airframes, and thus the focus of this investigation is identifying potential improvements to rotorcraft powerplants.

In particular, a select number of parameters were highlighted based on their influences on the airframe's performance, along with the insight gained through discussions with industry professionals. These include the engine's efficiency, specific power, one engine inoperable (OEI) capabilities (for airframes with multiple engines), and "hot and high" performance degradation. An engine's efficiency measures how well the powerplant is able to convert the chemical energy of its fuel into the mechanical power that enables flight, with high efficiencies desired to enable further travel, given a set amount of fuel. As a helicopter's flight profile is anticipated to result in varying degrees of power requirement, the efficiency throughout part-load and full-load operation (i.e. fractional through full rated power requirement) must be determined to

accurately predict an engine's performance. Furthermore, the engine's specific power is a reflection of how much power it produces per unit of weight (also identified as the power-to-weight ratio), indicating that a high specific power is desirable to minimize an engine's mass, due to the mass restrictions present in aircraft. These two parameters are essential to an engine's performance in rotorcraft applications and were the initial focus for identifying potential improvements and impacts of new technologies.

The remaining two parameters, OEI capability and hot and high performance, are measures of how well an engine responds to adverse conditions, and were identified as heavily influencing an engine's implementation. As stated in the condition's name, OEI pertains to situations where one engine fails during flight, requiring the remaining engine(s) to increase its power output for a short duration to safely counteract this loss [6]. To estimate this performance requirement, the evaluated airframes were assumed to be rated for takeoff in a Category A procedure, indicating that a multi-engine airframe is capable of continued stable flight or an aborted takeoff after an engine failure occurs [8]. Based on input from industry professionals, as well as this identified requirement, this analysis stipulated that each rotorcraft provide sufficient power to enable cruise capability of the airframe, which was estimated (and verified through inspection of airframe performance) to be approximately 70% of the required power during takeoff. Thus, each engine (in multi-engine configurations) must be sized to provide this additional power requirement to account for OEI scenarios.

Furthermore, hot and high performance refers to the derating of engine power due to operation at high ambient temperature and high altitude. The engine performance analysis discussed in Chapters 2 and 3 for hot and high conditions use an altitude of 1.22 kilometers (4,000 ft, where the ambient pressure is 87.5 kilopascals) and a temperature of 42° Celsius (35° Celsius greater than the International Standard Atmosphere temperature of 7° Celsius at this altitude), as these assumed conditions are considered the characteristic cruising altitude at the industry standard maximum helicopter temperature rating [1, 81, 82, 84, 86, 88, 91]. At this pressure and temperature, the engines were required to provide sufficient power for all portions of a flight path to ensure full operational capabilities.

## 1.4 Project Scope

The project was limited to a five-year technology horizon and did not consider possible but anticipated "blue-sky" technologies that, in theory, might out-perform combustion-based engines. Due to this requirement, in addition to the engine and aircraft parameters identified in the following chapters, the analysis begins by evaluating the performance of turboshaft engines to determine their baseline capabilities that are currently achieved. Following this study, alternative powerplant designs were identified, with their performance outlined and modeled, when applicable. Finally, various airframes were equipped with each promising configuration, in addition to the gas turbines, and modeled to identify the changes in their performance when equipped with different engine designs. The results of these comparisons were used to analyze the feasibility of each alternative technology, as well as the niche helicopter applications in which they are best suited. Based on these findings, the analysis provides recommendations on engine technologies to pursue and the airframes that are ideal for their implementation.

# Chapter 2

# Gas Turbines

Following the identification of the project goals, the investigation evaluated the current state of gas turbine engines, including their operational characteristics, performance trends, and limitations. Through these results, the project determined the turboshaft's advantages and disadvantages, which directed the analysis of potential alternative engine configurations and the feasibility of their implementation in rotorcraft applications.

## 2.1 Basic Operation and Applications

Gas turbines are internal combustion engines which use the air-standard Brayton cycle to generate power, with Figure 2-1 illustrating the engine's major components, along with the pressure-volume and temperature-entropy graphs of the ideal cycle. The gas turbine's operation begins with the compressor drawing and isentropically compressing ambient air between states 1 and 2. Following this compression, the air enters the combustor, where fuel is introduced and combusted at constant pressure (corresponding to the process between states 2 and 3). The combusted gases then enter the turbine, which extracts work by isentropically expanding the gas from state 3 to 4, with some of this work providing the required compressor work. Finally, these gases are exhausted to the environment, completing cycle.

Contrary to positive displacement (i.e. piston) engines, gas turbines spatially

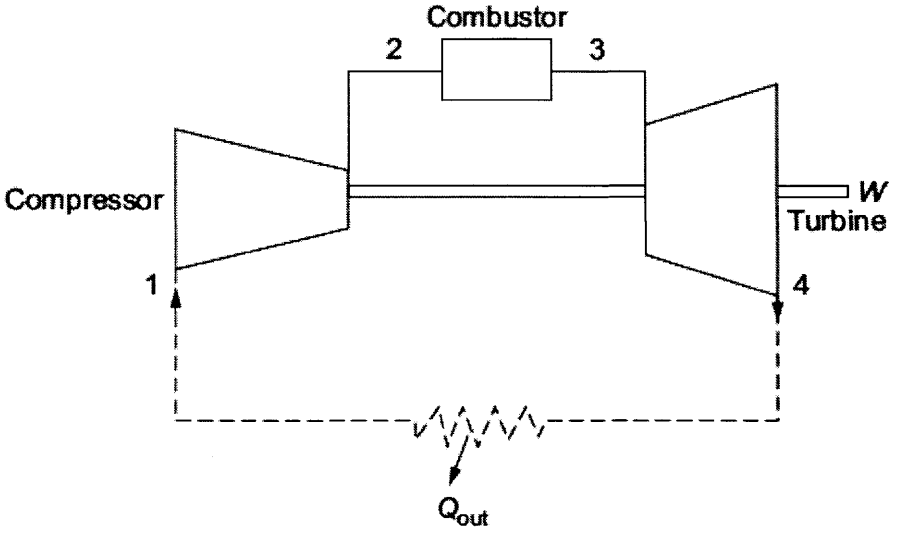


(a) Gas turbine components

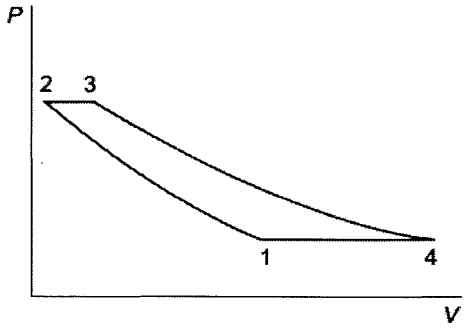


(b) The air-standard Brayton cycle P-V diagram

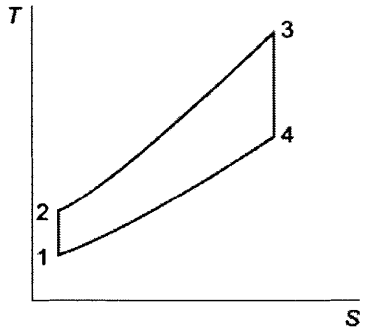


(c) The air-standard Brayton cycle T-S diagram

Figure 2-1: An overview of the gas turbine cycle, with (a) a schematic diagram of the engine's components, (b) a P-V diagram of the air-standard Brayton cycle used in the gas turbine, and (c) the corresponding T-S diagram [7].

(rather than temporally) separate their compression, combustion, and expansion processes. This physical separation enables the continuous combustion of air and fuel mixtures, allowing gas turbines to produce large amounts of power in modest packages and provide excellent reliability (due to their steady operation). The inherent advantages of these engines has led to their adoption in multiple applications, including aviation engines, marine powerplants, and industrial power generation [9]. Another benefit of gas turbines is their versatility in fuel requirement. Based on their design, modern gas turbines are able to operate using natural gas, diesel, naphtha, methane, crude oil (kerosene), gases with low heats of combustion, vaporized fuel oils, and biomass gases [7].

Despite this flexibility, gas turbine applications typically use a particular fuel based on their application. For aviation engines, kerosene is the predominate choice due to its high heating value, which minimizes fuel weight, and lack of corrosive elements (enabling longer engine lives, which is of added importance due to their high costs). Alternatively, marine engines almost exclusively use diesel because of the fuel's low cost and the engine's ability to handle the corrosive agents that are present, as they are already designed to operate in corrosive seawater conditions. Finally, industrial power generators commonly choose natural gas for the relative low cost, abundance, and acceptable amounts of corrosive elements [9].

## 2.2 Design Aspects

The design of a gas turbine must consider a variety of factors, with the engine's application dictating the majority of these considerations. Due to the scope of this project, the engine applications will be limited to aviation powerplants, with rotorcraft turboshafts receiving special attention. Within this category, there are two major classifications of gas turbines; turboshafts that provide mechanical power via an output shaft (termed turboprops if connected to an airplane propeller), and turbojets that produce thrust through the engine's exhaust jet, with the only difference being the medium through which the engine produces meaningful work [10].

For both turboshafts and turbojets, a significant portion of the design flexibility arises from the selection of compressors and turbines. This variance manifests itself in factors such as the type of compressors and turbines implemented and the number of stages of each device (i.e. how many of the components are stacked in series), as discussed in the following sections. While there are many parts that are essential to their operation, the compressor and turbine blades are the components that interact directly with the incoming air, facilitating the pressure rises created by the compressor and the extraction of power by the turbine. Thus, discussion of turbomachinery components will be limited to their blades.

### 2.2.1 Compressors

#### Functionality and Performance Parameters

For gas turbines, the compressor's key purpose is to increase the pressure of the air that flows through the engine. However, a consequence of the increased pressure is the corresponding increase in temperature, due to the isentropic relationship between pressure and temperature, as well as the inefficiency of the compressor [10]. Per the ideal gas law, this increased temperature reduces the density of the gas, counteracting the improved airflow rate.

A gas turbine's total compression ratio, defined as the final compressor outlet pressure divided by the inlet pressure, heavily influences the engine's overall efficiency,

$$\eta_f = 1 - \frac{1}{r^{\frac{\gamma-1}{\gamma}}}, \tag{2.1}$$

where $\eta_f$ is the maximum theoretical fuel conversion efficiency, $\gamma$ is the specific heat ratio of the gas, and $r$ is the compressor's total compression ratio [10]. Thus, given a constant engine geometry, high compression ratios in gas turbines are instrumental in achieving high power outputs through the associated impacts on both the airflow rate and engine efficiency.

### Design Types

Gas turbines implement three major compressor design types: axial-flow, radial-flow (or centrifugal), and axi-centrifugal designs that incorporate both axial and radial-flow stages. Axial-flow, or simply axial, compressors operate with air entering and exiting the compressor parallel to the axis of rotation. Alternatively, while still entering axially, the flow out of centrifugal compressors is perpendicular to the axis of rotation [7].

The main advantages of centrifugal compressors include a significantly lower unit cost, simplicity and ruggedness (resulting in high reliability), greater stability to flow variations, a larger operating range, acceptable performance at low airflow rates, and shorter engine length [7, 10, 21]. Centrifugal compressors do have limits that narrow their range of applicability. First, radial compressors suffer lower efficiency when placed in multiple stages, limiting their use to two stages due to the complexity and losses of ducting between stages [10, 18]. Additionally, the material restrictions of the rotor limit the centrifugal compressor speeds and temperatures, which restricts the range of mass flows and pressure ratios that are achievable in this configuration [18, 19, 20]. These factors are especially important in small power applications, making centrifugal compressors the better choice in small-scale engine designs.

Axial compressors, on the other hand, post significant advantages that have ushered in their widespread adoption. These designs are easily multistaged, enabling many rows of axial compressors to be stacked in series to create overall pressure ratios that approach 40:1, despite each individual stage contributing pressure ratios lower than 2:1 [10]. As stated in Section 2.2.1, the overall compressor pressure ratio is critical to a gas turbine's power output and efficiency, and thus is an important advantage of axial designs. Additionally, at high airflow rates, the individual stages of axial compressors are more efficient than centrifugal configurations. Axial designs contain controlled air velocities flowing axially to minimize flow losses, contrary to centrifugal compressors that inherently have difficulties achieving these conditions. Finally, axial compressors have significantly smaller frontal areas (reducing drag at high flight

speeds), which are usually accompanied by lower weights (due to the smaller engine diameters) [9, 18]. Thus, for many large-scale applications, axial compressors are the preferred design to maximize the engine's performance.

Despite these significant advantages, axial compressors are constrained in their range of applications. Manufacturing and material boundaries limit the compressor blades' roughness and both the leading and trailing edge thicknesses, which cause substantial efficiency losses in low flow rate conditions [18]. These manufacturing and material restrictions also complicate the management of blade tip clearances, which are the gaps between the rotating blades and the stationary casing of turbomachinery. The losses associated with these clearances, as discussed in Section 2.4, limit the feasibility of axial compressors in low mass flow rate applications.

Finally, axi-centrifugal designs incorporate axial stages upstream of a centrifugal stage to harness the advantages of each design, through increasing the pressure ratio via multiple stages while limiting the complexity, sensitivity, and length of the engine. Depending on the airframe's size and application, rotorcrafts have incorporated all three of these designs. However, the majority of turboshafts implement either a centrifugal or an axi-centrifugal compressor, with the exception of very high power classes in excess of 10,000 horsepower [9, 20].

### 2.2.2 Turbines

The functionality of turbines is similar to that of compressors, with a reversal in the direction of power transfer; instead of increasing the enthalpy of the working fluid, the turbine extracts energy through the reduction of a fluid's enthalpy. This extracted energy drives the engine's compressor and, for turboshafts, provides shaft power for the airframe's rotor or propeller, with the amount of available energy depending on the airflow rate, compression ratio, and amount of fuel injected in the combustor. Analogous to compressors, gas turbines implement both radial and axial turbines, depending on the engine's size and application.

Radial turbines are advantageous due to their high single-stage expansion ratios (reducing the number of required stages, and thus the engine length), significantly

lower unit cost, robustness when operating with particulates in the gas flow, and improved efficiency in very low capacity (or low airflow rate) applications [7, 18]. However, similar to centrifugal compressors, multi-stage radial turbine designs require complex inter-turbine ducting systems, which drastically reduce their feasibility. Additionally, manufacturing restrictions limit a radial turbine's diameter to approximately 0.5 meters, which caps the flow rates and expansion ratios that these turbines can achieve [18]. For these reasons, the favorability of radial turbines is limited to applications with low flow rates, and when particles are present in the working fluid (i.e. chemical industries), or where low-cost and simplicity are the major priorities [7].

When compared to radial flow designs, axial turbines are advantageous across a wide range of operating conditions. In standard applications, axial turbines provide higher efficiencies and better performance in multi-stage configurations, allowing gas turbines to achieve high airflow rates, pressure ratios, and power outputs. These features, as well as their lower frontal area (in highly loaded designs) and engine weight (due to the smaller engine diameter), result in the implementation of axial turbines in more than 95% of all gas turbine applications [7, 18, 20]. Despite these advantages, axial turbines suffer from distinct performance limitations in low power applications. Because small designs do not implement blade cooling, the turbine inlet temperature is limited by the blade material's maximum allowable temperature. Thus, as the gas turbine's efficiency is dependent on this temperature, the engine's performance capabilities are significantly restricted [7]. Moreover, for low airflow designs, axial turbines suffer from drastic losses in efficiency due to relative tip clearances, as discussed in Section 2.4.1. These factors combine to restrict axial turbines from very low airflow applications.

## 2.3 Performance Trends

Based on the discussion provided in Section 1.3, an engine's specific power, efficiency, hot and high derating, and OEI capability were identified as being crucial for rotor-

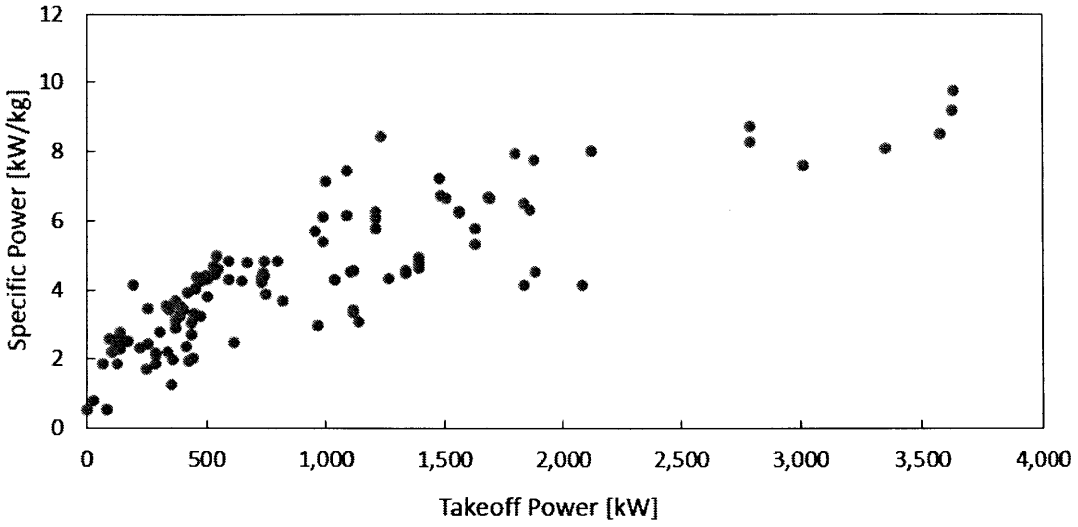


Figure 2-2: A database of modern turboshafts was used to compared the specific power and takeoff power rating for multiple engines to create a correlation between these parameters.

craft applications. Thus, these characteristics were evaluated for gas turbines using industry data and trends, as seen in the following sections.

### Efficiency and Specific Power

The efficiency and specific power describe an engine's performance in standard operating conditions, with both factors heavily influencing a rotorcraft's capabilities. To gain further understanding of these parameters, a database of modern turboshafts was created to compare the engines' specific powers and efficiencies at full-load with their rated power outputs [11, 12, 13]. First, using this data, Figure 2-2 was constructed to compare the engines' rated takeoff powers on the horizontal axis with their specific powers on the vertical axis. Here, gas turbines exhibit a wide range of specific powers, reaching in excess of 10 kilowatts per kilogram in power classes greater than 3,500 kilowatts, and falling to under 2 kilowatts per kilogram for rated takeoff powers less than 500 kilowatts. For comparison purposes, the specific power of automobile-sized gasoline engines is approximately 1 kilowatt per kilogram [10].

Additionally, the turboshaft database was used to create Figure 2-3, which com-

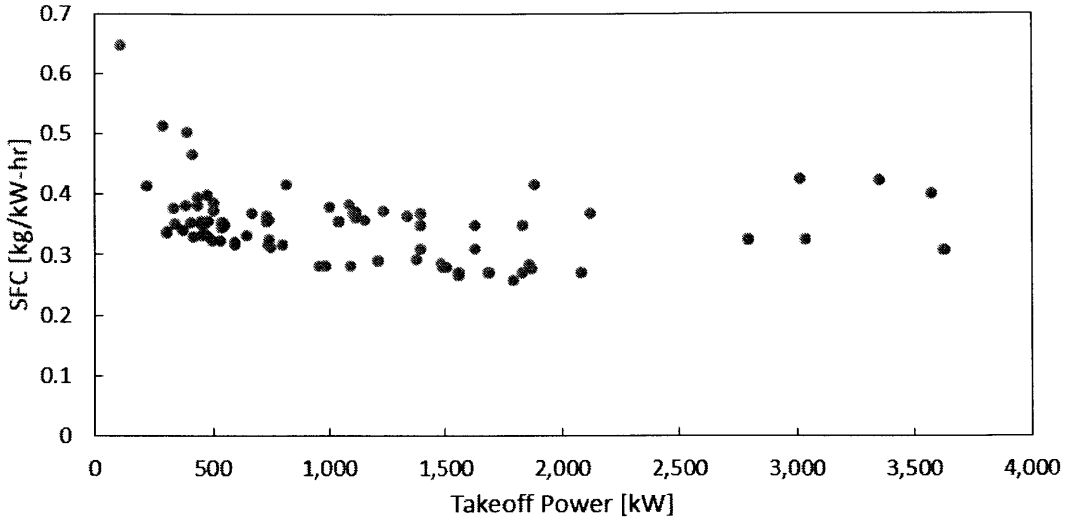


Figure 2-3: The turboshaft database was also used to evaluate trends in the engines' specific fuel consumption and takeoff power rating.

pared each engine's rated takeoff power on the horizontal axis with its efficiency at this power output on the vertical axis, listed as the specific fuel consumption. This specific fuel consumption (SFC) is commonly used to describe an engine's efficiency and corresponds to the engine's fuel mass flow rate divided by its power output (in kilograms per kilowatt-hour). Thus, a large SFC indicates an inefficient engine, as more fuel must be consumed per unit power output when compared to more efficient (i.e. lower SFC) engines. The graph indicates that, similar to Figure 2-2, the turboshafts achieve greater efficiencies (i.e. lower SFCs) at higher takeoff powers. In power classes lower than 1,000 kilowatts, the gas turbine SFCs generally exceed 0.3 kilograms per kilowatt-hour, while turboshafts with higher power ratings achieve SFCs that approach 0.25 kilograms per kilowatt-hour. For context, diesel engines, which are very efficient reciprocating piston engines, regularly achieve SFCs around 0.2 kilograms per kilowatt-hour [14].

While Figures 2-2 and 2-2 provide a wide range of data to evaluate, the scatter in these values indicates that the database contains engines with varying degrees of quality. As this investigation is characterizing the best achievable airframe performance, the database was distilled into the high-end turboshafts, which provide both

the highest specific power and lowest specified fuel consumption relative to other engines in their rated power class. Exceptions were made to this dual requirement for small (i.e. power output less than 300 kilowatts) turboshafts, as the majority of these engines did not provide SFC ratings. Furthermore, the additional data for the specific powers was necessary to ensure accurate trend predictions in this identified region, which was essential for this investigation (see Chapter 5).

The results of this analysis are shown in Figure 2-4, which are plots of the engine's specific power (2-4a) and the SFC (2-4b) versus the takeoff power ratings. Clear trends emerge from this distilled data. The data were fit using power relations,

$$P_{\text{specific}} = 0.245(P_{\text{takeoff rated}}{}^{0.456}), \tag{2.2}$$

$$SFC = 128(P_{\text{takeoff rated}}{}^{-1.23}) + 0.262, \tag{2.3}$$

where $P_{specific}$ is the engine's specific power in kilowatts per kilogram, $P_{takeoff\ rated}$ corresponds to the rated takeoff power in kilowatts, and $SFC$ represents the specific fuel consumption in kilograms per kilowatt-hour. These fits are shown as the dotted lines in Figure 2-4 and provide a performance baseline from which to compare other possible engine configurations in subsequent analyses.

### Part-Load Efficiency

The full load efficiency of an engine is insufficient to model a rotorcraft's performance over an entire flight profile, given that the engine will be operated at many power levels. To model the overall efficiency, a map of the engine's efficiency versus power output is necessary. To characterize this relationship, SFC data for two gas turbines at varying loads was obtained and plotted in Figure 2-5 [15, 130]. Here, the vertical axis is the fractional change in the engine's SFC, and the horizontal axis is the fraction change in the engine power compared to the rated takeoff power. Both examples illustrate a similar trend, where the engine's SFC rises substantially at part-load operation, while Engine 1 exhibits a less drastic rise (indicating better efficiency).

A polynomial fit of the data for Engine 1,

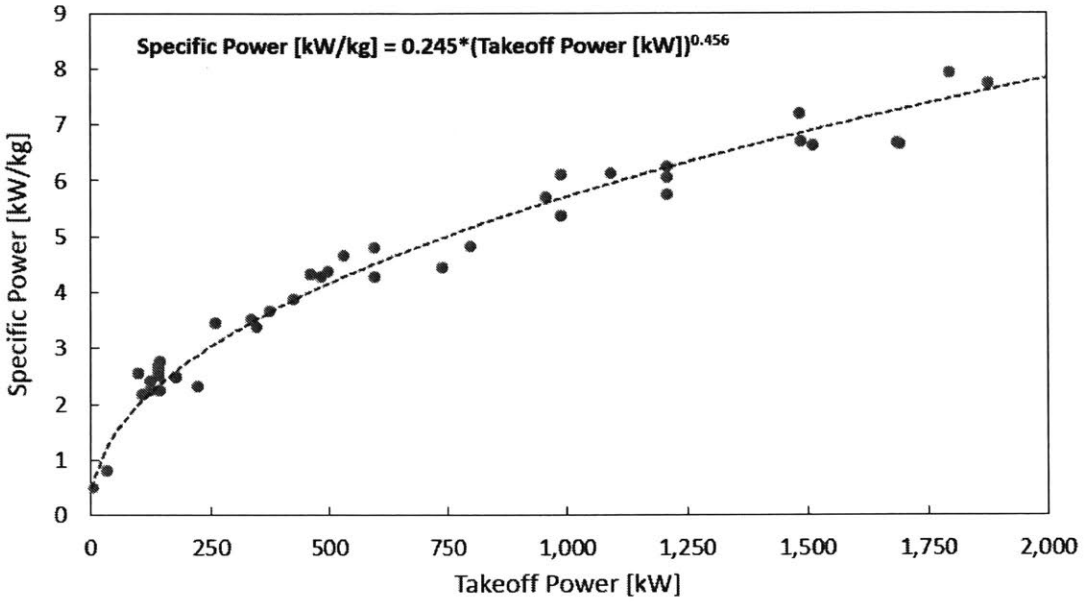


(a) Specific power

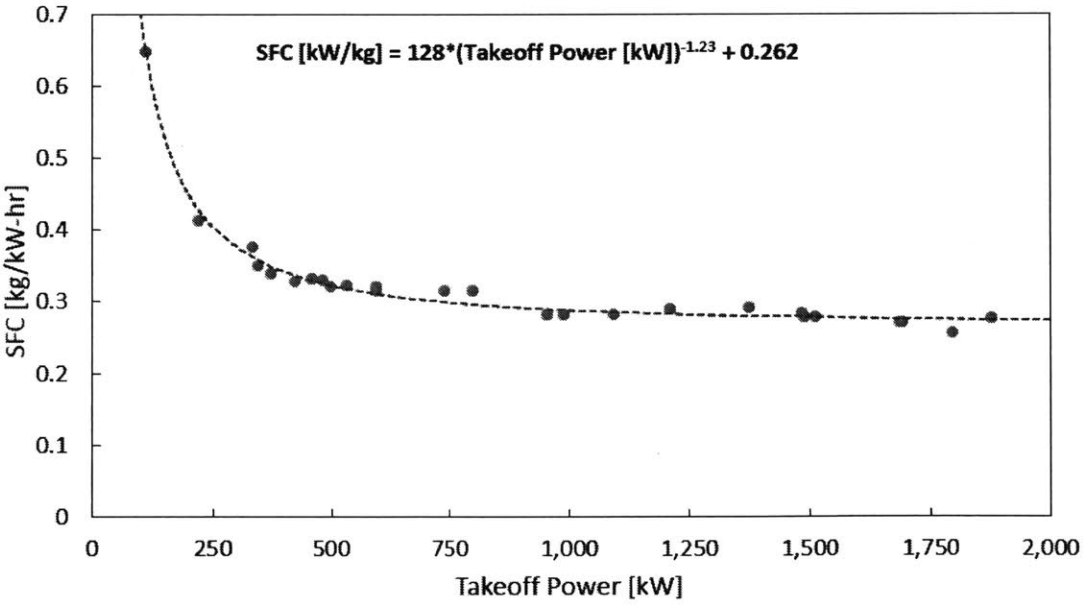


(b) Specific fuel consumption

Figure 2-4: The turboshaft database was distilled into the highest-performing engines, providing predictive trends used to estimate a gas turbine's specific power and SFC based on the engine's takeoff power rating.

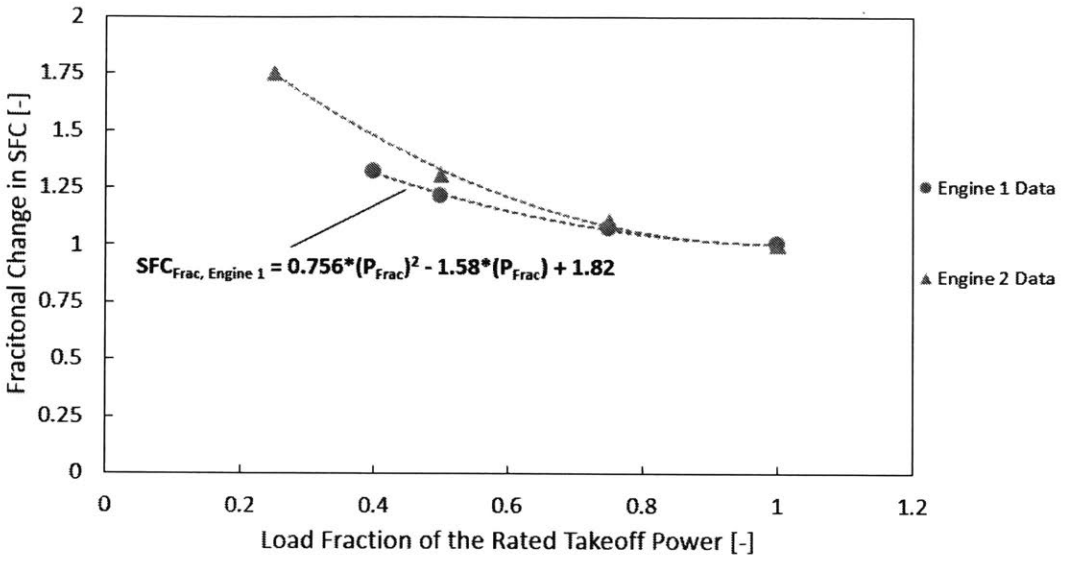


Figure 2-5: Data for the part-load efficiency of two characteristic gas turbine engines was used to create a predictive trend in turboshaft operation across varying power loads [15, 130].

$$SFC_{\text{Frac}} = 0.756(P_{\text{Frac}})^2 - 1.58(P_{\text{Frac}}) + 1.82 \tag{2.4}$$

where $SFC_{Frac}$ represents the fractional change in SFC at a given load, and $P_{Frac}$ is the load fraction of the rated takeoff power, is also plotted in Figure 2-5. This fit is more conservative (i.e. corresponds to better engine performance) than that of the data trend for Engine 2 and is used in subsequent sections to model the performance of high-end gas turbines.

### One Engine Inoperable and Hot and High Ratings

In addition to standard conditions, the gas turbine's performance in adverse scenarios was estimated to provide a full understanding of the engine's operation in rotorcraft applications. As determined in Section 1.3, an airframe's engines must provide sufficient takeoff power for hot and high conditions, as well as when engine failure occurs (i.e. OEI scenarios). First, for hot and high operation, multiple sources were compiled that evaluated gas turbine performance degradation at increasing altitude and

temperature [10, 16]. Using the specified conditions of 4,000 feet altitude pressure and a temperature 35° C greater than the ISA temperature at this altitude (i.e. 7° C), the gas turbine derating was estimated to be 25%, based on the provided trends. This effect is due to both the lower density of ambient air, which reduces the engine's airflow rate, as well as the higher temperature reducing the engine's component (and cycle) efficiencies [16, 92].

For OEI performance, gas turbines are capable of increasing their power output above the rated takeoff value for short durations, enabling rotorcraft to recover from this adverse situation. To determine a trend for this performance characteristic, turboshaft data was compiled to compare each engine's takeoff power with its rated OEI power increase [11, 12]. Figure 2-6 provides the result of this evaluation, where the rated OEI fractional increase in power is the vertical axis and the takeoff power corresponds to the horizontal axis. Here, the OEI rating exhibits considerable scatter across the sample engines, with maximum ratings that range between less than 5% and in excess of 40%. Based on this data, the analysis chose a characteristic gas turbine OEI rating that is 120% of the takeoff power, as this represents the higher end of these example engines while being close to the data average of 117%, as well as industry estimations [6].

## 2.4 Performance Limitations

Through both the specific power and SFC analyses conducted in Section 2.3, it is apparent that gas turbines experience decreased performance at lower rated powers. In addition to industry practices and material limitations, two physical interactions of scaling effects and changes in engine design assist in explaining this trend, as described in the following sections.

### 2.4.1 Scaling Effects

The reduced overall efficiency of small scale gas turbines can primarily be attributed to two effects. As the gas turbine decreases in size, the Reynolds number is a dimen-

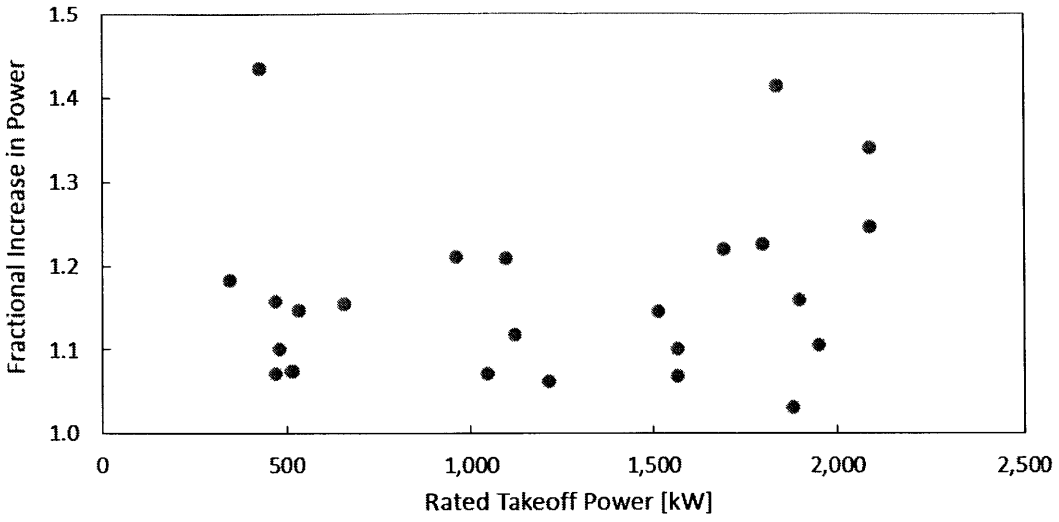


Figure 2-6: A database of turboshafts was compiled to evaluate the trend between the engine's OEI performance and rated takeoff power [11, 12].

sionless quantity that characterizes the magnitude of inertial versus viscous forces,

$$Re = \frac{\rho v L}{\mu}, \tag{2.5}$$

where $\rho$ is the density of the fluid in kilograms per cubic meter, $v$ is the fluid's characteristic velocity in meters per second, $L$ is the characteristic length scale in meters, and $\mu$ is the fluid's dynamic viscosity in kilograms per meter-second. Based on the Reynolds number's proportional dependence on the length dimension, as gas turbines decrease in geometric size, the Reynolds number will also decrease, assuming a constant characteristic velocity. This lowering of the Reynolds number causes a shift in the dynamics of the fluid flow, transitioning from inertial effects towards viscous effects.

Due to this change, fluids are more susceptible to flow separation effects (or boundary layer separation), as this is a viscous phenomenon [17]. The separation occurs when, under a strong adverse pressure gradient, the fluid flow reverses direction near an object, creating a vortex region proximal to the object's surface that transposes fluid away from the object towards the mainstream flow region [17]. Figure 2-7 dis-

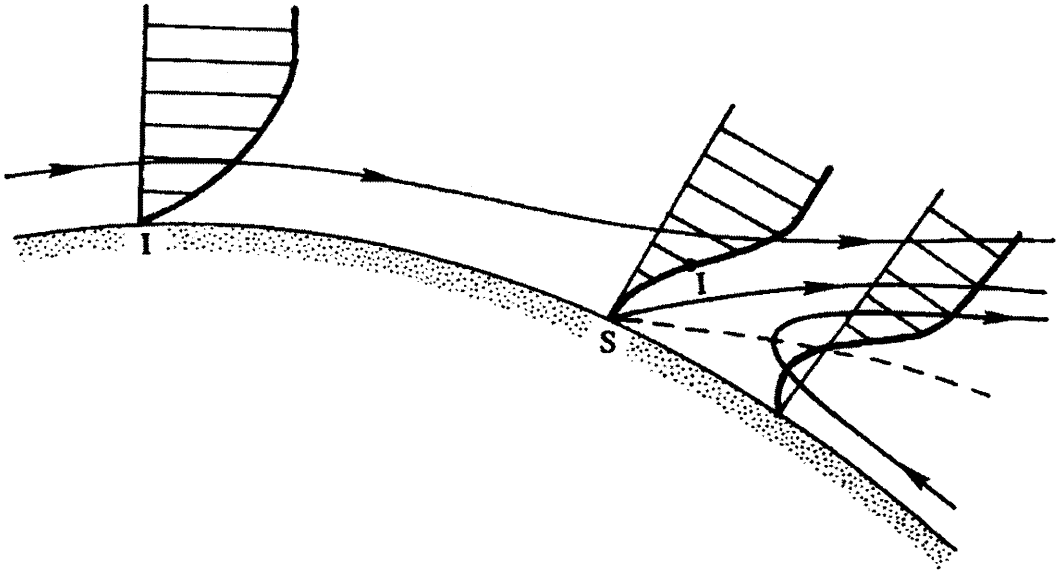


Figure 2-7: In low Reynolds number conditions, a fluid experience flow separation, occurring at point 'S', where fluid is transposed toward the mainstream flow region [17].

plays this interaction, where the separation occurs after point 'S'.

In gas turbines, this separation can result in a "blockage" in the flow path, which restricts the fluid flow rate and decreases the engine's efficiency and power output [7, 18]. Additionally, boundary layer separation can lead to flow unsteadiness, resulting in oscillatory blade stresses that can cause blade fatigue failure [20]. Thus, the compressors (where adverse pressure gradients arise) of smaller gas turbines are more susceptible to the detrimental effects of flow separation due to their smaller Reynolds numbers. However, based on the aerodynamics of how each design generates a pressure rise, axial compressors are significantly more sensitive to boundary layer separation when compared to centrifugal designs. This leads to radial compressors reaching significantly higher pressure ratios across each of their stages, as they are less limited by this separation [20].

The second effect is due to the clearances between the rotating rotor blades and the stationary casing scaling at a different rate than the engine's blade lengths (i.e. the clearances do not decrease at the same rate as the blade size). As mentioned in

Section 2.2.1, tip clearances are responsible for one of the major loss mechanisms in both the compressors and the turbines of gas turbines [7, 18]. For compressors, the performance loss occurs due a portion of the fluid flowing upstream from high-pressure regions, past the compressor's blade tips, to lower-pressure regions. This flow results in both the compressor consuming extra power and the narrowing of the operating range (i.e. range of acceptable mass flow rates and pressure ratios) of specific axial compressor designs [7, 18]. For turbines, the fluid bypasses the component's blade tips when flowing downstream between the high- and low-pressure regions, reducing the energy harnessed by the turbine, and thus reducing the power output (and efficiency) of the engine [7, 18]. While also harmful to radial turbomachinery, the architecture of axial compressors and turbines results in the creation of a pressure differences across each row of the component's blades, giving rise to extra sensitivity to these losses [18].

While important for all gas turbines, the tip clearances become a larger fraction of overall blade height as the engine size decreases. This increase in the gap to the blade height ratio allows an increase in the relative mass of fluids that bypass the flow through the turbomachinery blades. This bypass flow leads to a reduction in the output power of the engine. Thus, these losses significantly reduce the power output and efficiency of the engine at small engine sizes [7, 18]. Furthermore, scaling axial turbomachinery becomes impractical beyond the region where tip clearances remain constant, due to manufacturing constraints (occurring at different sizes for compressors and turbines). After this point, the tip clearance percentage of the overall blade height rises drastically, severely reducing the performance of the engine and rendering axial designs infeasible [18]. This effect, combined with the increase in tip clearance losses that accompany the reduction in size of all gas turbines, severely hinders the performance of axial turbomachinery in low airflow applications.

### 2.4.2 Changes in Engine Design

In addition to the scaling effects, the gas turbine's compressor and turbine designs change in low airflow (power class) engines. As stated in Section 2.2, axial turboma-

chinery are more efficient in high airflow applications, while radial compressors and turbines perform better in low airflow conditions (extremely low airflow conditions for the radial turbines). However, aside from the scaling effects outlined in Section 2.4.1, axial turbomachinery are the preferred designs when strictly considering power output and efficiency, due to the factors provided in Section 2.2. Despite this inclination, gas turbine designs change from axial to radial turbomachinery due to the previously referenced scaling effects as well as changes in design priorities.

Based on the discussion provided in Section 2.4.1, the scaling down of turbomachinery greatly reduces their performance capabilities, due to the increases in boundary layer separation and tip clearance losses. While these factors affect both design types, axial turbomachinery suffer significantly greater losses than radial designs in low power classes, resulting in radial turbomachinery gaining a performance advantage in these configurations. Additionally, while power output and efficiency are always important, low airflow applications place extra emphasis in simplicity, durability, low cost, and reliability [7, 10, 18]. Thus, as these factors received added focus, and the efficiency and power output of the engine become less important, radial turbomachinery are the advantageous designs.

Both of these considerations result in engines shifting from axial to radial configurations. For compressors, this change in design preference occurs over a range of medium airflow rates between 1.5 and 10 kilograms per second, depending on the application [18]. For turbines, the switch occurs at lower airflow rates, between approximate compressible flow values of 0.05 to 0.5 kilograms per second (measured as 0.05 to 0.1 ($kg\sqrt{K}/s/kPa$), with the conversion depending on operating parameters) [18]. As explained in Section 2.2.1, the change between axial and radial turbomachinery creates constraints in their maximum attainable pressure ratios, airflow rates, and efficiencies (see Section 2.2.1).

This required change in design preference, compounded with the growth of the scaling losses outlined in Section 2.4.1, results in gas turbine performance being limited to the trends identified in Figure 2-4, where the engine specific powers and efficiencies drastically fall at low power ratings. While extensive research has been

devoted to increasing the performance capabilities of gas turbines, the majority of this innovation aims at higher power classes whose applications are more common. Additionally, the restrictions outlined in this chapter have significantly constrained these developments in lower power configurations. For these reasons, the scope of this investigation was narrowed to focus on identifying alternative engine configurations for powering rotorcraft in low power class applications.

# Chapter 3

# Reciprocating Piston Engines

Reciprocating piston engines were the main alternatives to gas turbines that were analyzed in this study. Piston engines are the most common modern engine configuration, with applications that include land, sea, and air transportation along with stationary power generation [14]. Their widespread adoption is attributed to their successful combination of efficiency and cost-effectiveness, in part due to the piston engines' relative simplicity, ruggedness, and reasonable power-to-weight ratio [14, 22]. While their utilization in aircraft is a dated concept (see Section 1.1), piston engines are rarely implemented in modern airframes, mainly due to the engines' significantly heavier architecture compared to gas turbines. However, piston engines obtain advantages in other essential characteristics, such as higher efficiencies, which enable their use in niche applications. To determine the feasibility of replacing gas turbines with piston engines, the following sections will discuss piston engine features, performance trends, and limitations, with these results compared to those of the gas turbines.

## 3.1 Basic Design Principles

All reciprocating piston engines share common characteristics that facilitate their operation. Figure 3-1 provides an example of a piston engine's basic architecture, illustrating some of these universal features. The piston translates linearly within the cylinder walls between top dead center (TDC), where the volume between the piston

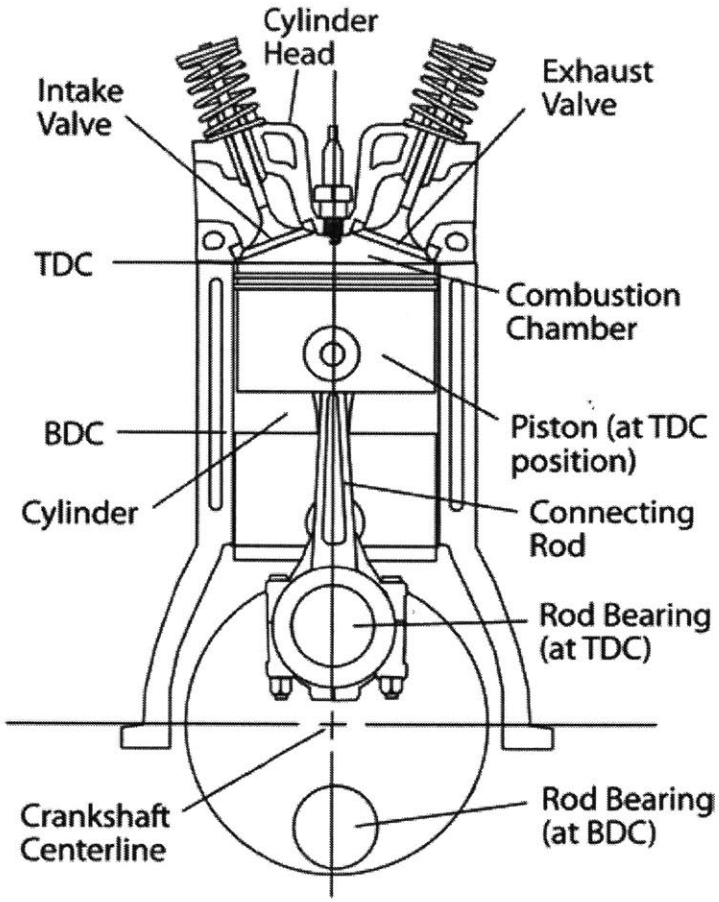


Figure 3-1: Basic piston engine architectures contain these common components to facilitate their operation [22].

and cylinder head is at a minimum (known as the clearance volume), and bottom dead center (BDC), where this volume is at a maximum. The volume between the piston and the cylinder head is referred to as the "combustion chamber," and the volume between BDC and TDC is known as the cylinder's displacement.

This basic architecture can be packaged in a variety of ways to fit specific applications, with Figure 3-2 illustrating four of the most common configurations: inline, vee, horizontally opposed, and radial. Inline is the most basic engine design, containing a row of pistons stacked "in line" with the engine's crankshaft. Increasing the design complexity, vee and horizontally opposed (HO) designs are essentially two inline piston banks separated by an angle (90° or less for vee and 180° for HO) [14]. Lastly,

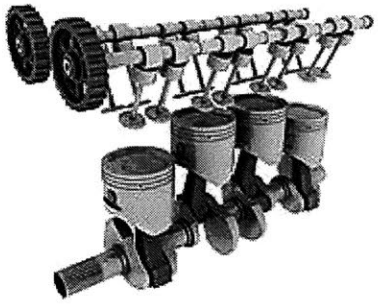

(a) Inline [26]

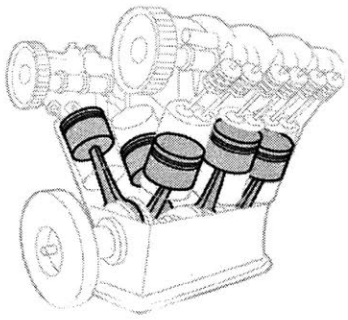

(b) Vee [25]

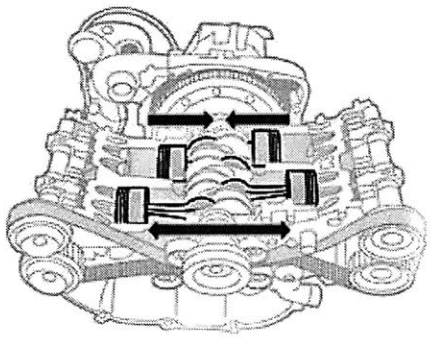

(c) Horizontally Opposed [25]

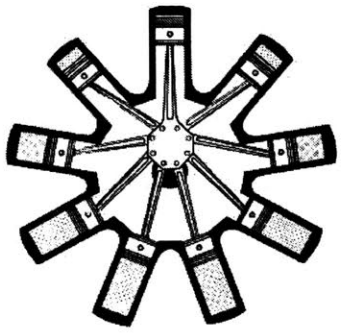

(d) Radial [27]

Figure 3-2: These four piston engine designs are common configurations, with widespread use both historically and in modern applications.

radial configurations wrap entire banks of cylinders in a circular pattern around the engine's crankshaft. Each design offers advantages and disadvantages in their packaging, complexity, and inherent balancing of combustion forces. While this analysis did not thoroughly evaluate these different configurations, the choice of engine architecture is crucial when considering their implementation.

For a particular application, determining an engine's ideal geometry entails a balance between multiple engine characteristics, including efficiency, magnitude of stresses, and overall engine size and weight. With increasing displacement (assuming a constant ratio between the cylinder diameter and height, known as the bore and stroke), the efficiency increases as the friction and heat losses become less significant factors, while the cylinder stresses grow due to hoop stress being proportional to the diameter and the cylinder head stress being proportion to its area (and thus the bore squared). Furthermore, the engine speed must be decreased with increasing stroke,

as the piston speed, which is limited due to lubrication of the cylinder walls, is proportional to the engine speed and stroke length. Finally, the relationship between engine displacement, size, and weight is very complex, with multiple factors affecting whether engine weight and size increases or decreases with varying cylinder dimensions. Estimating the resulting values for these parameters is not a trivial exercise, and must be completed on a case-by-case basis. Thus, when applicable, this analysis used standard industry geometry for the various evaluations.

Regardless of their architecture and geometry, reciprocating piston engines produce power by initiating the combustion of a gaseous air and fuel mixture inside the combustion chamber when the piston is near TDC. The combustion creates a drastic rise in pressure, transferring work from the gas to the piston by pushing the piston down towards BDC. This linear work is converted into the rotational energy of the crankshaft through a connecting road and crank mechanism (the latter is not depicted in Figure 3-1), with the crankshaft serving as the engine's power output shaft. Most piston engines operate on a four-stroke cycle, where one power-producing cycle requires four separate "strokes" (i.e. the piston moving from TDC to BDC, or vice versa). These four strokes function as follows, with Figure 3-3 illustrating each process:

1. Intake stroke - a fresh charge (either air or an air/fuel mixture) is drawn into the cylinder while the piston moves from TDC to BDC.

2. Compression stroke - the piston translates from BDC to TDC, compressing the fresh charge to a higher pressure and smaller volume. The ratio between the maximum and minimum volumes (piston at BDC and TDC, respectively) is defined as the engine's compression ratio (CR). Combustion is usually initiated near the end of this stroke.

3. Power (or expansion) stroke - as a result of combustion, the high-pressure charge pushes the piston from TDC to BDC, producing the engine's power.

4. Exhaust stroke - the piston moves from BDC to TDC, while the burned mixture is exhausted out of the cylinder in preparation of the next cycle.

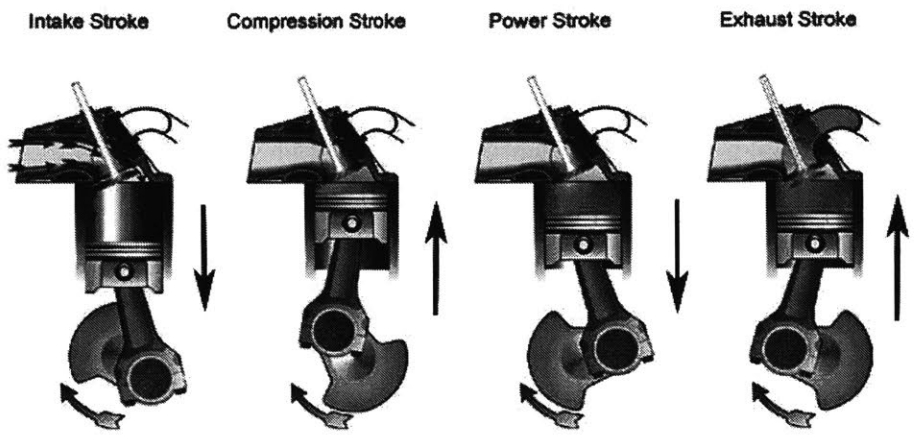


Figure 3-3: The four-stroke cycle is comprised of the intake, compression, power, and exhaust strokes [23].

The charge transfers (i.e. drawing in an intake charge, exhausting the burned mixture) are facilitated by the engine's intake and exhaust valves, with the most common design, poppet valves, depicted in Figure 3-1. In basic configurations, these valves are controlled by the engine's valve-train, consisting of a camshaft mechanically coupled to the crankshaft. The valve-train is tuned such that the intake and exhaust valves are opened and closed at specific times within the engine cycle to ensure sufficient airflow (for both the intake and exhaust processes), power output, and cycle efficiency [14]. Sections 3.2.3 and 3.6.1 will discuss alternative valve configurations and valve activation mechanisms, respectively.

As the combustion of fuel releases substantial amounts of energy, the engine must be cooled to prevent component degradation and failure. Piston engines accomplish this goal through implementing either air or liquid cooling, with each method providing unique advantages. Air-cooled engines incorporate large fins attached directly to their cylinders to increase the heat transfer between the high-temperature cylinder walls and the low-temperature ambient air, whereas liquid cooled designs pump coolant throughout the engine walls and reject heat through an auxiliary heat exchanger (such as an automobile's radiator). The main differences between the two

techniques are the amount of added weight and cooling capabilities; the fins are significantly lighter than the liquid coolant system, allowing for a lighter engine architecture, while liquid cooling rejects significantly more heat, and thus is required in the majority of high-performance applications [14]. Therefore, as this analysis is investigating engines for a high-performance application, all piston engines considered in this report are assumed to be liquid-cooled.

While all engines incorporate these basic principles, there are two main piston engine categories: spark ignition (SI) and compression ignition (CI) engines. The major difference between these designs is their method of initiating combustion; SI engines utilize a spark whereas CI engines rely on autoignition of their fuel from exposure to high pressures and temperatures. There are stark differences in the architecture and operation of SI and CI engines, as well as in the design process for each cycle, as described in Sections 3.1.1 and3.1.2.

### 3.1.1 Spark Ignition Engines

#### Operating Principles

The ideal Otto cycle is often used to model an SI engine's theoretical operating cycle, as seen in Figure 3-4. Despite actual performance differing from this concept, the cycle illustrates an SI engines' basic operating principles, with the following steps [14]:

- 1 - 2: Adiabatic and reversible (i.e. isentropic) compression of the intake charge, consuming engine power
- 2 - 3: Adiabatic, constant-volume combustion of the air/fuel mixture while the piston is at TDC
- 3 - 4: Isentropic expansion, generating the engine's power
- 4 - 1: Adiabatic exhausting of burned mixture and intake of fresh charge

In the combustion step between states 2 and 3 of Figure 3-4, SI engines are unique in their using a spark plug to initiate combustion. When the piston approaches TDC,

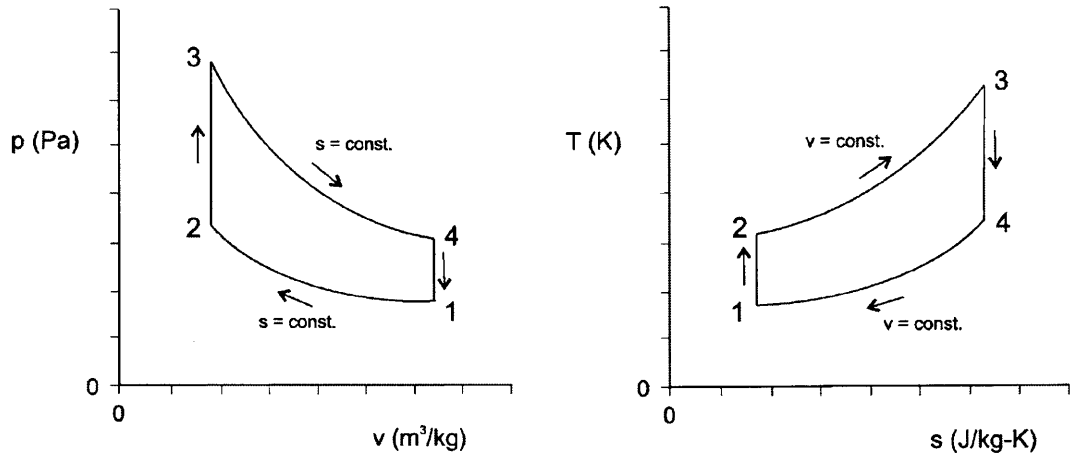


(a) Pressure - specific volume diagram

(b) Temperature - entropy diagram

Figure 3-4: The theoretical Otto cycle is comprised of an isentropic compression (1-2), constant-volume heat addition (2-3), isentropic expansion (3-4), and constant-volume heat rejection (4-1) [10].

a large voltage is applied across the spark plug's electrodes, inducing a spark. This spark creates a small flame kernel in the charge that begins propagating radially throughout the cylinder, burning the remaining air/fuel mixture until the flame front reaches the cylinder wall and is extinguished [14]. Section 3.2.2 will discuss the use of combustion timing to improve engine performance (i.e. increasing power and efficiency) and the associated trade-offs.

### SI Combustion

The combustion process described above is accomplished by premixing a combustible air and fuel mixture. In the presence of a spark or the propagating flame front, fuel (made of hydrocarbons) is oxidized by the air's oxygen, forming carbon dioxide and water vapor (among other undesired products), while releasing the energy that the engine harnesses into useful power [14]. A mixture is considered stoichiometric (or chemically correct) if its proportions of air and fuel result in complete combustion with no excess fuel or oxygen. For standard gasoline, the most common SI engine fuel, the stoichiometric air-fuel mass ratio is 14.6 [14].

Because the presence of an oxidizer (air) is required for combustion, the maxi-

mum amount of fuel that can be burned (and thus the maximum power that can be produced) in each cycle is dictated by both the engine's airflow rate and air-fuel ratio. The airflow rate is metered through the use of a throttle, which is an adjustable restriction in the intake flow path that lowers the airflow rate into the engine when operating at part load (i.e. less than maximum power output). This throttling has the negative consequence of creating a reduced pressure in the cylinder due to the flow restriction; the lower pressure creates a pumping loss (i.e. the engine consumes more energy having to draw in air at a lower pressure than ambient) during the intake stroke of the engine's cycle, reducing power output and efficiency [14]. Furthermore, changes to the air-fuel ratio have substantial effects on engine operation, such as power output, efficiency, and emissions. These factors will be discussed in further detail in the following sections.

### Fuel Introduction and Characteristics

SI engines are unique in their burning a premixed air and fuel charge, accomplished by introducing the fuel to the air through one of three separate designs: within a carburetor prior to entering the cylinder, implementing port injection at the intake valves, or using direct injection (DI) inside of the engine's combustion chamber. Carburetors are passive components that meter fuel introduction based on the airflow rate and ambient conditions (i.e. air temperature and pressure). These devices are low cost and allow for little control and flexibility after installation, making them suited for inexpensive applications where continuous optimization of the engine's performance is not essential [10]. Alternatively, port injection provides more control at the cost of added complexity and cost. In this configuration, fuel is injected onto the upstream side of the intake valve, as illustrated in Figure 3-5. Incoming air vaporizes the fuel while passing into the cylinder, creating the desired mixture. The amount of fuel injected onto the valve is dictate by variations in ambient conditions and the desired engine performance.

Lastly, many modern engines implement direct injection to introduce the fuel after the air charge has entered the cylinder. As seen in Figure 3-5, fuel injectors are

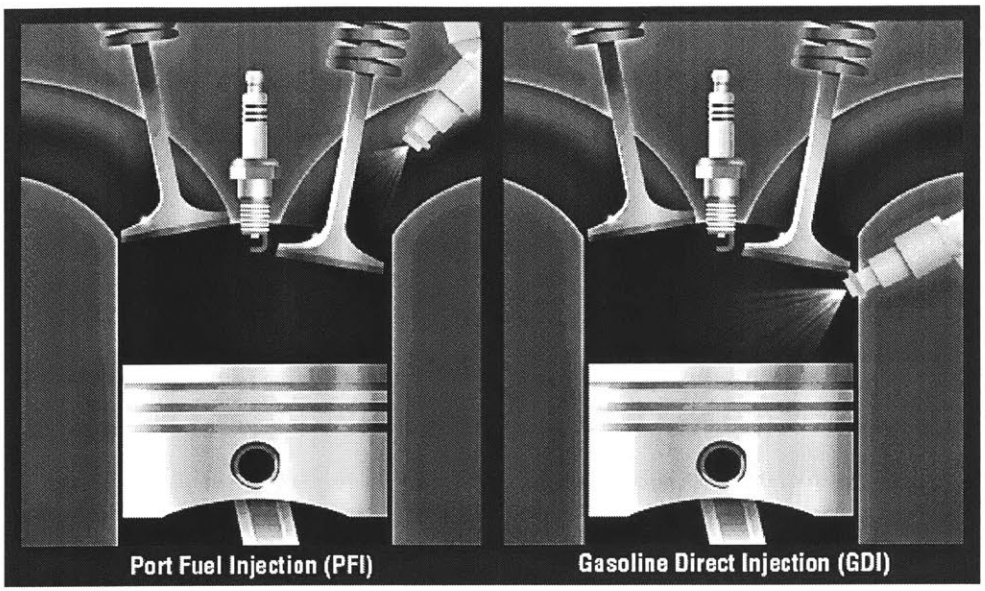


Figure 3-5: Port injection (left) deposits fuel onto the back of the intake valve, while direct injection (right) introduces the fuel directly into the cylinder [31].

installed into the cylinder head, with injection occurring during the initial portion of the intake stroke (between states 1 and 2 of Figure 3-4). DI provides two major advantages to SI engine performance by decreasing the charge temperature and providing improved control of the air-fuel ratio. First, because the fuel is vaporized inside of the cylinder, the temperature of the charge is reduced, lowering the fuel's "knock" tendencies (i.e. the spontaneous combustion of the fuel, a concept discussed in the following paragraph) while increasing the charge density. This increase in density allows more air and fuel to be introduced and burned per engine cycle, thus improving engine performance [40]. Second, DI enables more sophisticated control of the air-fuel ratio, which is instrumental in maximizing engine performance (see the following section). While carburetors and port injection are widely adopted due to their low costs and simple installations, this analysis will exclusively consider DI to leverage its improvements to the engine's performance and operational control [14].

Similar to these introduction methods, SI engines can operate using multiple fuels, with the most common fuel being gasoline. For these engines, one of the most important fuel characteristic is the resistance to spontaneous combustion, known as

knock (see Section 3.4). This resistance to knock is characterized as the fuel's "octane number", which is an empirical measure of whether or not a fuel will autoignite under specific operating conditions (higher numbers having more resistance to knock than lower numbers) [14]. The two techniques used to measure a fuel's octane number are the research method, providing the research octane number (RON), and the motor method, supplying the motor octane number (MON). The research method is conducted in less severe engine operating conditions than the motor method, resulting in the majority of fuels possessing a higher RON than MON. For reference, regular grade gasoline (used by standard automobile SI engines) has a RON of at least 91 and a MON of roughly 83, while aviation gasoline (Avgas, used in many SI aircraft engines) has a minimum MON of approximately 100 [14, 24].

### Air-Fuel Ratio

In specific operating conditions, a cycle's air-fuel ratio is often identified as a fraction of the stoichiometric (i.e. chemically correct) ratio, calculated by either of the following ratios[1],

$$Relative\ Air/Fuel\ Ratio,\ \lambda = \frac{(A/F)_{\text{actual}}}{(A/F)_{\text{stoichiometric}}}, \tag{3.1}$$

$$Fuel/Air\ Equivalence\ Ratio,\ \phi = \frac{(F/A)_{\text{actual}}}{(F/A)_{\text{stoichiometric}}}, \tag{3.2}$$

where $A$ and $F$ are the air and fuel masses within the cycle's charge, respectively [14]. For reference, SI engines typically operate with a fuel-air ratio (i.e. equivalence ratio, $\phi$) between 0.8 to 1.2 [14]. Mixtures with excess fuel (equivalence ratio greater than 1) are termed "rich", while charges with excess air (equivalence ratio less than 1) are called "lean". As previously mentioned, SI engines must carefully meter their air-fuel ratio to balance power output, efficiency, emissions, and knock tendencies.

Starting at unity, increasing the equivalence ratio will initially raise the engine's mean effective pressure (a measure of engine power). In the high temperature conditions that follow combustion, disassociation of molecules creates the presence of

[1]These ratios are the inverse of one another, providing the same information in different formats.

additional oxygen, which enables the burning of more fuel. Thus, a higher equivalence ratio increases the amount of combustion and power, with peak power output occurring at an equivalence ratio between 1 and 1.1. However, this increase in power comes at the cost of reduced engine efficiency: while excess fuel is required to utilize all available oxygen, a portion of the injected fuel does not combust, resulting in incomplete combustion and diminished efficiency [14].

Alternatively, the opposite effects occur when decreasing the equivalence ratio; engine power output falls while efficiency rises. By definition, leaner mixtures contain less fuel, resulting in less combustion and power output. Additionally, combustion of lean mixtures produces lower peak temperatures, which reduces the dissociation of the combustion byproducts carbon dioxide and water, a process that consumes energy. Thus, limiting this dissociation enables a larger fraction of the energy released from combustion to be converted into the useful work of the piston, increasing the fuel conversion efficiency. However, as mixtures become increasingly lean, the improvement in efficiency is reversed due to an increase in combustion duration, resulting in efficiency decreasing in very lean conditions [14]. These trade-off are illustrated in Figure 3-6a, where *imep*, *isfc*, and $\eta_{f,i}$ are the engine's *indicated* mean effective pressure, specific fuel consumption, and fuel conversion efficiency, respectively.[2] Here, the identified parameters are the vertical axes, with the horizontal axis corresponding to the air-fuel ratio.

In addition to power output and efficiency, the air-fuel ratio can significantly affect an engine's knock tendencies and emissions. For engines that utilize direct injection, increasing the equivalence ratio (i.e. injecting more fuel) will increase the charge cooling effect introduced in Section 3.1.1, as the addition fuel will vaporize and reduce the fuel's knock tendencies [14]. Furthermore, the equivalence ratio's effect on emissions is illustrated in Figure 3-6b, where emission production is the vertical axis and the horizontal axis corresponds to the air-fuel ratio. The relationship between the air-fuel ratio and carbon monoxide (CO) production is straightforward: increasing

[2]These *indicated* performance measures do not account for the engine's friction, but illustrate the parameter trends with respect to the equivalence ratio

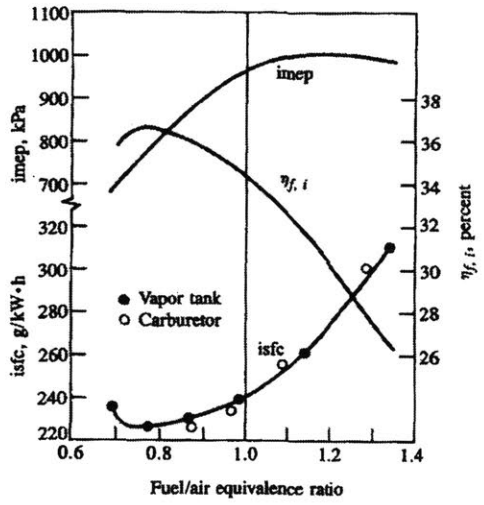


(a) IMEP (indicated mean effective pressure), isfc (indicated specific fuel consumption), and indicated efficiency vs equivalence ratio

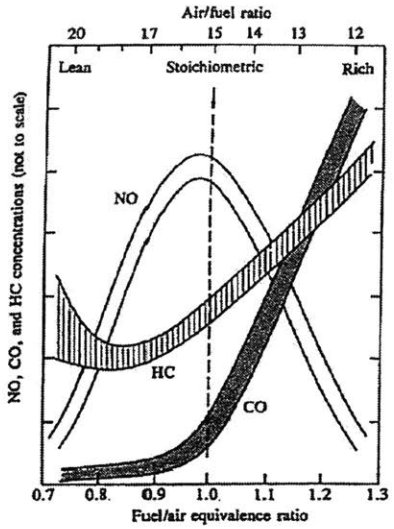


(b) NO, CO, and CH emissions vs equivalence ratio

Figure 3-6: An SI engine's performance (imep, isfc, and efficiency) and exhaust emissions drastically change as the engine's equivalence ratio is varied [14].

the equivalence ratio will increase CO emissions. Rich mixtures do not have sufficient oxygen to fully burn all of their fuel, resulting in the increased formation of CO instead of $CO_2$, the usual combustion byproduct [14].

On the other hand, hydrocarbon (HC) and nitric oxide (NO) emissions exhibit local extrema in lean conditions. HCs are exhausted due to incomplete combustion, which can be caused by either the shortage of oxygen that occurs in rich conditions or the mixture's combustion duration exceeding the available time, which is a side effect of excessively lean conditions. In more reasonably lean mixtures, these factors are balanced to create a minimum in HC production. Similarly, NO formation requires excess oxygen and high combustion temperatures, which are balanced in slightly lean conditions to achieve maximum nitric oxide production. In richer conditions, the reduction in available oxygen outweighs the initial increase in combustion temperatures caused by more fuel being burned, whereas in leaner mixtures, the reduced combustion temperatures dominate.

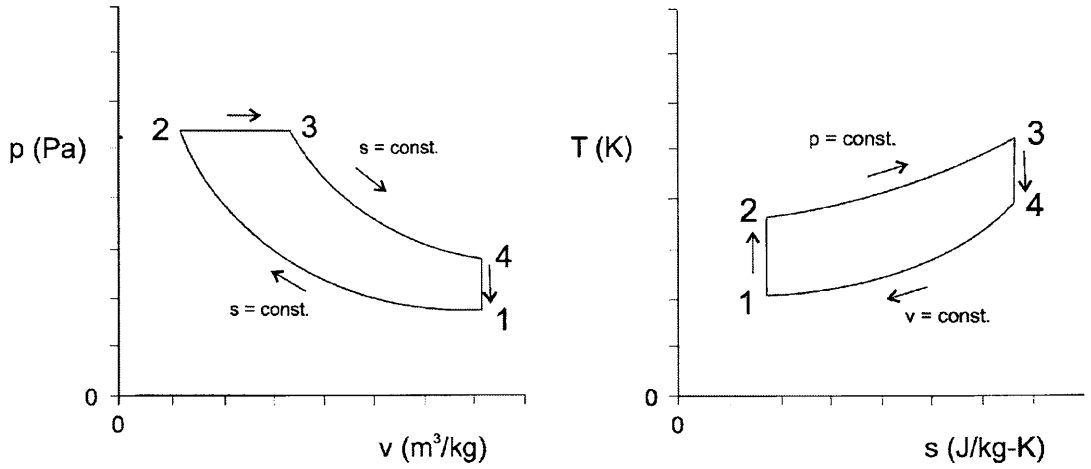


(a) Pressure - specific volume diagram

(b) Temperature - entropy diagram

Figure 3-7: The theoretical Diesel cycle consists of an isentropic compression (1-2), constant-pressure heat addition (2-3), isentropic expansion (3-4), and constant-volume heat rejection (4-1) [10].

### 3.1.2 Compression Ignition Engines

#### CI Operating Principles

Contrary to SI configurations, the ideal representation of CI engine operation is the Diesel cycle, which is illustrated in Figure 3-7 and operates as follows:

- 1 - 2: Adiabatic and reversible (i.e. isentropic) compression of the intake charge, consuming engine power
- 2 - 3: Adiabatic, constant-pressure combustion of the air/fuel mixture as the piston begins moving from TDC to BDC, generating a portion of the engine's power
- 3 - 4: Isentropic expansion, providing the remainder of the engine's power
- 4 - 1: Adiabatic exhausting of the burned mixture and intake of fresh charge

The major difference between the Diesel and Otto cycles is the combustion step between phases 2 and 3. As discussed in Section 3.1.1, an SI engine's combustion is approximated as a constant-volume process, with spark ignition of a premixed air

and fuel charge creating a drastic rise in pressure. Alternately, CI engine combustion occurs at a constant *pressure*, with the process initiated by autoignition of the fuel and maintained via a diffusion flame, as described below.

### CI Combustion

In the CI combustion process, liquid fuel is injected into the combustion chamber, where the fluid is atomized into droplets, evaporated, and mixed with fresh air to form combustible regions within the heterogeneous cylinder charge. At this point, the cylinder's pressure and temperature have exceeded the fuel's autoignition threshold, resulting in the spontaneous ignition of portions of the combustible regions after the fuel's ignition delay period (i.e. the time for a fuel exposed to the operating conditions to autoignite). The ensuing flame front rapidly expands to burn the remaining sections of sufficiently mixed fuel and air, while additional fuel is injected, mixed with fresh air via diffusion, and burned to continue the combustion process [14].

To facilitate this diffusion flame, CI engines operate at high pressures to enable the spontaneous combustion of their fuel, which is achieved, in part, by using high compression ratios (typically between 12 and 24 compared to 8 to 12 for SI engines). To control this flame and ensure proper combustion timing, the designs commonly utilize direct injection of fuels that possess sufficient ignition delay. Fuels with a short delay period result in ignition occurring before the majority of fuel has been injected, allowing the engine to control the combustion process using the rate of injection and charge mixing, enabling smoother operation [14]. Analogous to the octane number for antiknock tendency, a fuel's "cetane number" is a measure of its ignition delay, with a high cetane number indicating a short delay period. For reference, diesel fuels have cetane numbers that usually fall between 40 and 55 [14].

Because combustion (and the corresponding energy release) is continued until all of the injected fuel has burned, the power output of the engine is controlled by the duration of this injection. However, a cycle's maximum amount of combustible fuel is limited by time, as the engine requires the air and fuel to mix (and combust) within a specific crank angle interval. Because of this limited time frame, any additional

fuel cannot mix with air, which leads to inefficient combustion and unburned fuel that is a pollutant [14]. Due to this constraint, CI engines must operate with air fuel ratios that are a minimum of 20% leaner than stoichiometric. For reference, despite diesel fuel (the most common source for ground applications) having a stoichiometric air-fuel ratio of 14.5, CI engines using this fuel usually operate with ratios between a minimum of 18 at full load and upwards of 70 at part load (an equivalence ratio range of 0.8 to 0.2) [14]. Furthermore, CI engines operate with a relatively constant airflow rate across all load levels to eliminate the pumping losses that arise from throttling (as described in section 3.1.1) [14]. This feature, coupled with the direct relationship between fuel injection and power output, constrains the engine's operational flexibility; unlike SI designs, CI engines cannot use their air-fuel ratio to balance additional factors such as emissions and efficiency. Instead, these engines leverage their combustion timing to control their emissions, as described in Section 3.2.2.

## 3.2 Alternative Design Features

Building off the basic features provided in Section 3.1, there are multiple design avenues that are used to improve piston engine performance, including the adding of components (turbocharging and supercharging) and running a different cycle (two-stroke operation). These features can significantly augment engine performance and must be considered when evaluating the upper limits of piston engine capabilities.

### 3.2.1 Turbocharging and Supercharging

Because of the equivalence ratio limitations discussed in Section 3.1, an engine's airflow rate is crucial to its performance capabilities. Many reciprocating piston engines are naturally aspirated (NA), drawing air into the engine's cylinder directly from ambient conditions, due to this configuration's low cost and simplicity. However, high performance applications must improve their airflow rate by increasing the density of the intake charge, enabling more fuel to be combusted during each cycle. The two most common methods of accomplishing this goal are the implementation of

supercharging and turbocharging, which contain the following features.

### Compressors and Intercoolers

Superchargers and turbochargers use mechanical compressors to increase the air density at the intake port of the engine. The performance of these compressors is defined by the device's performance map, as illustrated in Figure 3-8. Here, $\pi_c$ is the pressure ratio, the ratio of the compressor's outlet pressure to the inlet pressure, $N$ is the compressor's rotational speed, $\dot{m}_{C,cor}$ represents the corrected air mass flow rate (adjusted based on temperature and pressure), and $\eta_C$ is the compressor's isentropic efficiency. The performance map indicates the range of operation for a specific compressor, showing what pressure ratios are attainable at a given (corrected) mass flow rate and compressor speed, with the corresponding efficiency [32]. Every compressor has a distinct performance map that heavily depends on the compressor's design type, size, and intended application.

In accomplishing the fundamental goal of increasing the intake air pressure (and density), the compressor inherently raises the working fluid's temperature. This is counter to the desired improvement in density that can be provided by the pressure rise and increases the knock tendencies of SI engines [14, 33]. Assuming an isentropic compression process and that the air is an ideal gas, the relationship between the air pressure and temperature is as follows,

$$\frac{T_2}{T_1} = \left(\frac{P_2}{P_1}\right)^{\frac{k-1}{k}}, \tag{3.3}$$

where $T_{1,2}$ are the inlet and outlet air temperatures in kelvin, $P_{1,2}$ are the inlet and outlet air pressures in pascals, and $k$ is the air's heat capacity ratio ($c_p/c_v$) [34]. In actual operation, the compressor will experience thermodynamic losses that result in fluid outlet temperatures exceeding those predicted by Equation 3.3 [34]. The relative magnitude of these thermodynamic losses are described by the compressor's isentropic efficiency,

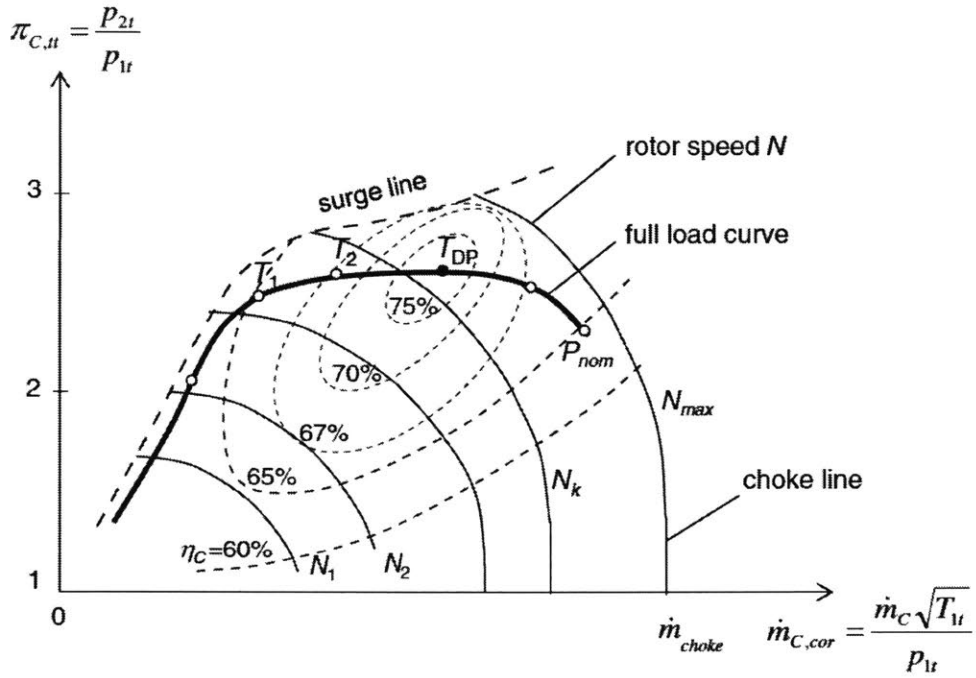


Figure 3-8: A compressor performance map illustrates the relationship between the compressor's pressure ratio ($\pi_C$), mass flow rate ($\dot{m}_C$), rotational speed ($N$), and efficiency ($\eta_C$) [32].

$$\eta_C = \frac{h_{2,s} - h_1}{h_{2,a} - h_1}, \tag{3.4}$$

where $h_1$, $h_{2,s}$, and $h_{2,a}$ are the air's inlet, (theoretical) isentropic outlet, and actual outlet specific enthalpies, respectively, in kilojoules per kilogram [32, 33]. Using the ideal gas and constant specific heat assumptions, the enthalpies of Equation 3.4 are simplified into their corresponding temperatures,

$$\eta_C = \frac{T_{2,s} - T_1}{T_{2,a} - T_1}, \tag{3.5}$$

where each $T$ is the air temperature for the states corresponding to the definitions provided for Equation 3.4 in kelvin [32, 33]. Thus, in addition to the requisite temperature rise described by the isentropic relationship in Equation 3.3, the compressor's inefficiency further increases its outlet air temperature. To reduce this temperature

rise, a heat exchanger (known as an intercooler or aftercooler) is installed after the compressor to cool the air charge and increase the density of the air introduced to the engine. These heat exchangers transfer energy from the high-temperature compressed air stream to a low-temperature stream that can be the ambient air or a liquid coolant. For transportation applications, air-to-air intercoolers are the most common designs due to their significantly lower weight compared to air-to-liquid heat exchangers [14].

### Power Source

Turbocharging and supercharging are differentiated by their power sources; turbochargers implement a turbine that extracts energy from the exhaust gases of the engine, while superchargers consume power directly from the engine's output shaft. As the latter encompasses a simple mechanical coupling, the remainder of this section will focus on the turbocharging system.

The turbocharger turbine expands the engine's high temperature and pressure exhaust gases, extracting the power required to drive the system's compressor. Similar to the compressor, Equation 3.3 provides the relationship between the exhaust gas pressure and temperature, assuming an isentropic expansion and an ideal gas [34]. Furthermore, the relationship between the turbine's isentropic efficiency and temperatures is

$$\eta_{\mathrm{T}} = \frac{T_{2,\mathrm{a}} - T_1}{T_{2,\mathrm{s}} - T_1}, \tag{3.6}$$

where $\eta_{\mathrm{T}}$ is the turbine's isentropic efficiency, $T_1$ represents the inlet temperature, $T_{2,s}$ is the isentropic outlet temperature, and $T_{2,a}$ represents the actual outlet temperature, with these temperatures in kelvin [32, 33]. Figure 3-9 provides a characteristic turbine performance map, which compares a turbine's reduced mass flow rate (corrected for temperature and pressure), combined isentropic and mechanical efficiency, and pressure ratio at varying rotational speeds [33]. This map is matched with a compressor's performance map, when considering their features (i.e. pressure ratios,

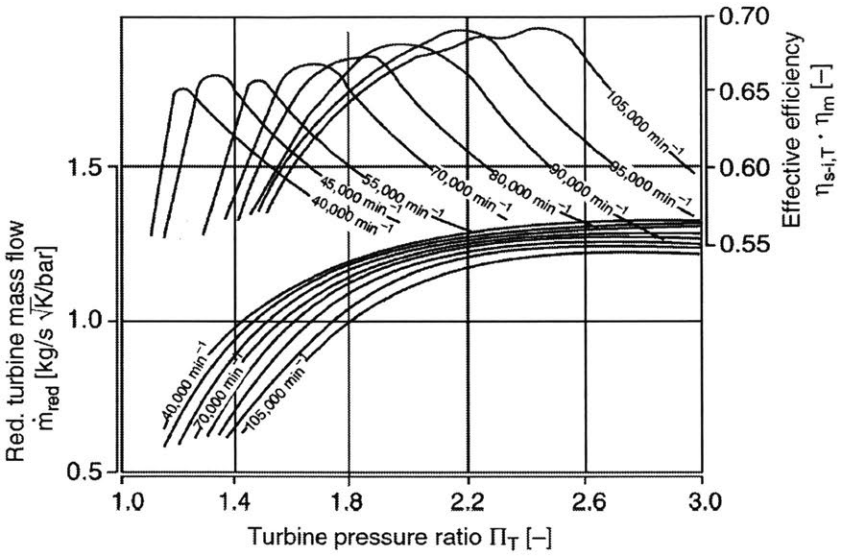


Figure 3-9: A turbine performance map shows the relationship between the turbine's mass flow rate ($\dot{m}$), pressure ratio ($\pi_T$), and efficiency ($\eta_T$) [33].

rotation speed, etc.) in specific conditions, to ensure desirable performance over the anticipated range of operation.

### Advantages and Disadvantages

An engine's application and performance requirements dictate the choice in implementing supercharging or turbocharging. Assuming equal engine performance, a turbocharger is inherently more efficient than a supercharger due to drawing the required power directly from the exhaust gases instead of the engine. However, the turbocharger's turbine creates back pressure in the exhaust path, hindering the engine's breathing and performance [33]. Furthermore, the turbocharger's dependence on the exhaust gases limits the system's response time in transient operation, as the turbocharger must speed up or slow down to produce a change in the intake manifold pressure, which requires time to overcome the system's inertia [33].

For some high-performance applications, a turbocharger and supercharger are installed in series; the supercharger provides fast adjustment in transient conditions while the turbocharger improves the system efficiency. Furthermore, multiple stages

of turbocharging or supercharging are commonly used to increase the overall pressure rise and efficiency, as an individual compressor's efficiency decreases with higher pressure ratios [33]. Finally, a select few high-performance engines implement turbo-compounding, where a power turbine (usually downstream of additional turbines or used with supercharging) is directly coupled to the engine's crankshaft, harnessing energy to increase the engine's power. This added power can provide upwards of a 5% improvement in engine efficiency [33]

### 3.2.2 Combustion Timing

The onset of combustion is often specified by the instantaneous angle of the crankshaft relative to an anchor point, such as TDC or BDC (i.e. the crankshaft's relative position before or after TDC/BDC when the event occurs, measured in degrees). In using a particular combustion timing, the engine balances trade-offs between power, efficiency, and emissions, based on the application and operating conditions [14].

Combustion initiation is controlled through the use of spark plugs and fuel injection for SI and CI engines, respectively. Early combustion (combustion advance) unnecessarily raises the cylinder pressure during the compression stroke, causing this cycle portion to consume more energy. Alternatively, late combustion (combustion delay) limits the peak cylinder pressure (and temperature), diminishing the work extracted during the power stroke [14]. The point where these forces are balanced is known as and engine's maximum brake torque (MBT) timing, where the engine's output torque is maximized. Figure 3-10 illustrates this balance for an SI engine, where the vertical axis is the normalized torque and the horizontal axis corresponds to the spark timing.

In addition to engine architecture, optimum combustion timing depends on operational factors that influence the rate of flame development and propagation, including engine speed, load (i.e. power output, dictating amount of air and/or fuel used per cycle), and intake manifold pressure and temperature [14]. Advancing or delaying combustion timing provides the engine with flexibility to maximize power output and efficiency by responding to these fluctuating operation parameters. Furthermore,

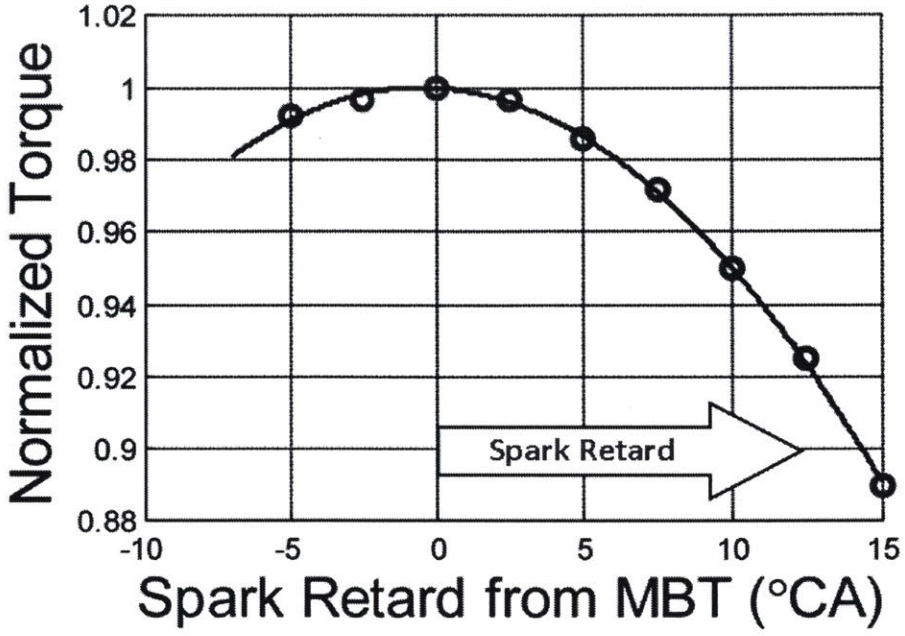


Figure 3-10: The combustion timing that maximizes an engine's torque is known as maximum break torque (MBT) timing. Advancing or delaying the timing from this point will decrease the engine's torque and thus its output power [28].

engines often advance or delay their combustion timing to achieve other purposes, such as increasing their overall power output through expanding the potential operating conditions and controlling their emissions output, as described in the following sections [14, 28].

### Improving Engine Power Output

While MBT timing ensures maximum power output for specific intake air conditions (i.e. temperature, pressure, and mass flow rate), combustion delay is an effective tool for increasing the maximum potential power output for a given engine design. In particular, SI engines heavily benefit from spark delay due to their performance being limited by knock considerations and the peak pressures that the engine's structure can handle. In delaying combustion and operating with the same airflow rate, the SI engine cylinders reach lower peak temperatures and pressures, which reduce the engine block stresses and the fuel's knock tendencies [28].

Because these limiting factors are lowered, the engine can increase its airflow rate and the amount of fuel burned per cycle without experiencing knock or structural failure of the engine. Thus, by increasing its power output without needing to strengthen the design (which adds cost and weight) or use fuels with higher knock resistance, an engine can significantly improve its specific power. However, the increase in power output comes at the cost of reduced engine efficiency, due to peak pressure occurring later than the optimal timing [29].

Figures 3-11a and 3-11b illustrate these concepts for SI engines. First, Figure 3-11a compares the engine's combustion timing and peak pressure on the vertical axes vs. increasing brake mean effective pressure (BMEP) on the horizonta axis. Here, the combustion timing is identified as the crank angle at which 50% of the cycle's fuel has burned (CA50), and BMEP is used as a performance measure that normalizes an engine's power output into a theoretical pressure.[3] As illustrated in the top two traces (the average peak pressure and the average plus 3 sigma peak pressure that accounts for the uncertainty in individual cycles), increasing BMEP causes the engine's peak pressure to rise until spark delay (manifested as the retarding of the 50% burn angle) is utilized. As seen in the bottom trace, the combustion timing is delayed after exceeding a BMEP of approximately 14 bar, which enables the engine's power to continue increasing without peak pressure rising above the maximum limit. Furthermore, Figure 3-11b plots the engine's efficiency on the vertical axis with varying spark timing on the horizontal axis. The provided data illustrates the significant penalty in efficiency that occurs when implementing spark delay, due to the pressure release timing being retarded past ideal operation [30].

As identified in Section 3.3, piston engines suffer low specific powers when compared to gas turbines. Thus, in an effort to increase the engine's power output, this analysis will utilize the benefits of spark delay to identify the upper limits of piston engine performances. However, to fully leverage this technique, an engine must be designed to produce the higher airflow (and fuel) rate that is enabled. This includes

[3]BMEP is calculated as follows: BMEP $= \frac{Pn_R}{V_d N}$, where $P$ is the engine's power output, $n_R$ is the number of crankshaft revolutions per each power output stroke, $V_d$ is the engine's displacement volume, and $N$ is the engine speed.

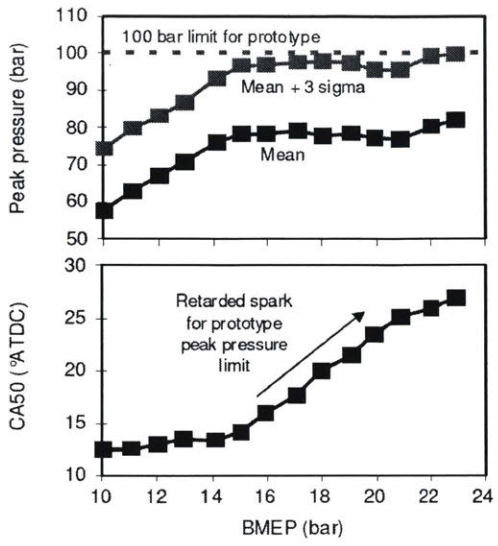


(a) Peak pressure vs BMEP, with increasing spark delay

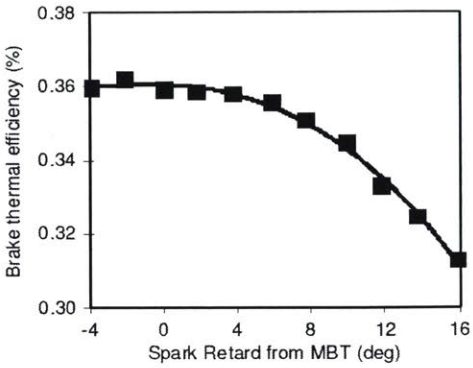


(b) Thermal efficiency vs. spark delay

Figure 3-11: Spark delay limits an engine's peak pressure, (a) allowing more power to be produced without exceeding the allowable pressure limit, (b) at the expense of reduced efficiency [30].

a boosting system (turbocharging or supercharging) that produces a higher outlet pressure, an intercooler with higher cooling capacity, and larger piping components to minimize pressure drops. These larger components will increase the system weight, partially counteracting the engine's improvement in specific power. Thus, the amount of added weight must be accounted for when determining the performance advantages provided by spark delay.

While there are clear benefits for SI engines using spark delay, this technique does not significantly improve CI engine performance or design capabilities. This is because, in addition to not having knock considerations, their power output is predominantly limited by the diffusion process and not peak pressures. Thus, this report only considered the use of spark delay for improving SI engine performance.

### Emissions

Combustion timing is strongly connected to an engine's emissions, including the production of nitrogen oxides ($NO_x$, consisting of NO and $NO_2$), unburned hydrocarbons

(HC), and particulates.[4] High combustion temperatures drastically increase $NO_x$ production, while slightly decreasing the formation of HCs (at low loads) and particulates. Thus, spark delay is commonly used to limit cylinder temperature and $NO_x$ formation, but must be moderated due to the increased production of particulates and HCs [14]. However, to justify their implementation in rotorcraft applications, piston engines must first overcome their significant disadvantage in specific power before controlling their emissions becomes a priority. Thus, this study did not focus combustion timing's effect on emissions.

### 3.2.3 Two-Stroke Operation

Alternative to the four-stroke operation mode, some engine designs utilize a two-stroke cycle; instead of completing four strokes during each cycle, the engine only requires two stokes, and thus one crankshaft rotation, to produce work. Figure 3-12 illustrates the following two-stroke processes [14]:

1. Compression stroke - the inlet and exhaust valves are closed, followed by the compression of the cylinder's charge and initiation of combustion near TDC.

2. Power (expansion) stoke - the cylinder charge is expanded, producing the engine's power until the exhaust valve(s) is opened. At this point, the majority of the high-pressure burned gas mixture is exhausted before the intake valve(s) is opened, enabling fresh gas to flow into the cylinder in preparation of the next cycle.

By producing work during each crankshaft revolution, an engine's power output per unit displacement volume (i.e. the engine's volumetric size) is substantially increased, with a theoretical limit of twice as large. However, this advantage is diminished by the complications of a two-stroke engine's breathing. Because of the limited time available for the intake and exhaust processes, high-pressure fresh charge must

[4]With regards to particulates, CI engines predominately produce soot (combustion generated carbonaceous material), with some absorbed organic compounds. SI engines produce sulfates, lead (when using leaded fuel), and organic particulates (including soot) [14].

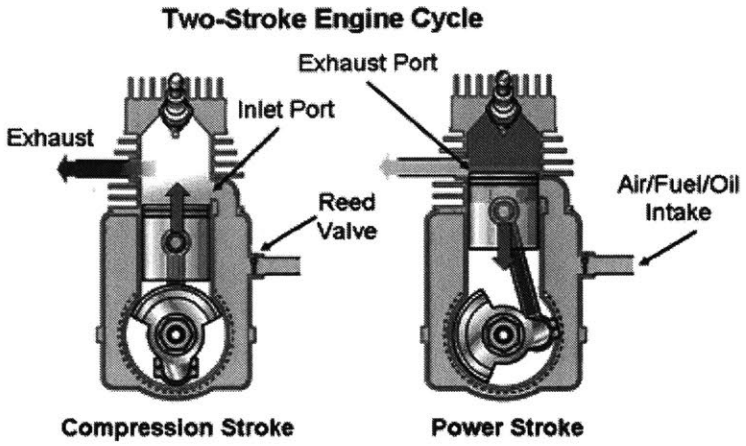


Figure 3-12: The two-stroke cycle reduces the four-stroke cycle into a compression and power stroke that are completed during a single rotation of the crankshaft [35].

be used to help displace the previous cycle's burned gas, a process known as scavenging. This process results in a significant amount of fresh charge (either air or an air/fuel mixture) passing through the cylinder and out the exhaust valve (known as short-circuiting), which reduces the fresh charge density, increases the boosting system's power consumption, and, if direct injection is not implemented, drastically increases the engine's fuel consumption [14].

The scavenging process is often assisted by implementing port valves, as illustrated in Figure 3-12. Counter to the poppet valve configuration, port valves are passive designs, with their activation dictated by the piston's position. The valves are closed by the piston as it moves towards TDC and reopened as the piston translates back to BDC, resulting in the port valve timing (i.e. when the port is opened and closed) being fixed across all operating ranges [14]. Two-stroke engines favor these valves, as they can be shaped and positioned to increase airflow rate, limit short-circuiting, improve mixing, and effectively scavenge the previous cycle's residual burned gases [14]. However, due to the piston translating across these valves in the cylinder wall, the piston's lubricated surface is constantly disrupted. Thus, a downside to port valves configurations is the need for oil to be mixed with the engine's fuel to constantly re-lubricate the cylinder walls, causing a significant increase in oil consumption [14].

Based on their valve configuration, two-stroke engines are classified into cross-scavenged, loop-scavenged, and uniflow-scavenged designs. Cross- and loop-scavenged configurations use port valves for both the intake and exhaust, while (in standard engine configurations[5]) uniflow-scavenged engines utilize intake port valves and poppet exhaust valves [14]. Each category requires careful designing of the engine's pistons and cylinders to maximize their scavenging and mixing capabilities.

For gasoline designs, two-stroke operation is usually restricted to small applications, where low cost and high specific power are important factors, including motorcycles and boat outboard engines [14]. On the other hand, two-stroke diesel engines are very common in large applications, such as locomotive, marine, and stationary power generation. In these large configurations, the engine speeds are very low, allowing scavenging to be easily accomplished. Furthermore, due to the combustion characteristics of diesel engines, only intake air is lost during short-circuiting, thus eliminating the efficiency penalty of fuel passing through the engine without combusting [14].

## 3.3 Performance Trends

Piston engines exhibit distinct trends in performance capabilities that illustrate the potential applications in which they are best suited. In particular, the piston engine's SFC and mass (thus the specific power) are the most influential parameters for rotorcraft applications and will be evaluated in the following sections.

### 3.3.1 Specific Fuel Consumption

First, each identified piston engine design's SFC was characterized to be compared with the gas turbine capabilities. While there is a wide spread in efficiencies based on specific designs, this analysis focused on identifying the upper limit of feasible performance, and thus, despite the design process for an actual engine dictating its

[5]For an alternative engine design where each cylinder contains two opposed pistons, uniflow-scavenging is achievable using both inlet and exhaust port valves [14].

efficiency, it was assumed that a particular engine design's SFC is constant across varying power output using the maximum attainable efficiencies. With this assumption, Figure 3-13 was populated using the lowest anticipated SFC values that each identified engine design can achieve, based on industry trends and aircraft engine data [14, 36, 62]. Here, the vertical axis is the engine SFC at the rated takeoff power and the horizontal axis corresponds to the power output. In addition to the piston engines, the best-performing gas turbine engines are included for reference.

The diesel four-stroke engine provides the lowest SFC of 0.2 kilograms per kilowatt-hour, while the gasoline two-stroke design has the highest SFC of 0.375 kilograms per kilowatt-hour. Between these bookend values, the diesel two-stroke and gasoline four-stroke engines have estimated SFCs of 0.225 and 0.25 kilograms per kilowatt-hour, respectively. With the exception of the gasoline two-stroke engine, these values are substantially lower than the high-end turboshaft data until the takeoff power ratings exceed approximately 1,500 kilowatts, at which point the gas turbine efficiency approaches the gasoline four-stroke engines. Thus, in direct implementation, the gasoline two-stroke configuration does not appear to have a distinct advantage over gas turbines, while the remaining piston engine designs are competitive up to high takeoff power ratings.

Furthermore, as the engines must operate over a range of power outputs, the gasoline and diesel four-stroke engines' part-load SFC were estimated using data acquired on two turbocharged example aircraft engines, chosen due to their high performance capabilities [63, 97]. Figure 3-14 provides the results, where the engine's fractional SFC, normalized to the takeoff power rating, are the vertical axes, the horizontal axis corresponds to the engine's load as a fraction of the takeoff power, and the resulting trends are included for reference.

Both engine's experience initial declines in their SFC, falling to approximately 94% and 92% for the diesel and gasoline engines, respectively. However, as the diesel data extends further into part-load operation, the SFC rebounds to a higher level, displaying a minimum SFC that exists around 60% of the rated takeoff power. For the gasoline engine, this trend is not immediately clear from the data, as the engine's

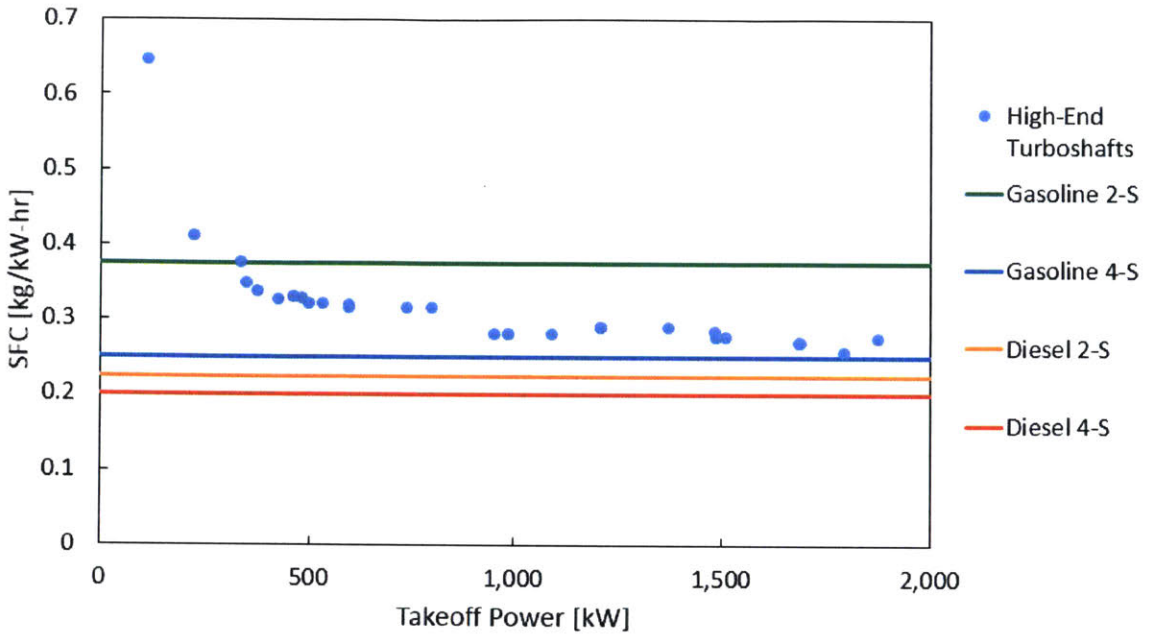


Figure 3-13: The piston engine SFC trends were plotted with the high-end gas turbine engines to illustrate the difference in their performance.

SFC was only provided at a minimum power fraction of roughly 60%. However, based on the trend fit, as well as additional gasoline aircraft engine data, a similar rebound in SFC is predicted [65]. This trend of reduced SFC at part-load is counter to the gas turbine's characteristics, where the engine's efficiency rises with falling power output (see Section 2.3). As aircraft operate at part-load through most of their flight (see Chapter 5), this provides the piston engines with a significant advantage.

Due to limited available data, these trends were assumed to also represent two-stroke engine operation. As these engines are often restricted by breathing, the lower loads (i.e. engine speed, or airflow rate) would likely provide a substantial benefit to the two-stroke configurations, and thus these trends were justified as appropriate approximations [14]. Additionally, it is important to note that the gasoline trend is based on a turbocharged engine; naturally aspirated gasoline engines suffer from poor part-load efficiencies due to the required throttling of the intake air [14]. As this analysis is investigating high-performance engines with boosting systems, the part-load efficiency trend provided in Figure 3-14 is an accurate description.

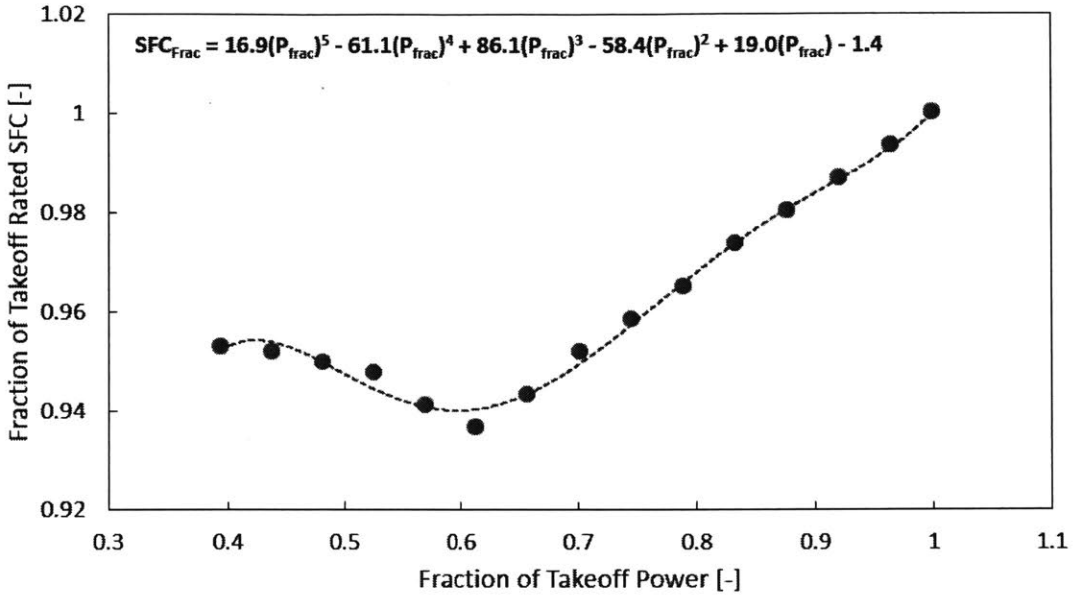


(a) Continental CD-155, Diesel [97]

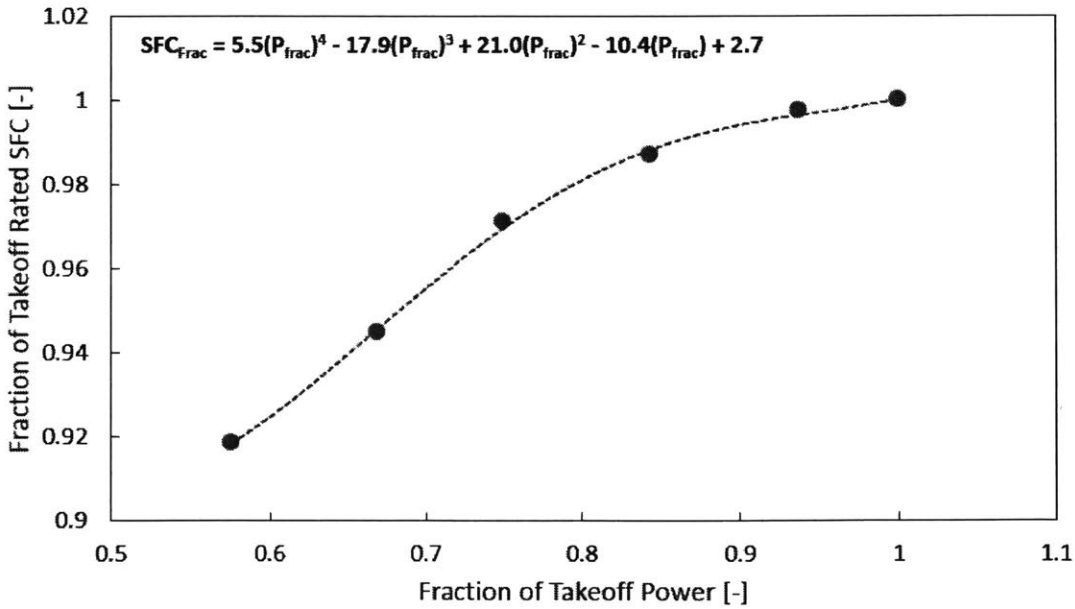


(b) Limbach L2400 DX, Gasoline [63]

Figure 3-14: Two example aircraft engines, one diesel and the other gasoline, were used to compile a part-load SFC trend.

### 3.3.2 Engine Mass

While the piston engines possess advantages in operational efficiency, their masses are the main limiting factor to their implementation in rotorcraft applications. To characterize this feature, example aircraft piston engine data was acquired through various manufacturer documentation, certifications from government agencies, and multiple commercial databases, providing trends in engine mass versus power output for the four-stroke gasoline, four-stroke diesel, and two-stroke diesel engines. Due to limited available data, trends could not be determined for two-stroke gasoline engines, and, hence, the trends for these engines were determined through modeling, which is described in Chapter 4. Figure 3-15 illustrates the resulting relationships, where the vertical axis corresponds to engine mass, the horizontal axis is the rated takeoff power, and the resulting trends are included for reference.

The data was used to determine correlations of dry mass to takeoff power[6],

$$m_{\text{gasoline four-stroke, dry}} = 0.531 * P_{\text{engine}} + 55.6, \tag{3.7}$$

$$m_{\text{diesel four-stroke, dry}} = 1.21 * P_{\text{engine}}, \tag{3.8}$$

$$m_{\text{diesel two-stroke, dry}} = 0.809 * P_{\text{engine}} + 13.0, \tag{3.9}$$

where $m_{engine}$ is the identified engine configuration's dry mass in kilograms and $P_{engine}$ represents the engine's takeoff power in kilowatts. Each engine design experiences a different trend in mass versus power output, as indicated by the differences in the correlations. Here, the slope of the line is related to the inverse of the engine's specific power; a low slope indicates the engine's mass modestly increases at higher power ratings, resulting in a high specific power, while larger slopes correspond to higher engine masses and lower specific powers. Thus, as expected and verified by these trends, the gasoline four-stroke engines have the highest piston engine specific powers (i.e. the lowest slope), followed by the diesel two-stroke and four-stroke engines, in

[6]Due to the diesel four-stroke engine data's best fit curve resulting in a negative y-intercept, the trend provided by Equation 3.8 was artificially constrained to pass through the origin to ensure that negative engine masses could not be predicted.

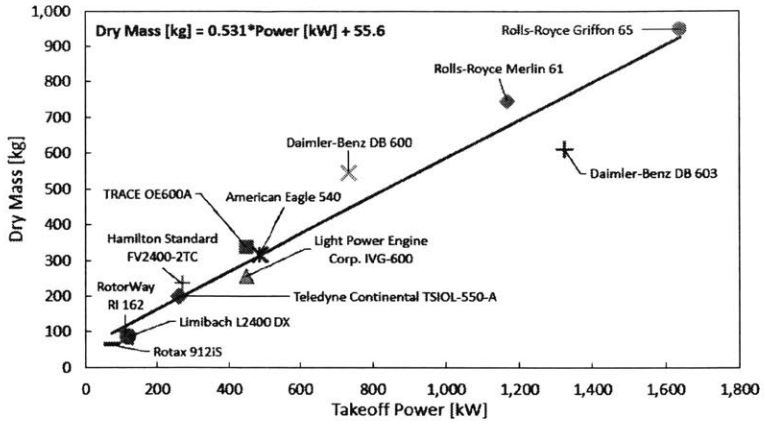


(a) Gasoline four-stroke trend

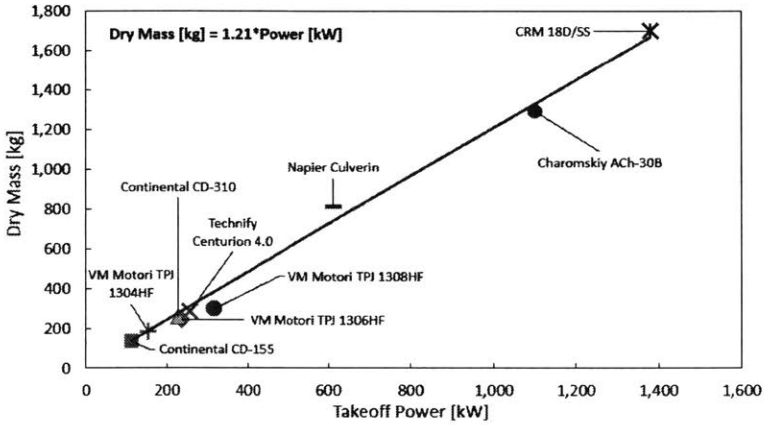


(b) Diesel four-stroke trend

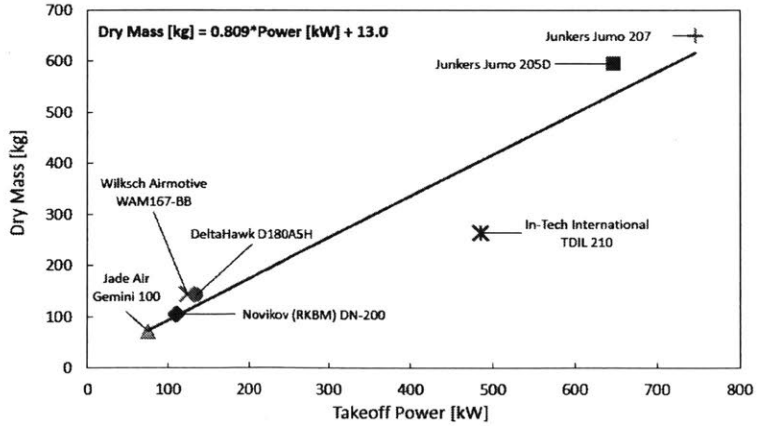


(c) Diesel two-stroke trend

Figure 3-15: The identified piston engines were graphed to illustrate the mass vs. takeoff power trends for gasoline four-stroke, diesel four-stroke, and diesel two-stroke engines [11, 13, 61, 62, 63, 64, 65, 66, 93, 94, 95, 96].

that order. However, as identified in Section 3.3.1, the trends in efficiency exhibit the opposite relationship, where the diesel four-stroke engines achieve the lowest SFC, and the gasoline four-stroke engine has the highest SFC of these designs. Based on these counteracting trends, the three engines provide separate design points with varying degrees of emphasis on efficiency and mass.

Furthermore, in addition to the dry mass, the engine coolant fluid and oil contribute to the system mass and must be accounted for when comparing these designs with gas turbines. As all of the configurations considered in this study are liquid-cooled, a database was created to evaluate the coolant volume and rated power output for a set of liquid-cooled piston engines, comprised mainly of automobile engines due to the limited availability of coolant data for aviation piston engines. Additionally, a similar trend between an engine's oil volume and rated power output was compiled using manufacturer data for the example aircraft engines that are identified in Section 4.3. These values are provided in Figure 3-16, which compares each selected engine's power output on the horizontal axes to the system's coolant fluid (3-16a) or oil volume (3-16b) on the vertical axes, with the data sets' characteristic trends included for reference.

Fits of this data were developed to estimate a piston engine configuration's fluid masses based on its power output[7],

$$m_{\text{coolant}} = 0.503({P_{\text{engine}}}^{0.552}) * 1.076, \tag{3.10}$$

$$m_{\text{oil}} = 0.0528({P_{\text{engine}}}^{0.895}) * 0.875, \tag{3.11}$$

where $m_{coolant}$ and $m_{oil}$ are the coolant and oil masses in kilograms and $P_{engine}$ is the engine's rated power output in kilowatts. Additionally, as the data provided in Figure 3-16 corresponds to the fluid volumes, the fits were modified to correlate

[7]The coolant and oil calculations were kept constant for two- and four-stroke engine models. While two-stroke engines generally require more oil and coolant, due to the increase in power cycles and port valves requiring oil to be mixed with the fuel, the engines are also assumed to be in smaller configurations, because their power density is significantly higher. As these factors counteract one another and arise from complex relationships, this analysis assumed equal coolant and oil calculations for both engine designs.

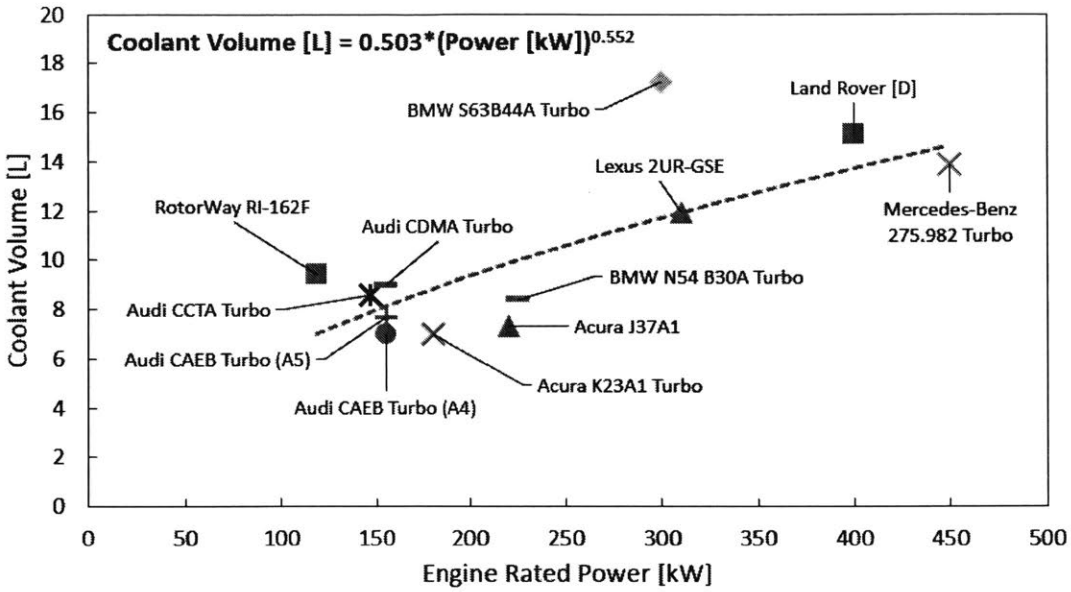


(a) Coolant volume trend [66, 104, 105, 106, 107, 108, 109, 110, 111, 112, 113, 114, 115, 116, 117, 118, 119, 120, 121, 122, 123, 124, 125]

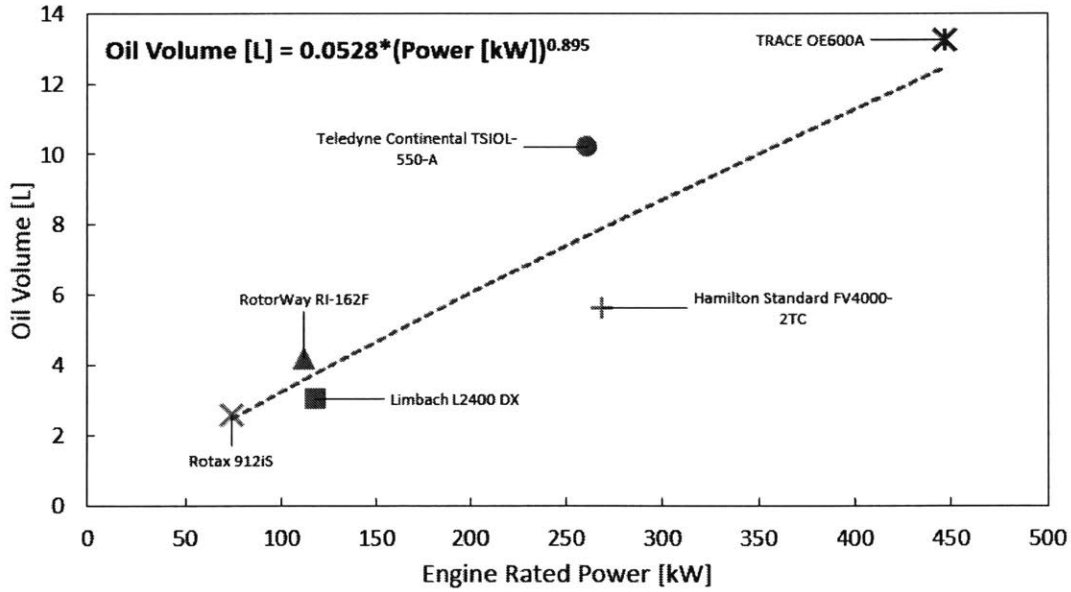


(b) Oil volume trend [60, 62, 65, 66, 67, 70]

Figure 3-16: A set of liquid-cooled automobile engines (in addition to the RotorWay RI-162F aircraft engine) and the example aviation piston engines were graphed to compare their (a) coolant and (b) oil volumes, respectively, with their rated power output. The automobile engines were included due to limited available data on aircraft engine coolant.

the fluid masses by multiplying the volume trends by the average densities of the example aircraft engines' coolant and oil. Using the fluids that are specified by the manufacturers, the coolant and oil densities were calculated to be 1.076 kilograms per liter and 0.876 kilograms per liter, respectively [60, 62, 65, 66, 67, 70]. These equations, combined with either Equation 3.7, 3.8, or 3.9 (for gasoline four-stroke, diesel four-stroke, or diesel two-stroke engines, respectively), provide an estimation for an engine configuration's wet mass given its power output,

$$m_{\text{engine, wet}} = m_{\text{engine, dry}} + m_{\text{coolant}} + m_{\text{oil}}. \tag{3.12}$$

To compare these trends with gas turbines, each piston engine's specific power was estimated using Equation 3.12, with the dry mass calculated by the equation corresponding to the particular engine type. Figure 3-17 provides this result, with the specific power on the vertical axis, the takeoff power on the horizontal axis, and the high-end gas turbine data included for context. As shown in this plot, the high power turboshaft engines have significantly higher specific powers compared to that of the piston engines. Thus, at high power classes, the large piston engine masses put these configurations at a significant disadvantage with respect to the gas turbine.

## 3.4 Performance Limitations

Similar to gas turbines, piston engine performance in limited by multiple factors, which differ between design categories. These restrictions reflect the challenges of improving a piston engine's feasibility for rotorcraft applications, due to their impacts on the performance trends provided in Section 3.3.

### Mixing Time

To facilitate combustion, proper mixing between the fuel and fresh air is required for both gasoline and diesel engines. For the former, this is not a major limiting factor, as the premixing of the gasoline and fuel prior to combustion, injection techniques

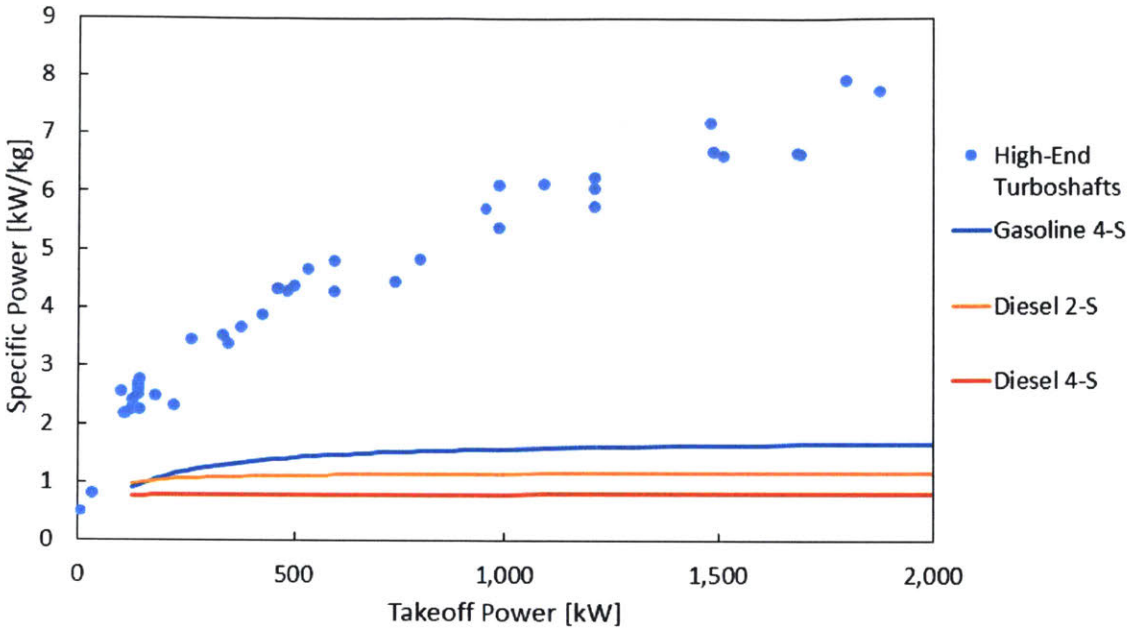


Figure 3-17: The piston engine mass trends were used to estimate their specific powers. These results were plotted with the high-end gas turbine engines to illustrate the difference in their performance.

discussed in Section 3.1.1, and advanced cylinder head, piston, and port designs ensure proper mixing for a wide range of high-performance operation (i.e. high engine speeds, high air mass flow rates) [14].

However, for diesel engines, this mixing is extremely influential on the engine's performance. As outlined in Section 3.1.2, the diesel engine's combustion process requires a diffusion flame, where the air and fuel must mix and burn in the same space. The timescale of this process is a limiting factor for diesel engine speeds (in small to medium-sized applications), which directly limits their power output and specific power. Despite being improved by common techniques that increase the charge's turbulence and mixing, this factor is a major limitation to diesel engine performance [14].

### Engine Architecture

Both diesel and gasoline engines produce power through reaching high cylinder pressures (and the corresponding temperatures), caused by the combustion of their fuel. These adverse conditions require the engines to be designed with sufficient structural integrity, which results in the their heavy masses [14]. This coupling necessitates a balance in engine design; higher cylinder pressures will improve the engine's performance at the expense of a heavier design, which counteracts the improvement in specific power gained from this added performance. The use of ignition delay, described in Section 3.2, helps limit the cylinder's peak pressure, but at the expense of poor efficiency.

Furthermore, the size of an engine's pistons and cylinders can limit the attainable operational speeds. For diesel engines, this effect is less pronounced, as the engine must operate at moderate speeds to facilitate proper mixing (as discussed in the previous section). Alternatively, large gasoline engines become restricted by their piston sizes, due to the large forces cause by heavy reciprocating components. This causes the engines to operate at slower speeds, which directly limits the configuration's specific power [14].

### Knock Tendencies

Finally, for gasoline engines, knock is a major limitation to their performance capabilities. As described in Section 3.1.1, knock is the spontaneous combustion of fuel that occurs ahead of the cylinder's induced flame front, causing detrimental pressure rises that can destroy an engine. An engine's knock tendency grows directly with its cylinder pressures and temperatures (as seen in Section 4.2), which directly limits the performance of the engine.

## 3.5 Piston Engine Niche

Based on the performance trends and limitations identified in the previous sections, piston engines are best suited in applications that minimize the impact of the engine's

weight while maximizing its efficiency advantage. As rotorcraft require high specific powers in addition to adequate efficiencies, the piston engine's heavy architecture is the major limiting parameter than must be overcome to exceed the performance of gas turbines. Thus, the range of potential airframe sizes was restricted to a maximum of 5,500 kilograms with power requirements less than 1,000 kilowatts per engine. In this spectrum, the efficiencies of piston engines are substantially higher than that of gas turbines (see Section 3.3.1), while the specific powers are anticipated to remain competitive, although much lower (see Section 3.3.2). Before evaluating these standard engine configurations, alternative designs were investigated for improving the performance of pistons engines, as described in Section 3.6.

## 3.6 Performance Improvement Investigations

Based on the performance trends and limitations described in Sections 3.3 and 3.4, this analysis sought alternative configurations to leverage the piston engine's advantage of high efficiency and reduce its disadvantage of low specific power. After literature review, two additional engine designs were identified as having the potential to significantly improve the piston engine's performance, which are outlined in the following sections.

### 3.6.1 Two/Four-Stroke Engine

The first identified alternative configuration was the two/four-stroke engine, a concept that was initially conceived to improve the performance of passenger vehicles by leveraging the high specific power of the two-stroke cycle with the efficiency advantage of four-stroke operation [37]. For rotorcraft applications, the engine would use two-stroke operation during takeoff and climb when extra power is required. Then, once the airframe reaches cruising altitude, the engine would switch to four-stroke operation, leveraging the improved efficiency to increase the airframe's range. By improving the engine's specific power while maintaining a high efficiency, the two/four-stroke configuration could substantially improve the piston engine's capabilities.

In this platform, direct injection is required to ensure adequate efficiency during two-stroke operation, as other fuel introduction methods result in fuel being lost in the short-circuiting of the flow path through the cylinder [14]. Furthermore, to enable switching between the two operation modes, the valve and spark timing must be varied rapidly over a wide range of values. While the spark is easily changed through the engine's spark plug, the valve timing is not readily variable in standard valve-train configurations. This can be overcome by using alternative designs for actuating the poppet valves, or through different valve configurations. For changing poppet valve configurations sufficiently to run both two and four-stroke operation, variable valve actuation (VVA) is required, including cam switching, variable cam phasing, electromechanical, hydraulic/electro-hydraulic, and electromagnetic designs [42, 43, 44, 45, 46, 47]. To varying degrees, these technologies have been utilized in applications and are viable options to enable the two/four-stroke engine's operation.

However, assuming that the VVA technologies are able to successfully switch the engine between two and four-stroke operation, the poppet valves present a considerable limit to the performance of this engine platform, as two-stroke engines greatly prefer port valves to enhance their operation (see Section 3.2.3). By limiting the engine design to poppet valves, the power advantage of two-stroke operation is partially mitigated due to the restriction of the engine's breathing [37, 38, 39]. Alternatively, this analysis considered the use of port intake valves with the capability of switching their timing (i.e. sleeve vales) in a similar fashion to the identified VVA technology. This technology has previously been implemented in aviation piston engines and, in addition to the previously discussed improvement to the intake airflow, allows the engine to increase the size of its exhaust valves, which further improves the engine's breathing and performance [48, 49]. This analysis evaluated both poppet and port intake valve configurations, with Section 4.4 describing the results of modeling each configuration, and the overall performance of the two/four-stroke switching engine. Based on these simulations, the capabilities of the configuration were compared with baseline engines to determine the feasibility of the alternative design.

### 3.6.2 Dual-Fuel: Ethanol-Gasoline

The second alternative engine configuration considered in this report was the ethanol-gasoline design, which uses both ethanol and gasoline as fuel sources. In this architecture, the engine leverages the ethanol to improve the engine's performance through both an increased octane number and significant charge cooling, as discussed in the following sections.

#### Octane Effect

Ethanol has a substantially higher octane rating than standard gasoline, which allows the engine to operate at higher pressures and temperatures before experiencing knock. This characteristic was evaluated in an investigation conducted by Kasseris and Heywood, where a research engine was tested using fuels with varying amounts of ethanol while measuring the onset of knock. The results were correlated with a gasoline knock prediction integral to provide an estimation for each ethanol blend's "effective" RON that can be used with traditional gasoline knock prediction methods, which was required during the modeling described in Chapter 4 [41].

Figure 3-18 plots the results of this analysis, where the effective octane number is the vertical axis and the volumetric content of ethanol in the fuel corresponds to the horizontal axis. The ethanol blends provide significantly higher RONs, reaching a maximum of approximately 115 at blends near 50% ethanol. This higher octane rating provides the engine with higher knock resistance, which enables substantial improvements to engine performance.

#### Cooling Effect

The second benefit of ethanol fuel is the increased charge cooling effect of the fluid. When introduced through direct injection, an engine's fuel vaporizes within the cylinder charge, which consumes energy and lowers the temperature of the surrounding gas. This lower temperature increases the density of the cylinder charge during each cycle (when injection occurs with the intake valve open, which is a common practice),

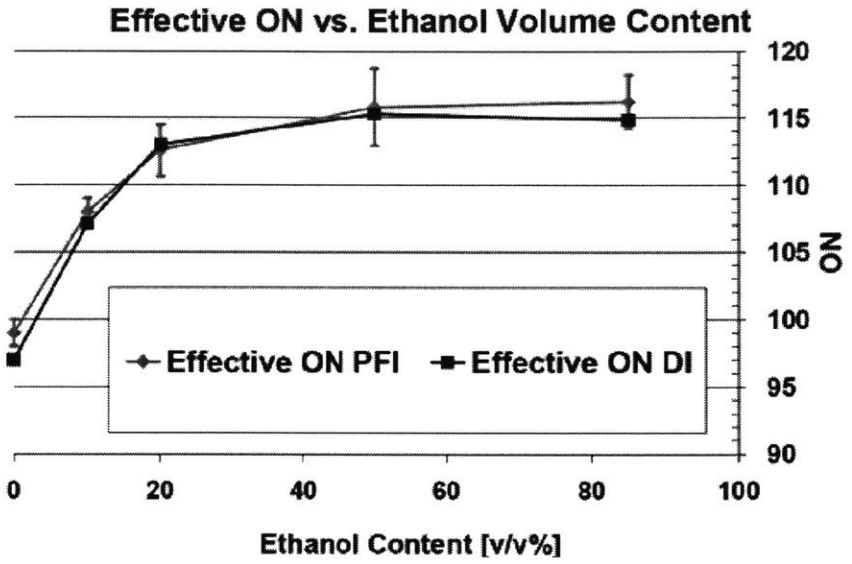


Figure 3-18: A research engine was tested with fuel using varying amount of ethanol, while measuring the onset of knock. The results were correlated with a gasoline knock prediction integral to provide an estimation of each ethanol blend's effective RON [41].

in addition to lowering the knock tendency of the charge [14, 40]. While gasoline also provides this benefit, ethanol has a significantly higher heat of vaporization, resulting in lower cylinder temperatures and more substantial advantages.

Figure 3-19 illustrates this effect, where a characteristic engine's intake conditions were used to compare the effect of injecting varying concentrations of ethanol with gasoline. Here, the vertical axis is the maximum potential change in cylinder charge temperature after all fuel has been injected, while the horizontal axis corresponds to the fuel's volumetric ethanol content. From the steep rise in temperature change that occurs with increasing ethanol content, the results verify that ethanol provides a substantial improvement in charge cooling (and thus density) over that of standard gasoline. This benefit, as well as the RON trend described in Section 3.6.2, was built into the modeling described in Chapter 4, which evaluated this configuration's capabilities. Based on these results, the ethanol-gasoline engine was compared with the standard designs to determine the feasibility of the concept's implementation in rotorcraft applications.

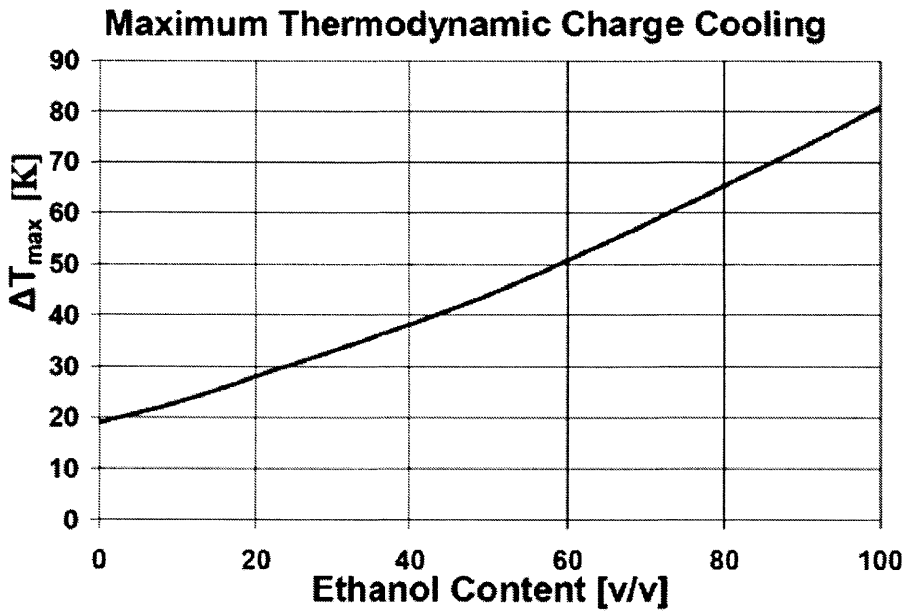


Figure 3-19: The charge cooling associated with the heat of vaporization of an engine's fuel is drastically increased when using blends of ethanol [40].

# Chapter 4

# Engine Performance Modeling

Thus far, the baseline piston engine performance characteristics and potential avenues for their improvement have been outlined in Chapter 3. However, to conduct an accurate comparison between the gas turbines and alternative configurations, the latter designs' performances must be modeled to identify their realistic capabilities in both the standard and adverse conditions that are prevalent in rotorcraft applications. To accomplish this goal, the commercial software GT-POWER was utilized for modeling the promising engine configurations. The following sections will outline the software's essential design parameters and will discuss the setup and results of modeling a set of modern aviation engines, a baseline engine configuration, and the alternative design avenues.

## 4.1 Simulation Design Parameters

GT-POWER is an industry standard engine simulation software that enables sophisticated modeling of engine performance capabilities, including power output, airflow rate, and fuel consumption [50]. The program was used to model the various engine configurations that this analysis identified as promising, resulting in a more accurate understanding of their capabilities and feasibility in rotorcraft applications. Figure 4-1 illustrates a representative simulation architecture, where ambient air enters the system on the left side of the model, passes through a single-stage supercharger and

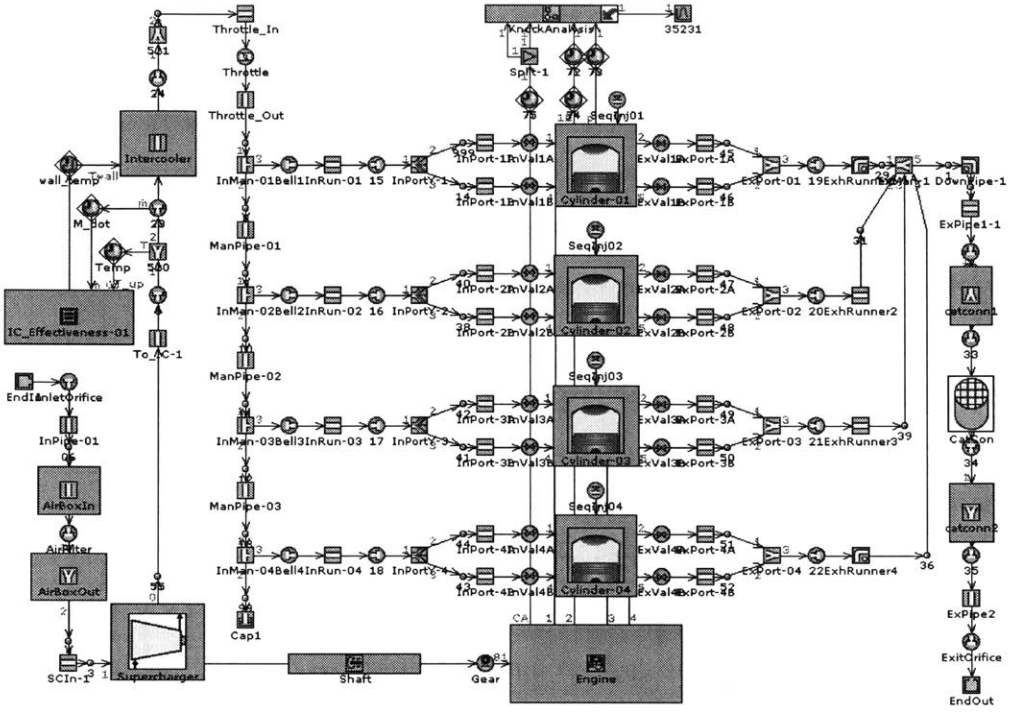


Figure 4-1: This representative GT-POWER model is a four-stroke supercharged gasoline engine using poppet valves and direct injection.

intercooler, flows through the four cylinders, and exits the model on the bottom right.

Each model was constructed by altering the example engine configurations that are provided in the GT-POWER software package, which are predominately four-cylinder engines and include features such as two- and four-stroke operation, SI and CI cycles, and naturally aspirated, turbocharged, and supercharged intake systems. As the designs were based on automotive applications, the engine sizes are significantly smaller than most rotorcraft piston engines (see Section 3.3). However, many component parameters were directly implemented in subsequent models, while the remainder were sized to accommodate the changes in engine architecture. The following sections discuss these important engine components, including their parameters and effects on engine performance.

### Ambient Conditions

As mentioned in Section 1.3, rotorcraft must be capable of operating in low pressure and high temperature environments, which hinders the performance of their engines. To attain an approximation of this effect on piston engines, each configuration was modeled as operating in both standard sea level (1 bar, 298 K) and hot and high conditions (0.875 bar, 315.2 K). The difference in performance between the two operating conditions provided an estimate of the configuration's hot and high derating.

### Engine Piping and Manifolds

An engine's ducting, consisting of the piping that connects each component and the intake and exhaust manifolds, facilitates the flow of intake and exhaust gases throughout the system. In GT-POWER, each section of ducting is specified by its geometry (length, diameters, and/or volume), thermal attributes, and pressure drop characteristics. For all engine models, the thermal traits were based on the example configuration's parameters, which include a basic heat transfer correlation, initial wall temperature, and transient wall temperature solver. Furthermore, the pressure drop characteristics were maintained as being calculated based on the ducting and surrounding component diameters and lengths. Thus, the geometry was the only direct change to the example engine ducting parameters.

In altering the geometry, the modeling scaled the piping and manifold sizes according to the engine's operation; if higher airflow rates were required, the component diameters would be increased to mitigate their pressure drops and improve the engine's breathing. Additionally, the piping length can be adjusted to minimize these pressure drops, but this flexibility is limited by feasible geometric constraints within the engine architecture (i.e. connections between components cannot be reduced to negligible lengths). Lastly, the manifold volumes were increased if higher airflow rates required more stable conditions for the intake air entering the cylinders (intake manifold) or the exhaust air upstream from the turbocharger turbine (exhaust manifold).

### Boosting Systems

The majority of the engine models contained either a supercharger or turbocharger configuration to boost their intake air pressure (and density). Each of these boosted configurations implemented a compressor that utilized the baseline performance maps provided in GT-POWER, which related the compressor's speed, mass flow rate (corrected for temperature and pressure), pressure ratio, efficiency, and power consumption. For superchargers, the gearing ratio that couples the engine's crankshaft to the compressor's input shaft controls the relationship between the rotational speeds of these components. Based on the compressor's performance map and the engine speed, this gearing ratio heavily influences the performance of the compressor and thus the entire system. In models that implemented supercharging, this ratio was varied to achieve desirable engine conditions, with an imposed maximum allowable compressor pressure ratio of 2.5. This was chosen as a conservative limit to ensure reliable performance and is consistent with various industry models [51, 52, 53, 54].

As the modeling pushed the compressors into regions that fell outside of their baseline maps, device "multipliers' were used to increase the map ranges by a multiplication factor. In particular, the mass flow rate and efficiency parameters were adjusted to accurately model compressors that are designed for higher flow rate applications. While the mass flow rate was not capped at a maximum value, the efficiency was aimed to be approximately 70%, which is a reasonable upper-value for these compressors. As it was anticipated that altering these multipliers may affect GT-POWER's compressor power consumption prediction, an external analysis was conducted on the supercharger to calculate this power, which is described in Appendix C, and was accounted for in the results of each simulation. Furthermore, both boosting systems utilize a predictive intercooler based on the example GT-POWER engine designs, which adjusts the intake air's outlet temperature based on the mass flow rate and the component's heat transfer effectiveness data. These intercoolers were placed after each compression stage for every engine model.

Finally, for the turbocharging systems, the exhaust turbine performance map

was also inherited from a baseline GT-POWER engine, relating its speed, mass flow rate, pressure ratio, and efficiency. The turbine's operation, given constant exhaust conditions, was controlled via a waste gate, which is a feature that allows the exhaust flow to bypass the turbine to reduce its power output and rotational speed. Given that the turbine is directly coupled to the compressor, the adjustable waste gate enables control over the compressor's speed and operation (i.e. amount of boost), which dictates the engine's performance.

### Intake and Exhaust Valves

The engine's initial intake and exhaust valve characteristics were based on the GT-POWER example engines, including their diameters, lift profiles (i.e. how far the valve head is displaced into the cylinder), discharge coefficients (the actual mass flow rate divided by the ideal rate), and timing. For large cylinder volumes, the lift profiles were slightly increased (i.e. less than 20%) to enable the higher flow rates that were required. Additionally, the valve diameters were scaled according to the changes in the cylinder geometry; the poppet valve areas were increased proportionally with the larger bore sizes, while the port valve areas were scaled proportionally with the increase in cylinder surface area (influenced by both the bore and stroke). Furthermore, by removing the intake poppet valves, the port intake valve configurations enabled significantly larger exhaust valves due to the increase in available space, with the maximum diameters restricted by the geometric constraints of the cylinder bore.

For the poppet valves, the discharge coefficient data maps were used to relate this coefficient to the ratio of the valve's lift divided by its diameter. In simulations where the engine geometry exceeded the range provided in the example engine models, the map was extended to accommodate the larger ratio by maintaining the baseline trend in the line slope (see Figure 4-2). Finally, each engine model's valve timing was varied throughout the operation ranges to facilitate proper airflow and achieve the desired performance.

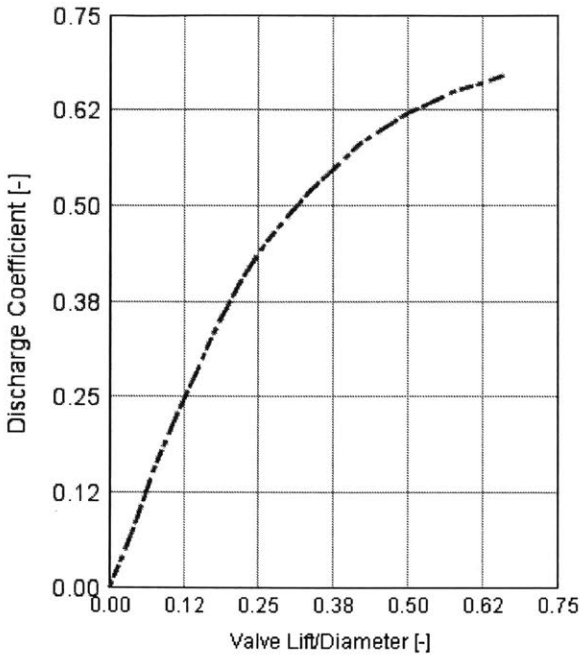


Figure 4-2: The GT-POWER discharge coefficient data was extended to reach operating conditions that exceeded the original range by maintaining the data trend of decreasing slope with increasing values.

### Fuel Type and Injection

All engine simulations used direct injection of their fuel, with the injection timing and rate held relatively constant based on the example engine parameters. The amount of fuel injected per cycle was specified by the engine's air-fuel ratio, which was adjusted to accommodate the engine's performance requirements (i.e. to increase power or reduce knock tendencies). For the ethanol modeling, the analysis used E85, which is defined as containing 85% ethanol by volume. This mixture was chosen due to wide availability, extensive literature data, and the diminishing performance advantage gained with increasing ethanol volume at this level of concentration (see Section 3.6.2) [28, 40, 41].

Unless otherwise noted, the gasoline engine models used Avgas 100 (known as aviation gasoline) for their fuel, which has combustion characteristics similar to standard gasoline and a minimum motor octane number (MON) of approximately 100

[24]. Despite this minimum MON being a specified parameter, Avgas does not have a rated research octane number (RON), due to the aviation fuel testing procedures differing from the standard automobile techniques [55]. However, as discussed in Section 4.2, the GT-POWER simulations require the fuel's RON to accurately predict the engine's knock characteristics. To estimate this value, a set of high-performance gasoline octane numbers was used to correlate Avgas's MON and RON, with this analysis provided in Appendix B. Based on this result, the simulations were conducted using an Avgas RON of 110.

### Cylinders and Combustion

As part of GT-POWER, models for heat transfer, friction, and the scavenging processes are provided. In this work, these models (based on geometry and operating conditions) were used to calculate the impact of these processes on the engine performance.

The burn duration for each engine's operating point was first estimated using correlations that were developed by extrapolating the burn rates measured in an experimental setup operating with both gasoline and E85. These trends were fitted as a function of the engine speed and manifold pressure[1],

$$CA_{10\text{-}90,\ \text{gasoline}} = 24.84 + 0.002767 * EngineSpeed - 8.058 * MAP, \tag{4.1}$$

$$CA_{10\text{-}90,\ \text{E85}} = 22.75 + 0.0033155 * EngineSpeed - 7.057 * MAP, \tag{4.2}$$

where $CA_{10\text{-}90}$ represents the number of crank angle degrees that pass between 10% and 90% of the fuel burning, engine speed is specified in rpm, and MAP (the engine manifold absolute pressure) is measured in bar [28]. Once these values were calculated, final burn durations were scaled using the engine configuration's bore dimension,

[1]This method for approximating the burn duration is not complete, as other factors will influence the time of combustion, such as the cylinder temperature, pressure, and the air/fuel ratio. Additionally, the modeling conducted in this report exceeded the verified range that was tested in referenced paper, creating uncertainty in the prediction validity [28]. However, this approach provides a reasonable estimation for the purposes of this analysis.

$$CA_{10\text{-}90,\,f} = CA_{10\text{-}90,\,i} * \left(\frac{B}{86}\right), \tag{4.3}$$

where $B$ is the cylinder bore in millimeters, and 86 is the bore size (in millimeters) for the engine that was used to derive this correlation [28]. The adjustment accounts for the difference in the flame propagation distance (and thus the overall burn duration), due to the differences in the engine bores (i.e. cylinder diameters).

Furthermore, the spark timing was varied in each simulation based on the operating conditions and the model's purpose; for current engines configurations, the spark timing was based on available manufacture data, while, for the alternative engine designs, the timing was varied to maximize engine performance. In all models, it was assumed that approximately 100% of the injected fuel was combusted to provide an upper limit on the engines' performance. Finally, cylinder characteristics such as engine speed, cycle mode (two- vs four-stroke), and geometry (i.e. bore, stroke, compression ratio) were specified based on the model's purpose, such as simulating an existing engine's operation or estimating the performance of a new design. The essential outputs of each model (i.e. peak pressure, power output, etc) are described in the following section.

## 4.2 Modeling Outputs

After conducting simulations on an engine platform, GT-POWER produces a wide range of performance data that describes the engine's operation characteristics, as well as the interaction of individual components with the intake and exhaust gases. Specifically, as the basic goal of the GT-POWER modeling was to provide upper limits on the capabilities of the various engine configurations, the predicted engine power was the most essential output for these simulations. While an engine's efficiency is crucial to its performance in rotorcraft applications, the factors that influence this parameter (i.e. in-cylinder mixing, crevices, and incomplete combustion) were not the target of this investigation, and thus GT-POWER was not used for predicting efficiency.

In addition to the performance (power output) capabilities, an engine's cylinder conditions are instrumental in evaluating the feasibility of the engine design. Specifically, as discussed in Section 3.4, gasoline engines are limited by their peak pressures and fuel knock tendencies, with the former dictating the engine structure's mass and the latter predicting if the engine can operate safely. While the cylinder's peak pressure is readily available in GT-POWER, knock tendency was measured through a customized technique to ensure sufficient prediction capabilities. This method, known as the Livengood-Wu integral, is based on an empirically derived induction time correlation that is integrated over a portion of the engine cycle to determine if knocking will occur,

$$\int_{t=0}^{t_f} \frac{dt}{\tau}, \tag{4.4}$$

where $\tau$ is the induction time, $t = 0$ is the time when the intake valve closes, and $t_f$ is time at which one of two ending conditions are reached [14, 56]. First, the integral can reach unity during the cycle, at which point Equation 4.4 predicts the engine will experience knock. Second, the integral is terminated if less than 10% of the total fuel mass remains unburned, as this amount of fuel is assumed to be too dispersed for significant knock to occur [57]. The most widely recognized correlation for the induction time was implemented with Equation 4.4,

$$\tau = 17.68 \left(\frac{ON}{100}\right)^{3.402} p^{-1.7} exp\left(\frac{3800}{T}\right), \tag{4.5}$$

where $ON$ is the fuel's road octane number (RON), and $p$ and $T$ are the instantaneous cylinder pressure and temperature in atmospheres and kelvin, respectively [14, 58]. These equations were built into GT-POWER to ensure adequate prediction of each engine configuration's knock. While Equation 4.4 predicts knock when reaching unity, the models' maximum allowable integral values were limited to lower values to ensure stable operation, with this imposed restriction defined in the following sections.

## 4.3 Example Aircraft Engines

Prior to simulating the alternative design configurations proposed in Section 3.6, further understanding of piston engine performance was gathered by modeling six aviation engines using manufacturer and certification data, as seen in Table 4.1 with additional parameters provided in Appendix A.1. Specifically, a baseline knock integral value was desired to ensure that the two/four-stroke and ethanol-gasoline engines were simulated with a realistic buffer before knocking would occur. By using the method provided in Section 4.2, the final knock integral values were modeled for each example engine, with the results displayed in Table 4.1.

These engines provided a wide spread of knock integral values, ranging from 0.60 for the Continental TSIOL-550-A up to 0.96 for the TRACE OE600A. From reviewing the simulation data, the Continental knock integral result was deemed to be an outlier, due to the value being significantly lower than the next closest ending knock integral. Thus, after discarding this data point, the example engine modeling resulted in a median knock integral of 0.92, which was used as the target integral value for all of the subsequent testing. This value provides an engine with sufficient knocking cushion from adverse conditions and operational variance, while not being so low as to hinder the potential performance of the simulated engine models.

Table 4.1: The example aircraft engine data and modeling results [11, 60, 61, 62, 63, 64, 65, 66, 67, 68, 69, 70]

| **Engine Parameters** | **Hamilton Standard FV4000-2TC** | **Limbach L2400 DX** | **Rotax 912iS** | **RotorWay RI-162F** | **Teledyne Continental TSIOL-550-A** | **TRACE OE600A** |
|---|---|---|---|---|---|---|
| Rated power (kW) | 268.5 | 118.0 | 73.5 | 111.9 | 261 | 447 |
| Wet mass (kg) | 253.7[a] | 92.3 | 68.3 | 99.1 | 220.7[a] | 365.3[a] |
| Specific Power (kW/kg) | 1.06 | 1.28 | 1.08 | 1.13 | 1.18 | 1.22 |
| SFC[b] (kg/kW/hr) | 0.305 | 0.255 | 0.278 | 0.256 | 0.304 | 0.268 |
| Knock integral | 0.82 | 0.94 | 0.92 | 0.73 | 0.60 | 0.96 |

[a] These engines' coolant masses were estimated using trend data compiled from the other example aviation piston engines, as seen in Section 3.3.2.

[b] The SFC is measured when operating at the rated power output.

## 4.4 Two/Four-Stroke Engine Simulation

### 4.4.1 Modeling Parameters

As described in Section 3.6.1, the two/four-stroke switching engine harnesses the specific power advantage of two-stroke operation while leveraging the efficiency of a four-stroke engine. To determine this engine configuration's capabilities, the technology was modeled by separately implementing the two operation modes in a core engine platform, which is outlined in Table 4.2. As discussed in Section 3.4, designing an engine's cylinder geometry is a complex task that must consider multiple factors aside from the performance requirements. Since this exercise falls out of the scope of this analysis, the two/four-stroke platform's bore, stroke, maximum engine speed, and compression ratio were chosen to emulate the standard aviation piston engine designs described in Section 4.3.

Table 4.2: The two/four-stroke engine architecture.

| | |
|---|---|
| Bore | 100 mm |
| Stroke | 86.07 mm |
| Number of cylinders[a] | 4 |
| Compression ratio | 8.5:1 |
| Maximum engine speed | 4,400 rpm |
| Boosting system | Supercharged |
| Fuel grade | Avgas 100 |
| Valve configuration | Port intake, poppet exhaust valves |

Initially, the two/four-stroke platform incorporated turbocharging to leverage the inherent efficiency benefit. However, when operating in two-stroke mode, the turbocharger's turbine created substantial back pressure in the exhaust path, which severely limited the engine's breathing and performance. Thus, to improve the two-stroke operation, the modeling switched to supercharging. With regards to the valve configuration, the modeling first utilized poppet intake and exhaust valves, due to their widespread adoption and simplistic implementation. However, through iterations of design, it was determined that this configuration would not fully leverage the engine's capabilities. Despite previous investigations using poppet intake valves, this modeled engine size is significantly larger than a standard automotive engine's architecture, thus resulting in the configuration's performance being restricted by breathing [37, 38, 39]. Due to this restriction, the final configuration implemented port intake valves with poppet exhaust valves.

In addition to calculating the potential power output of these models, the anal-

ysis required an approximation of the engine's mass to optimize the two/four-stroke engine's specific power, given that this parameter is the design's crucial advantage over standard piston engines. To accomplish this goal, the engine takeoff power vs. mass trend provided in Section 3.3 was used to estimate the platform's mass. However, this trend was populated using conventional piston engine data, and thus the performance of this two/four-stroke switching engine would not provide an accurate result. Therefore, the core engine platform outlined in Table 4.2 was modified to accommodate conventional operation by using poppet intake valves.

With this new configuration, a third simulation was conducted to determine the performance of the conventional design. First, the simulated power output provided an estimation of the engine platform mass by using Equations 3.7, 3.10, and 3.11. Then, due to two-stroke operation creating a higher demand on the boosting system from the greater air mass flow rate, the change in mass between the standard and two-stroke configurations' boosting systems was estimated and added to the initial platform mass, as outlined in Appendix C. The final two/four-stroke engine mass prediction, along with the configuration's power output, enabled the two-stroke GT-POWER model to be tuned for maximum specific power, providing the optimum performance capability for rotorcraft applications.

Finally, for all three simulations, the compressor characteristics (i.e. the gear ratios and the mass flow rate and efficiency multipliers) were initially sized to maximize engine performance at standard ambient conditions. Afterwards, these parameters were used as fixed values for modeling engine performance in hot and high conditions, while the remaining unfixed variables (i.e. spark and valve timing) were used to optimize the engine's power output. The difference in power provided an initial estimate for the hot and high effect on piston engines, which is an essential consideration for rotorcraft applications.

### 4.4.2 Simulation Restrictions

Using the common platform provided in Table 4.2, the two and four-stroke models were optimized to maximize their specific power and net power output, respectively,

while being limited by the maximum allowable ending knock value and peak cylinder pressure. As discussed in Section 4.3, 0.92 was chosen to be the maximum ending knock integral value, as this provides a cushion before detrimental knock would occur in adverse operating conditions and is consistent with the aviation piston engine modeling results.

Furthermore, the maximum allowable cylinder pressure was selected by considering the balancing of improving an engine's performance through attaining higher pressures with the associated increase in the engine's mass. Based on literature review, the peak pressure was capped at 120 bar. This is an attainable value for high performance gasoline engines, provides high performance capabilities to illustrate an upper limit on the engine's performance, and is not sufficiently high to cause the engine structure to approaches diesel engine designs, which would result in significantly heavier architectures [30, 78, 79]

### 4.4.3 Modeling Results

The variable parameters identified in Section 4.1 were used to tune and optimize each engine configuration, resulting in the engine performance and operational parameters provided in Table 4.3 and Appendix A, respectively. The two-stroke configuration drastically outperformed both four-stroke models, achieving a power output (and power density) that was 33% and 42% higher than that of the four-stroke port and standard configurations, respectively. This improvement in power output was obtained at the expense of added mass, with the configuration resulting in an estimated engine mass of 219 kilograms, compared to 202 kilograms for the standard four-stroke model. Accounting for this difference, the two-stroke platform still achieved a significant performance advantage, with a 36% increase in specific power over the traditional four-stroke platform.

Table 4.3: The two/four-stroke engine modeling results

| **Engine Performance Parameter** | **Two-Stroke, Port Valve Model** | **Four-Stroke, Port Valve Model** | **Four-Stroke, Standard Model** |
|---|---|---|---|
| Net power output[a] (kW) | 344 | 259 | 243 |
| Estimated wet mass[b] (kg) | 210 | 210[c] | 203 |
| Specific power (kW/kg) | 1.64 | 1.23[c] | 1.20 |
| Power density (kW/L) | 127 | 96 | 90 |
| Hot and high power loss[d] | -19% | -16% | -12% |

[a] This power output accounts for the supercharger's power consumption.

[b] The engine masses were estimated using the power vs mass trends located in Section 3.3.2 and adjusted based on supercharging and intercooler mass considerations, as seen in Appendix C.

[c] The four-stroke port valve modeling estimated the change in power when switching between the two- and four-stroke operation modes. Thus, their engine masses were assumed to be equal.

[d] The hot and high power loss is the configuration's percent decrease in maximum available power when the engine is operating in ambient air conditions of 315.2 K and 0.875 bar.

However, the performance of the two-stroke port valve and four-stroke poppet valve models are not directly comparable, as the standard configuration is sized for a smaller power application. To distill a direct comparison between the two configurations when designed for the same application, the engine mass vs. power rating trend provided in Section 3.3 was used to estimate the mass of a standard engine configuration sized to produce 344 kilowatts (the power produced by the two-stroke model), resulting in an engine mass of 260 kilograms and a specific power of 1.32 kilowatts per kilogram. Thus, in this direct comparison, the two/four-stroke configuration provides a 24% increase in specific power, less than the previously referenced 31% improvement, due to the standard configuration's specific power increasing with higher power ratings. Through these results, it is evident that implementing the two-stroke port valve configuration enables significant increases in performance, both over

the four-stroke port valve operation mode and the conventional platform.

In addition to the significant performance improvements, consideration must be given to the configuration's effect on engine efficiency and hot and high power loss. As mentioned in Section 3.6.1, the major advantage of the two/four-stroke engine is the ability to provide a rotorcraft with the power required for takeoff (and climb) by operating in the two-stroke mode, and attain a high efficiency through the four-stroke mode during the remainder of the flight to maximize range, all while operating in a light engine architecture. These two features improve the airframe's range in different manners; a high specific power enables the rotorcraft to carry more fuel due to the lighter engine (which can still provide sufficient power), while high efficiencies increase how far the helicopter can travel given a set amount of fuel. Despite the importance of its efficiency, as stated in Section 4.2, the GT-POWER simulations were not suitable for estimating the engine platform efficiency, and this report was unable to conduct the optimization of specific power vs efficiency. Additionally, since no efficiency modeling was completed, this analysis assumed that the two/four-stroke engine's SFC in the two- and four-stroke modes were equal to the values provided in Section 3.3 (0.25 and 0.375 kilograms per kilowatt-hour, respectively), as well as the engine's part-load efficiency obeying the trends outlined in this same discussion.

Furthermore, as seen in Table 4.3, hot and high operation is detrimental for all three configurations, resulting in an 19%, 16%, and 12% decrease in power output for the two-stroke, four-stroke port valve, and four-stroke standard engine models, respectively. This significant impact is partially caused by each engine using the maximum amount of available boost in standard conditions, resulting in the boosting system being unable to compensate for the adverse ambient temperature and pressure reducing the air mass flow rate. In particular, the two-stroke model was substantially derated in hot and high conditions due to the configuration's optimum performance in standard temperatures and pressures occurring with minimum spark delay, as the engine's knock tendency and peak pressures were sufficiently low. Thus, when operating in adverse ambient temperature and pressure, the engine cannot utilize its spark timing to counteract the reduction in airflow. This hot and high derating significantly

impacts the engine's sizing for rotorcraft applications, due to the helicopter's powerplant being required to provide sufficient performance for a full flight profile when operating in adverse ambient conditions, as discussed in Section 1.3.

However, if additional boost was available (i.e. dual-staged supercharging), this performance degradation would be partially mitigated by the increase in airflow rate. To analyze this scenario, the two-stroke model was simulated with a compressor ratio that exceeded the limit of 2.5 during both standard and hot and high conditions, with the former scenario aiming to optimize its specific power and the latter attempting to achieve maximum power output. Due to the uncertainty in both the sizing of the superchargers and the stability of delayed combustion in two-stroke configurations, the models were restricted to operating at maximum break torque (MBT) timing, which minimized the engine's dependence on increasing the boosting to achieve greater performance. Table 4.4 lists the resulting performance characteristics, with the operational parameters and mass estimations provided in Appendices A and C, respectively.

Table 4.4: The revisited two-stroke engine modeling results

| | |
|---|---|
| Net power output[a] | 395 kW |
| Estimated wet mass[b] | 247 kg |
| Specific power | 1.60 kW/kg |
| Power density | 146 kW/L |
| Hot and high power loss[c] | -13% |

[a] This power output accounts for the supercharging power consumption.

[b] The engine mass was estimated using the baseline four-stroke configuration mass listed in Table 4.3 and adjusted based on supercharging and intercooler mass considerations, as seen in Appendix C.

[c] The hot and high power loss is the decrease in maximum available power when the engine is operating in ambient air conditions of 315.2 K and 0.875 bar.

The redesigned configurations provide significantly more power at the expense of heavier components, resulting in a new wet mass of 247 kilograms and a specific power of 1.60 in standard operation. However, hot and high derating still occurs, albeit to a lesser extent, with a 13% reduction in power. These results were used to develop a correlation by modifying the gasoline four-stroke engine's dry mass prediction equation (see Section 3.3),

$$m_{\text{engine, dry}} = 0.531 * \left( \frac{P_{\text{engine, max}}}{C_{\text{power}}} \right) + 55.6, \tag{4.6}$$

where $m_{engine,\ dry}$ is the engine's dry mass in kilograms, $P_{engine}$ is the power output capability of the two-stroke operation mode in kilowatts, and $C_{power}$ is a power correction factor, which approximates the engine's fractional increase in power output when switching from the four-stroke mode to two-stroke operation. By selecting an appropriate constant for $C_{power}$, the equation provides an estimation of the two/four-stroke model's dry mass, which, when combined with Equations 3.10 and 3.11 (i.e. the coolant and oil mass trends), predicts the engine's configurations wet mass and specific power. Using the revisited power output and wet mass as data points, $C_{power}$ was calculated to be 1.26. However, as the GT-POWER modeling was not optimized to strike a balance between standard and hot and high optimization, a compromise in the engine's specific power and hot and high derating was conducted to further balance these effects. Additionally, as the intercooler was not adjusted across models, it is anticipated that this component could be designed to better handle the adverse ambient temperature and pressure, further reducing the hot and high penalty. Thus, the analysis modified the $C_{power}$ constant from 1.26 to 1.25, while also decreasing the hot and high power derating from 13% to 10%,

$$m_{\text{two/four-stroke engine, dry}} = 0.531 * \left( \frac{P_{\text{engine, max}}}{1.25} \right) + 55.6. \tag{4.7}$$

Furthermore, as the modeling's boosting system was also not optimized for adverse ambient conditions, the standard gasoline engines were assumed to experience the same 10% hot and high derating, with this value falling in a similar range as two

example aircraft engines (the Rotax 912iS and the ULPower UL520) [65, 71]. Finally, due to the project's time constraints, gasoline engine configurations were exclusively modeled in GT-POWER, resulting in hot and high estimates for these engine designs only. As no other data was available, the diesel engine hot and high power loss was also assumed to be 10%. This is a reasonable estimation as both gasoline and diesel engines require sufficient airflow to maximize their performance, and thus the lower density hot and high conditions will decrease a diesel engine's power output in a similar manner. These ratings will be influential in the airframe engine sizing process, as described in Chapter 5.

## 4.5 Dual-Fuel: Ethanol-Gasoline

From the analysis conducted in Section 3.6.2, operating with a combination of ethanol and gasoline fuels can provide substantial improvements to an engine's performance, due to ethanol's higher charge cooling capabilities and octane number [40, 41]. To identify the potential for implementing this configuration in rotorcraft applications, the Limbach L2400 DX example aircraft engine model was modified to compare the configuration's performance when operating with gasoline and E85, with this engine being chosen due to its high efficiency and specific power (see Table 4.1). The basic engine architecture was held constant, aside from varying the fuel and introducing dual-staged turbocharging when necessary. This additional boosting capability was simplified by altering the turbocharger's intake air conditions to simulate an upstream compressor. The pressures and temperatures were specified based on modeling the process of an isentropic compression with an enthalpy balance across the compressor. The intake air pressure (and the corresponding temperature) was chosen to facilitate the modeling requirements, as discussed in the following paragraph. Despite the inherent inaccuracy, this method allowed for an initial approximation for evaluating the engine's operation and feasibility in rotorcraft applications.

To compare the engine's performance when operating with the two separate fuel sources, two spark sweeps (i.e. changing the spark timing across a range of possi-

ble ignition times) were completed, while separately maintaining a constant knock integral of 0.92 or a maximum peak pressure of 91 bar.[2] At each spark timing, the engine's boost conditions and operating parameters were varied to adhere to these fixed performance characteristics, as seen in Appendix A. The results of the first spark sweep, where the knock integral was held constant, are shown in Figure 4-3, with the engine's spark delay (measured against the baseline MBT of 7° ATDC) varied across the horizontal axis and the corresponding engine power output or peak cylinder pressure plotted on the vertical axis.

Figure 4-3a demonstrates the ethanol's power improvement when holding the knock integral constant, which is gained by leveraging the fuel's higher octane number and charge cooling. However, this advantage requires significantly higher peak pressures, as increasing the engine's power output to roughly 250 kilowatts results in the engine cylinder's peak pressure reaching nearly 180 bar, requiring an engine structure as strong (and thus as heavy) as a diesel engine [30]. Due to the importance of specific power in rotorcraft applications, this requisite peak pressure rise heavily mitigates the performance improvement provided by ethanol. To compare performance in the same engine architecture (i.e. with the same mass), a second spark sweep was conducted while holding the engine's peak pressure constant. Figure 4-4 displays the result, with the engine's spark delay varied across the horizontal axis and the power output or final knock integral plotted on the vertical axis.

The engine produces nearly equivalent power output when using either fuel source, while E85 results in a lower knock integral value. These trends are due to E85's advantages; ethanol has a higher octane number and provides greater charge cooling, thus limiting the knock integral values. However, with heavy spark delay, the engine performance becomes limited by peak pressure and not knock, which mitigates the benefit of E85. Thus, given the equal performance at constant peak pressure and the mass considerations that limit their advantage at high peak pressures, ethanol-gasoline engines were not considered an attractive option for rotorcrafts.

[2] 91 bar was the peak pressure when operating at a CA50 of 7° ATDC, identified as the engine's baseline MBT timing, and thus was used for the pressure-limited spark sweep.

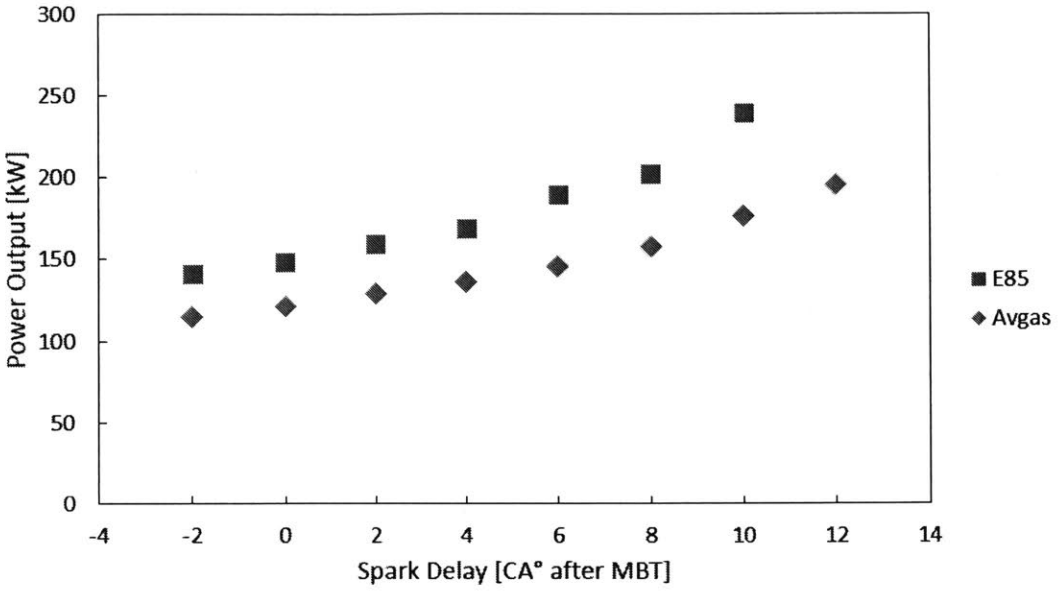


(a) Engine power output, with knock integral held constant

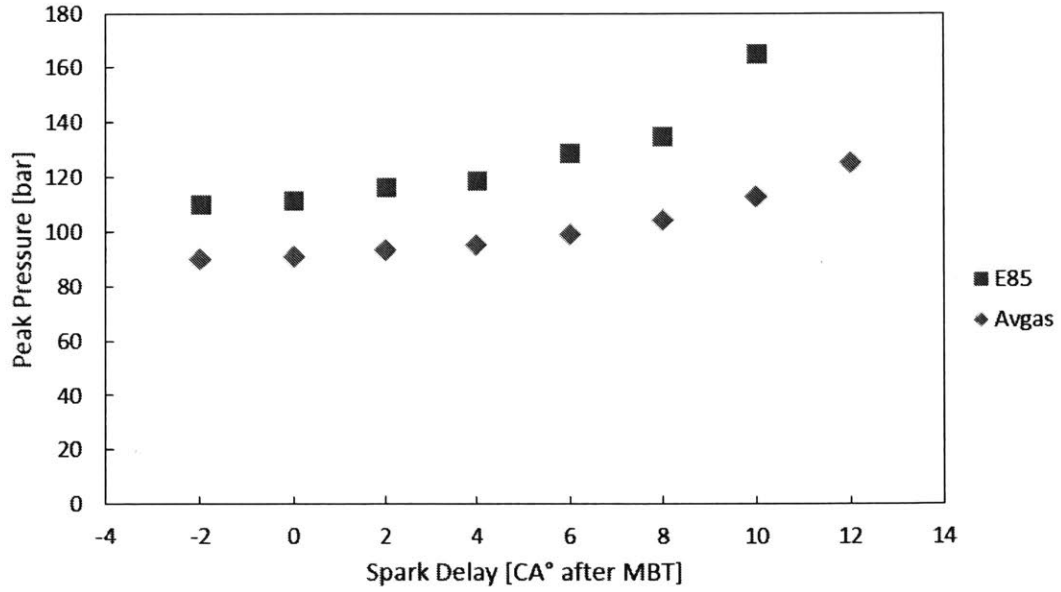


(b) Engine peak pressure, with knock integral held constant

Figure 4-3: The GT-POWER ethanol-gasoline model simulated a spark sweep while maintaining a constant knock integral, resulting in the engine producing significantly larger power output when operating with E85, at the expense of large peak pressures.

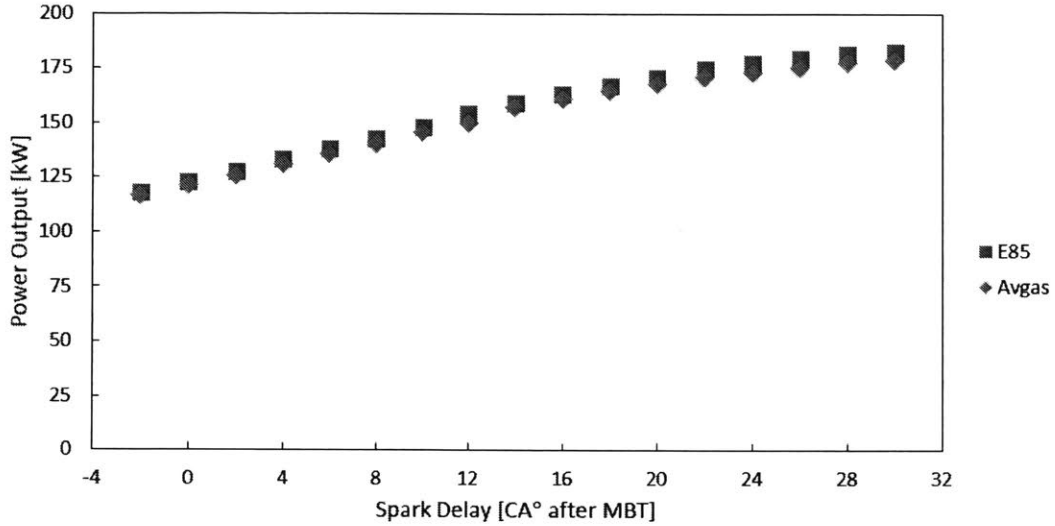


(a) Engine power output, with peak pressure held constant

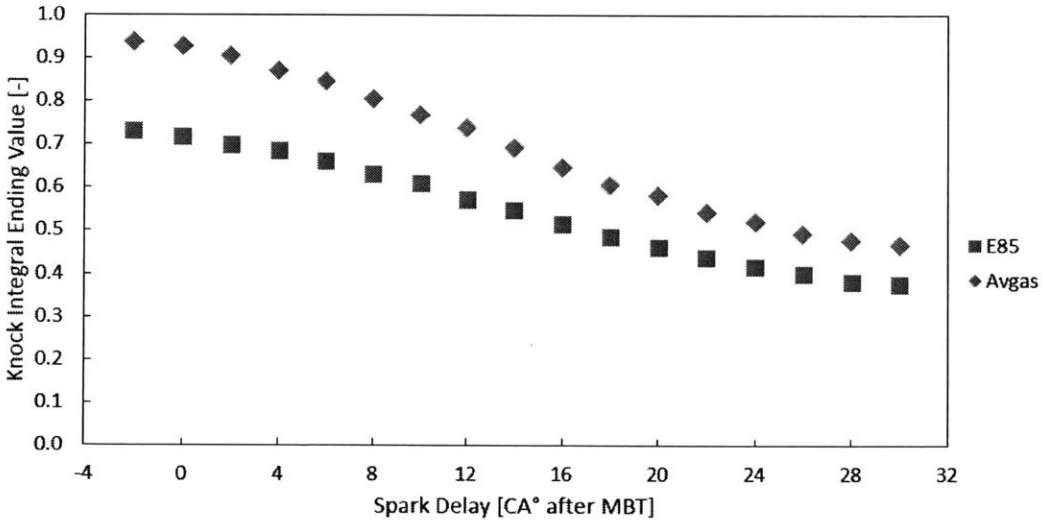


(b) Engine power output, with peak pressure held constant

Figure 4-4: The GT-POWER ethanol-gasoline model simulated a spark sweep while maintaining a constant peak pressure, resulting in the engine producing very similar power output when operating with either fuel source, while having a significantly lower knock integral when running on E85.

# Chapter 5

# Flight Profile Modeling

To determining the feasibility and niche applications for alternative engine configurations, a flight profile model was constructed to simulate a characteristic helicopter flight path and evaluate the airframe's performance when equipped with various engine designs. Specifically, the simulations were conducted with gas turbines, gasoline, and diesel piston engines, including the two-stroke diesel and two/four-stroke gasoline engine configurations. These designs were modeled in multiple combinations when equipped in a variety of airframe sizes to determine their applicability, as discussed in the following sections.

## 5.1 Modeling Construction

The flight profile model was built to simulate a realistic flight path consisting of takeoff, climb, cruise, reserve, descent, and landing flight segments. Within each segment, the airframe's instantaneous power requirement was calculated to size and estimate the aircraft's engine, as well as estimate its performance throughout the flight path. The following sections discuss the development of the flight profile modeling architecture.

### 5.1.1 Instantaneous Power Requirements

At each point during the flight profile, the airframe's instantaneous power requirement is calculated to determine the helicopter's engine load and the corresponding fuel consumption. The engine counteracts the aerodynamic and gravitational forces to provide forward and vertical flight capabilities,

$$P_{\text{total}} = \frac{P_{\text{i}} + P_{\text{o}} + P_{\text{p}} + P_{\text{c,d}}}{x_{\text{m}}}, \tag{5.1}$$

where $P_{total}$ is the total power required by the helicopter's engines, $P_i$ represents the airframe's induced power that produces lift, $P_o$ is the profile power caused by the rotor's viscous losses, $P_p$ is the parasitic power that corresponds to the airframe's drag, $P_{c,d}$ represents the power required for the helicopter to climb vertically or the reduction in power when descending, and $x_m$ is a correction factor that accounts for the miscellaneous airframe power requirements, including the tail rotor, transmission losses, and auxiliary equipment. Based on industry approximations, the correction factor is assumed to be 0.91 for forward flight and 0.85 during hovering (i.e. stationary flight) [3, 6].

Figure 5-1 illustrates characteristic power curves for level forward flight, with flight speed on the horizontal axis and each power requirement (i.e. induced, profile, parasitic, and climb or descent), along with the total airframe power, on the vertical axis. Before evaluating each power component, a handful of terms must be defined that will be used in the subsequent calculations. Table 5.1 lists these parameters, along with their symbols and implications, with Figure 5-2 providing context to the physical interpretation of the terms in a characteristic forward flight path. The following sections outline how these parameters are used to calculate each power component.

#### Parameter Calculations

The terms identified in Table 5.1 are required to determine the instantaneous power requirements in the following sections, which are derived from the physical relationships shown in Figure 5-2, as well as additional features of rotorcraft flight [3]. First,

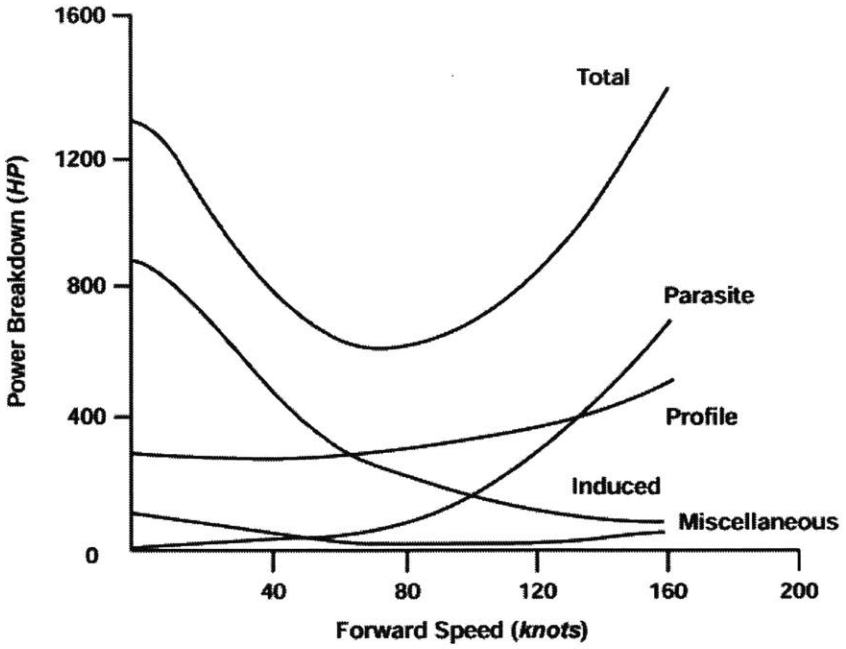


Figure 5-1: A characteristic forward flight power curve illustrates the change in each power component and the overall power requirement when varying forward speed [6].

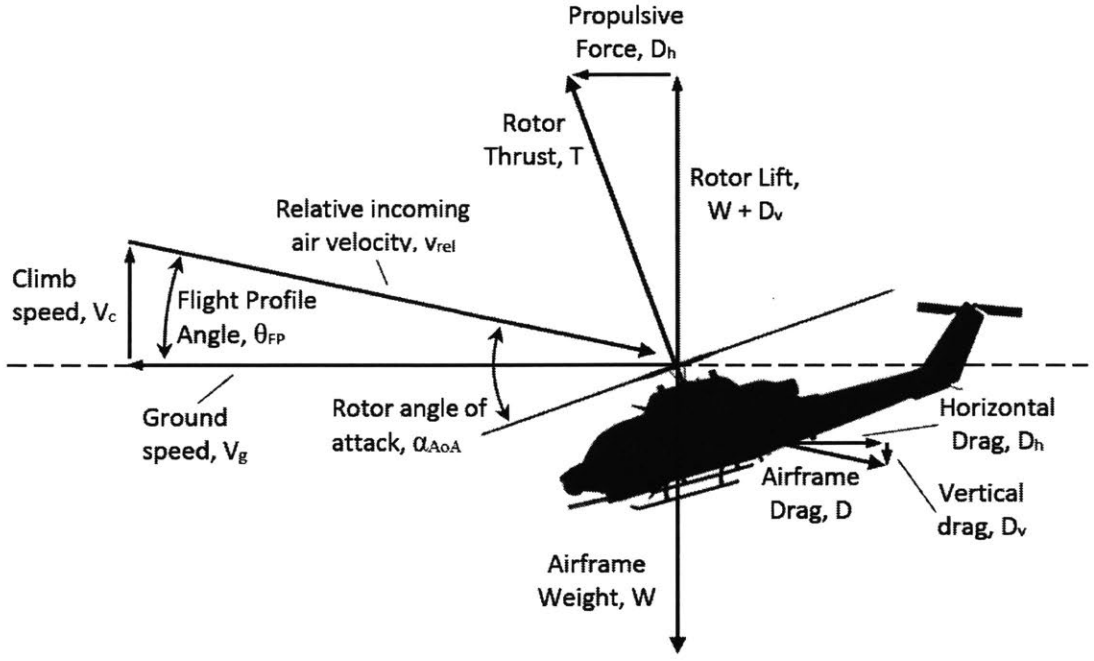


Figure 5-2: The forces and characteristics of a stable and balanced flight path illustrate a portion of the terms that are used to calculate the helicopter's instantaneous power requirements (adapted from [3]).

Table 5.1: The important terms used when calculating an airframe's instantaneous power requirement [3]

| **Term name** | **Symbol** | **Description** |
|---|---|---|
| Rotor disc area ($m^2$) | $A_{prop}$ | The total swept rotor area, calculated as a circle with the propeller's radius |
| Fuselage drag coefficient | $C_{Df}$ | The fuselage drag coefficient, based on a reference drag area, that is used to calculate the equivalent fuselage wetted area |
| Airfoil profile drag coefficient | $C_{do}$ | The coefficient used to calculate the rotor's aerodynamic drag force |
| Drag force (N) | $D$ | The aerodynamic drag force that opposes flight |
| Equivalent fuselage wetted area ($m^2$) | $f$ | The aggregate area used to account for the drag of the fuselage, hub, and other components, not including the rotor |
| Blade profile power correction factor | $K$ | The empirical correction factor used to adjust the airfoil profile power |
| Reference drag area ($ft^2$) | $S_{ref}$ | A reference area arbitrarily defined and used to calculate the equivalent fuselage wetted area |
| Rotor thrust (N) | $T$ | The total force the rotor produces to counteract the airframe weight and drag forces |
| Blade tip speed (m/s) | $v_{blade}$ | The tangential speed of the rotor blade tip |
| Climb or descent speed (m/s) | $v_{c,d}$ | The vertical speed at which the airframe increases or decreases its altitude |
| Ground speed (m/s) | $v_g$ | The horizontal speed at which that the aircraft travels |
| Relative ambient velocity (m/s) | $v_{rel}$ | The velocity of the ambient air relative to the rotor |
| Airframe total weight (N) | $W_{tot}$ | The total weight of the airframe at an instantaneous point during the flight path |
| Rotor attack angle (rad) | $\alpha_{AoA}$ | The angle between the relative velocity of the incoming air and the rotor plane |
| Induced power correction factor | $\kappa$ | The correction factor used to account for non-ideal physical effects on the rotor, including tip losses, nonuniform inflow, wake swirl, finite blade, etc. |
| Rotor inflow ratio | $\lambda$ | The ratio between the induced velocity of the incoming ambient air perpendicular to the rotor plan and the rotor blade tip speed |
| Rotor advance ratio | $\mu$ | The ratio between the component of the incoming ambient air velocity parallel to the rotor plane and the rotor blade tip speed |
| Ambient air density ($kg/m^3$) | $\rho_{amb}$ | The density of the ambient air |
| Rotor solidity | $\sigma$ | The fraction of the rotor disc area that is occupied by the total area of the rotor blades |
| Flight path angle (rad) | $\theta_{FP}$ | The instantaneous vertical angle of the flight path, measured from the horizon |

the helicopter's reference drag area is used to calculate the aircraft's equivalent wetted area,

$$S_{\text{ref}} = \left( \frac{W_{\text{tot}}}{9.81} * 2.2046 \right)^{2/3}, \tag{5.2}$$

where $S_{ref}$ is the reference drag area in square feet and $W_{tot}$ is the total helicopter weight in newtons. With this area, the airframe's equivalent fuselage wetted area is calculated,

$$f = (C_{\text{Df}} * S_{\text{ref}})0.099 \quad (m^2) \tag{5.3}$$

where $f$ is the equivalent wetted area in square meters, $C_{Df}$ is the fuselage drag coefficient, and $S_{ref}$ is the reference drag area calculated in Equation 5.2. Next, the equivalent fuselage wetted area enables the calculation of the aircraft's aerodynamic drag,

$$D = \frac{1}{2} \rho_{\text{amb}} ({v_{\text{rel}}}^2) f \tag{5.4}$$

where $D$ is the airframe's total drag (excluding the rotors) in newtons, $\rho_{amb}$ is the ambient air density in kilograms per cubic meter, $f$ represents the equivalent fuselage wetted area in square meters as calculated by Equation 5.3, and $v_{rel}$ is the velocity of the incoming ambient air relative to the rotor disc in meters per second. This latter parameter is determined from the flight path velocities (assuming no wind),

$$v_{\text{rel}} = \sqrt{{v_{\text{c,d}}}^2 + {v_{\text{g}}}^2} \tag{5.5}$$

where $v_{rel}$ is the velocity of the incoming ambient air relative to the rotor disk in meters per second, $v_c$ is the airframe's vertical climb (or descent) rate in meters per second, and $v_g$ is the helicopter's horizontal (or ground) speed in meters per second. After calculating the aircraft's aerodynamic drag (using the relative velocity), the total thrust required by the rotor is calculated,

$$T = \sqrt{D^2 + {W_{\text{tot}}}^2} \tag{5.6}$$

where $T$ is the thrust produced by the rotor in newtons, $D$ is the airframe's aerodynamic drag in newtons, and $W_{tot}$ is the total weight of the helicopter in newtons. Furthermore, using the aircraft's aerodynamic drag, the flight path angle is determined,

$$\theta_{\text{FP}} = \arctan\left(\frac{v_{\text{c,d}}}{v_{\text{g}}}\right) * D^2 + {W_{\text{tot}}}^2 \tag{5.7}$$

where $\theta_{FP}$ is the flight path angle in radians, $v_{c,d}$ is the helicopter climb (or descent) rate in meters per second, $v_g$ is the horizontal speed in meters per second, $D$ is the airframe's aerodynamic drag in newtons and calculated by Equation 5.4, and $W_{tot}$ is the helicopter's total weight in newtons. With this flight path angle, the rotor's angle of attack can be evaluated,

$$\alpha_{\text{AoA}} = \theta_{\text{FP}} + \arctan\left(\frac{D}{W_{\text{tot}}}\right) \tag{5.8}$$

where $\alpha_{AoA}$ is the rotor's angle of attack in radians, $\theta_{FP}$ represents the airframe's flight path angle in radians, $D$ corresponds to the aircraft's aerodynamic drag in newtons and calculated by Equation 5.4, and $W_{tot}$ is the helicopter's total weight in newtons. With this angle of attack, the rotor's advance ratio is determined,

$$\mu = \frac{v_{\text{rel}} \cos(\alpha_{\text{AoA}})}{v_{\text{blade}}} \tag{5.9}$$

where $\mu$ is the rotor's advance ratio, $v_{rel}$ is the velocity of the ambient air relative to the rotor in meters per second and calculated in Equation 5.5, $\alpha_{AoA}$ is the rotor's angle of attack in radians, and $v_{blade}$ is the rotor blade tip speed in meters per second. Finally, with these parameters, the rotor's inflow ratio is calculated,

$$\lambda = \mu \tan(\alpha_{\text{AoA}}) + \frac{T}{2\rho_{\text{amb}} * A_{\text{prop}} * {v_{\text{blade}}}^2(\mu^2 + \lambda^2)} \tag{5.10}$$

where $\lambda$ is the rotor's inflow ratio, $\mu$ is the rotor's advance ratio, $\alpha_{AoA}$ is the rotor's

angle of attack in radians, $T$ is the thrust produced by the rotor in newtons, $\rho_{amb}$ is the ambient air density in kilograms per cubic meter, $A_{prop}$ is the total swept rotor area in square meters, and $v_{blade}$ is the rotor blade tip speed in meters per second. These parameters will be used to calculate the individual power requirements in the following sections.

### Induced Power

As seen in Figure 5-1, induced power is the dominant power source during low flight speeds, and quickly decreases as forward velocity increases. This power is related to the lift produced by accelerating air through the rotor disk,

$$P_{\text{induced}} = \frac{\kappa * T^2}{2\rho_{\text{amb}} * A_{\text{prop}} * v_{\text{blade}}\sqrt{\lambda^2 + \mu^2}}, \tag{5.11}$$

where $P_{induced}$ is the airframe's induced power in watts, $\kappa$ is the induced power correction factor, $T$ is the thrust produced by the rotor in newtons and calculated in Equation 5.6, $\rho_{amb}$ is the ambient air density in kilograms per cubic meter, $A_{prop}$ is the total swept rotor area in square meters, $v_{blade}$ is the blade tip speed in meters per second, $\lambda$ is the rotor inflow ratio calculated in Equation 5.10, and $\mu$ is the rotor advance ratio calculated in Equation 5.9 [3].

### Profile Power

The profile power contributes a substantial amount of the total airframe power required during all operation conditions and slightly increases at higher flight speeds, as seen in Figure 5-1. This power represents the rotor's viscous losses,

$$P_{\text{profile}} = \frac{\sigma * C_{\text{do}}}{8}(1 + K * \mu^2)\rho_{\text{amb}} * A_{\text{prop}} * {v_{\text{blade}}}^3, \tag{5.12}$$

where $P_{profile}$ is the profile power in watts, $\sigma$ is the rotor solidity, $C_{do}$ is the airfoil profile drag coefficient, $K$ is the blade profile power correction factor, $\mu$ is the rotor advance ratio calculated in Equation 5.9, $\rho_{amb}$ is the ambient air density in kilograms per cubic meter, $A_{prop}$ is the total swept rotor area in square meters, and $v_{blade}$ is the

blade tip speed in meters per second [3].

### Parasitic Power

The airframe's parasitic power is very small factor during slow flight speeds, but rapidly increase in high speeds, as seen in Figure 5-1. This power defines the airframe's drag force,

$$P_{\text{parasitic}} = \frac{1}{2}\rho_{\text{amb}} * f * v_{\text{blade}}{}^{3}, \tag{5.13}$$

where $P_{parasitic}$ is the parasitic power in watts, $\rho_{amb}$ is the ambient air density in kilograms per cubic meter, $f$ is the equivalent wetted area in square meters, and $v_{blade}$ is the blade tip speed in meters per second [3].

### Climb or Descent Power

The airfoil climb power is required to increase the airframe's altitude, while the descent power reduces the airframes power requirement while descending,

$$P_{\text{climb, descent}} = W_{\text{tot}}(1 + x)v_{\text{c,d}}. \tag{5.14}$$

Here, $P_{climb,\ descent}$ is the climb or descent power in watts, $W_{tot}$ is the total airframe weight in newtons, $v_{c,d}$ is the climb or descent velocity in meters per second, and $x_f$ is an adjustment factor that accounts for the fuselage vertical drag. This latter parameters is approximated to equal 0.05 during climb, -0.05 when descending, and 0.00 during hover based on industry assumptions [3].

### Hover Power

While the previous sections provide the power calculations during forward flight, the total airframe power correlation can be simplified during hover conditions (i.e. no forward or vertical velocities),

$$P_{\text{hover}} = \frac{\frac{\kappa * {W_{\text{tot}}}^{3/2}}{\sqrt{2\rho_{\text{amb}} * A_{\text{prop}}}} + \frac{\rho_{\text{amb}} * A_{\text{prop}} * {v_{\text{blade}}}^{3} * \sigma * C_{\text{do}}}{8}}{0.85}, \tag{5.15}$$

where $\kappa$ is the induced power correction factor, $W_{tot}$ is the total airframe weight in newtons, $\rho_{amb}$ is the ambient air density in kilograms per cubic meter, $A_{prop}$ is the total swept rotor area in square meters, $v_{blade}$ is the blade tip speed in meters per second, $\sigma$ is the rotor solidity, $C_{do}$ is the airfoil drag coefficient, and the 0.85 factor represents the miscellaneous power correction factor ($x_m$) in hover conditions [3]. As outlined in Section 5.2.1, the rotorcraft's hover power is essential for sizing an airframe's engine, due to this portion of flight requiring the maximum amount of power (see Figure 5-1).

### Hot and High Consideration

In addition to an engine's performance, ambient pressure and temperature directly impacts an airframe's instantaneous power requirement, due to the ambient air density's influence on the induced, profile, parasitic, and simplified hover power calculations. As the anticipated flight path ranges between sea level and cruise altitude, the ambient air density is estimated throughout the flight profile,

$$\rho_{\text{amb}} = \rho_{\text{o}} * \left(\frac{T_{\text{o}}}{T_{\text{o}} - 0.0065h}\right) * \left(1 - 0.0065\frac{h}{T_{\text{o}}}\right), \tag{5.16}$$

where $\rho_{amb}$ is the ambient air density in kilograms per cubic meter, $\rho_o$ represents the International Standard Atmosphere (ISA) density at sea level (1.225 kilograms per cubic meter), $T_o$ is the ISA mean temperature of air at sea level (288.15° kelvin), and $h$ is the pressure altitude in meters [91]. Furthermore, as identified in Section 1.3, the helicopter must be capable of takeoff at a pressure altitude of 4,000 feet (1,219 meters) and ambient temperature that is 35° Celsius greater than the ISA temperature for that altitude (i.e. 7 + 35 = 42° Celsius). Thus, Equation 5.16 is modified to account for this specification when sizing an airframe's takeoff power requirement,

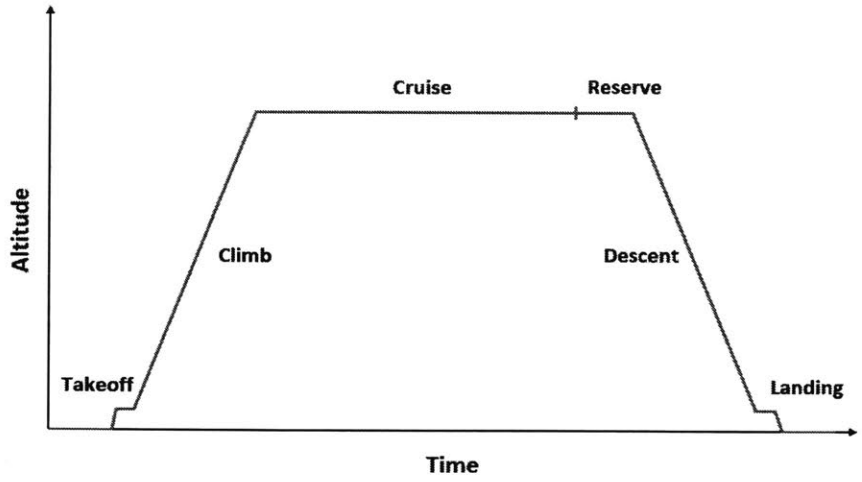


Figure 5-3: The flight profile is broken into the takeoff, climb, cruise, reserve, descent, and landing segments. The times of each segment are not to scale, with the takeoff, climb, reserve, descent, and landing portions lasting for minutes compared to the cruise segment which lasts for hours. Additionally, the cruise altitude is assumed to be 1,219 meters, while takeoff is approximated to occur at ground level.

$$\rho_{\text{amb}} = \rho_{\text{o}} * \left( \frac{T_{\text{o}}}{T_{\text{o}} + 35^{\circ} - 0.0065h} \right) * \left( 1 - 0.0065 \frac{h}{T_{\text{o}}} \right), \tag{5.17}$$

where the 35° increase is accounted for when calculating the ambient temperature at hot and high takeoff conditions.

### 5.1.2 Flight Segments

As illustrated in Figure 5-3, the flight path is broken into six separate segments: takeoff, climb, cruise, reserve, descent, and landing. Each of these flight portions are modeled to provide a realistic flight profile, and to evaluate the performance of the airframe across all associated operating conditions. The following sections evaluate the six segments in further detail.

#### Takeoff and Climb

The airframe's takeoff and climb procedures are the initial portions of the flight profile that the helicopter utilizes to reach its cruising altitude. As a simplified approach,

the modeling assumed a one-minute vertical ascent at approximately hovering conditions, followed by two climb segments. First, the airframe accelerated vertically and horizontally until reaching the desired climb velocity, including the ground speed and vertical climb speed. The ideal ground speed is identified as the airframe's horizontal speed that produces a minimum power requirement for the airframe, with this minimum illustrated in Figure 5-1. The vertical initial climb speed for each airframe is calculated based on a trend observed in example helicopters, with this analysis provided in Appendix D. However, due to various engine architectures changing the total available power, this speed is allowed to be reduced if the available engine power could not facilitate the baseline climb speed. Upon reaching the desired climb velocity, the airframe continued to climb until reaching the cruising altitude, which is set to a typical industry value of 4,000 feet (1,219 meters) [84].

### Cruise

After climbing to the cruise altitude, the airframe travels horizontally at the speed that maximizes its range, until the remaining fuel is the minimum amount necessary for the reserve, descent, and landing portions of the flight profile. This optimum value is illustrated in Figure 5-4, which plots a characteristic airframe's fuel consumption rate across a range of flight speeds. Here, maximum range is achieved when the ratio between the fuel consumption rate and the flight speed is minimized, with this ratio being equivalent to the slope of a line that passes through the origin and intersects with a point on the curve. Thus, due to the desire to minimize this slope while being restricted by the aircraft's operational characteristics, the maximum range speed arises when the line is tangent to the curve [3].

For the flight profile modeling, this speed is directly calculated through comparing the ratio of the fuel consumption rate and flight speed over a range of speeds, until the minimum is determined. The variations in the airframe's fuel consumption rate profile arise from the flight speed's effect on the airframe power requirement and the corresponding effect on the engine's SFC, with the former illustrated in Figure 5-1 and the latter discussed in Sections 2.3 and 3.3.

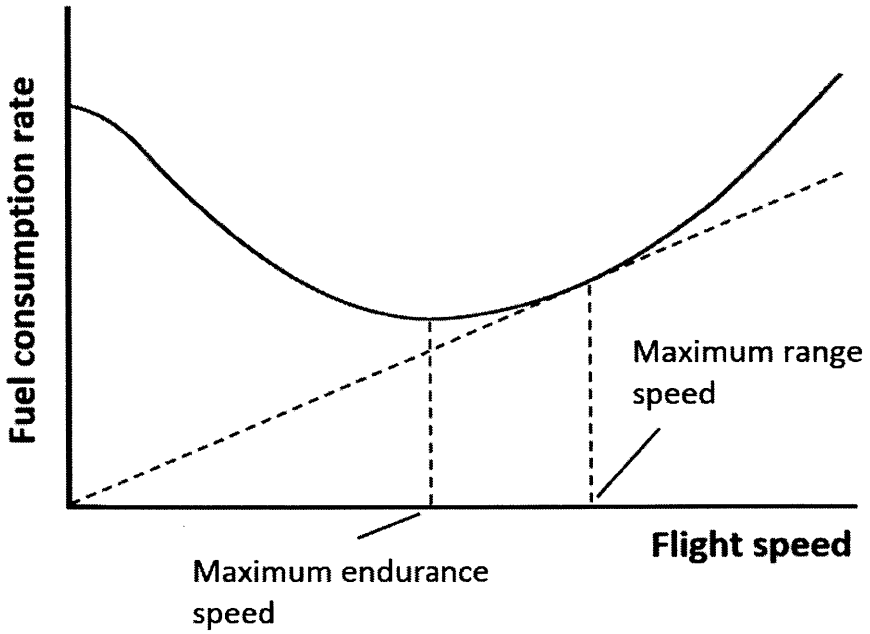


Figure 5-4: The airframe will travel at the maximum endurance/minimum power speed during the climb and reserve flight segments, while cruising at the maximum range speed (adapted from [6]).

### Reserve

After cruising for most of the mission, the rotorcraft transitions into the reserve portion of flight. Based on the legal requirements for fuel during rotorcraft flight, airframes are typically sized with enough reserve fuel to travel for 30 minutes after the maximum cruise duration [84, 90]. This requisite amount of fuel is calculated with the airframe traveling at the maximum endurance speed, as seen in Figure 5-4, which is standard industry practice [82, 88]. Similar to the best range speed, the modeling calculated the maximum endurance speed by determining the minimum power requirement speed, which is a common approximation[1] [3, 6]. With the reserve fuel specified, the airframe is modeled as traveling at the best range speed until consuming all of the reserve fuel (with sufficient fuel left for descent and landing), as

[1] A more accurate approach entails calculating the minimum fuel consumption rate speed, similar to the maximum range speed procedure. However, as calculating the required amount of reserve fuel only impacts how much fuel is available during cruise vs. reserve (with the cumulative amount remaining constant), and considering that both the reserve and cruise best range speeds are calculated in the same manner, this approximation does not impact the aircraft's overall range prediction.

this provides the maximum potential range for the airframe and is common practice in reporting a helicopter's range [1, 80, 81, 83, 84, 86, 88].

### Descent and Landing

Finally, the airframe is modeled as descending from altitude at the minimum power (and fuel consumption rate) flight speed, with a vertical descent rate of 2.5 meters per second. This speed was chosen to insure that the rotorcraft flight does not fall into a region where vortex rings begin to form, resulting in adverse operation and dangerous flight conditions [3]. However, this portion of the flight represents a small fraction of the overall fuel consumption, and thus an accurate determination of descent speed is not crucial. To finish the flight, the helicopter landing procedure is modeled as a one minute hover, analogous to the takeoff assumption.

## 5.2 Engine Configurations

For each airframe, multiple engine configurations are compared to evaluate their effect on the rotorcraft's performance, comprised of gas turbine, diesel, and gasoline engines implemented in a variety of combinations. In addition to a standard swap where the gas turbines are directly replaced by the piston engines, two alternative configurations are identified in this analysis to further leverage the piston engine's advantages and mitigate their limitations: the hybrid and auxiliary engine designs. The hybrid concept implements both a gas turbine and a piston engine to leverage each engine's advantages while mitigating their disadvantages; the gas turbine provides a portion of the required takeoff power in a light package due to the engines high specific power, while the piston engine's high efficiency is used to maximize the airframe's range.

Similarly, the auxiliary engine configuration utilizes a small gas turbine to assist in takeoff and OEI conditions, while one or two main engines (depending on the aircraft size) provide the remainder of the airframe's power. This additional engine is capable of improving the airframe's performance in multiple ways. If sized with a sufficient

power rating, gas turbine have higher specific powers than piston engines (see Section 2.3), and thus, when paired with main piston engines, the auxiliary engine reduces the airframe's total engine mass. Additionally, the configurations' main engines do not need to be sized to solely handle OEI conditions during hot and high takeoff, as the auxiliary engine provides a secondary source of power in these situations. This reduces the overall power requirement of the airframe, which lowers the aircraft's total engine mass. Finally, when the auxiliary engine is paired with gas turbines, the decrease in the main engine power rating enables these gas turbines to operate at power outputs that are closer to their maximum rating, which substantially improves their operating efficiency (see Section 2.3).

Each configuration is required to provide sufficient power in both hot and high and, if applicable, OEI conditions. Thus, the required hovering power in hot and high conditions are used as engine sizing requirement, due to the assumption that hovering requires the most power during the flight profile (see Figure 5-1), and that the hot and high condition is the most stringent case for each engine's power output. Additionally, for conditions that required OEI considerations, each engine is sized to provide sufficient OEI power during the baseline hot and high takeoff requirement. The engine designs, as well as the sizing requirements, are outlined in the following sections.

### 5.2.1 Engine Sizing Considerations

For each configuration, the engine sizing process is based on ensuring an airframe is capable of takeoff in hot and high conditions when, if applicable, experiencing OEI. Per the discussion in Section 1.3, the former stipulation entails that the engine must provide the total airframe power required to takeoff in hot and high conditions that are equivalent to the pressure at an altitude of 1,219 meters at 35° C greater than the ISA temperature at that altitude, with this airframe power requirement identified as $P_{hover,\ H\&H}$. Additionally, the latter consideration requires that, in OEI conditions, the remaining functional engine(s) provides 70% of the takeoff decision point (TDP) power output (see Section 1.3). As discussed in Section 2.3, gas turbines are estimated

to have a derating of 25% under these hot and high conditions, due to the lower air density and negative effects of high air temperature [10, 16, 92]. Similarly, as discussed in Section 4.4.3, the piston engine hot and high derating is approximated as 10%, with the negative affects being limited by the excess boosting capabilities that are achieved through proper design. These hot and high power adjustments are identified in the following sections as $x_{GT,H\&H}$ for the gas turbines and $x_{Pist,H\&H}$ Furthermore, per the data and discussion provided in Section 2.3, gas turbines are estimated to be capable of providing a 20% increase in power output during OEI operation, which is referred to in subsequent sections as $x_{GT,OEI}$. Finally, as piston engine data is based on maximum performance, this analysis assumes that attempting to gain higher output power would result in rapid engine destruction, due to higher speeds (and thus greater stresses) causing the rotating and reciprocating components to fail, and/or higher peak pressures damaging the cylinders and cylinder heads while causing the onset of knock. Thus, the piston engine configurations are not rated for increased performance in OEI conditions. Each of these factors and parameters are used to estimate the required engine sizing for the following configurations, with each configuration's procedure provided in Appendix E.

### Standard Implementations

First, five standard designs are separately modeled in each airframe, including the baseline gas turbine, diesel two- and four-stroke engines, gasoline four-stroke engine, and two/four-stroke gasoline engine. These engines are sized by considering hot and high performance and, when applicable, OEI capabilities. For the gas turbine, the configurations resulted in the following sizing requirements for the single- and dual-engine airframes,

$$P_{\text{single-engine}} = \frac{P_{\text{hover, H\&H}}}{x_{\text{GT, H\&H}}} = \frac{P_{\text{hover, H\&H}}}{0.75}, \tag{5.18}$$

$$P_{\text{dual-engine}} = \frac{1}{2}\left(\frac{1.4P_{\text{hover, H\&H}}}{x_{\text{GT, OEI}} * x_{\text{GT, H\&H}}}\right) = 0.78P_{\text{hover, H\&H}}, \tag{5.19}$$

where $P_{single\text{-}engine/dual\text{-}engine}$ are the power ratings required in the single- and dual-engine configurations. Alternatively, for the piston engines, the resulting engine sizing requirements for the single- and dual-engine airframes are as follows, using the same $P_{single\text{-}engine,\ dual\text{-}engine}$ nomenclature,

$$P_{\text{single-engine}} = \frac{P_{\text{hover, H\&H}}}{x_{\text{Pist, H\&H}}} = \frac{P_{\text{hover, H\&H}}}{0.9}, \tag{5.20}$$

$$P_{\text{dual-engine}} = \frac{1}{2}\left(\frac{1.4P_{\text{hover, H\&H}}}{x_{\text{Pist, H\&H}}}\right) = 0.78P_{\text{hover, H\&H}}. \tag{5.21}$$

Note that the sizing requirements for the dual-engine gas turbine and piston engine configurations are equivalent by coincidence only, as these equations are derived using different hot and high performance adjustments and only the gas turbine is rated as having an OEI power increase. The derivations for these equations are provided in Appendix E.

### Hybrid Implementation

The hybrid configuration is the second design category evaluated in this analysis, where the four piston engine architectures are separately paired with a gas turbine on each airframe. As both of the configuration's engines must provide sufficient hot and high and OEI capabilities, the hybrid design's gas turbine and piston engine power calculations are identical to Equations 5.19 and 5.21, respectively, which are used for the standard implementation configuration. The derivations for these equations are provided in Appendix E.

### Auxiliary Engine Implementation

Finally, the third engine design incorporated an auxiliary gas turbine with the standard piston engine and gas turbine configurations serving as the main engines. To mimic the original airframe designs, one main engine is paired with the auxiliary engine for single-engine airframes and two main engines are implemented in dual-engine rotorcraft, as described in Section 5.3.3. Despite the potential for improvement, the

auxiliary configurations must balance the negative effect of decreasing the main engines' size; the specific power for both gas turbines and piston engines increase with increasing power while the gas turbine's efficiency also rises with power (see Sections 2.3 and 3.3). Furthermore, due to OEI considerations, the allowable range of auxiliary engine power allocation is restricted to ensure that the airframe can produce 70% of the power required at the takeoff decision point, per the discussion provided in Section 1.3.

This stipulation results in upper and lower bounds in the allocation of power between the main and auxiliary engines, based on situations where either the auxiliary engine or, for dual-main-engine configurations, one of the main engines fail. In the former scenario, the main engine(s) must have sufficient power to produce the requisite OEI power, and thus this failure mode corresponds to the lower limit for the main engine sizing. On the other hand, when one of the main engines fail in the dual-main-engine configurations, only half of the power allocated to the main engines is available. Thus, as increasing the main engine power allocation would decrease the airframe's capabilities, this scenario provides the upper limit for the dual-main-engine sizing.

For single-main-engine configurations, the analysis assumed that the design must only ensure OEI capabilities for the main engine, as this provides the same likelihood of catastrophic failure when compared to the standard design (i.e. the standard single engine is as likely to fail as the main engine). Thus, the upper limit for the percent of total power provided by the single-main-engine was determined to be 100%. For the gas turbine configurations, the total airframe power requirement and ranges of allowable main engine power allocation are calculated as follows,

$$P_{\text{total}} = 1.33 P_{\text{hover, H\&H}}, \tag{5.22}$$

$$0.583 \leq x_{\text{main frac, single-engine}} \leq 1.000, \tag{5.23}$$

$$0.583 \leq x_{\text{main frac, dual-engine}} \leq 0.833, \tag{5.24}$$

where $P_{total}$ corresponds to the total power required by engine configuration and

$x_{main\ frac,\ single\text{-}engine/dual\text{-}engine}$ are the fraction of the total engine configuration power allocated to the main engines in the single- and dual-engine airframes. Similarly, the piston engine configurations' total airframe power requirement and ranges of allowable main engine power allocation are determined by the following relationships,

$$P_{\text{total}} = \frac{P_{\text{hover, H\&H}}}{0.9 + 0.15x_{\text{main frac}}}, \tag{5.25}$$

$$0.660 \leq x_{\text{main frac, single-engine}} \leq 1.000, \tag{5.26}$$

$$0.660 \leq x_{\text{main frac, dual-engine}} \leq 0.676, \tag{5.27}$$

using the same nomenclature as Equations 5.22 through 5.24. Appendix E provides the derivation of each allocation limit, as well as the engine power requirements.

Within the ranges provided in Equations 5.23, 5.24, 5.26, and 5.27, the flight profile modeling optimizes the main engine power allocation to balance the advantages and disadvantages of the auxiliary engine configuration. This optimization entails running the modeling with varying allocation values until achieving the maximum airframe range, with the process completed for each main engine design and airframe. The resulting power allocations are provided in Section 5.4.

### 5.2.2 Engine Mass and Specific Fuel Consumption

Following the calculation of their required power output, the engine masses are estimated to fully determine the designs' impacts on the each airframe's performance. To facilitate this evaluation, the mass versus power output trends compiled in Sections 2.3, 3.3, and 4.4 are used for the gas turbines, standard piston engines, and the two/four-stroke configuration, respectively. Using these masses, the mass allocation process is conducted on each airframe, where the change in engine mass must be balanced with a equal and opposite alteration to the aircraft's fuel and the corresponding fuel tank mass (see Appendix D).

The airframe's power requirement also dictates the gas turbine's specific fuel consumption (SFC, rated at takeoff power), as predicted by the trends discussed in Section 2.3. The standard piston engine designs are assumed to have SFCs of 0.2 kilograms per kilowatt-hour for the diesel two- and four-stroke engines and 0.25 kilograms per kilowatt-hour for the four-stroke gasoline engine across all power ratings (See Section 3.3). Additionally, the two/four-stroke engine is modeled as having a SFC of 0.25 and 0.375 kilograms per kilowatt-hour when operating in the four-stroke and two-stroke modes, respectively (as discussed in Section 3.6.1). Furthermore, the modeling adjusted each engine's SFC when operating at part-load based on the trends provided in Sections 2.3 and 3.3 for the gas turbines and piston engines, respectively. In the analysis of the two/four-stroke engine configurations, the engine's SFC is assumed to follow the same part-load efficiency trends of the standard gasoline engines.

## 5.3 Airframe Design

To facilitate the comparison of each engine configuration's effect on rotorcraft performance, baseline airframes are designed using industry standard practices for gas turbine-powered helicopters. This entailed identifying trends in designs of modern airframes, as well as tuning the model to accurately predict the performance capabilities of a set of modern aircraft examples.

### 5.3.1 Helicopter Design Trends

The following industry trends in airframe parameters are used to design the baseline aircraft that are evaluated in this analysis. The correlations are derived from multiple sets of aircraft databases, and partially provide the structure for designing a generic airframe.

#### Propeller Radius

To determine appropriate rotor radii for the airframes, data was collected on example rotorcraft to create a trend between the propeller radius and the gross takeoff mass.

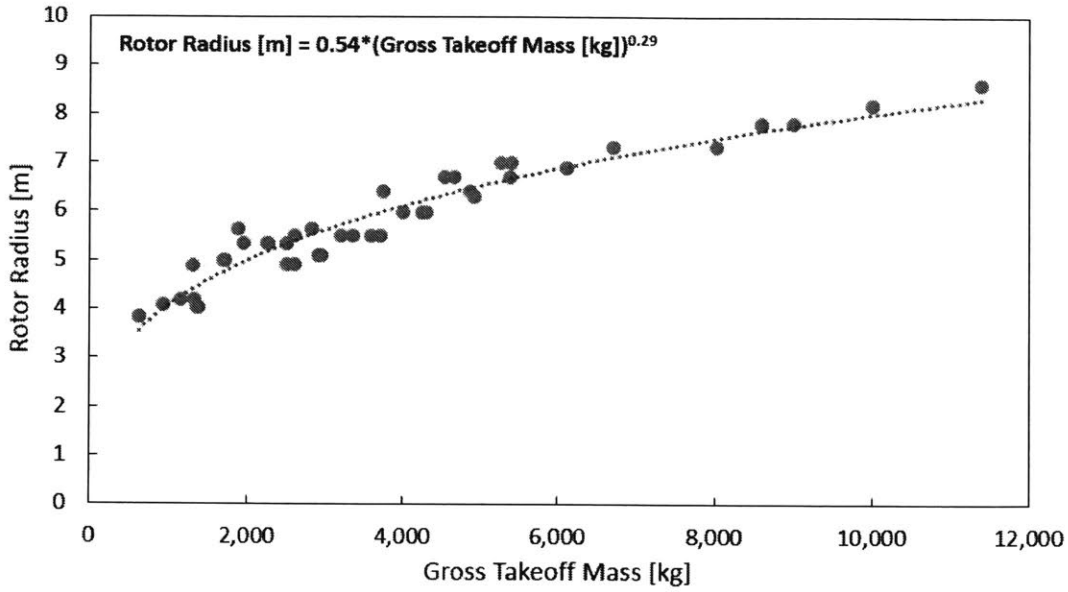


Figure 5-5: The propeller radius and gross takeoff mass are compared for a variety of rotorcraft, providing a trend in this relationship [1, 3, 80, 81, 82, 83, 84, 85, 86, 87, 88, 89].

The results are displayed in Figure 5-5, where the rotor radius is the vertical axis and the airframe's gross takeoff mass corresponds to the horizontal axis. Additionally, the best-fit curve is included and is as follows,

$$R_{\text{propeller}} = 0.55 \left(m_{\text{GTOM}}\right)^{0.29}, \tag{5.28}$$

where $R_{propeller}$ is the helicopter's propeller in meters and $m_{GTOM}$ is the airframes gross takeoff mass in kilograms. This correlation is used to specify the rotor radius of each baseline airframe, with the resulting values provided in Appendix D.

### Fuel Fraction of Gross Takeoff Mass and Climb Speed

A set of example airframe data was used to create a trend in an airframe's fuel fraction of the gross takeoff mass and the helicopter's climb speed, as seen in Figures 5-6 and 5-7. Here, the airframe's gross takeoff mass corresponds to each horizontal axis, while the fuel fraction of gross takeoff mass and the vertical climb speed are the vertical

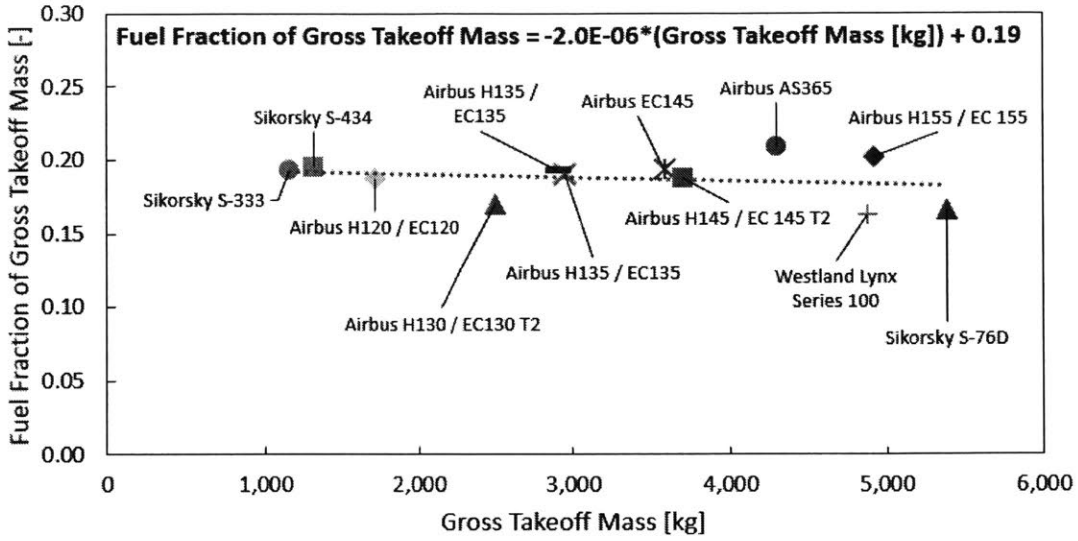


Figure 5-6: The fraction of gross takeoff mass dedicated to fuel is compared for the example aircraft listed in Appendix D [1, 80, 81, 82, 83, 84, 85, 86, 87, 88].

axes, respectively. The fuel fraction best-fit is included and determined to be as follows,

$$m_{\text{fuel fraction}} = -2.0e{-}6\,(m_{\text{GTOM}}) + 0.19, \tag{5.29}$$

where $m_{fuel\ fraction}$ is the fraction of the airframe's gross takeoff mass and $m_{GTOM}$ is the gross takeoff mass in kilograms. Furthermore, the illustrated climb speed correlation is as follows,

$$v_{\text{climb}} = 0.0003\,(m_{\text{GTOM}}) + 6.3, \tag{5.30}$$

where $v_{climb}$ is the helicopter's climb speed in meters per second and $m_{GTOM}$ is the gross takeoff mass in kilograms. These trends are used to calculate each baseline airframe's total fuel capacity and climb speed, based on their gross takeoff mass.

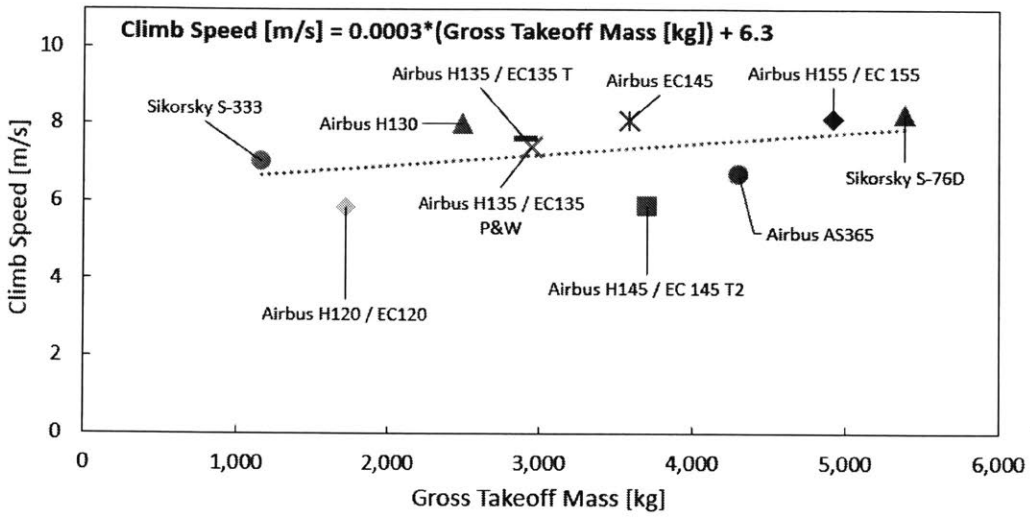


Figure 5-7: The climb speed and gross takeoff mass of the example aircraft listed in Appendix D are graphed to identify their relationship. The Westland Lynx airframe is not included as its climb speed is an outlier [1, 80, 81, 82, 83, 84, 85, 86, 87, 88].

### Rotor Solidity

A database containing the rotor solidity and gross takeoff mass of multiple aircraft was created to compare these parameters, with the results provided in Figure 5-8. Here, the horizontal axis is the airframe's gross takeoff mass and the vertical axis corresponds to the rotor solidity. Furthermore, the best-fit data trend is plotted for reference and is described as follows,

$$\sigma_{\mathrm{R}} = 6.0e{-}6\,(m_{\mathrm{GTOM}}) + 0.051, \tag{5.31}$$

where $\sigma_R$ is the rotor solidity and $m_{GTOM}$ is the airframe's gross takeoff mass in kilograms. This correlation is used to estimate the rotor solidity for all of the baseline airframes developed in this analysis.

### Fuel Tank Mass

Based on the amount of fuel that an airframe carries, the fuel tank is estimated to be 17% of the fuel mass from using a literature correlation [130]. This factor is

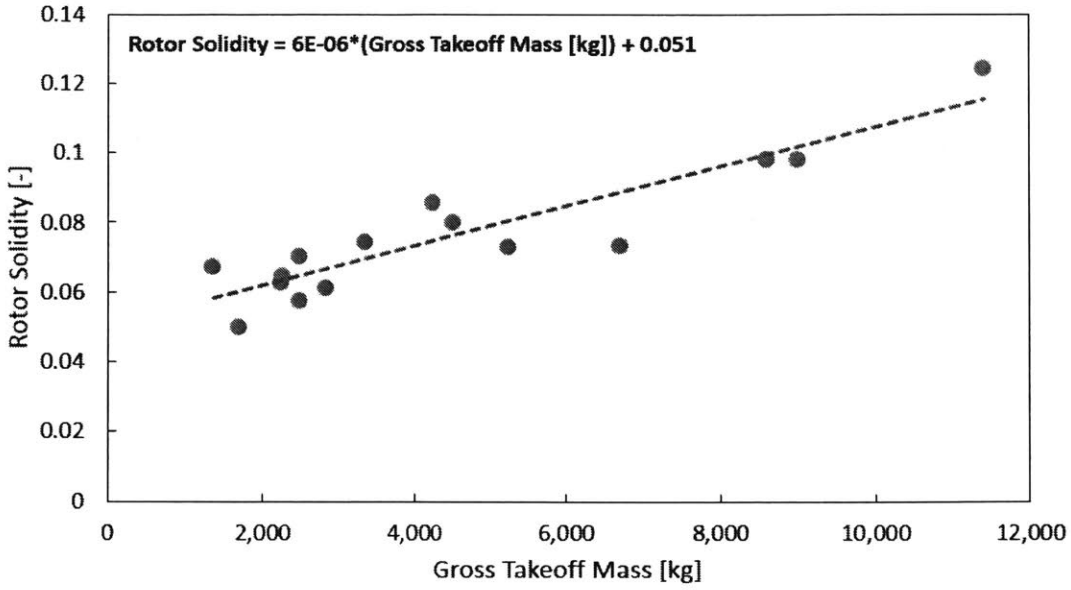


Figure 5-8: A database of airframes was used to create a trend between a helicopter's rotor solidity and gross takeoff mass [89].

accounted for when adjusting each aircraft's mass allocation due to changes in engine configurations.

### Blade Tip Speed

The airframe's blade tip speed must strike a balance between multiple counteracting forces, including high speeds delaying blade stall while lower velocities mitigate compressibility effects at increasing flight speed [3]. Based on industry references, each airframe's rotor tip speed is specified as 220 meters per second [3, 89].

### Power Factors

As defined in Section 5.1.1, two constants are used to adjust a helicopter's instantaneous power requirement; $K$ is a blade profile power correlation factor and $\kappa$ is the induced power correction factor that accounts for the aerodynamic losses and nonuniform flow. Based on the suggestions made form empirical analyses, 4.675 and 1.15 are selected as $K$ and $\kappa$ values, respectively [3, 89].

### Payload

In addition to the gross takeoff mass, each airframe is identified by its payload mass, which further describes the aircraft's mission capabilities. The baseline payloads are calculated using an industry-guided estimation,

$$m_{\text{payload}} = (1 - 0.55)(m_{\text{GTOM}}) - m_{\text{fuel}} - m_{\text{pilot}}, \tag{5.32}$$

where $m_{payload}$ is the helicopter's payload mass, $m_{GTOM}$ represents the aircraft gross takeoff mass, $m_{fuel}$ is the fuel mass, and $m_{pilot}$ is the pilot mass, all in kilograms [6]. The pilot mass is assumed to be 85 kilograms for all airframes, while the remaining parameters are based on the particular airframe and engine configuration.

## 5.3.2 Varied Parameters and Modeling Verification

After using the correlations identified in Section 5.3.1 to calculate the majority of the baseline airframe's parameters, estimations are required for the airfoil profile drag coefficient, $C_{do}$, that is used to predict the rotor drag force, and the airframe drag coefficient, $C_{Df}$, which predicts the total airframe drag (see Section 5.1.1). However, a wide range in each coefficient's potential values was observed, and thus a general estimation was not obtained from industry trends. Additionally, an estimation of the modeling accuracy was desired to ensure reasonable predictions of the baseline airframe performance characteristics.

To accomplish both goals, a set of twelve example aircraft were modeled using manufacturer and certification data, including the gross takeoff, fuel, and engine masses, rated takeoff power, propeller radius, climb speed, and engine specific fuel consumption (SFC). Appendix D lists these values that are specified by the aircraft documentation, while the remaining airframe performance parameters are calculated using the correlations provided in Section 5.3.1. From the manufacturer data, each helicopter's actual range was identified and used as the modeling target to verify the simulation's accuracy, with the airfoil profile and airframe drag coefficients tuned to improve this accuracy. After completing this process, the resulting airfoil profile and

airframe drag coefficients are 0.01 and 0.07 for the dual-engine configurations and 0.008 and 0.055 for the single-engine configurations, respectively, which fall within the range of standard industry values [3, 89][2].

Figure 5-9 displays the final comparison between the modeling predicted and manufacturer specified ranges when using these drag coefficient values. Here, each example aircraft is listed on the vertical axis with the airframe ranges corresponding to the horizontal axis. In reviewing the results, the Westland Lynx and Sikorsky S-76D have significant discrepancies in the modeling and manufacturer ranges. For the Westland Lynx, this is potentially explained by the design being a military helicopter, and thus it is like to have significantly different performance parameters. For the Sikorsky S-76D, the difference in values was not reconciled, but could be due to the manufacturer using different airframe parameters or configurations (i.e. an extra fuel tank) in their estimation. Despite these discrepancies, the remainder of the rotorcraft resulted in similar range values when comparing the manufacture data and modeling results, providing verification that the simulation parameters are appropriate estimations. Furthermore, as the modeling is used for a direct comparison between engine configuration performances when implemented in the same airframes, the absolute accuracy is not essential for this analysis.

[2]These values are allowed to be different based on the assumption that dual-engine configurations will result in a greater amount of drag

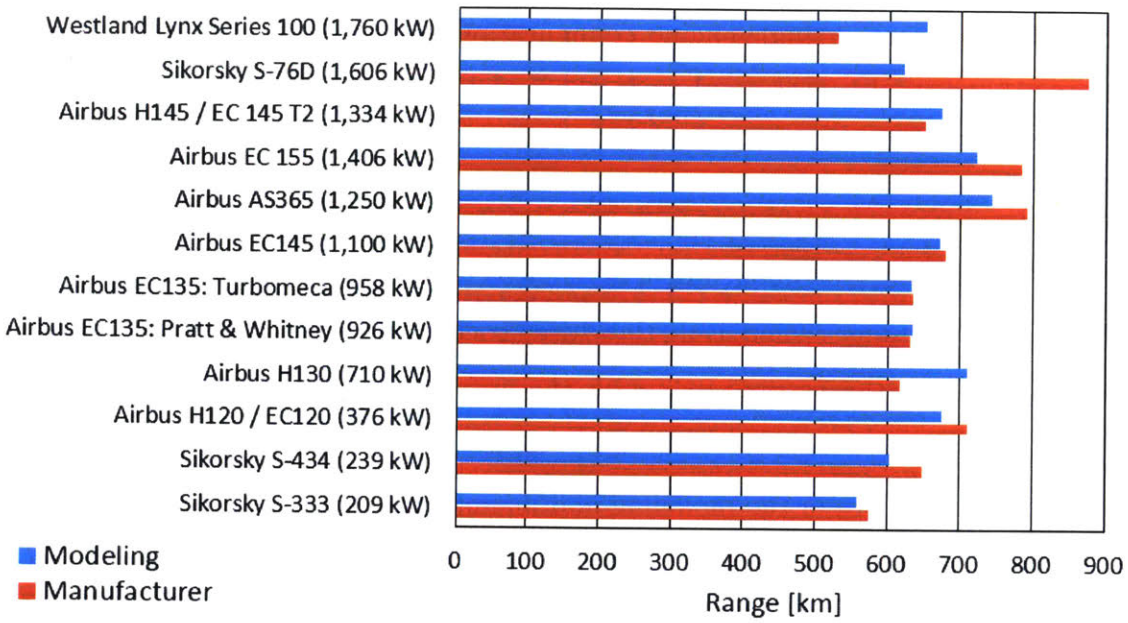


Figure 5-9: The example aircraft were tested in the flight profile model, with the output range compared to the values specified by the manufacturers [1, 80, 81, 82, 83, 84, 85, 86, 87, 88].

### 5.3.3 Baseline Airframe Characteristics

Based on the helicopter design trends that are obtained in the previous sections, a set of ten baseline airframes are designed to facilitate the comparison of each alternative engine configuration's effect on rotorcraft performance. Table 5.2 provides the resulting airframe characteristics, with additional parameters listed in Appendix D. The range of airframe gross takeoff masses (i.e. less than 6,000 kilograms) is selected based on the expectation that piston engines will only be competitive in this size region, as discussed in Section 3.5. Furthermore, the number of engines is increased from one to two after the airframe gross takeoff mass exceeded 2,500 kilograms to emulate modern helicopter trends (see Appendix D).

Table 5.2: The baseline airframe characteristics

| Airframe Number (Number of Engines) | Gross Takeoff Mass (kg) | Fuel mass (kg) | Payload (kg) | Total Power Required[a] (kW) |
|---|---|---|---|---|
| 1 (1) | 1,000 | 193 | 172 | 204 |
| 2 (1) | 1,500 | 288 | 302 | 318 |
| 3 (1) | 2,000 | 382 | 433 | 439 |
| 4 (1) | 2,500 | 475 | 565 | 565 |
| 5 (2) | 3,000 | 567 | 698 | 846 |
| 6 (2) | 3,500 | 658 | 832 | 1,009 |
| 7 (2) | 4,000 | 784 | 967 | 1,176 |
| 8 (2) | 4,500 | 837 | 1,103 | 1,347 |
| 9 (2) | 5,000 | 926 | 1,240 | 1,522 |
| 10 (2) | 5,500 | 1,013 | 1,377 | 1,702 |

[a] The total power required includes both engines if the airframe implements dual-engines, and is sized for gas turbine performance characteristics, as discussed in Section 5.2.1.

## 5.4 Airframe Performance Comparison

To summarize the overall modeling process, Figure 5-10 provides the flow of each step outlined in the preceding sections, which are described as follows. First, as part of the development of the baseline rotorcraft designs, the baseline airframes' engine (gas turbine), fuel, fuel tank, and total aircraft masses are determined based on industry trends and data. Using the baseline airframes' gross takeoff masses, the alternative engine configurations are sized to ensure adequate hot and high and, if applicable, OEI capabilities, based on the particular engine's performance trends. Following this sizing, the alternative engine configurations are conceptually mounted onto each aircraft (creating the modified airframes), while holding constant both the helicopter's gross takeoff mass and the portion of this mass allocated to the identified components (i.e. engine(s), fuel, and fuel tank). Based on the changes in the engine mass that are dictated by the engine's performance trends, the fuel and fuel tank are altered to

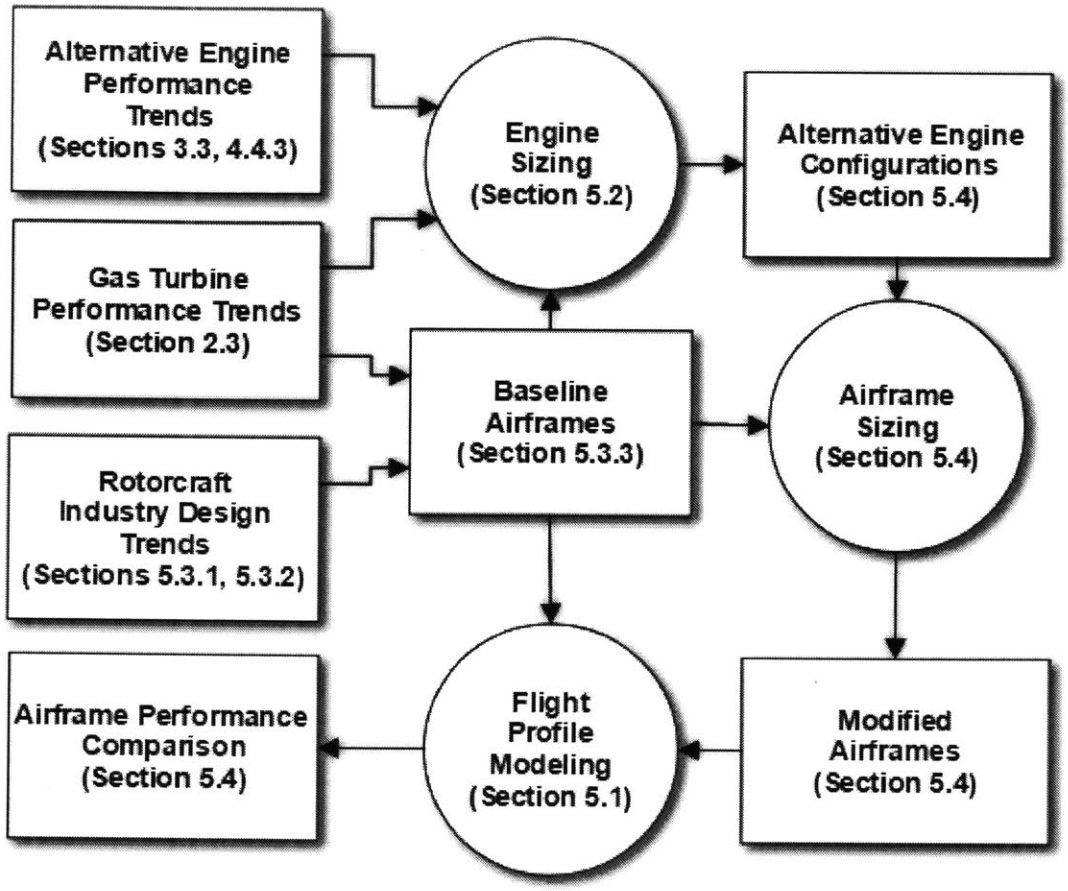


Figure 5-10: The flight profile modeling diagram shows the steps that are implemented to compare the performance of gas turbines and alternative engine configurations.

maintain the amount of the gross takeoff mass allocated to the combination of these components, which ensures that the remainder of the aircraft's design is held constant. After completing the conceptual engine swap, the modified airframes containing the new engine configurations are tested in the flight profile modeling, along with the baseline airframes. The resulting performances are then evaluated to identify the advantages and disadvantages of the alternative engines compared to those of the standard gas turbines across various aircraft sizes, providing the feasibility of their implementation in rotorcraft applications. The following sections outline the results for each alternative engine configuration.

### 5.4.1 Standard Implementation

For the standard configurations, the piston engines are evaluated across each airframe, with the four-stroke diesel engine providing the heaviest and most efficient architecture, and the two/four-stroke gasoline engine representing a lighter design with lower efficiency. After conceptually swapping the gas turbine engines with the four piston engine designs, the airframe's mass allocation (i.e. distribution of available mass between the engine, fuel, and fuel tank) is shifted based on the particular configuration, with Appendix D providing the individual mass values for each airframe. Figure 5-11 shows the general results, where the vertical axes correspond to the mass of each identified category, and the horizontal axes list each airframe equipped with the various engine designs, using the following abbreviations: gas turbine (GT), four-stroke diesel engine (4-S D.), two-stroke diesel engine (2-S D.), four-stroke gasoline engine (4-S G.), and two/four-stroke gasoline engine (2/4-S G.). For this allocation, the airframe mass is sectioned into the fuel, engine(s), payload, and balance (i.e. the remainder of the aircraft, including the fuel tank), adding up the airframe's gross takeoff mass. As illustrated by these results, the piston engines are significantly heavier than the gas turbines, which drastically reduces the amount of fuel that the aircraft can carry. In particular, for all of the dual-engine airframes, the four-stroke diesel engine masses are greater than the allowable amount, with the two-stroke diesel engines experiencing the same scenario in airframes 9 and 10. This results in the total airframe mass exceeding the specified limit, indicating that these particular combinations of engines and airframes are unfit for implementation.

After calculating these distributions of masses, the flight profile modeling evaluated each airframe when equipped with the identified engine designs to determine the resulting changes in performance. In addition to the amount of fuel that is carried (and consumed), the airframe's range is calculated and compared between the engine designs as the most important performance parameter. Figure 5-12 provides this result, where the aircraft range corresponds to the vertical axes and is compared across each identified airframe and engine configuration listed on the horizontal axes.

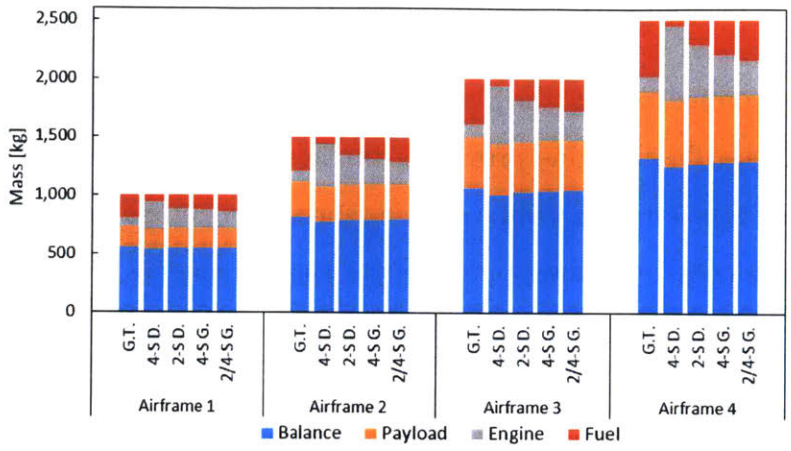


(a) Single-engine aircraft

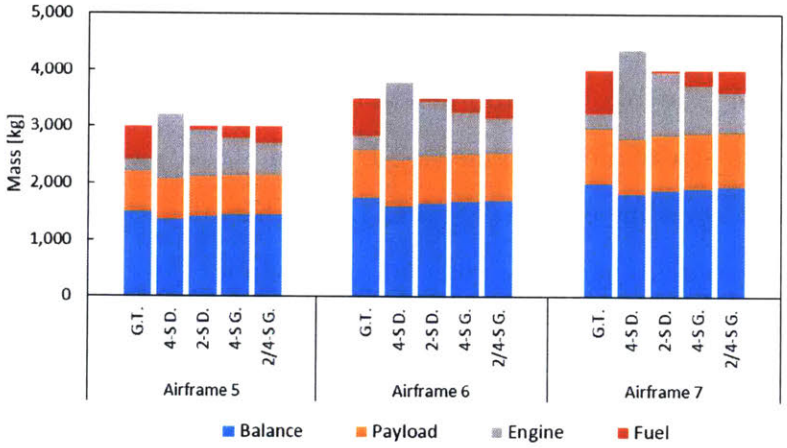


(b) Dual-engine aircraft, part 1

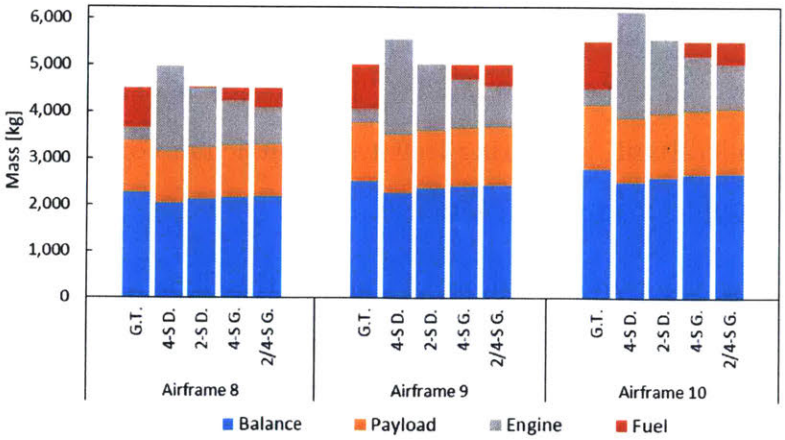


(c) Dual-engine aircraft, part 2

Figure 5-11: The changes in mass between engine configurations requires an adjustment to the amount of fuel that an airframe can carry, with the significantly heavier piston engines displacing a large portion of the airframe's fuel.

Here, a portion of the standard piston engine configurations achieve substantial range improvement in single-engine configurations, with the lone exception being the four-stroke diesel design. For all four of the single-engine aircraft, the two/four-stroke gasoline engine provided the largest advantage, with a peak range improvement of 47% for the first airframe. Furthermore, the four-stroke gasoline engine exhibited improved range in all four of these aircraft, while the two-stroke diesel design achieved an advantage in airframes one and two. Despite these advantages, all four piston engine configurations exhibited declining performance relative to the gas turbines as the airframe sizes increased. This is particularly evident in Figures 5-12b and 5-12c, where, in addition to the two- and four-stroke diesel engines not having enough fuel to fly (with the exception of the fifth airframe for the two-stroke), the remaining gasoline engines experience declining range values while the gas turbine configuration exhibits the opposite trend. Thus, when considering the impact on the aircraft's range, the results indicate that the standard piston engine configurations are only suited in small, single-engine airframes where the engine mass does not outweigh the improvements in efficiency. Specifically, the two/four-stroke engine provides the best option for these aircraft, while both the four-stroke gasoline and two-stroke diesel configurations show promise in the smallest airframes.

Furthermore, the best-range cruise speed is compared between the standard implementation designs, resulting in Figure 5-13. Here, the vertical axes plot the average cruise speed of each standard engine configuration and airframe, as specified by the horizontal axes. Due to the gas turbine and piston engine SFC trends provided in Sections 2.3 and 3.3, the configurations have different optimum power loads; gas turbines are most efficient when operating at their rated power output, while piston engines reach an optimum efficiency between approximately 50% and 70% of their rated maximum power. Because of this difference, the best-range speed for piston engines is significantly lower than that of gas turbines. Thus, aside from the improvement in fuel consumption, the piston engine configurations must cruise at lower speeds to achieve their maximum range.

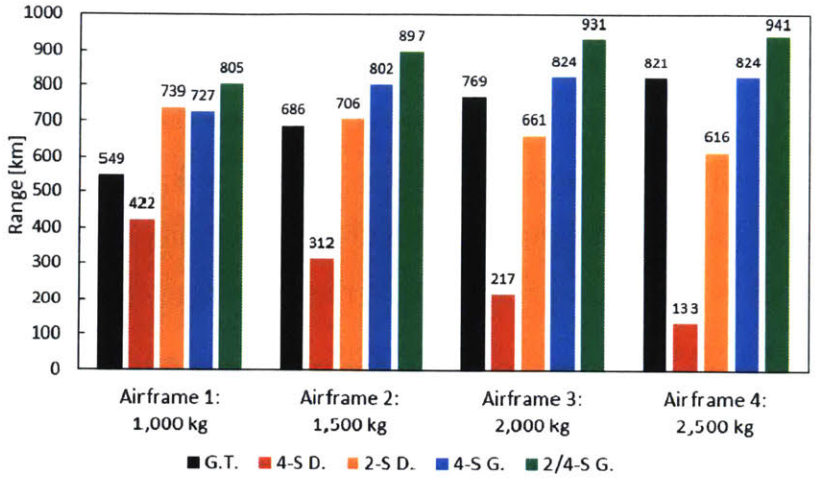


(a) Single-engine aircraft

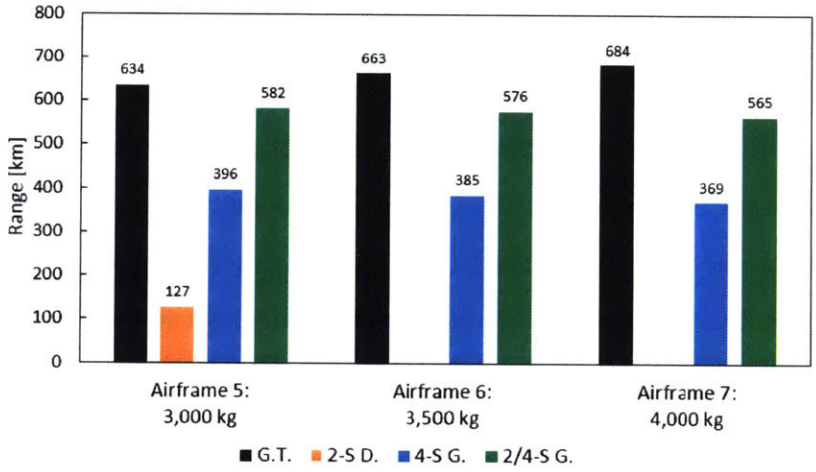


(b) Dual-engine aircraft, part 1

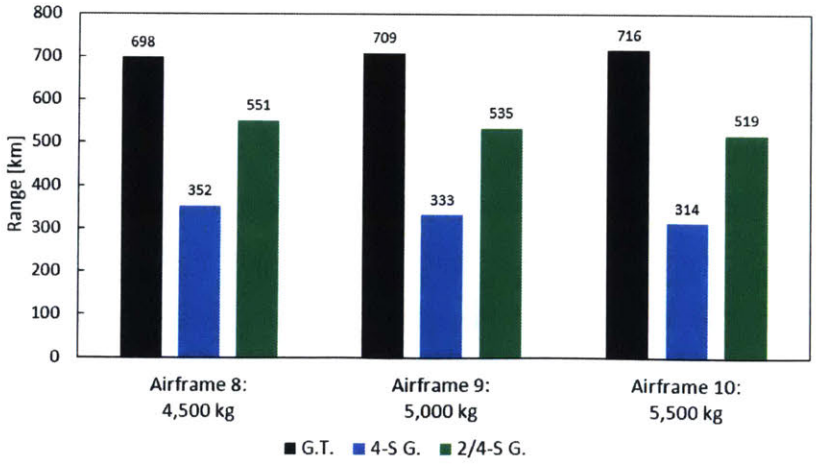


(c) Dual-engine aircraft, part 2

Figure 5-12: The modified airframes are modeled to compare each engine configuration's effect on the aircraft range.

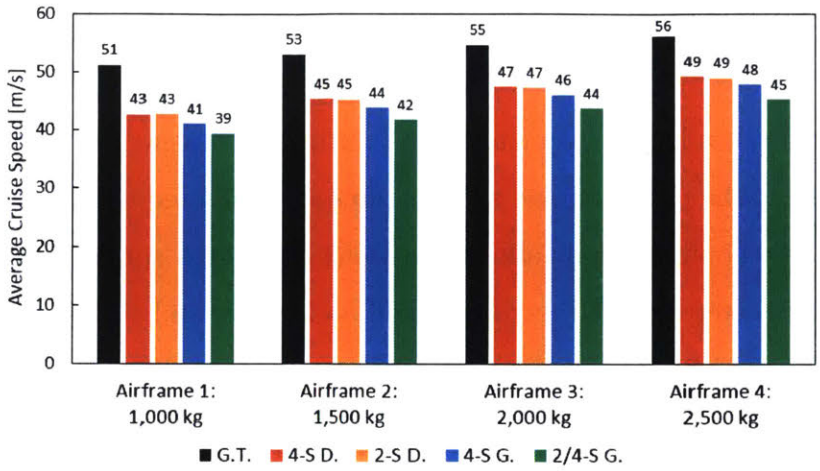


(a) Single-engine aircraft

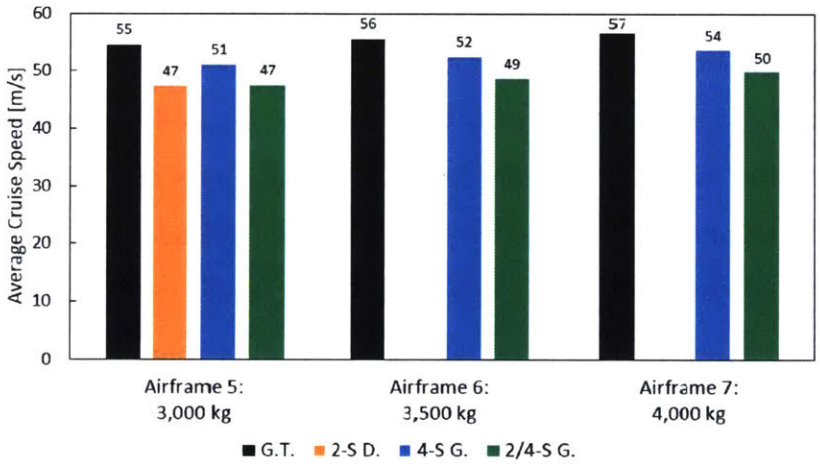


(b) Dual-engine aircraft, part 1

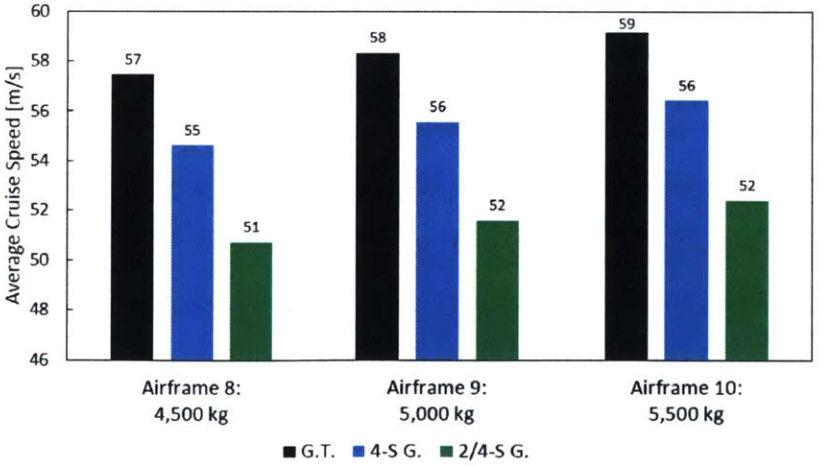


(c) Dual-engine aircraft, part 2

Figure 5-13: The operational characteristics of each engine configuration results in different best-range cruise speeds.

### 5.4.2 Hybrid Design

In addition to the standard implementation, four hybrid designs incorporating a gas turbine and each of the piston engine architectures are evaluated during the flight profile modeling. The configurations aimed to combine the high specific power of a gas turbine, with its power required during takeoff and climb, and the high efficiency of the piston engine, which exclusively provides the power needed for cruising. For these configurations, the power required by the gas turbine and piston engine are calculated to be equal, based on their hot and high deratings and the gas turbine's OEI power boosting capability (see Section 5.2.1). Figure 5-14 illustrates the results of each airframe's mass allocation, in addition to the standard gas turbine data for reference, with Appendix D provides the individual mass values and additional parameters for each airframe. Here, similar to Figure 5-11, the vertical axis represents the mass of each identified category, divided into the fuel, engines, payload, and balance (i.e. the remainder of the aircraft), and the horizontal axis provides each airframe equipped with the various engine designs, using the following abbreviations: gas turbine engine(s) (GT), a four-stroke diesel engine and gas turbine (H. 4-S D.), a two-stroke diesel engine equipped with a gas turbine (H. 2-S D.), a four-stroke gasoline engine and gas turbine (H. 4-S G.), and a two/four-stroke gasoline engine paired with a gas turbine (H. 2/4-S G.).

As anticipated, the piston engines account for significantly more mass than the gas turbines, illustrating the discrepancy between the engine designs' specific powers as the engines are sized to produce equal power output (see Appendix D). Following these allocations, each modified airframe is modeled to evaluate the associated changes in aircraft performance (i.e. range and cruise speed). Figure 5-15 provides the first of these results, where the aircraft range corresponds to the vertical axis for each hybrid engine pairing identified on the horizontal axis. For the traditional single-engine aircraft, the hybrid two-stroke implementation provides the highest performance in airframe 1, with a 21% increase in range over that of the standard gas turbine. Alternatively, the two/four-stroke engine achieves the greatest range in airframes

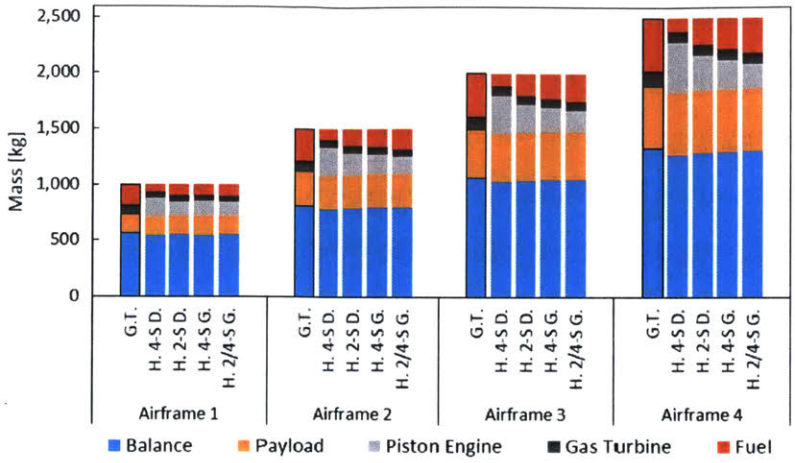


(a) Traditional single-engine aircraft

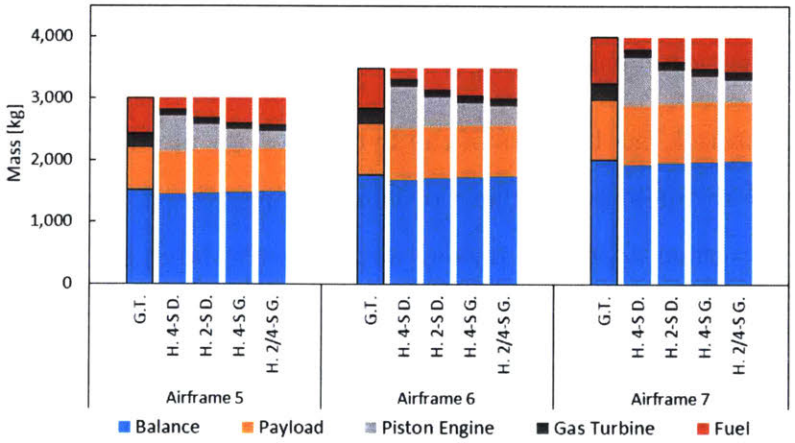


(b) Traditional dual-engine aircraft, part 1

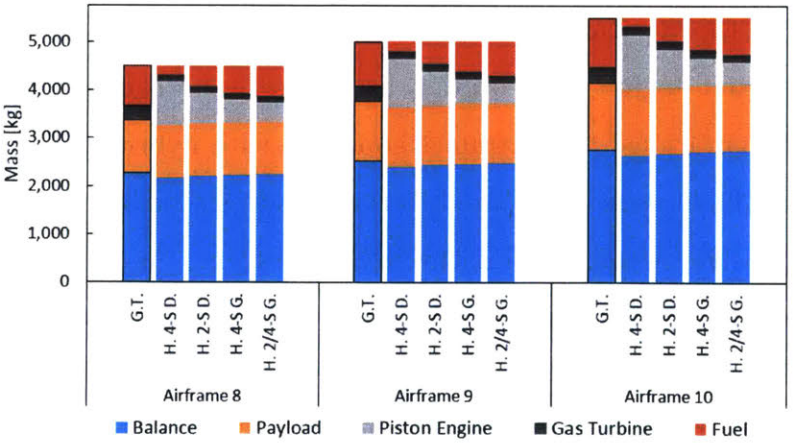


(c) Traditional dual-engine aircraft, part 2

Figure 5-14: The changes in mass between the hybrid engine configurations requires adjustments to the amount of fuel that an airframe can carry, as is evident when compared to the standard gas turbine configuration, included and outlined for reference.

2 and 3, with modest improvements of 6% and 3%, respectively. Similar to the standard configurations, these benefits are mitigated at higher airframe sizes, where, for airframe 4, only the two/four-stroke hybrid design is capable of matching the gas turbine configuration's performance. Furthermore, these trends are repeated in the traditional dual-engine aircraft, where the two/four-stroke gasoline engine's range exceeds all configurations for each airframe. This benefit is at a maximum for airframe 5 with a 29% increase in range over the standard gas turbine implementation, and is diminished at higher helicopter sizes, with a final range improvement of 10% for airframe 10. As evident in both the single- and dual-engine categories, the hybrid designs provide the greatest advantage in smaller aircraft, while gas turbines become more competitive with increasing size.

As previously stated, the benefits of the hybrid designs are due to the helicopter's allocation of power throughout the flight profile. During takeoff, the airframe requires both engines to produce adequate power, and thus the large specific power of the gas turbine minimizes the require engine mass. On the other hand, while cruising, the airframe deactivates the gas turbine and runs exclusively on the piston engine, leveraging the higher efficiency. This latter feature occurs at the cost of lower best-range cruise speed (due to less power being used during flight), as illustrated in Figure 5-16. Here, the vertical axis is the best-range cruise speed which is compared for each airframe and engine configuration listed on the horizontal axis. Similar to the standard configurations, the airframes equipped with hybrid designs cruise at a significantly lower flight speed compared to those with gas turbines, with this trend arising from a similar mechanism for the hybrid designs. As these configurations maximize their range by exclusively drawing power from their piston engine during cruise, only half of the total available airframe power is accessible during this portion of flight. The reduction in available cruise power, in addition to the piston engine's efficiency rising in part-load operation (see Section 3.3), results in the best cruise speed shifting to lower values. Thus, despite improvements in fuel consumption, the hybrid airframe designs must travel at lower cruise speeds to achieve their maximum range.

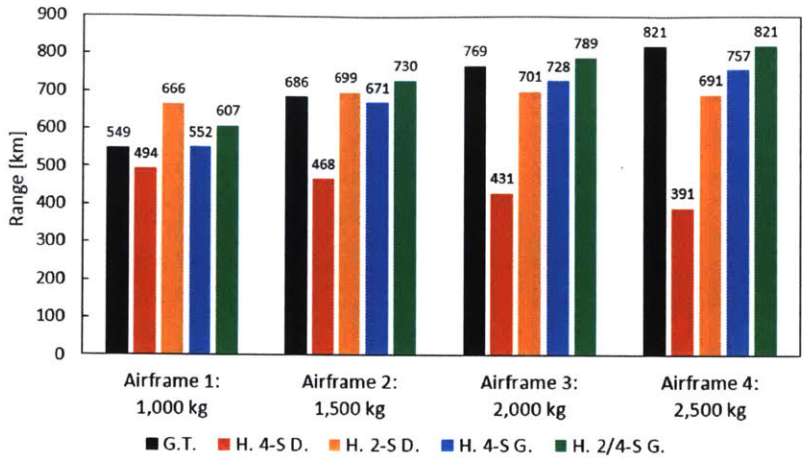


(a) Traditional single-engine aircraft

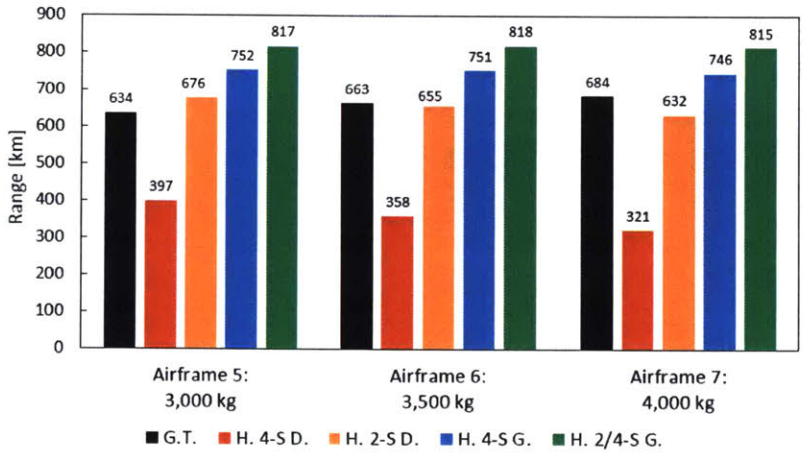


(b) Traditional dual-engine aircraft, part 1

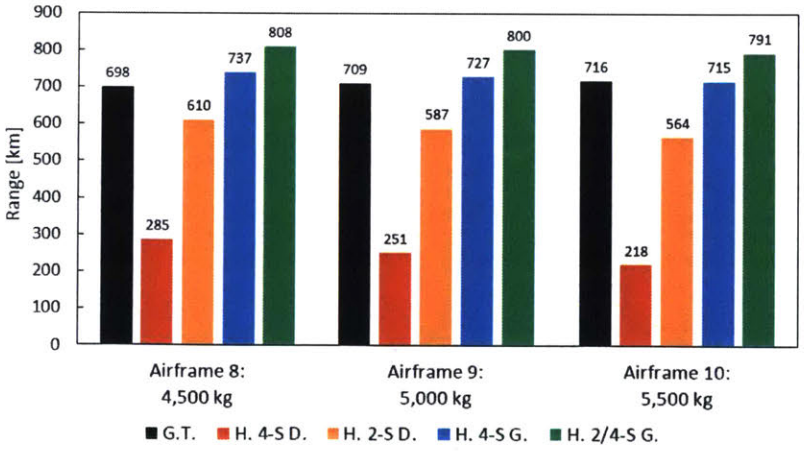


(c) Traditional dual-engine aircraft, part 2

Figure 5-15: The modified airframes with hybrid engine designs are modeled to compare each configuration's effect on the aircraft ranges. For reference, the standard gas turbine configuration is included.

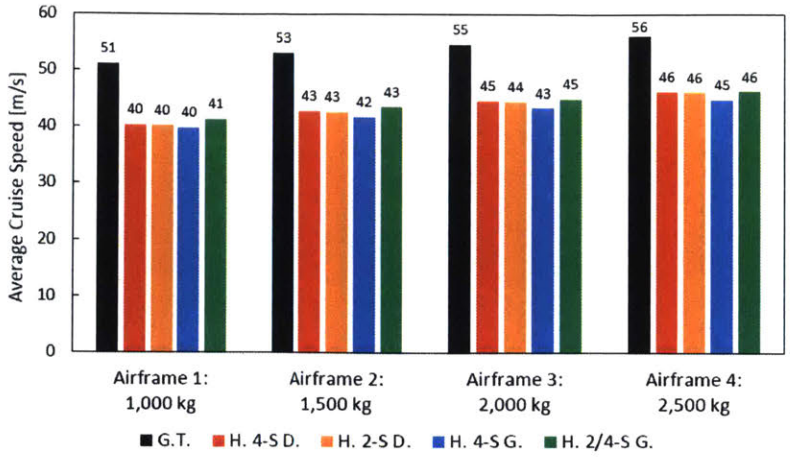


(a) Traditional single-engine aircraft

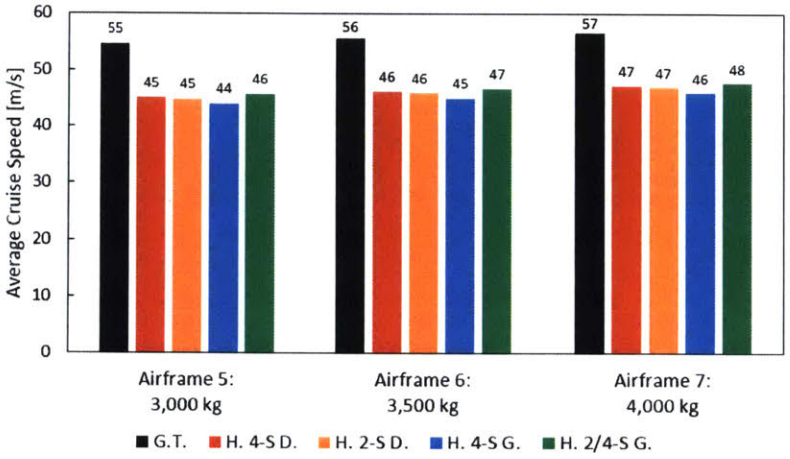


(b) Traditional dual-engine aircraft, part 1

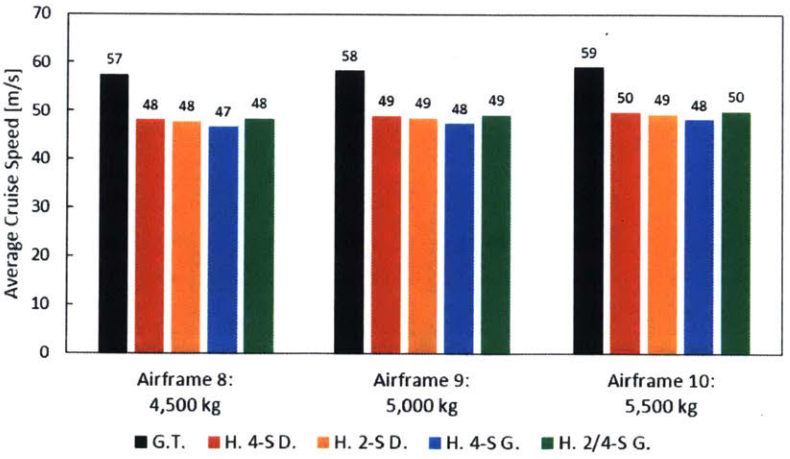


(c) Traditional dual-engine aircraft, part 2

Figure 5-16: While each hybrid design incorporates a gas turbine, the piston engines cause the cruise speeds to be substantially lower to maximize range, due to the different optimum operating points for these configurations.

### 5.4.3 Auxiliary Engine Configurations

Finally, the auxiliary engine configurations are evaluated and compared to the standard gas turbine implementations. These designs incorporated either single or dual main piston and gas turbine engines, matching the traditional single- or dual-engine airframes, while installing an auxiliary gas turbine. The auxiliary engine serves to provide power when needed during takeoff and OEI scenarios, while the main engines handle the remainder of the flight. This allows the airframe to leverage the piston engines' superior efficiency or, for the gas turbine auxiliary configurations, enables the two main engines to operate at high loads in cruise, which improves their SFC (see Section 2.3). The distribution of the total available power between the main and auxiliary engines is optimized to maximize the configuration's range, while ensuring sufficient OEI and hot and high capabilities. Figures 5-17 and 5-18 show the resulting mass and power allocations, with Appendix D providing values for the individual masses, power allocations, and the associated parameters for each airframe.

For Figure 5-17, the vertical axes correspond to the mass of each identified category, including the fuel, engines, payload, and balance (i.e. the remainder of the aircraft). For Figure 5-18, the vertical axes are the percent of the total rated takeoff power allocated to the main and auxiliary engines. In both charts, the horizontal axis identifies each airframe equipped with the various engine designs, using the following abbreviations: gas turbine engine(s) (GT, Std. for standard implementation, Aux. for auxiliary engine configuration), four-stroke diesel main engine(s) (Aux. 4-S D.), two-stroke diesel main engine(s) (Aux. 2-S D.), four-stroke gasoline main engine(s) (Aux. 4-S G.), and two/four-stroke gasoline main engine(s) (Aux. 2/4-S G.).

In the single-main-engine airframes, the optimization results in different trends for the various engine designs. For the gas turbine and two/four-stroke gasoline main engine configurations, the airframe's range is maximized by minimizing the auxiliary engine's size, suggesting that these designs do not benefit substantially from an auxiliary configuration. On the other hand, the four- and two-stroke diesel main engine configurations allocate a substantial fraction of their total power to the auxil-

iary engine in each of these single-main-engine airframes, showing that these designs are improved by the auxiliary engine. Falling between these two extremes, the optimization of the four-stroke gasoline main engine design results in minimum auxiliary engine power when equipped in airframes 1 through 3, with this trend reversing in airframe 4. In this aircraft design, a substantial portion of the airframe's power is allocated to the auxiliary engine, which indicates that this design benefits form the auxiliary engine in larger airframe sizes.

For each of the dual-main-engine aircraft, the auxiliary engines account for a significant portion of the total engine mass, with limited variations in the power allocations across different configurations and airframes. These two trends are partially caused by the hot and high and OEI restrictions that are imposed on the power allocation process, as described in Section 5.2[3].

The flight profile modeling is conducted using these configurations, with the results shown in Figure 5-19. The auxiliary configurations show substantial range improvements for all modeled airframes when compared to the standard gas turbine designs. Specifically, the two/four-stroke gasoline engine achieves the maximum range for airframes 1 through 6, which encompasses all of the single-main-engine aircraft (airframes 1 through 4), as well as the first two dual-main-engine airframes (5 and 6). These improvements in range vary between a maximum of a 46% increase for airframe 1 down to a 10% improvement for airframe 6. For the remainder of the dual-main-engine aircraft (i.e. airframes 7 through 10), the gas turbine auxiliary configuration achieves the greatest range, with a maximum improvement of 16% over the standard gas turbine implementation for airframe 10.

A comparison of the aircraft's best range speed is shown in Figure 5-20, where the airframe's cruise speed is the vertical axis vs. the auxiliary configuration pairings provided on the horizontal axis, with the standard gas turbine's speed included for reference. Similar to the hybrid designs, the auxiliary configurations travel at significantly lower cruise speeds to optimize the airframes' ranges, with the lone exception being the auxiliary gas turbine design incorporated in the single-main-engine

[3]The limited spread in these power allocations is also due to these performance restrictions.

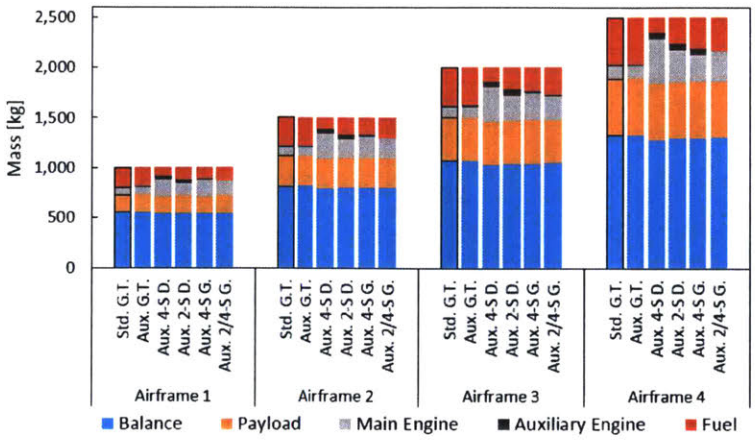


(a) Single-main-engine aircraft

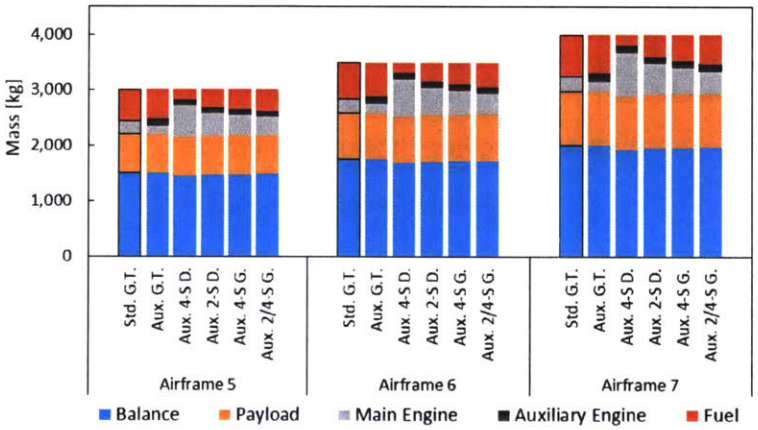


(b) Dual-main-engine aircraft, part 1

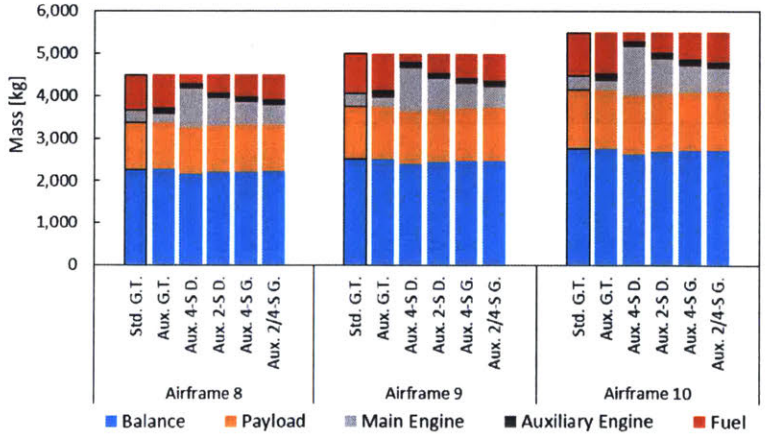


(c) Dual-main-engine aircraft, part 2

Figure 5-17: The amount of power allocated to the main and auxiliary engines is optimized for each airframe and auxiliary engine configuration pairing, resulting in different mass allocations.

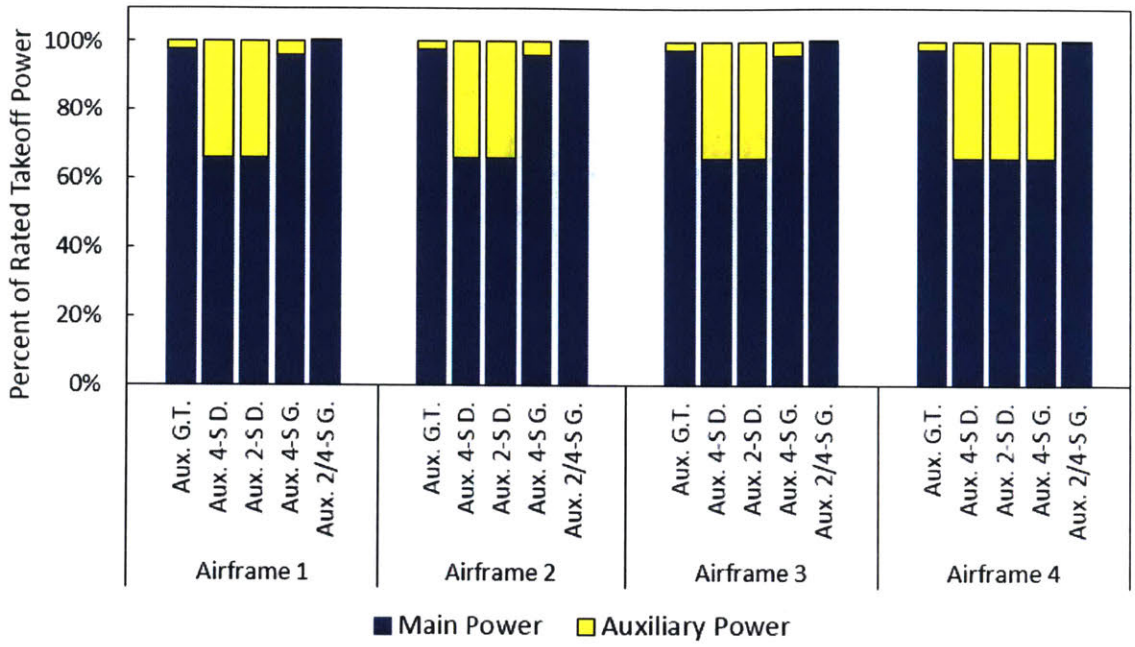


(a) Single-main-engine aircraft

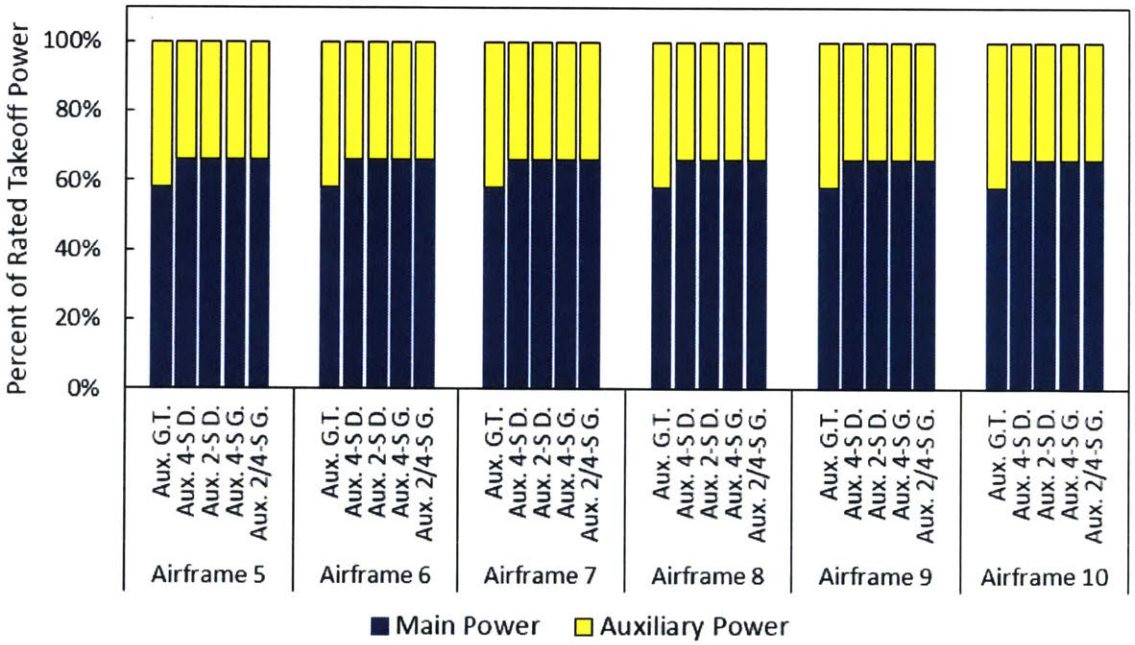


(b) Dual-main-engine aircraft

Figure 5-18: The auxiliary engine configurations optimized the power allocation between the main and auxiliary engines to maximize each airframe's range. The allowable allocation limits restricted this process to ensure the airframe possessed adequate OEI capabilities, as calculated in Appendix E.

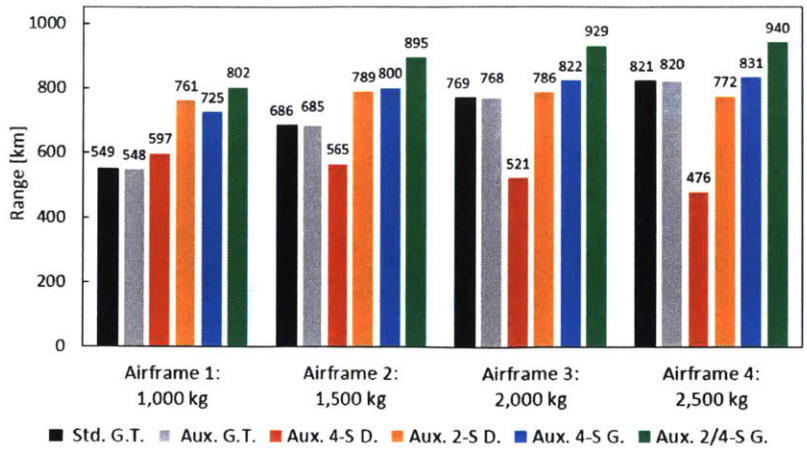


(a) Single-main-engine aircraft

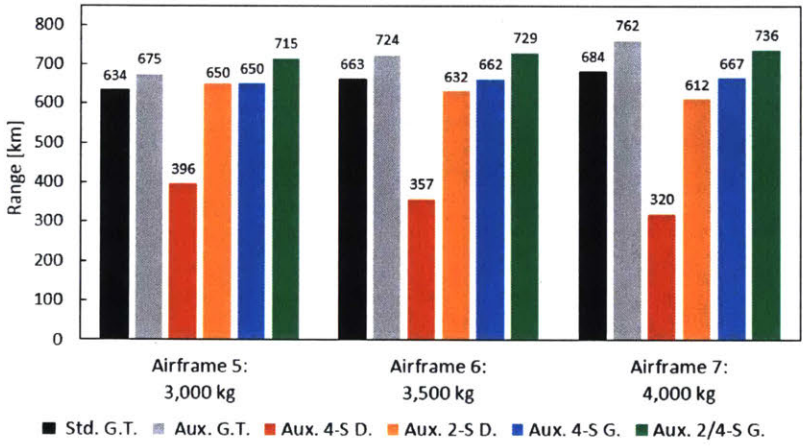


(b) Dual-main-engine aircraft, part 1

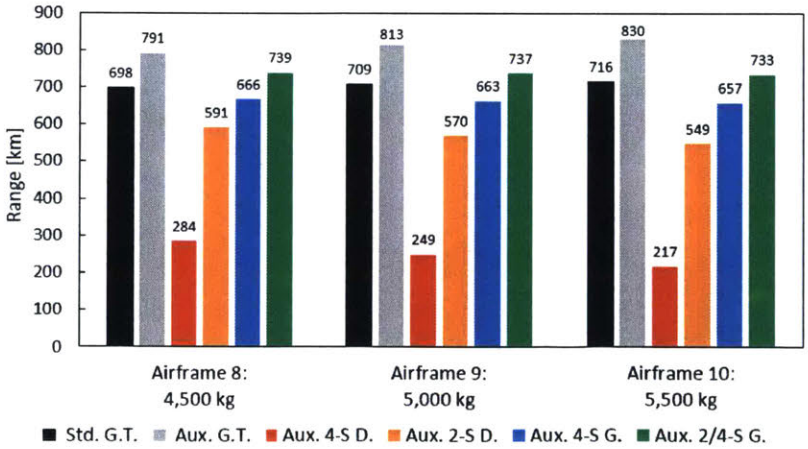


(c) Dual-main-engine aircraft, part 2

Figure 5-19: The auxiliary engine configurations achieved varying degrees of range improvement, as demonstrated by comparing their results with the standard gas turbine implementation.

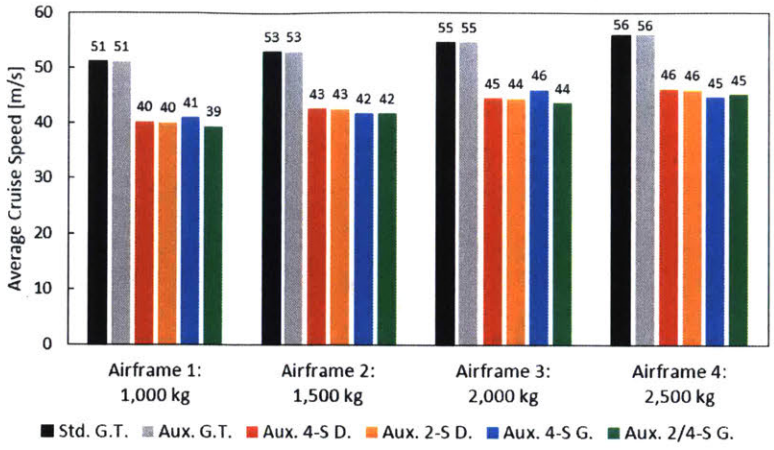


(a) Single-main-engine aircraft

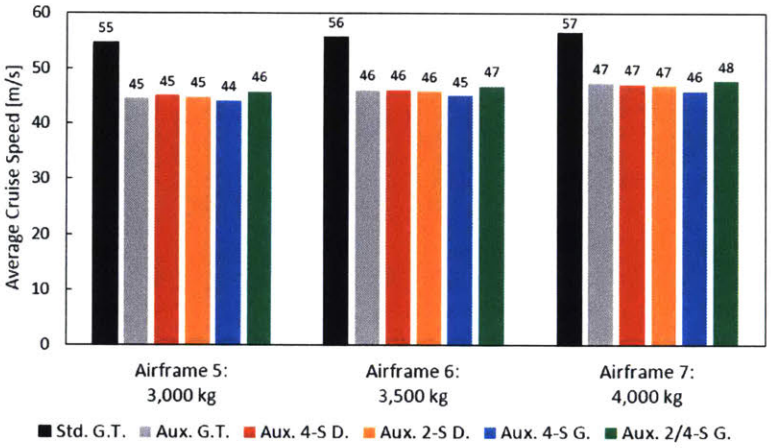


(b) Dual-main-engine aircraft, part 1

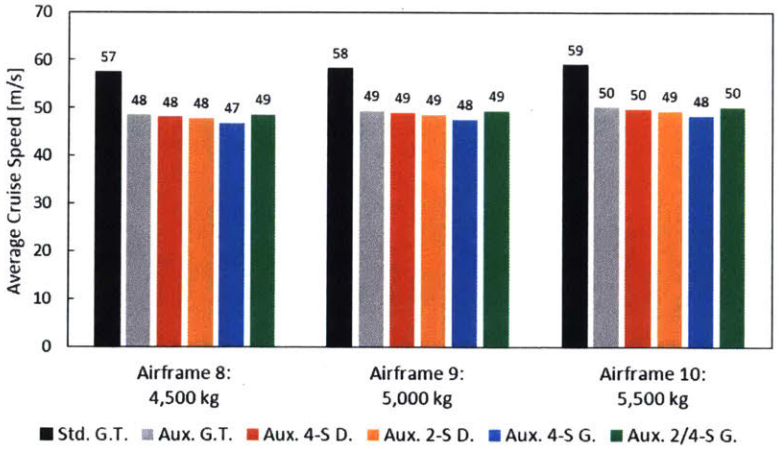


(c) Dual-main-engine aircraft, part 2

Figure 5-20: While the gas turbine auxiliary engine configuration achieves similar cruise speeds in the traditional single-engine airframes, the piston engine designs, as well as the gas turbine auxiliary design in dual-main-engine airframes, travel at significantly lower flight speeds.

airframes (due to the minimal impact of the small auxiliary engine). The combination of lower power available for the main engines (all auxiliary configurations) and the SFC trends at part-load (piston configurations) are the driving forces that require the airframes to travel at lower speeds to maximize their range.

### 5.4.4 Combined Range Comparison

After evaluating each implementation strategy independently, the results are combined to identify the trends in airframe performance. In this final analysis, the data is parsed to exclusively consider configurations that exceeded the standard gas turbine's performance in at least one of the airframes. Furthermore, this evaluation is completed by normalizing the configurations' range values by the baseline gas turbine's range, providing a comparisons of the fractional change in range for each engine design and airframe. The results are split into Figures 5-21 and 5-22 for the traditional single-engine and dual-engine airframes, respectively. Here, the vertical axes represent the fractional change in range of the various engine designs compared to the baseline gas turbine configuration, and the horizontal axes plot each airframe, with the gross takeoff mass listed on the bottom of the chart and the corresponding airframe payload provided above the figure.

#### Traditional Single-engine Airframes

Many engine configurations achieved substantial range improvements when equipped in the traditional single-engine aircraft, led by the two/four-stroke standard design with range improvements between 47% for airframe 1 (1,000 kilogram gross takeoff mass, GTOM) and 15% for airframe 4 (2,500 kilogram GTOM). For the diesel piston engines, the four-stroke auxiliary engine design provided a modest increase in range for airframe 1 (albeit lower than the majority of other engines), but dropped off drastically in larger aircraft. For the two-stroke diesel engines, the auxiliary design achieved performance advantages in airframes 1 through 3, while the standard and hybrid designs provided improvements in range up to airframe 2 (1,500 kilogram

GTOM). Thus, when comparing these diesel configurations for the traditional single-engine airframes, the two-stroke auxiliary design provides the highest airframe range due to the ideal allocation of power and efficiency.

Alternatively, the gasoline hybrid and auxiliary designs achieved varying degrees of range improvement. For the two/four-stroke engine, the hybrid design provided a modest advantage, which, with increasing airframe size, is diminished to matching the performance of the gas turbine in airframe 4 (2,500 kilogram GTOM). On the other hand, both the four-stroke and two/four-stroke gasoline auxiliary engine designs improved each airframe's range, but only matched the performance of the piston engine architectures' standard implementations. Thus, due to the added complexity of incorporating two different engines, the standard configuration is the favored four-stroke and two/four-stroke implementations in these airframes.

However, despite these improvement capabilities, each piston engine configuration experienced significant declines in performance with increasing airframe sizes. This indicate that, for single-engine configurations, many piston engine designs would become further limited in airframes that exceed 2,500 kilograms in gross takeoff mass. While these engine combinations experienced a diminishing advantage with increasing aircraft size, each identified designs shows potential for feasibility in, at a minimum, a portion of the considered sizes of single-engine aircraft.

### Traditional Duel-Engine Airframes

For the traditional dual-engine airframes, the number of configurations that provided range improvements over the standard gas turbine is lower, with only auxiliary and hybrid designs and no diesel four-stroke engines. While smaller than the traditional single-engine airframe results, the alternative engine configurations provided improvements in range across the entire set of airframes. For the piston engines, the hybrid two/four-stroke gasoline engine design provided the largest range advantage, with a maximum of a 29% increase when equipped in airframe 5 (3,000 kilogram GTOM), while the auxiliary gas turbine configuration achieved the largest improvements in airframes 9 and 10 (5,000 and 5,500 kilogram GTOM), reaching a maximum of a

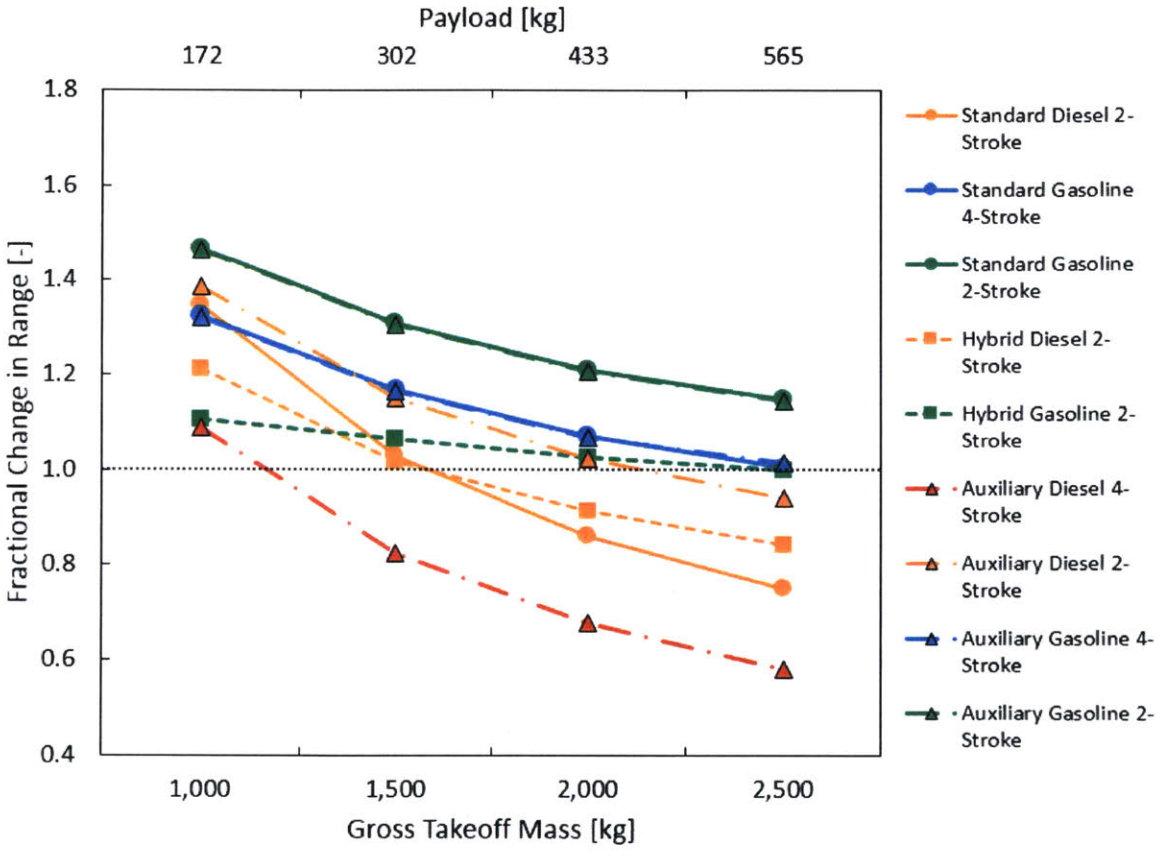


Figure 5-21: The fractional changes in range achieved by the best performing engine configurations are plotted for the traditional single-engine airframes.

16% increase in range for airframe 10. For the four-stroke and the two/four-stroke gasoline designs, the hybrid configurations outperformed the auxiliary engine implementation across all ten airframes; the four-stroke auxiliary and hybrid gasoline designs provided range advantages up until airframes six (3,500 kilogram GTOM) and ten (5,500 kilogram GTOM), respectively, while the two-stroke auxiliary and hybrid implementations achieved improved range in all modeled dual-engine airframes. Similarly, the diesel two-stroke hybrid configuration provides slightly higher ranges than the auxiliary implementation, with both designs initially achieving improvements in range that are lost in airframes 6 through 10.

However, analogous to their implementation in the traditional single-engine airframes, each piston engine design experienced a significant decline in performance with increasing airframe size, culminating in airframe 10, where only the two/four-stroke hybrid and auxiliary engines achieve an improvement in range. Based on this trend, the performance advantages are mitigated in greater aircraft sizes for all piston engine designs, with the exception of the two/four-stroke hybrid implementation. Alternatively, the auxiliary gas turbine configurations experiences the opposite trend, where the design's range improvement increases with the airframe sizes. Thus, when considering the sizes of aircraft evaluated in this analysis, the alternative engine configurations provide significant improvements in range and fuel consumption compared to the standard gas turbine implementations, at the expense of lower flight speeds (with the exception of the auxiliary gas turbine configuration in traditional single-engine airframes).

## 5.5 Uncertainty Impact

The results evaluated in the previous sections were developed using multiple trends compiled from industry data, including engine masses, fluid volumes, SFCs, and part-load efficiencies. With these trends comes inherent uncertainty in their accuracy, due to the variations in the collected data. To estimate the impact of the potential errors, the results are calculated after accounting for the variance in the piston engine mass

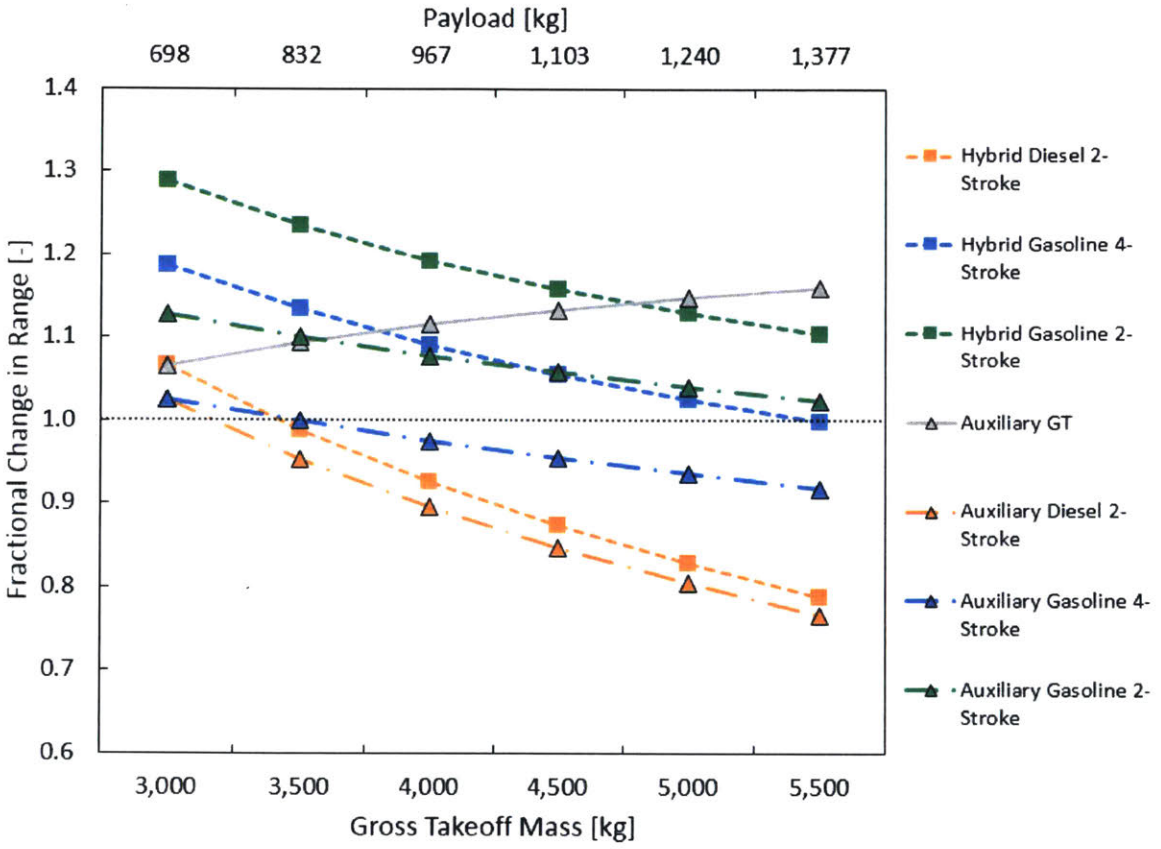


Figure 5-22: The fractional changes in range achieved by the best performing engine configurations are plotted for the traditional dual-engine airframes.

predictions, including the dry engine and fluid masses. While uncertainty exists in all of the populated trends, the impact of the engine masses demonstrates the sensitivity of these results to changes in the input data.

### 5.5.1 Uncertainty Calculation

For the piston engine dry masses, confidence bounds of one standard deviation (i.e. 64.2%) for each linear curve fit's coefficients were calculated by MATLAB's "confint" function, with these bounds defining the interval that has a 64.2% probability of containing the true curve fit. Using the resulting coefficients, the upper and lower bound trends for the diesel four-stroke, diesel two-stroke, and gasoline four-stroke engines were compiled,

$$m_{\text{D. 4-S, dry, UB}} = 1.233 * P_{\text{engine}}, \tag{5.33}$$

$$m_{\text{D. 4-S, dry, LB}} = 1.182 * P_{\text{engine}}, \tag{5.34}$$

$$m_{\text{D. 2-S, dry, UB}} = 0.923 * P_{\text{engine}} + 61.3, \tag{5.35}$$

$$m_{\text{D. 2-S, dry, LB}} = 0.695 * P_{\text{engine}} - 35.4, \tag{5.36}$$

$$m_{\text{G. 4-S, dry, UB}} = 0.571 * P_{\text{engine}} + 87.1, \tag{5.37}$$

$$m_{\text{G. 4-S, dry, LB}} = 0.490 * P_{\text{engine}} + 24.2, \tag{5.38}$$

where each $m$ refers to the particular engine's predicted dry mass in kilograms, D. is the abbreviation of diesel, G. is the abbreviation for gasoline, 2-S and 4-S represent two- and four-stroke configurations, respectively, UB corresponds to the engine's upper bound trend, LB is the engine's lower bound trend, and $P_{engine}$ represents the engine's rated takeoff power in kilowatts. The mass-power relationship for two/four-stroke gasoline engines is based on the four-stroke relations (Equations 5.37 and 5.38). The four-stroke trends were modified to account for the 25% increase in power when switching form four-stroke operation to the two-stroke mode, as well as the increase (and uncertainty) of the mass of the supercharging system for the two/four-stroke

configuration,

$$m_{\text{G. 2/4-S, dry, UB}} = 0.571 * \left(\frac{P_{\text{engine}}}{1.25}\right) + 87.1 + 12.5, \tag{5.39}$$

$$m_{\text{G. 2/4-S, dry, LB}} = 0.490 * \left(\frac{P_{\text{engine}}}{1.25}\right) + 24.2 - 12.5. \tag{5.40}$$

Here, $m_{G.\ 2/4\text{-}S,\ dry}$ refers to the two/four-stroke engine's predicted dry mass in kilograms, UB and LB correspond to the engine's upper and lower bound trends, respectively, $P_{engine}$ represents the engine's rated takeoff power in kilowatts, and the +/- 12.5 (kilograms) factor corresponds to half of the assumed increase in mass for the two/four-stroke engine's supercharging system (see Section 4.4). This latter adjustment is made to incorporate the approximate uncertainty in the supercharging mass prediction, as the value was assumed based on sparse industry data. To illustrate the difference between the original trends and the new fits that account for the uncertainty in the data, Figure 5-23 was compiled for the four-stroke diesel, two-stroke diesel, and four-stroke gasoline engines. Here, the vertical axes provide the engine's mass, the horizontal axes represents the engine's rated takeoff power, and the identified trends are included for comparison. Based on these graphs, it is evident that the diesel two-stroke engine provides the most uncertain results, due to the scarcity of data and the wide spread in values. On the other hand, the diesel four-stroke engines provide the most accurate fit, with the gasoline four-stroke engines falling in-between.

In addition to the piston engine dry masses, the coolant and oil volumes were predicted using industry trends with inherent uncertainty. Due to their minimal impact on the overall engine masses and the limited data used to compile the trends, the uncertainty in these values is taken to equal the largest difference between the data points and their corresponding trend-predicted volumes. This resulted in data spreads of six liters for the coolant fluid and two liters for the oil, with these volumes added or subtracted to the baseline trend-predicted values to account for the upper and lower uncertainty bounds in the data.

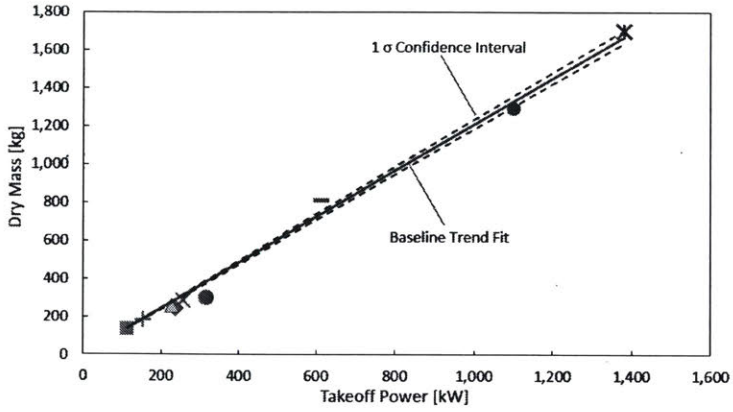


(a) Diesel four-stroke engines

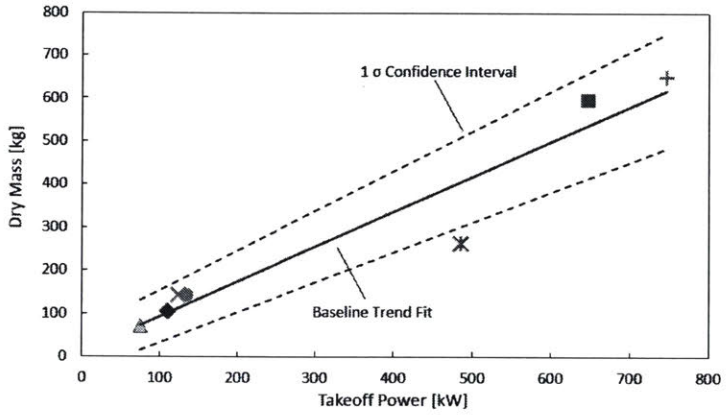


(b) Diesel two-stroke engines

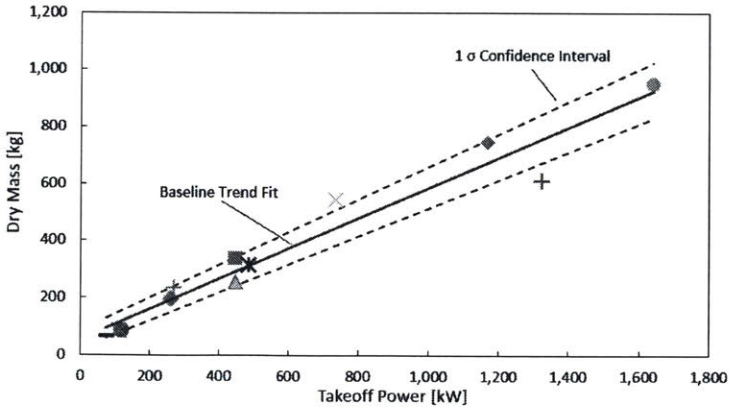


(c) Gasoline four-stroke engines

Figure 5-23: The variation in the industry data results in uncertainty in the calculated piston engine trends, represented by the standard deviation confidence bounds.

### 5.5.2 Modeling Impact

Using the upper and lower engine mass bounds, in addition to the coolant and volume corrections, the flight profile modeling is reevaluated to provide the impact of these mass uncertainties. From the change in the results, the sensitivity of each airframe's range with respect to the engine masses is evaluated to provide context when considering a specific application for the identified engine configurations. This analysis is separated into the single- and dual-engine airframes, with the following sections discussing these results.

#### Single-Engine Airframes

First, for the single-engine airframes equipped with the piston engine configurations that provided an improvement in performance (as identified in Section 5.4), Figure 5-24 illustrates the impact of using the upper (5-24a) and lower (5-24c) piston engine mass uncertainty bounds compared to the baseline trend results (5-24b). Here, each vertical axis corresponds to the fractional change in range from the standard gas turbine configuration and the horizontal axes are the gross takeoff mass (bottom) and payload mass (top). From these results, it is evident that the variation in piston engine mass trends results in drastic changes to the predicated airframe ranges when equipped with each configuration. When using the upper standard deviation bound, all piston engine implementations fail to match the performance of the standard gas turbine design. On the other hand, using the lower standard deviation bound, each configuration achieves substantial improvements in range across all four airframes (with the exception of the auxiliary diesel four-stroke design), with the two-stroke standard and auxiliary configurations providing in excess of 120% improvements in range in the first airframe (1,000 kilogram GTOM).

To further evaluate these effects, the best performing configuration (largest improvement in range, based on the original mass trends) for each of the four piston engine categories (i.e. two- and four-stroke diesel, four-stroke gasoline, and two/four-stroke gasoline) are individually plotted with their upper, baseline, and lower trend

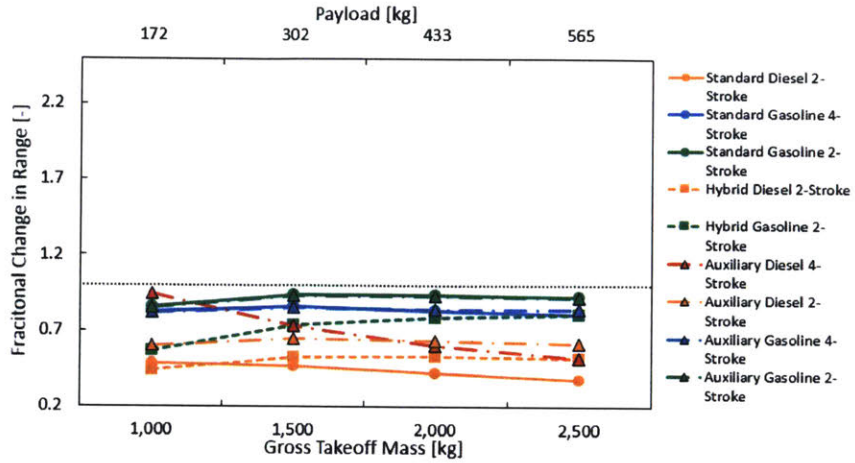


(a) Piston engine masses plus one sigma

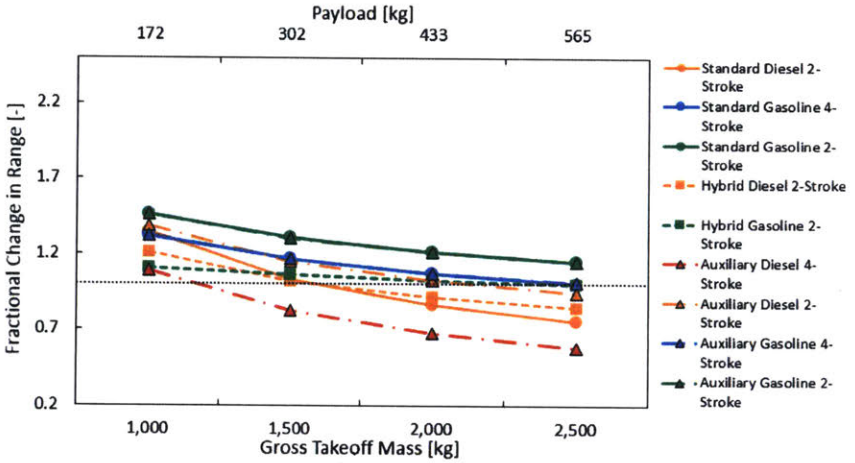


(b) Baseline piston engine mass trends

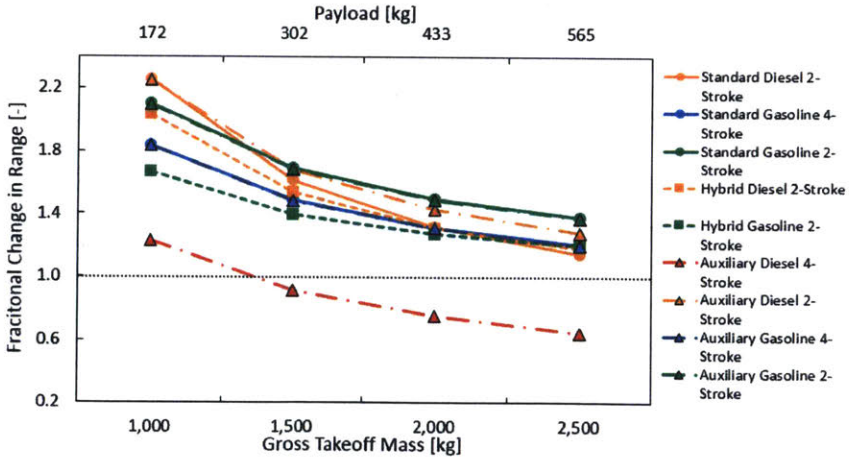


(c) Piston engine masses minus one sigma

Figure 5-24: The impacts of the upper and lower standard deviation bounds for the piston engine mass trends are illustrated by the significant variations in the single-engine airframe ranges.

results. Figure 5-25 provides these results, where each vertical axis is the fractional change in range form the standard gas turbine configuration, and the horizontal axes corresponds to each airframe's gross takeoff mass (bottom) and payload mass (top). As anticipated, the diesel two-stroke and four-stroke auxiliary designs exhibit the widest and smallest variance in range, respectively, as the two-stroke engine's mass trend had the greatest uncertainty and the four-stroke design contained the lowest uncertainty (see Figure 5-23). For the diesel two-stroke auxiliary configuration, these uncertainty bounds resulted in a fractional change in range that varied for the first airframe (1,000 kilogram GTOM) between an improvement greater than 120% to a decrease of approximately a 40%. On the other hand, the diesel four-stroke auxiliary design's variance in range is significantly smaller for this airframe, falling between an increase slightly greater than 20% and a decrease less than 10%. Based on these wide changes in range, the sizing an engine for a specific application is essential; an airframer must obtain accurate estimates for an engine's mass to ensure that the anticipated performance can be achieved. Additionally, if an engine design can exceed the baseline trends identified in this analysis (i.e. better efficiency and specific power), the aircraft is capable of achieve substantially higher performance, further demonstrating the feasibility of implementing the engine configuration.

### Dual-Engine Airframes

The same single-engine airframe range comparison is conducted on the dual-engine airframes equipped with the piston engine configurations that provided improvements in range, with Figure 5-26 illustrating the results of using the upper (5-26a) and lower (5-26c) piston engine mass uncertainty bounds compared to the baseline trend results (5-26b). Here, the vertical axes correspond to the fractional change in range compared to the standard gas turbine designs, and the horizontal axes are each airframe's gross takeoff (bottom) and payload masses (top). While less pronounced than in the single-engine airframes, the mass uncertainties significantly change the aircraft ranges achieved with each engine configuration. When modeling the piston engine upper mass bounds, only the gasoline four-stroke and two/four-stroke engines provided im-

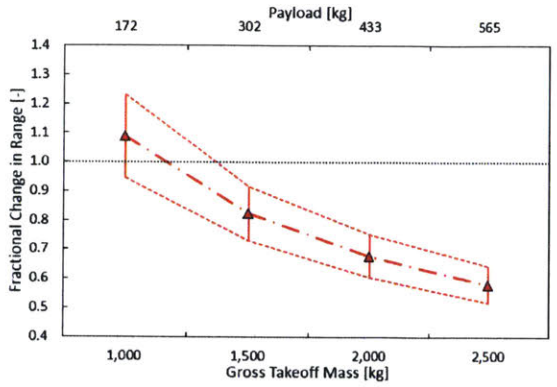


(a) Diesel four-stroke auxiliary configuration

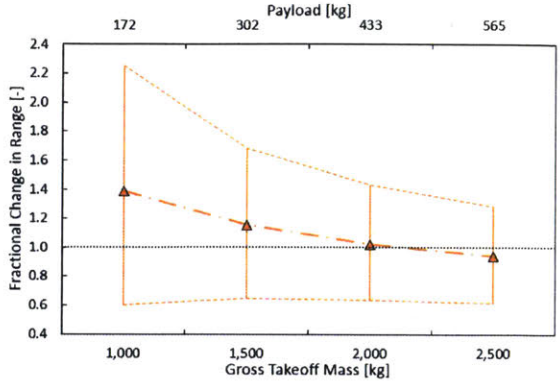


(b) Diesel two-stroke auxiliary configuration

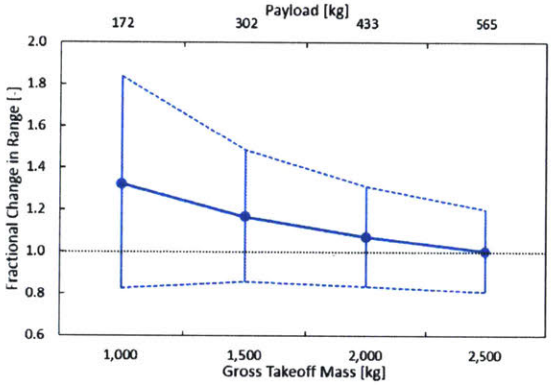


(c) Gasoline four-stroke standard configuration

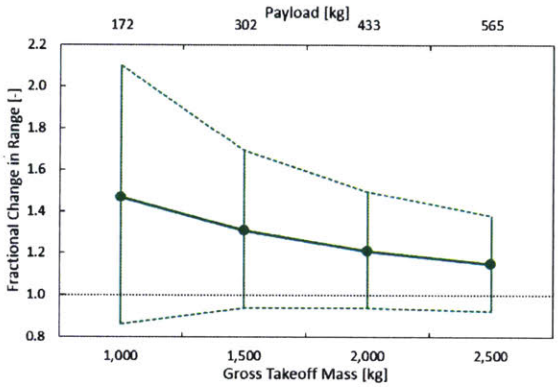


(d) Gasoline two/four-stroke standard configuration

Figure 5-25: The best-performing configurations for each of the piston engine designs in single-engine airframes are individually evaluated to illustrate the impact of their upper and lower uncertainty bounds.

provements in range for any of the aircraft. Alternatively, when using the lower mass bounds, each configuration resulted in increased range across all airframes, with the auxiliary diesel configuration nearly achieving a 60% increase in range in the first dual-engine airframe (3,000 kilogram GTOM).

Furthermore, the individual mass uncertainty impacts are evaluated for the best performing (largest improvement in range, based on original mass trends) configurations of each piston engine category, with the results provided in Figure 5-27. Here, each vertical axis is the fractional change in range from the standard gas turbine configuration, and the horizontal axes corresponds to each airframe's gross takeoff mass (bottom) and payload mass (top). Due to the two-stroke diesel engine's mass

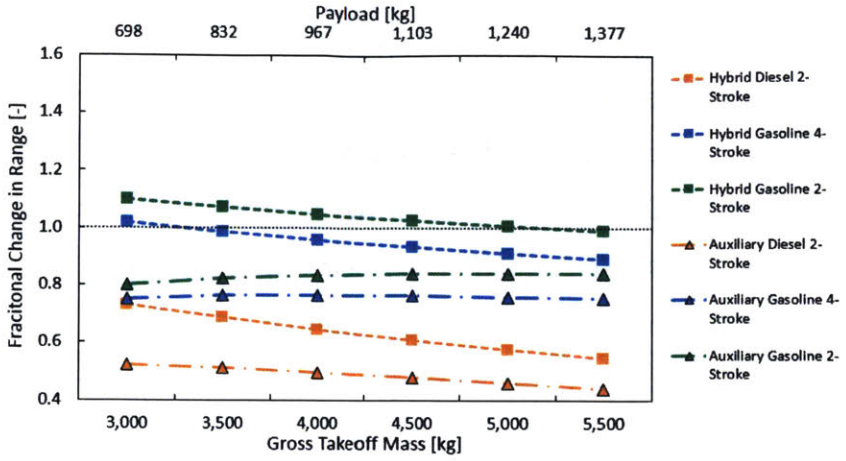


(a) Piston engine masses plus one sigma

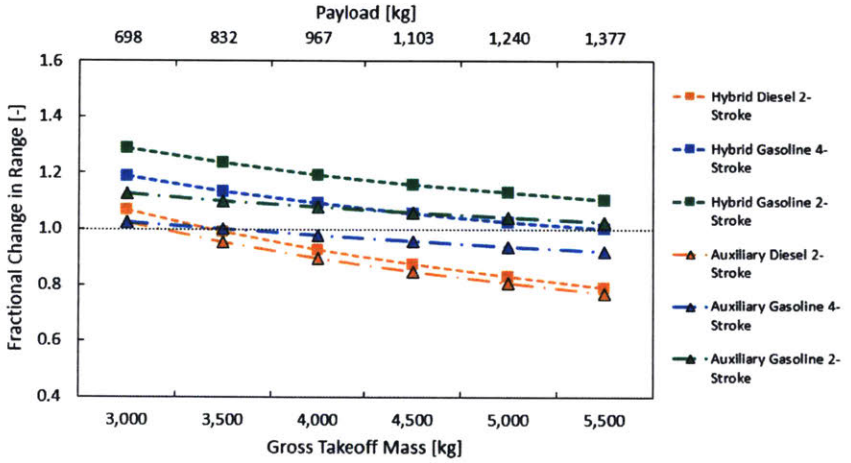


(b) Baseline piston engine mass trends

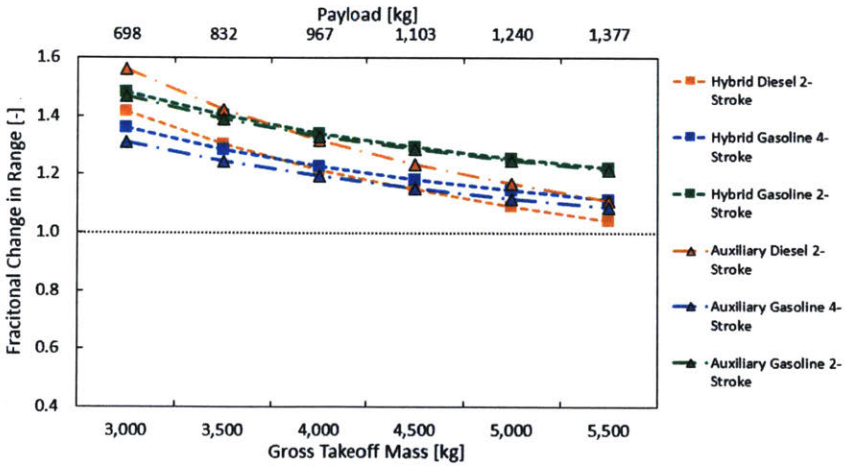


(c) Piston engine masses minus one sigma

Figure 5-26: The impacts of the upper and lower standard deviation bounds for the piston engine mass trends are illustrated by the significant variations in the dual-engine airframe ranges.

trend having the greatest uncertainty and the four-stroke diesel design containing the lowest uncertainty (see Figure 5-23), the hybrid two-stroke and four-stroke configurations exhibited the widest and smallest variances in range, respectively. For the diesel two-stroke hybrid design, the interval of the resulting ranges varied for the first dual-engine airframe (3,000 kilogram GTOM) between an increase of approximately 40% and a decrease of nearly 30%, while the diesel four-stroke hybrid configuration's interval is contained within decreases of approximately 30% and 45%. This variation indicates that, while less sensitive than single-engine airframes, the engine mass must be carefully estimated for specific dual-engine airframe applications to ensure adequate performance. Additionally, if the engine's is capable of exceeding performance trends identified in this report (i.e. better efficiency and specific power), an airframe's advantages can be substantially increased, further emphasizing the feasibility of implementing these engine designs.

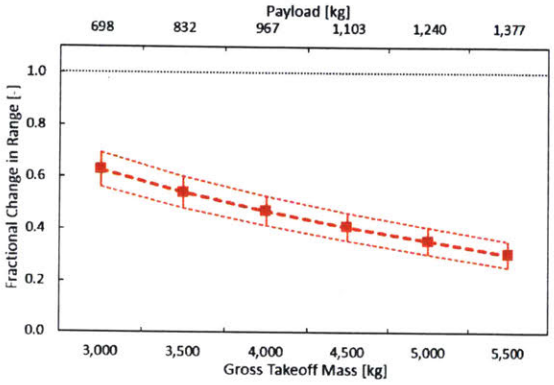


(a) Diesel four-stroke hybrid configuration

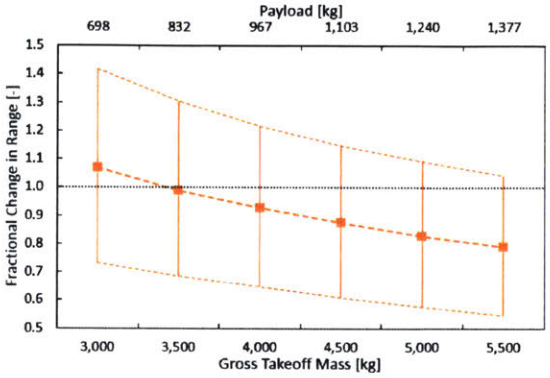


(b) Diesel two-stroke hybrid configuration

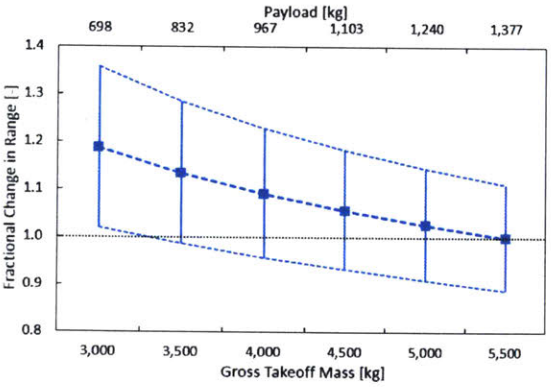


(c) Gasoline four-stroke hybrid configuration

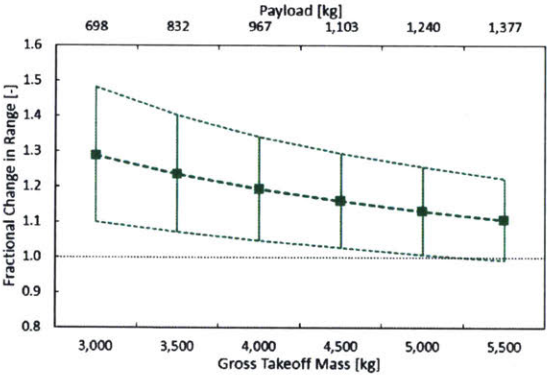


(d) Gasoline two/four-stroke hybrid configuration

Figure 5-27: The best-performing configurations for each of the piston engine designs in dual-engine airframes are individually evaluated to illustrate the impact of their upper and lower uncertainty bounds.

# Chapter 6

# Summary and Conclusions

This project considered multiple avenues to improve the performance of rotorcraft powerplants through the use of alternative engine configurations, with the main goal of increasing a helicopter's range. To approximate a realistic operation profile, the rotorcraft performance required adequate capabilities in the adverse conditions of high altitude and temperatures, as well as during scenarios where engine failure occurs. Through these lenses, the airframe's powerplant was identified as being instrumental to the helicopter's performance, and thus was the focus of this thesis. In particular, the engine's specific power, efficiency, and performance in the specified adverse conditions were identified as the essential parameters to be considered for improvement.

As gas turbines are implemented in the vast majority of modern airframes, these engines were evaluated across a range of power classes to identify the baseline rotorcraft powerplant capabilities, as well as determine the factors that dictate their advantages, disadvantages, and limitations. This analysis was conducted through compiling multiple turboshaft databases, identifying industry trends, and evaluating changes to gas turbine operation and architecture at varying sizes. Through these results, this investigation determined that gas turbines are severely limited in low power class operation (thus small airframe sizes), due to changes in the engine architecture and the scaling issues that inhibit their performance in these designs (gas turbine efficiency and specific power drops as these engines become smaller). This region of low gas turbine efficiency provides a niche where alternative engine configurations

have a potential for significant performance improvements.

Following this exercise, standard gasoline and diesel piston engines were considered as alternative powerplant configurations. These engines were evaluated by compiling industry trends and engine data to determine performance capabilities and limitations, similar to what was done in the gas turbine analysis. From these results, the piston engines were shown to possess significant advantages in efficiency in the low power classes, at the cost of high engine weights (low specific powers). Two/four-stroke switching engine designs and ethanol-gasoline designs were considered as avenues to mitigate the piston engine's specific power disadvantage. The former configuration improves the engine's specific power by operating in two-stroke mode when required and otherwise running in four-stroke mode to maximize efficiency. In the case of the ethanol-gasoline engine, the use of the two fuels increased the engine's specific power by leveraging ethanol's improved knock resistance and charge cooling. These configurations were modeled using the GT-POWER simulation software to determine their capabilities and performance characteristics, in addition to providing hot and high performance data for standard piston engines. While the two/four-stroke engine provided substantial improvement in specific power over the baseline four-stroke gasoline engine, the ethanol-gasoline engine did not attain improvements due to the need for heavier engines to fully utilize the ethanol's advantages.

Using these results, flight profile modeling was conducted using a variety of airframes that were within the niche region investigated by this project, including both single- and dual-engine designs. The rotorcraft were created using industry standard practices with gas turbine engine characteristics predicted by high-end performance trends. Using each identified engine design, these virtual aircraft were then equipped with multiple configurations, including standard engine swaps that replaced the gas turbines with piston engines, hybrid designs that incorporated both a gas turbine and piston engine, and the auxiliary engine configurations that included a small gas turbine in addition to the standard gas turbines or piston engines. With these configurations separately installed, the aircraft were simulated as conducting a characteristic flight path to compare the changes in the airframe's performance with those

achieved using the baseline gas turbine engines. From this modeling, the advantages and disadvantages of the various designs were identified, as well as the regions of applications that would achieve greater performance with particular alternative engine configurations. Finally, the uncertainties in the piston engine mass trends, along with their impact on the flight profile modeling, were evaluated to provide context on the importance of sizing an engine for specific applications.

## 6.1 Main Conclusions

Through this investigation, the following conclusions were drawn regarding the feasibility of replacing current gas turbine engines with alternative configurations, including the difference in engine configuration advantages as well as their impacts on airframe performance.

### Engine Comparisons

When compared to gas turbines, the piston engine designs poses distinct advantages in efficiency at the expense of significantly heavier architectures. These effects shift from each design, with the two extremes being the diesel four-stroke configuration, achieving the highest efficiency and mass, and the two/four-stroke gasoline engine, which has the poorest efficiency (when considering the effect of operating in two-stroke mode during a portion of the flight) and the lightest architecture.

With regards to adverse operation, both gas turbines and piston engines possess separate advantages. In OEI situations, gas turbines are able to boost their power output for short durations, decreasing the takeoff power rating required to handle these scenarios. On the other hand, piston engines are better suited to handle hot and high conditions, which limits the required power buffer that ensures the airframe can achieve full flight capabilities in the anticipated envelope of operation. In addition to an aircraft's power requirement in standard conditions, these performance parameters dictate how large the engines must be sized to handle the adverse scenarios. The resulting power requirement directly impacts the total engine mass, which

alters the mass of fuel that an airframe can carry and thus the maximum range that the helicopter can travel.

### Airframe Performance

When equipped in rotorcraft, select alternative engine configurations achieved substantial advantages in range and fuel consumption for each of the modeled airframes when compared to the standard gas turbines. In the traditional single-engine airframes (i.e. gross takeoff masses less than 3,000 kilogram) the two/four-stroke gasoline standard and auxiliary configurations achieved the highest range (nearly identical between the two designs) for airframes 1 through 4 (1,000, 1,500, 2,000, and 2,500 kilogram GTOMs).

Furthermore, for the traditional dual-engine airframes (i.e. gross takeoff masses of 3,000 kilograms and higher), multiple configurations provided significant improvements in airframe range when compared to the standard gas turbines. In airframes 5 (3,000 kilogram GTOM), 6 (3,500 kilogram GTOM), 7 (4,000 kilogram GTOM), and 8 (4,500 kilogram GTOM), the two/four-stroke hybrid design achieved the highest range, while the auxiliary gas turbine configuration provided the farthest ranges in airframes 9 and 10 (5,000, and 5,500 kilogram GTOMs).

In total, the following configurations provided significant (i.e. greater than 5%) improvements in range for the identified airframes. The particular airframes are specified using their gross takeoff mass, with their range improvements included:

- Standard diesel two-stroke: 1,000 kg (35%)
- Standard gasoline four-stroke: 1,000 (32%), 1,500 (17%), and 2,000 kg (7%)
- Standard gasoline two/four-stroke: 1,000 (47%), 1,500 (31%), 2,000 (21%), and 2,500 kg (15%)
- Hybrid diesel two-stroke: 1,000 (21%) and 3,000 kg (7%)
- Hybrid gasoline four-stroke: 3,000 (19%), 3,500 (13%), 4,000 (9%), and 4,500 kg (6%)

- Hybrid gasoline two/four-stroke: 1,000 (11%), 1,500 (6%), 3,000 (29%), 3,500 (23%), 4,000 (19%), 4,500 (16%), 5,000 (13%), and 5,500 kg (10%)
- Auxiliary gas turbine: 3,000 (6%), 3,500 (9%), 4,000 (11%), 4,500 (13%), 5,000 (15%), and 5,500 kg (16%)
- Auxiliary diesel four-stroke: 1,000 kg (9%)
- Auxiliary diesel two-stroke: 1,000 (39%) and 1,500 kg (15%)
- Auxiliary gasoline four-stroke: 1,000 (32%), 1,500 (17%), and 2,000 kg (7%)
- Auxiliary gasoline two/four-stroke 1,000 (46%), 1,500 (30%), 2,000 (21%), 2,500 (14%), 3,000 (13%), 3,500 (10%), 4,000 (8%), and 4,500 kg (6%)

However, these improvements in range are achieved at the expense of reductions in the airframe's best-range cruise speed. This change is due to the gas turbines and piston engines experiencing opposite trends in their efficiency when operating in part-load conditions; turboshaft efficiency falls when producing less than the takeoff rated power, while piston engine efficiency rises in part-load operation. Thus, the optimal cruise speed of piston engines is reduced to take advantage of this increase in efficiency, while the gas turbine configurations travel at higher speeds to counteract their reduction in efficiency. Additionally, the auxiliary gas turbine configuration's best-range cruise speed was also lower than the standard gas turbines in the traditional dual-engine aircraft, due to the reduction in the available power for the main engines. Therefore, the alternative engine configurations are capable of providing significant improvements in range and fuel consumption, at the expense of lower flight speeds.

Finally, a helicopter's performance is very sensitive to the predicted engine masses, as illustrated by the modeling of the uncertainty in the engine mass trends. To consider implementing one of the identified engine configurations, an airframer must carefully estimate the engine's characteristics (i.e. mass and efficiency) to ensure the aircraft is capable of achieving the desired performance, due to the wide variance in engine performances. Furthermore, if an engine is identified as exceeding the

performance trends provided in this analysis, an airframe's range can be substantially increased, further emphasizing the feasibility of implementing these configurations.

## Recommendations

Based on these results, the analysis recommends that airframers investigate the identified engine configurations in the airframe sizes in which they are capable of achieving improved performance over that of the gas turbines. In particular, the two/four-stroke switching engine exhibits the greatest piston engine performance capability in the standard and hybrid implementations for the single- and dual-engine airframes, respectively. To verify these capabilities, it is recommended that an engine manufacture provide more detailed evaluations of the configurations implementation, including the development time and feasible performance capabilities based on the manufacturer's expertise. Furthermore, for designs that could be implemented today, the diesel two-stroke auxiliary configuration provides substantial benefits in small single-engine airframe sizes, the gasoline four-stroke hybrid design exhibits improvements in range for the small and medium sized dual-engine airframes, and the auxiliary gas turbine configuration shows significant increases in range for all dual-engine airframes.

However, when considering the feasibility of these designs, an organization must obtain accurate estimations of engine masses and efficiencies to determine if the configuration can match or exceed the performance trends identified in this investigation. Due to the significant variance in these parameters, in addition to an aircraft's sensitivity to their changes, a specific application must size an engine's characteristics and evaluate the airframe's performance on a case-by-case basis. Additionally, the evaluation must be conducted on the specific airframe considered for the engine's implementation, as the aircraft performance parameters influences the helicopter's response to different engine configurations. While this analysis indicates the feasibility of the identified designs, an airframer must finalize the engine capabilities in specific airframes to ensure adequate performance can be achieved.

## 6.2 Future Work

Due to the time constraints imposed on this project, multiple topics were not fully vetted and require additional evaluation. These investigations must be analyzed to fully determine the feasibility of implementing the identified alternative engine configurations in rotorcraft applications, as discussed in the following sections.

### 6.2.1 Engine Considerations

First, the future work required for the engines evaluated in this modeling was determined. Each item must be considered when investigation the total implications of utilizing the engine designs.

#### Supercharging

Due to limited data, the supercharger maximum single-stage pressure ratio and mass were estimated using specific designs points found on example supercharging systems. However, to obtain a more accurate predictions, the boosting system must be designed for a specific engine, as the relationships between the airflow rate, pressure ratio, and mass are complex and experience too much variance to enable broad estimations. As these features are essential to a piston engine's performance, particular applications must individually conduct this sizing.

#### Turbocharging

The two-stroke operation mode was unable to accommodate turbocharging during the GT-POWER modeling because of the sensitivity to the resulting exhaust back pressure. However, turbocharging provides an inherent advantage in engine efficiency, as the power is drawn directly from the engine's exhaust. Thus, for the potential dual-stage boosting models in particular, turbocharging should be considered to further augment the two/four-stroke engine's performance.

### Emissions Impact

While referenced during the piston engine discussion, emission production was not considered in this investigation. In particular, the piston engines were modeled under the assumption that Avgas was used as a fuel, which contains lead as an anti-knock additive. With rising concerns on the impact of aircraft on the environment, the changes in emissions between each engine, as well as the extent of their impacts, must be considered in actual implementation.

### Engine Geometry

As mentioned in this analysis, a particular piston engine's ideal geometry is difficult to approximate, as the relationships between the various dimensions (i.e. bore and stroke, number of engines, etc.) complicates the process. Despite the substantial benefits outlined in this analysis, further consideration is required to design an engine for a particular application, with the potential for achieving greater performance than with the geometry specified in this report. Furthermore, the engine's overall dimensions (i.e. length, width, and height) are crucial to their implementation in rotorcraft applications, as the airframe's available space must be able to accommodate the engine size. This feature of the new engine configurations is an essential parameter to evaluate when considering implementing an engine design in a helicopter.

### Experimental Investigation of Two/Four-Stroke Engine

The two/four-stroke engine was discovered in literature, where a handful of studies have experimentally verified its basic operation. However, these evaluations were in engine sizes that are dwarfed by those considered in this analysis, and were not tested at the engine's maximum capabilities. Thus, the concept proposed in this analysis requires extensive experimental research to ensure that the platform can achieve the performance identified through the GT-POWER modeling, in addition to identifying realistic efficiencies in the two- and four-stroke operating modes and ensuring reliable mode switching and performance throughout the lifetime of the engine.

### Diesel Engine Characteristics

Despite the investigation of gasoline performance using GT-POWER, diesel engines were not modeled during this analysis. Thus, to more accurately predict their capabilities (i.e. hot and high derating), additional modeling and data is required for both four-stroke and two-stroke diesel engines.

### Auxiliary Mass Considerations

While the engine, fuel, and fuel tank masses were considered when swapping engines within an airframe, multiple auxiliary factors will influence the final change in mass between configurations. These include the changes in the structural mounting of the fuel tank, engines, and their associated components, as well as the alterations or additions to the transmission(s) (i.e. the coupling between the engine and the rotor). These secondary features are important when determining the final change in mass between configurations, and require further analysis to fully vet the associated impacts.

### Gas Turbine Wet Mass

Similar to piston engines, gas turbines incorporate lubrication oil to facilitate their operation. While the amount of this fluid is significantly less than the coolant and oil used in piston engines, their mass must be considered to fully compare piston engine and gas turbine wet masses and specific powers.

### Cost Analysis

This investigation exclusively considered the performance impacts of the identified engine configurations. However, in actually applications, the rotorcraft costs are critical to their feasibility. Thus, a comprehensive analysis of the costs associated with implementing the identified configurations is required to determine the feasibility in industry applications. These costs include the development and purchasing of the piston engines for particular application sizes (as well as the price of gas turbines),

changes in the engine maintenance and replacement frequencies, fuel price and consumption rates, and the monetary value of the changed airframe performance (i.e. further range at a lower speed).

### 6.2.2 Modeling Considerations

In addition to the future work regarding the engine technologies, further investigation into the modeling of these configurations is necessary to provide a full evaluation of the alternative engine designs' impacts on airframe performance. The applicable topics are listed in the following sections.

#### Additional Mission Profiles

The flight profile modeling evaluated a characteristic flight path that includes the basic takeoff, climb, cruise, reserve, descent, and landing segments. However, many airframes are designed and operated to accomplish specific missions, including reconnaissance, search and rescue, and transportation. To achieve more accurate results for specific applications, the flight profile modeling would require modification to its flight path to mimic the desired mission. Furthermore, the required airframe capabilities in OEI and hot and high conditions (in addition to the definition of hot and high) significantly impact the sizing of engines for a particular airframe. Thus, these features require attention when considering the feasibility of an engine design in specific applications.

#### Varying Performance Parameters

The simulated airframes were designed using industry trends to provide a general prediction of aircraft performance features, which heavily influence the rotorcraft's flight characteristics and capabilities. While these estimations provided baseline results, the specific parameters must be updated to match a particular airframe that is being considered for implementing the alternative configurations.

### Modeling Altitude Adjustment for Engine Performance

Finally, while included during the engine sizing procedures, the modeling did not account for changes in engine performance when at altitude during the flight path. To provide more realistic results, each engine configuration would require their performance trends to be built into the modeling to estimate their change in capabilities during the entire flight profile.

# Appendix A

# GT-POWER Simulation Parameters

The following sections outline the final modeling parameters for the example aviation piston engines, two/four-stroke simulations, and the ethanol-gasoline configurations. These parameters include specified characteristics that were emulated in the model, as well as variable parameters that were used to tune the engine for optimization (two/four-stroke, ethanol-gasoline engines) or to achieve a desired performance level (example aircraft engines). Each section will further describe these parameters in addition to the goals of the simulations.

## A.1 Example Aircraft Engines

For the example aviation piston engines modeled in GT-POWER, a combination of variable and fixed parameters were used to duplicate the engines' performance characteristics and provide better understanding of their operation. Specifically, the results were used to determine a maximum final knock integral value to be used in subsequent modeling. The data referenced in Section 4.3 was compiled by utilizing manufacturer and certification documentation describing the engines' parameters, with this information provided in Tables A.1 through A.6. Through the GT-POWER engine models, the example aircraft knock tendency trends were calculated using the imposed knock integral specified in Section 4.2, which provided a baseline value that served as the knock integral target for subsequent simulations.

Table A.1: The Hamilton Standard FV4000-2TC engine specifications

| **Fixed Engine Parameters** | |
|---|---|
| Rated power | 268.5 kW |
| SFC (at rated power) | 0.305 kg/kW/hr |
| Wet mass[a] | 253.7 kg |
| Bore x stroke | 87 x 83 mm |
| Number of cylinders | 8 |
| Compression ratio | 9.7:1 |
| Max engine speed | 5,200 rpm |
| Boosting system | Turbocharged |
| Fuel grade | Avgas 100LL |
| Cooling method | Liquid |
| Manifold Pressure | 1.46 bar |
| **Variable Engine Parameters** | |
| Ignition timing (50% CA) | 6.5° ATDC |
| Intake valve open timing | 317° ATDC |
| Exhaust valve open timing | 120° ATDC |
| Equivalence ratio | 1.28 |

[a] The coolant mass was estimated using trend data compiled from the other example aviation piston engines, as seen in Appendix 3.3.2.

Table A.2: The Limbach L2400 DX engine specifications

| **Fixed Engine Parameters** | |
|---|---|
| Rated power | 118.0 kW |
| SFC (at rated power) | 0.255 kg/kW/hr |
| Wet mass | 92.3 kg |
| Bore x stroke | 97 x 82 mm |
| Number of cylinders | 4 |
| Compression ratio | 8:1 |
| Max engine speed | 3,000 rpm |
| Boosting system[c] | Turbocharged |
| Fuel grade | 98 RON |
| Cooling method | Liquid-cooled cylinder heads, air-cooled cylinders |
| Manifold Pressure | 1.63 bar |
| **Variable Engine Parameters** | |
| Ignition timing (50% CA) | 11° ATDC |
| Intake valve open timing | 292° ATDC |
| Exhaust valve open timing | 142° ATDC |
| Equivalence ratio | 1.10 |

Table A.3: The Rotax 912iS engine specifications

| **Fixed Engine Parameters** | |
|---|---|
| Rated power | 73.5 kW |
| SFC (at rated power) | 0.278 kg/kW/hr |
| Wet mass | 68.3 kg |
| Bore x stroke | 84 x 61 mm |
| Number of cylinders | 4 |
| Compression ratio | 10.8:1 |
| Max engine speed | 5,800 rpm |
| Boosting system | Naturally aspirated |
| Fuel grade | 95 RON |
| Cooling method | Liquid-cooled cylinder heads, air-cooled cylinders |
| Manifold Pressure | 0.88 bar |
| Ignition timing[a] (50% CA) | 4.8° ATDC |
| **Variable Engine Parameters** | |
| Intake valve open timing | 309° ATDC |
| Exhaust valve open timing | 118° ATDC |
| Equivalence ratio | 1.17 |

[a] The manufacturer specifies a spark timing of 26° BTDC, which is equivalent to a 50% CA of 4.8° ATDC, based on the combustion modeling used in GT-POWER.

Table A.4: The RotorWay RI-162F engine specifications

| **Fixed Engine Parameters** | |
|---|---|
| Rated power | 111.9 kW |
| SFC (at rated power) | 0.256 kg/kW/hr |
| Wet mass | 99.1 kg |
| Bore x stroke | 102 x 82 mm |
| Number of cylinders | 4 |
| Compression ratio | 9.4:1 |
| Max engine speed | 4,250 rpm |
| Boosting system | Naturally aspirated |
| Fuel grade | 98 RON |
| Cooling method | Liquid-cooled |
| **Variable Engine Parameters** | |
| Ignition timing[a] (50% CA) | 6.25° ATDC |
| Manifold Pressure[b] | 0.88 bar |
| Intake valve open timing | 311° ATDC |
| Exhaust valve open timing | 125° ATDC |
| Equivalence ratio | 1.07 |

[a] The manufacturer specifies a spark timing between 14 - 38° BTDC, with the final timing set to 24.6° BTDC after optimizing the simulation. This is equivalent to a 50% CA of 6.25° ATDC, based on the combustion modeling used in GT-POWER.

[b] The manufacturer does not specify a manifold pressure, and thus this pressure target is based on the manifold pressure of the Rotax 912iS, which is also naturally aspirated.

Table A.5: The Teledyne Continental TSIOL-550-A engine specifications

| **Fixed Engine Parameters** | |
|---|---|
| Rated power | 261 kW |
| SFC (at rated power) | 0.304 kg/kW/hr |
| Wet mass[a] | 220.7 kg |
| Bore x stroke | 133 x 108 mm |
| Number of cylinders | 6 |
| Compression ratio | 7.5:1 |
| Max engine speed | 2,700 rpm |
| Boosting system | Turbocharged |
| Fuel grade | Avgas 100 or 100LL |
| Cooling method | Liquid-cooled |
| Ignition timing[b] (50% CA) | 4° ATDC |
| Manifold Pressure | 1.29 bar |
| **Variable Engine Parameters** | |
| Intake valve open timing | 314° ATDC |
| Exhaust valve open timing | 125° ATDC |
| Equivalence ratio | 1.22 |

[a] The coolant mass was estimated using trend data compiled from the other example aviation piston engines, as seen in Appendix 3.3.2.

[b] The manufacturer specifies a spark timing of 20° BTDC, which is equivalent to a 50% CA of 4° ATDC, based on the combustion modeling used in GT-POWER.

Table A.6: The TRACE OE600A engine specifications

| **Fixed Engine Parameters** | |
|---|---|
| Rated power | 447 kW |
| SFC (at rated power) | 0.268 kg/kW/hr |
| Wet mass[a] | 365.3 kg |
| Bore x stroke | 113 x 102 mm |
| Number of cylinders | 8 |
| Compression ratio | 8:1 |
| Max engine speed | 4,400 rpm |
| Boosting system | Turbocharged |
| Fuel grade | Avgas 100LL |
| Cooling method | Liquid-cooled |
| Ignition timing[b] (50% CA) | 6.8° BTDC |
| Manifold Pressure | 1.76 bar |
| **Variable Engine Parameters** | |
| Intake valve open timing | 295° ATDC |
| Exhaust valve open timing | 126° ATDC |
| Equivalence ratio | 1.03 |

[a] The coolant mass was estimated using trend data compiled from the other example aviation piston engines, as seen in Appendix 3.3.2.

[b] The manufacturer specifies a spark timing of 38° BTDC, which is equivalent to a 50% CA of 6.8° ATDC, based on the combustion modeling used in GT-POWER.

## A.2 Two/Four-Stroke Engine

The four simulations outlined in Section 4.4 were completed with the parameters listed in Tables A.7 through A.8. The two-stroke configuration was optimized to maximize specific power in standard ambient conditions, with two different test scenarios. First, the configuration was modeled with the compressor pressure ratio limited to 2.5 to simulate a single supercharger. However, as this resulted in the configuration's performance being restricted by its boosting capability, the second test scenario allowed the model to increase the pressure ratio above 2.5 to approximate dual-supercharging. Furthermore, the four-stroke port valve configuration was simulated to determine the approximate change in power output when switching between the two- and four-stroke operation modes, while the four-stroke poppet valve engine was modeled to estimate the engine platform's mass before accounting for the added supercharging and intercooler masses necessary for two-stroke operation. Each simulation was restricted by a peak pressure limit of 120 bar, a knock integral maximum value of 0.92, and, with the exception of the second two-stroke hot and high analysis previously described, a compressor pressure ratio limit of 2.5. The remaining parameters provided in Section 4.1 enabled the tuning of each engine configuration to optimize the desired performance (i.e. power output or specific power), with the resulting mass calculations provided in Appendix C.

Table A.7: The two-stroke engine operation parameters

| **Engine Performance Parameter** | **Two-Stroke, Initial** | **Two-Stroke, Revisited** |
|---|---|---|
| Net power output[a] (kW) | 344 | 395 |
| Estimated wet mass[b] (kg) | 210 | 247 |
| Specific power (kW/kg) | 1.64 | 1.60 |
| Power density (kW/L) | 127 | 146 |
| Hot and high power loss[a] | -19% | -13% |
| Standard and (hot and high) operating parameters and characteristics | | |
| Intake valve opening (° ATDC) | 150 (154) | 161 (154) |
| Exhaust valve opening (° ATDC) | 104 (106) | 114 (104) |
| Spark timing (50% CA, ° ATDC) | 5 (5) | 7 (6) |
| Equivalence ratio | 0.97 (0.96) | 0.97 (0.97) |
| Peak pressure (bar) | 104 (86) | 119 (108) |
| Final knock integral value | 0.83 (0.58) | 0.92 (0.83) |
| Compressor pressure ratio | 2.50 (2.46) | 3.15 (3.02) |

[a] This power output accounts for the supercharging power consumption.

[b] The engine masses were estimated by using the output power vs engine mass trends located in Section 3.3 and were adjusted based on the supercharging and intercooler mass considerations, as described in Appendix C.

[c] The hot and high power loss is the configuration's percent decrease in maximum available power when the engine is operating in ambient air conditions of 315.2 K and 0.875 bar.

Table A.8: The four-stroke engine operation parameters

| **Engine Performance Parameter** | **Four-Stroke, Port Valve Model** | **Four-Stroke, Standard Model** |
|---|---|---|
| Net power output[a] (kW) | 259 | 243 |
| Estimated wet mass[b] (kg) | 219[c] | 202 |
| Specific power (kW/kg) | 1.18[c] | 1.20 |
| Power density (kW/L) | 96 | 90 |
| Hot and high power loss[d] | -16% | -12% |
| Standard and (hot and high) operating parameters and characteristics | | |
| Intake valve opening (° ATDC) | 300 (302) | 309 (326) |
| Exhaust valve opening (° ATDC) | 131 (127) | 138 (130) |
| Spark timing (50% CA, ° ATDC) | 13 (8) | 16 (13) |
| Equivalence ratio | 0.97 (0.97) | 0.975 (0.91) |
| Peak pressure (bar) | 120 (114) | 110 (103) |
| Final knock integral value | 0.91 (0.91) | 0.92 (0.92) |
| Compressor pressure ratio | 2.50 (2.49) | 2.50 (2.50) |

[a] This power output accounts for the supercharging power consumption.

[b] The engine masses were estimated by using the output power vs engine mass trends located in Section 3.3 and were adjusted based on the supercharging and intercooler mass considerations, as described in Appendix C.

[c] The four-stroke port valve configuration modeling was conducted to estimate the change in power available when switching between the two- and four-stroke operation modes. Thus, the engine mass was assumed to be equal to the two-stroke configuration.

[d] The hot and high power loss is the configuration's percent decrease in maximum available power when the engine is operating in ambient air conditions of 315.2 K and 0.875 bar.

## A.3 Ethanol-Gasoline Engine

The two sets of ethanol-gasoline simulations varied the engine's spark timing while either keeping the knock integral or cylinder peak pressure constant for both E85 and Avgas fuel sources. Throughout the spark sweep, the engine's variable parameters were tuned to achieve maximum power output, given the testing restrictions. Tables A.9 through A.12 provide the results and the parameters used to achieve these performances, with every E85 and Avgas test case having operated with equivalence ratios of 0.92 and 0.9, respectively.

Table A.9: The E85 configuration's constant knock integral parameters

| **Spark Timing (50% CA, ° ATDC)** | **Intake Valve Opening (° ATDC)** | **Exhaust Valve Opening (° ATDC)** | **Compressor Inlet Temperature and Pressure (bar, K)** |
|---|---|---|---|
| 5 | 297 | 147 | 1, 293 |
| 7 | 297 | 147 | 1, 293 |
| 9 | 295 | 148 | 1, 293 |
| 11 | 295 | 145 | 1, 293 |
| 13 | 295 | 145 | 1.67, 359 |
| 15 | 295 | 145 | 1.67, 359 |
| 17 | 295 | 143 | 1.67, 359 |

Table A.10: The E85 configuration's constant peak pressure parameters

| Spark Timing (50% CA, ° ATDC) | Intake Valve Opening (° ATDC) | Exhaust Valve Opening (° ATDC) | Compressor Inlet Temperature and Pressure (bar, K) |
|---|---|---|---|
| 5 | 297 | 147 | 1, 293 |
| 7 | 297 | 147 | 1, 293 |
| 9 | 297 | 148 | 1, 293 |
| 11 | 295 | 145 | 1, 293 |
| 13 | 295 | 145 | 1, 293 |
| 15 | 295 | 145 | 1, 293 |
| 17 | 295 | 143 | 1, 293 |
| 19 | 295 | 143 | 1.33, 332 |
| 21 | 295 | 143 | 1.33, 332 |
| 23 | 295 | 143 | 1.33, 332 |
| 25 | 295 | 143 | 1.33, 332 |
| 27 | 295 | 143 | 1.33, 332 |
| 29 | 295 | 143 | 1.58, 352.5 |

Table A.11: The Avgas configuration's constant knock integral parameters

| **Spark Timing (50% CA, ° ATDC)** | **Intake Valve Opening (° ATDC)** | **Exhaust Valve Opening (° ATDC)** | **Compressor Inlet Temperature and Pressure (bar, K)** |
|---|---|---|---|
| 5 | 295 | 148 | 1, 293 |
| 7 | 295 | 146 | 1, 293 |
| 9 | 295 | 148 | 1, 293 |
| 11 | 295 | 147 | 1, 293 |
| 13 | 295 | 147 | 1, 293 |
| 15 | 295 | 147 | 1, 293 |
| 17 | 295 | 143 | 1.58, 353 |
| 19 | 295 | 143 | 1.58, 353 |

Table A.12: The Avgas configuration's constant peak pressure parameters

| Spark Timing (50% CA, ° ATDC) | Intake Valve Opening (° ATDC) | Exhaust Valve Opening (° ATDC) | Compressor Inlet Temperature and Pressure (bar, K) |
|---|---|---|---|
| 5 | 295 | 146 | 1, 293 |
| 7 | 297 | 146 | 1, 293 |
| 9 | 297 | 148 | 1, 293 |
| 11 | 295 | 147 | 1, 293 |
| 13 | 295 | 145 | 1, 293 |
| 15 | 295 | 145 | 1, 293 |
| 17 | 295 | 143 | 1, 293 |
| 19 | 295 | 143 | 1, 293 |
| 21 | 295 | 143 | 1.58, 353 |
| 23 | 295 | 143 | 1.58, 353 |
| 25 | 295 | 143 | 1.58, 353 |
| 27 | 295 | 143 | 1.58, 353 |
| 29 | 295 | 143 | 1.58, 353 |

# Appendix B

# Avgas RON Estimation

As described in Section 4.1, the GT-POWER simulations required the RON for each engine configuration's fuel to enable the estimation of knock tenancies. Thus, since Avgas does not have a specified RON, a correlation between the MON and RON of high-performance fuel was created to provide an adequate estimation for this parameter. Figure B-1 illustrates the resulting relationship, with each fuel's MON plotted on the horizontal axis and RON displayed on the vertical axis.

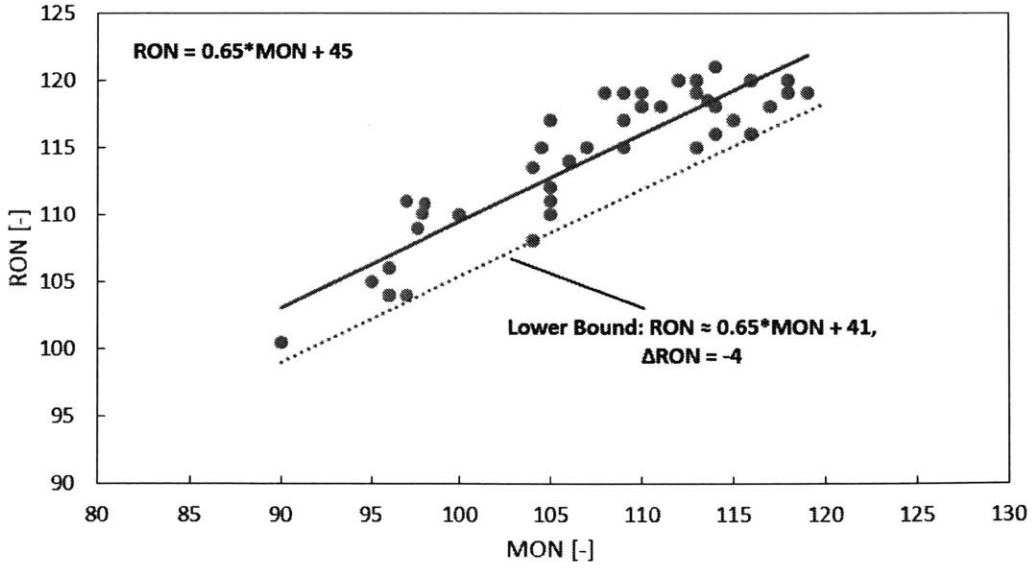


Figure B-1: The sample high-performance racing fuel was plotted to determine a characteristic relationship between a fuel's RON and MON [129].

Based on the best fit curve for this data, and the specified Avgas MON of 99.8, the fuel's approximated RON is calculated to be 110. However, as seen in Figure B-1, there is scatter in the data trend, with a worst case RON prediction of 106. Thus, while the example aircraft and two/four-stroke engine GT-POWER configurations analyses were based on the best fit curve, these models was also evaluated with the worst case scenario RON to determine how the RON uncertainty would impact each engine's knock prediction. The results of these tests are provided in the following sections.

## B.1 Example Aircraft Engine Testing

Three of the identified aviation piston engines, the Hamilton Standard FV4000-2TC, Teledyne Continental TSIOL-550-A, and TRACE OE600A, operate with Avgas as their minimum fuel requirement. For each of these engines, the GT-POWER modeling was designed to maximize performance when assuming an Avgas RON of 110, with the same operating parameters tested when using RON of 106. Table B.1 provides the changes in each engine's knock integral.

Based on these results, the worst-case potential for the Avgas RON would create significant changes to the example engines' knock integrals, averaging an increase of 0.14. However, as the TRACE OE600A exceeds the knock threshold of unity in this scenario, Avgas is likely to have a RON higher than 106. Furthermore, if the target knock integral target was updated using these higher values, the limit would be increased from the original 0.92 value. Thus, as subsequent testing was conducted with a maximum knock integral value of 0.92, the modeling would provide a conservative estimation of the engine capabilities, assuming their fuel's RON is accurate (see following sections).

Table B.1: The final knock integral values for the example aircraft engines that utilize Avgas, when assuming 110 RON and 106 RON

| **Example Engine** | **110 RON Knock Integral** | **106 RON Knock Integral** | **Change in Knock Integral** |
|---|---|---|---|
| Hamilton Standard FV4000-2TC | 0.82 | 0.96 | 0.14 |
| Teledyne Continental TSIOL-550-A | 0.60 | 0.70 | 0.10 |
| TRACE OE600A | 0.96 | 1.13 | 0.17 |

## B.2 Ethanol-Gasoline Engine Testing

For the ethanol-gasoline simulations, two separate test runs were conducted, with the first evaluation restricting the knock integral final value and the second case limiting the cylinder's peak pressure. For the first set of simulations, after evaluating the Avgas test case knock integrals with 106 RON, the final values jumped from the target of 0.92 to 1.08, resulting in operation that would cause knocking. With the second set of simulations, the differences in knock integral values between the baseline 110 RON and 106 RON conditions are displayed in Figure B-2, where the engine's spark delay is varied across the horizontal axis and the final knock integral values are plotted on the vertical axis. Here, the difference in knock integrals is as high as 0.16 at a spark advance of 2° (0.94 for 110 RON, 1.10 for 106 RON) and decreases to 0.09 at a spark delay of 22° (0.54 for 110 RON, 0.63 for 106 RON).

Despite the change in the Avgas RON causing knock in both simulation sets, the impact of the testing results does not change; to fully leverage the benefits of ethanol, the engine must have very high peak pressures. This requires substantially stronger (and thus heavier) engines, with the resulting increase in mass mitigating the basic goal of increasing the engine's specific power. Furthermore, based on the

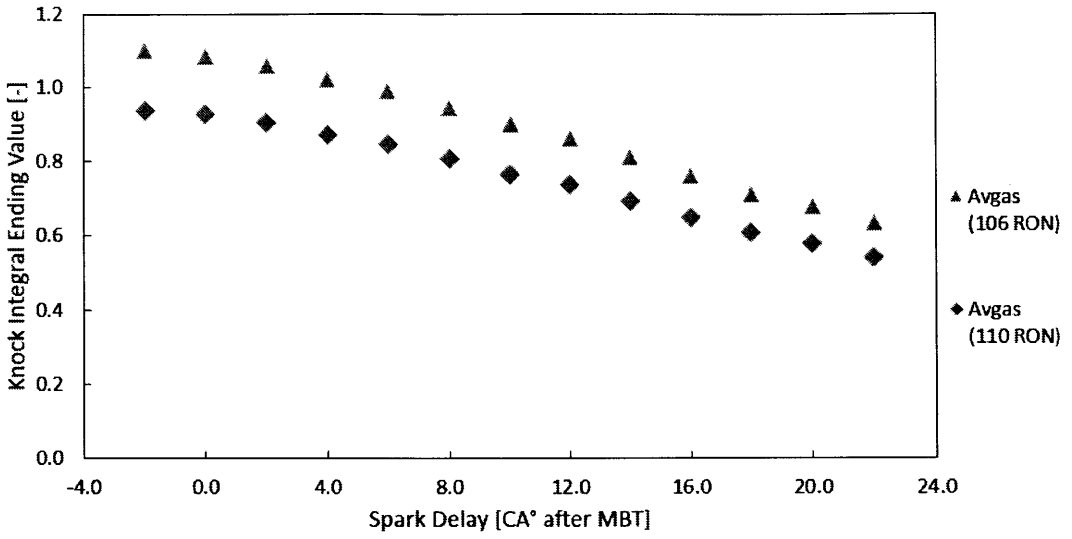


Figure B-2: The Avgas vs. E85 fixed pressure simulations were conducted with an Avgas RON of 110 and 106 to determine the lower RON's effect on the final knock integrals.

constant peak pressure analysis, ethanol does not provide a significant advantage when compared with Avgas in a representative gasoline engine architecture, despite the potentially lower Avgas RON. The simulation utilized heavy spark delay to maximize the engine's power output, which eliminated knock as a performance restriction. Therefore, regardless of the potential variance in the Avgas RON, the ethanol-gasoline configuration was deemed to be unfit for implementation in rotorcraft applications and was not considered in the flight profile modeling.

## B.3 Two/Four-Stroke Engine Testing

Finally, the two/four-stroke engine was simulated using an Avgas RON of 110 and 106, with Tables B.2 and B.3 providing the results. The change in the final knock integral values was significant for all configurations, causing both the four-stroke port valve and four-stroke poppet valve configurations to knock. Based on these results, the two/four-stroke engine's performance is sensitive to its fuel's RON due to multiple engine platforms being restricted by knock. However, as there are additional high-

performance gasoline fuels that provide a RON greater than or equal to 110, this analysis based its results on running Avgas with a RON of 110 under the assumption that a different fuel source with an adequate RON could be used if necessary [129].

Table B.2: The change in the final knock integral values for the four-stroke engine models

| **Engine Configuration** | **Four-stroke, port valve** | **Four-stroke, poppet valve** |
|---|---|---|
| 110 RON Standard and (Hot and High) Knock Integrals | 0.91 (0.91) | 0.92 (0.92) |
| 106 RON Standard and (Hot and High) Knock Integrals | 1.07 (1.07) | 1.08 (1.08) |
| Change in Standard and (Hot and High) Knock Integrals | 0.16 (0.16) | 0.16 (0.16) |

Table B.3: The change in the final knock integral values for the two-stroke engine models

| **Engine Configuration** | **Two-Stroke, Initial Modeling** | **Two-Stroke, Revisited Modeling** |
|---|---|---|
| 110 RON Standard and (Hot and High) Knock Integrals | 0.83 (0.58) | 0.92 (0.83) |
| 106 RON Standard and (Hot and High) Knock Integrals | 0.97 (0.68) | 1.08 (0.98) |
| Change in Standard and (Hot and High) Knock Integrals | 0.14 (0.10) | 0.16 (0.15) |

# Appendix C

# Supercharging Power and Mass Adjustment

During the GT-POWER modeling, an estimation of the supercharging system power consumption and mass was required to provide a full comparison of each configuration's specific power, as these features directly affect the performance predicted by the engine simulations and are used in the flight profile modeling. The former was completed using an external first law energy balance, while the latter was estimated using trends taken from industry superchargers. These analyses are provided in the following sections.

## C.1 Power Adjustment

As referenced in Section 4.1, the GT-POWER supercharger power requirement was verified through an external calculation to correct for any discrepancies that arose due to the altering of the compressor mass flow rate and efficiency multipliers. For each simulation, a first law energy balance was created for the compressor, based on the model's mass flow rate and the compressor's inlet and outlet air temperatures,

$$\dot{m}_{\text{air}} * h_{\text{in}} + \dot{W}_{\text{compressor}} = \dot{m}_{\text{air}} * h_{\text{out}}, \tag{C.1}$$

where $\dot{m}_{air}$ is the compressors mass flow rate in kilograms per second, and $h_{in}$ and $h_{out}$ are the specific enthalpies of the inlet and outlet air, respectively, in joules per kilogram (calculated using the air temperatures). Tables C.1 through C.4 display the data taken from each two/four-stroke GT-POWER simulation, along with the resulting calculated enthalpies, supercharging power consumption, and difference in the GT-POWER and external power estimations. Each simulation was updated with their supercharging power adjustment, ensuring accurate performance predictions.

Table C.1: The two-stroke configuration's compressor conditions and the resulting power consumption

| **Parameter** | **Standard Conditions** | **Hot and High Conditions** |
|---|---|---|
| Mass flow rate (kg/s) | 0.381 | 0.315 |
| Inlet temperature, enthalpy (K, kJ/kg) | 298, 298 | 313, 314 |
| Outlet temperature, enthalpy (K, kJ/kg) | 425, 426 | 441, 443 |
| Calculated compressor power (kW) | 48.8 | 40.1 |
| GT-POWER predicted compressor power (kW) | 26.1 | 19.2 |
| Change in compressor power (kW) | 22.7 | 20.9 |

Table C.2: The revisited two-stroke configuration's compressor conditions and the resulting power consumption

| **Parameter** | **Standard Conditions** | **Hot and High Conditions** |
|---|---|---|
| Mass flow rate (kg/s) | 0.472 | 0.403 |
| Inlet temperature, enthalpy (K, kJ/kg) | 298, 298 | 313, 313 |
| Outlet temperature, enthalpy[a] (K, kJ/kg) | 464, 467 | 481, 483 |
| Calculated compressor power[a] (kW) | 79.8 | 68.5 |
| GT-POWER predicted compressor power[a] (kW) | 25.3 | 17.5 |
| Change in compressor power[a] (kW) | 54.5 | 51 |

[a] These compressor outlet conditions and power values are based on the single supercharger with a pressure ratio that was allowed to exceed 2.5. Thus, these values are not equivalent to an actual system of two superchargers in series.

Table C.3: The four-stroke port valve configurations' compressor conditions and the resulting power consumption

| **Parameter** | **Standard Conditions** | **Hot and High Conditions** |
|---|---|---|
| Mass flow rate (kg/s) | 0.281 | 0.233 |
| Inlet temperature, enthalpy (K, kJ/kg) | 298, 298 | 313, 313 |
| Outlet temperature, enthalpy (K, kJ/kg) | 425, 427 | 445, 447 |
| Calculated compressor power (kW) | 36.2 | 31.2 |
| GT-POWER predicted compressor power (kW) | 27.5 | 22.7 |
| Change in compressor power (kW) | 8.7 | 8.5 |

Table C.4: The four-stroke standard configurations' compressor conditions and the resulting power consumption

| **Parameter** | **Standard Conditions** | **Hot and High Conditions** |
|---|---|---|
| Mass flow rate (kg/s) | 0.270 | 0.223 |
| Inlet temperature, enthalpy (K, kJ/kg) | 297, 297 | 311, 312 |
| Outlet temperature, enthalpy (K, kJ/kg) | 431, 433 | 450, 453 |
| Calculated compressor power (kW) | 36.6 | 31.4 |
| GT-POWER predicted compressor power (kW) | 26.1 | 20.8 |
| Change in compressor power (kW) | 10.5 | 10.6 |

## C.2 Mass Adjustment

The two/four-stroke engine mass estimation began with simulating the power output of a conventional engine design (i.e. poppet valves, single-stage supercharging), as outlined in Section 4.4. With this data, the standard engine configuration's wet mass was calculated using Equations 3.7, 3.10, and 3.11, per the discussion in Section 3.3.2.

Then, after modeling the two/four-stroke platform, the additional supercharging and intercooling requirements were determined for both of the two-stroke engine configurations (i.e. sized for standard and hot and high operation conditions) and the four-stroke operating mode. Due to the complexity of superchargers, variations in their designs, and lack of available data, a direct prediction trend was not achievable, and thus the modeling used example automotive racing supercharger systems as design points. Based on various manufacturers, a single high-performance supercharger system was estimated to have a mass of 50 kilograms [72, 73, 74, 75, 76]. Additionally, as the two-stroke operating mode required additional boosting capability, the configuration was assumed to increase the supercharging system mass by 50% (resulting in a total mass of 75 kilograms). This amount of additional mass is inline with smaller industry compressors, and the extra supercharging capabilities are assumed to require less mass than the initial main compressor [77].

Furthermore, the standard engine configuration's intercooler heat transfer rate was taken to represent a mass of 9 kg, based on devices that are implemented in similar sized high-performance applications [127, 128]. Using the assumption that the intercooler's mass is proportional to its heat transfer rate, the two- and four-stroke models' intercooler masses were approximated,

$$m_{\text{intercooler}} = \left( \frac{\dot{Q}_{\text{out,new}}}{\dot{Q}_{\text{out,baseline}}} \right) * 9, \tag{C.2}$$

where $m_{intercooler}$ is the intercooler mass estimation in kilograms, $\dot{Q}_{\text{out,new}}$ is the simulated intercooler heat transfer rate for the applicable configuration, and $\dot{Q}_{\text{out,baseline}}$ is the heat transfer rate for the standard model's intercooler. Tables C.5 and C.6 provide These results, as well as the wet engine mass and supercharger mass calculations.

Table C.5: The two/four-stroke initial modeling mass analysis data

| **Engine Parameters** | **Two/Four-Stroke, Standard Conditions** | **Two/Four-Stroke, Hot and High Conditions** | **Standard Four-Stroke Engine** |
|---|---|---|---|
| Net power output[a] (kW) | 344 | 280 | 243 |
| Trend-predicted engine dry mass (kg) | N/A | N/A | 185 |
| Compressor mass (kg) | 50 | 50 | 50 |
| Intercooler mass (kg) | 12 | 11 | 9 |
| Final engine dry mass[b,c] (kg) | 188 | 188 | 185 |
| Final engine wet mass[c] (kg) | 210 | 210 | 204 |

[a] This power output accounts for the supercharging power consumption.

[b] The dry engine mass was calculated using the baseline four-stroke configuration's predicted dry mass, and adjusting this value with the increased supercharger and intercooler masses.

[c] These values are equivalent as the engine platform is shared between the two operation modes.

Table C.6: The revisited two/four-stroke modeling mass analysis data

| **Engine Parameters** | **Two/Four-Stroke, Standard Conditions** | **Two/Four-Stroke, Hot and High Conditions** |
|---|---|---|
| Net power output[a] (kW) | 395 | 344 |
| Trend-predicted engine dry mass (kg) | N/A | N/A |
| Compressor mass (kg) | 75 | 75 |
| Intercooler mass (kg) | 21 | 22 |
| Final engine dry mass[b] (kg) | 222 | 222 |
| Final engine wet mass[c] (kg) | 247 | 247 |

[a] This power output accounts for the supercharging power consumption.

[b] The dry engine mass was calculated by taking the baseline four-stroke poppet valve configuration's predicted dry mass, and adjusting this value based on the increased supercharger and intercooler masses.

[c] These values are equivalent as the engine platform is shared between the two operation modes.

# Appendix D

# Airframe Characteristics and Performance Parameters

As a part of the flight profile modeling conducted in Chapter 5, baseline airframe characteristics and performance parameters were required to simulate each engine configuration's effect on the airframe's capabilities. These values were determined through a combination of industry standards and example airframes, and were initially designed with gas turbines as their engines. As a part of the modeling process, the airframes were modified to be equipped with each alternative engine configuration considered in this analysis. The flight profile modeling was then conducted, with the performance achieved by the baseline and modified airframes compared to evaluate the advantages and disadvantages of each engine configuration. The specific characteristics for the example aircraft used to tune the modeling, the baseline airframes, and the modified airframes are provided in the following sections.

## D.1 Example Rotorcraft

To assist the development of the flight profile modeling simulations, twelve airframes were identified and characterized through their manufacturer documentation and external sources, with the features identified in Tables D.1 through D.12. These rotorcraft were used to develop the appropriate performance parameters listed in Section

5.3.2 by modeling their range capabilities while varying the specified aircraft parameters. Once the fidelity of the developed models was verified by predicting a range similar to what is reported by the airframe's documentation, the developed airframe parameters could be used to simulate the constructed airframes.

Table D.1: The Sikorsky S-333 rotorcraft specifications [12, 83]

| **Airframe parameters** | |
|---|---|
| Gross takeoff mass | 1,157 kg |
| Rated takeoff power | 209 kW |
| Rotor radius | 4.2 m |
| Fuel mass | 223 kg |
| Climb speed | 7.0 m/s |
| **Engine parameters** | |
| Engine name (number of engines) | Rolls-Royce 250-C20W (1) |
| Engine mass | 73.5 kg |
| Engine SFC (rated at takeoff power) | 0.395 kg/kW/hr |

Table D.2: The Sikorsky S-434 rotorcraft specifications [12, 83]

| **Airframe parameters** | |
|---|---|
| Gross takeoff mass | 1,315 kg |
| Rated takeoff power | 239 kW |
| Rotor radius | 4.2 m |
| Fuel mass | 257 kg |
| Climb speed[a] | 7.0 m/s |
| **Engine parameters** | |
| Engine name (number of engines) | Rolls-Royce 250-C20W (1) |
| Engine mass | 73.5 kg |
| Engine SFC (rated at takeoff power) | 0.395 kg/kW/hr |

[a] The climb speed is taken from the S-333 due to these airframes' similarities.

Table D.3: The Airbus H120/EC120 rotorcraft specifications [12, 1]

| **Airframe parameters** | |
|---|---|
| Gross takeoff mass | 1,715 kg |
| Rated takeoff power | 376 kW |
| Rotor radius | 5.0 m |
| Fuel mass | 321 kg |
| Climb speed | 5.8 m/s |
| **Engine parameters** | |
| Engine name (number of engines) | Turbomeca Arrius 2F (1) |
| Engine mass | 103 kg |
| Engine SFC (rated at takeoff power) | 0.338 kg/kW/hr |

Table D.4: The Airbus H130 rotorcraft specifications [12, 86]

| **Airframe parameters** | |
|---|---|
| Gross takeoff mass | 2,500 kg |
| Rated takeoff power | 710 kW |
| Rotor radius | 5.4 m |
| Fuel mass | 425 kg |
| Climb speed | 8.0 m/s |
| **Engine parameters** | |
| Engine name (number of engines) | Turbomeca Arriel 2D (1) |
| Engine mass | 133 kg |
| Engine SFC (rated at takeoff power)[a] | 0.332 kg/kW/hr |

[a] This data is based on the Arriel 2C2 turboshaft engine.

Table D.5: The Airbus EC135: Pratt & Whitney rotorcraft specifications [87]

| **Airframe parameters** | |
|---|---|
| Gross takeoff mass | 2,950 kg |
| Rated takeoff power | 926 kW |
| Rotor radius | 5.1 m |
| Fuel mass | 560 kg |
| Climb speed | 7.4 m/s |
| **Engine parameters** | |
| Engine name (number of engines) | Pratt & Whitney PW206B3 (2) |
| Engine mass | 238 kg |
| Engine SFC (rated at takeoff power) | 0.330 kg/kW/hr |

Table D.6: The Airbus EC135: Turbomeca rotorcraft specifications [12, 87]

| **Airframe parameters** | |
|---|---|
| Gross takeoff mass | 2,910 kg |
| Rated takeoff power | 958 kW |
| Rotor radius | 5.1 m |
| Fuel mass | 560 kg |
| Climb speed | 7.6 m/s |
| **Engine parameters** | |
| Engine name (number of engines) | Turbomeca Arrius 2B2plus (2) |
| Engine mass | 228 kg |
| Engine SFC (rated at takeoff power)[a] | 0.328 kg/kW/hr |

[a] This SFC data is based on the Arrius 2B2 turboshaft engine.

Table D.7: The Airbus EC145 rotorcraft specifications [12, 81]

| **Airframe parameters** | |
|---|---|
| Gross takeoff mass | 3,585 kg |
| Rated takeoff power | 1,100 kW |
| Rotor radius | 5.5 m |
| Fuel mass | 694 kg |
| Climb speed | 8.1 m/s |
| **Engine parameters** | |
| Engine name (number of engines) | Turbomeca Arriel 1E2 (2) |
| Engine mass | 250 kg |
| Engine SFC (rated at takeoff power) | 0.349 kg/kW/hr |

Table D.8: The Airbus AS365 rotorcraft specifications [12, 88]

| **Airframe parameters** | |
|---|---|
| Gross takeoff mass | 4,300 kg |
| Rated takeoff power | 1,250 kW |
| Rotor radius | 6.0 m |
| Fuel mass | 897 kg |
| Climb speed | 6.7 m/s |
| **Engine parameters** | |
| Engine name (number of engines) | Turbomeca Arriel 2C (2) |
| Engine mass | 256 kg |
| Engine SFC (rated at takeoff power) | 0.333 kg/kW/hr |

Table D.9: The Airbus EC155 B1 rotorcraft specifications [12, 82]

| **Airframe parameters** | |
|---|---|
| Gross takeoff mass | 4,920 kg |
| Rated takeoff power | 1,406 kW |
| Rotor radius | 6.3 m |
| Fuel mass | 993 kg |
| Climb speed | 5.86 m/s |
| **Engine parameters** | |
| Engine name (number of engines) | Turbomeca Arriel 2C2 (2) |
| Engine mass | 256 kg |
| Engine SFC (rated at takeoff power) | 0.332 kg/kW/hr |

Table D.10: The Airbus H145/EC145 T2 rotorcraft specifications [12, 80]

| **Airframe parameters** | |
|---|---|
| Gross takeoff mass | 3,700 kg |
| Rated takeoff power | 1,334 kW |
| Rotor radius | 5.5 m |
| Fuel mass | 694 kg |
| Climb speed | 8.1 m/s |
| **Engine parameters** | |
| Engine name (number of engines) | Turbomeca Arriel 2E (2) |
| Engine mass | 278 kg |
| Engine SFC (rated at takeoff power)[a] | 0.330 kg/kW/hr |

[a] This value is the average SFC for the Arriel 2C2 and Arriel 2S1 turboshaft engines.

Table D.11: The Sikorsky S-76D rotorcraft specifications [84]

| **Airframe parameters** | |
|---|---|
| Gross takeoff mass | 5,386 kg |
| Rated takeoff power | 1,606 kW |
| Rotor radius | 6.7 m |
| Fuel mass | 893 kg |
| Climb speed | 8.3 m/s |
| **Engine parameters** | |
| Engine name (number of engines) | Pratt & Whitney PS210S (2) |
| Engine mass | 325 kg |
| Engine SFC (rated at takeoff power)[a] | 0.296 kg/kW/hr |

[a] The SFC is the predicted value at the rated power output, using the trend provided in Section 2.3.

Table D.12: The Westland Lynx Series 100 rotorcraft specifications [12]

| **Airframe parameters** | |
|---|---|
| Gross takeoff mass | 4,875 kg |
| Rated takeoff power | 1,760 kW |
| Rotor radius | 6.4 m |
| Fuel mass | 792 kg |
| Climb speed | 12.6 m/s |
| **Engine parameters** | |
| Engine name (number of engines) | Rolls-Royce Gem Mk. 530 (2) |
| Engine mass | 192 kg |
| Engine SFC (rated at takeoff power)[a] | 0.310 kg/kW/hr |

[a] The SFC is based on the Gem 42-1 turboshaft engine.

## D.2 Baseline Airframes

Based on the completion of the airframe design process provided in Chapter 5, the baseline airframes' final design characteristics are listed in Table D.13. The range of gross takeoff masses and the choice of which airframes implemented single- and dual-engine configurations were based on the trends observed for the example airframes listed in Section D.1. Furthermore, these rotorcraft were designed based on the industry practices used to size an airframe with gas turbine engines. Thus, each aircraft's gas turbine engine characteristics are provided in Table D.14, with the SFC calculated based on the high-end turboshaft correlation provided in Section 2.3.

Table D.13: The baseline airframe characteristics

| Airframe Number | Gross Takeoff Mass (kg) | Fuel mass (kg) | Payload (kg) | Propeller Radius (m) | Climb Speed (m/s) | Rotor Solidity, $\sigma$ |
|---|---|---|---|---|---|---|
| 1 | 1,000 | 193 | 172 | 4.1 | 6.7 | 0.0565 |
| 2 | 1,500 | 288 | 302 | 4.6 | 6.8 | 0.0595 |
| 3 | 2,000 | 382 | 433 | 5.0 | 6.9 | 0.0625 |
| 4 | 2,500 | 475 | 565 | 5.3 | 7.1 | 0.0655 |
| 5 | 3,000 | 567 | 698 | 5.6 | 7.2 | 0.0685 |
| 6 | 3,500 | 658 | 832 | 5.9 | 7.4 | 0.0715 |
| 7 | 4,000 | 784 | 967 | 6.1 | 7.5 | 0.0745 |
| 8 | 4,500 | 837 | 1,103 | 6.3 | 7.7 | 0.0775 |
| 9 | 5,000 | 926 | 1,240 | 6.5 | 7.8 | 0.0805 |
| 10 | 5,500 | 1,013 | 1,377 | 6.7 | 8.0 | 0.0835 |

Table D.14: The baseline airframes' engine characteristics

| Airframe Number (Number of Engines) | Engine Mass[a] (kg) | Power Output[a] (kW) | SFC[b] (kg/kW/hr) |
|---|---|---|---|
| 1 (1) | 72 | 204 | 0.443 |
| 2 (1) | 92 | 318 | 0.367 |
| 3 (1) | 111 | 439 | 0.333 |
| 4 (1) | 128 | 565 | 0.314 |
| 5 (2) | 217 | 846 | 0.336 |
| 6 (2) | 240 | 1,009 | 0.322 |
| 7 (2) | 261 | 1,176 | 0.311 |
| 8 (2) | 282 | 1,347 | 0.304 |
| 9 (2) | 303 | 1,522 | 0.298 |
| 10 (2) | 322 | 1,702 | 0.293 |

[a] The engine mass and power output includes both engines if the airframe is a dual-engine configuration.

[b] The SFC is the predicted value when operating at the rated power output, using the trend provided in Section 2.3.

## D.3 Modified Airframes

During the flight profile analysis provided in Chapter 5, the baseline airframes were modified to accommodate a variety of engine designs. Given the changes in engines, the mass allocation of each airframe was updated, with the following sections providing the results. Here, the helicopter mass was sectioned into the fuel, engine(s), payload, and balance (i.e. the remainder of the aircraft).

### D.3.1 Standard Implementation

First, the piston engines were installed in standard configurations, where the gas turbines were conceptually swapped with each piston engine design. Figures D-1 and D-2 provide the resulting mass allocation for the altered airframes, where the vertical axes plot the mass of each specific component, and the following abbreviations are used: gas turbine (GT), four-stroke diesel engine (4-S D.), two-stroke diesel engine (2-S D.), four-stroke gasoline engine (4-S G.), and two/four-stroke gasoline engine (2/4-S G.). Furthermore, Table D.15 lists the airframes' power required for the piston engine configurations. The powers are equal across all piston configurations due to the hot and high and OEI restrictions, as discussed in Appendix E.

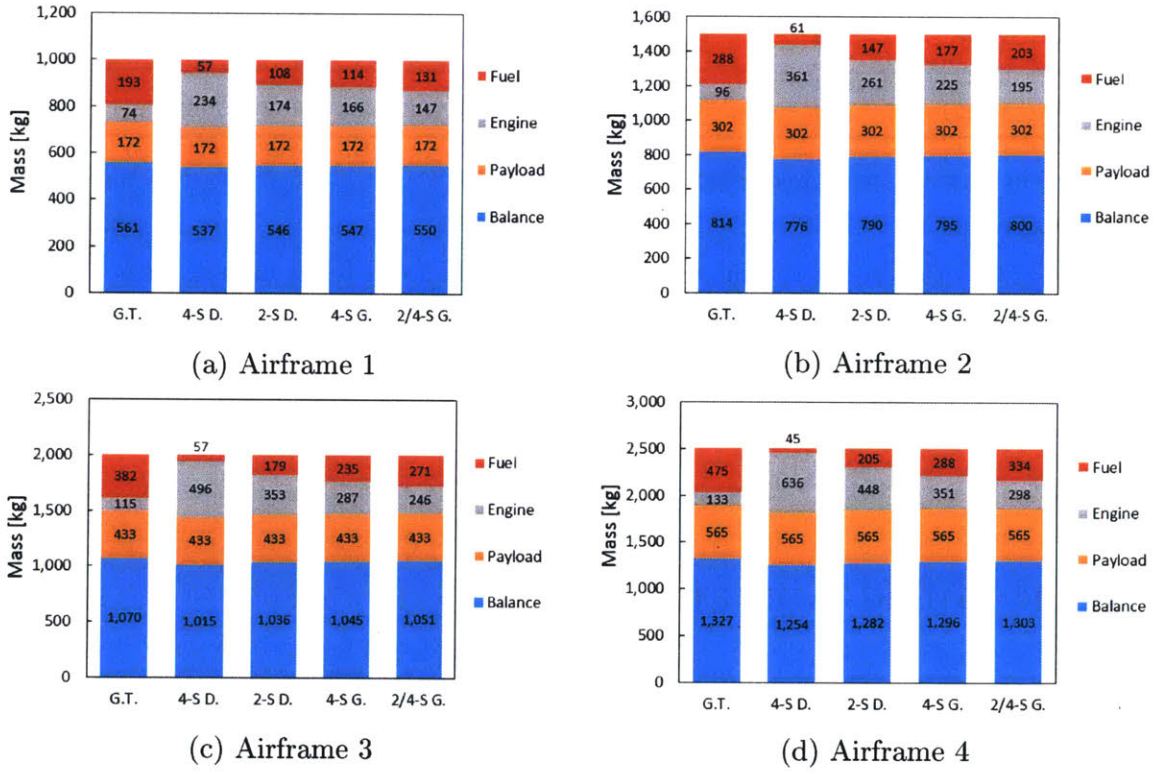


(a) Airframe 1

(b) Airframe 2

(c) Airframe 3

(d) Airframe 4

Figure D-1: The changes in mass between the single-engine configurations requires an adjustment to the amount of fuel that an airframe can carry.

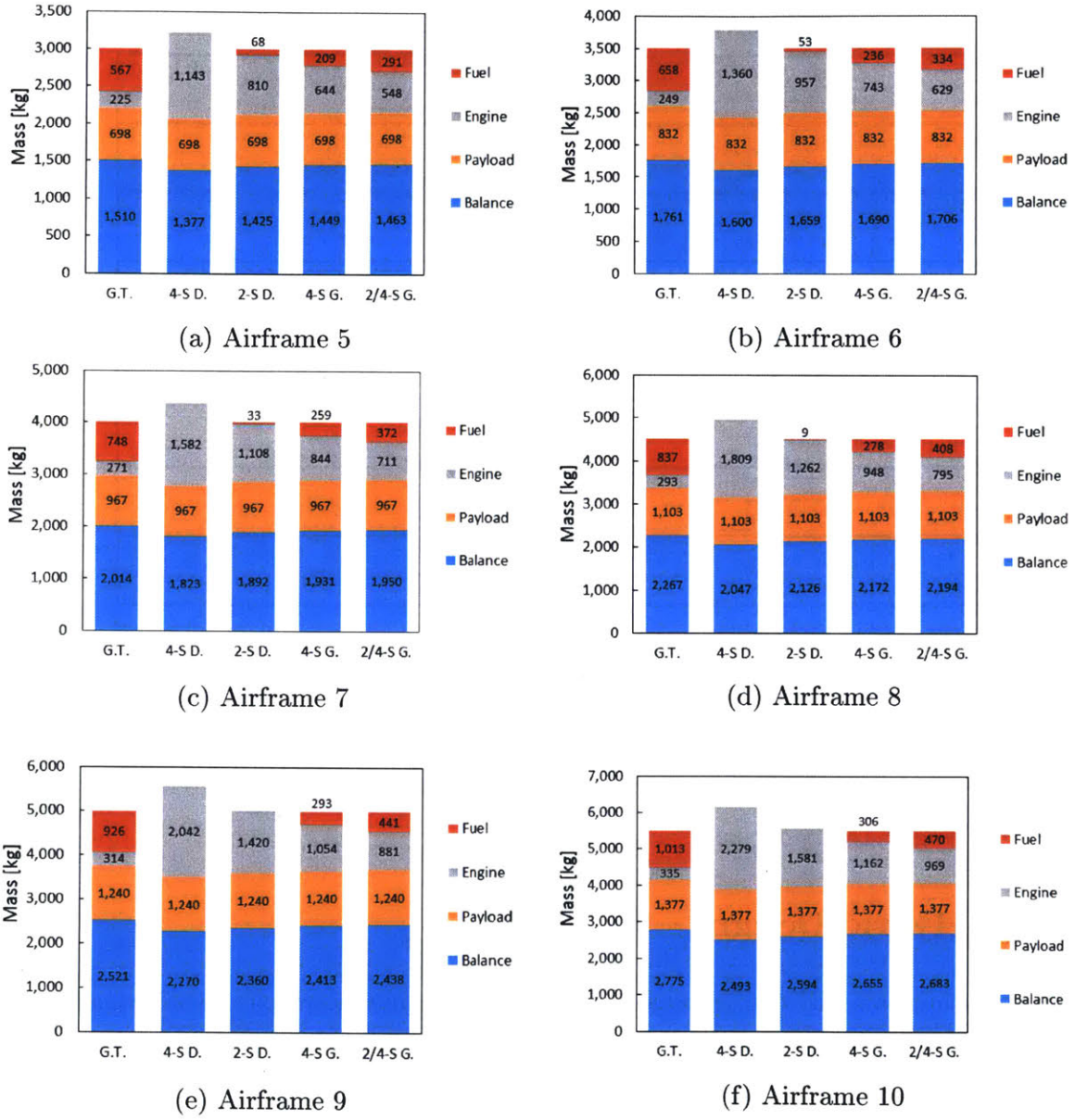


(a) Airframe 5

(b) Airframe 6

(c) Airframe 7

(d) Airframe 8

(e) Airframe 9

(f) Airframe 10

Figure D-2: The changes in mass between the dual-engine configurations requires an adjustment to the amount of fuel that an airframe can carry.

Table D.15: The airframes' required piston engine power output

| Airframe Number (Number of Engines) | Required Power Output[a](kW) |
|---|---|
| 1 (1) | 182 |
| 2 (1) | 283 |
| 3 (1) | 390 |
| 4 (1) | 503 |
| 5 (2) | 903 |
| 6 (2) | 1,076 |
| 7 (2) | 1,254 |
| 8 (2) | 1,437 |
| 9 (2) | 1,624 |
| 10 (2) | 1,815 |

[a] The engine power output includes both engines if the airframe is a dual-engine configuration.

### D.3.2 Hybrid Designs

Following the standard configurations, the piston engines were paired with gas turbines in hybrid configurations to leverage the strengths of each engine. Figures D-3 and D-4 provide the resulting mass allocation for the airframes, where the vertical axes plot the mass of each specific component, and the following abbreviations are used: gas turbine (GT), a four-stroke diesel engine paired with a gas turbine (H. 4-S D.), a two-stroke diesel engine and a gas turbine (H. 2-S D.), a four-stroke gasoline engine combined with a gas turbine (H. 4-S G.), and a two/four-stroke gasoline engine installed with a gas turbine (H. 2/4-S G). Additionally, Table D.16 contains each airframes' power required for each piston and gas turbine engine. The powers are

equal across all piston configurations due to the hot and high and OEI restrictions, as discussed in Appendix E.

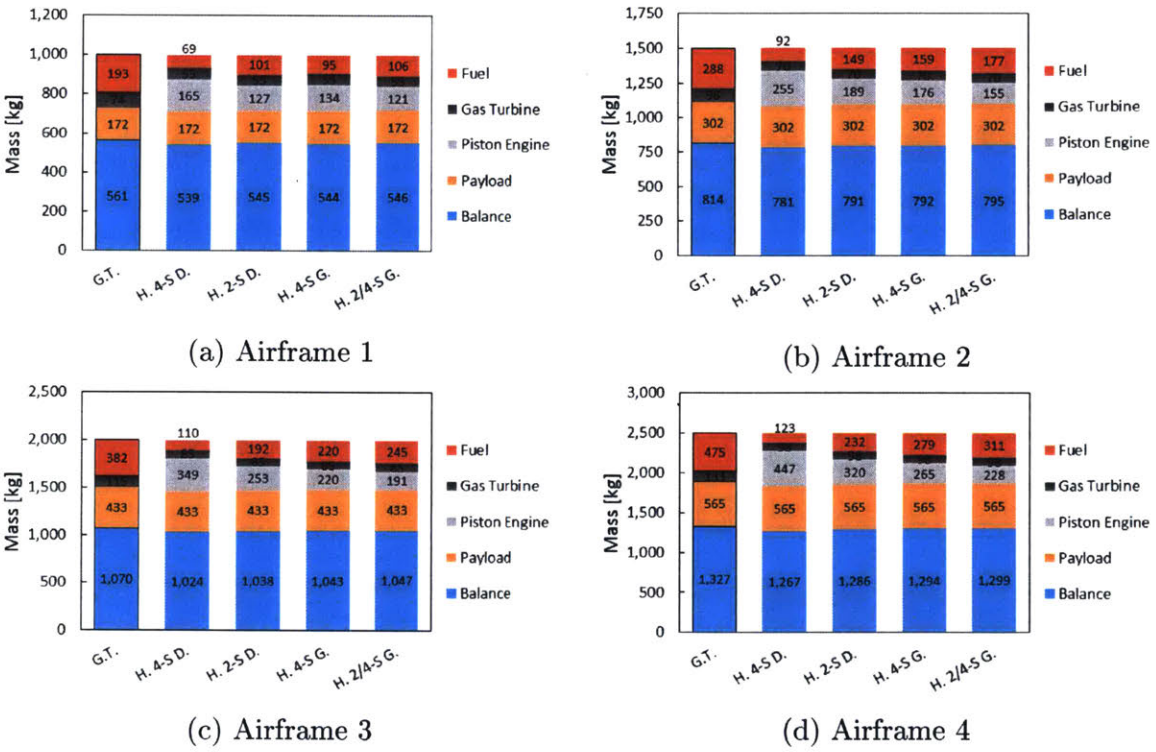


(a) Airframe 1

(b) Airframe 2

(c) Airframe 3

(d) Airframe 4

Figure D-3: The standard configurations are altered by pairing both a gas turbine and piston engine for the hybrid designs, which increases the engine mass in traditional single-engine airframes.

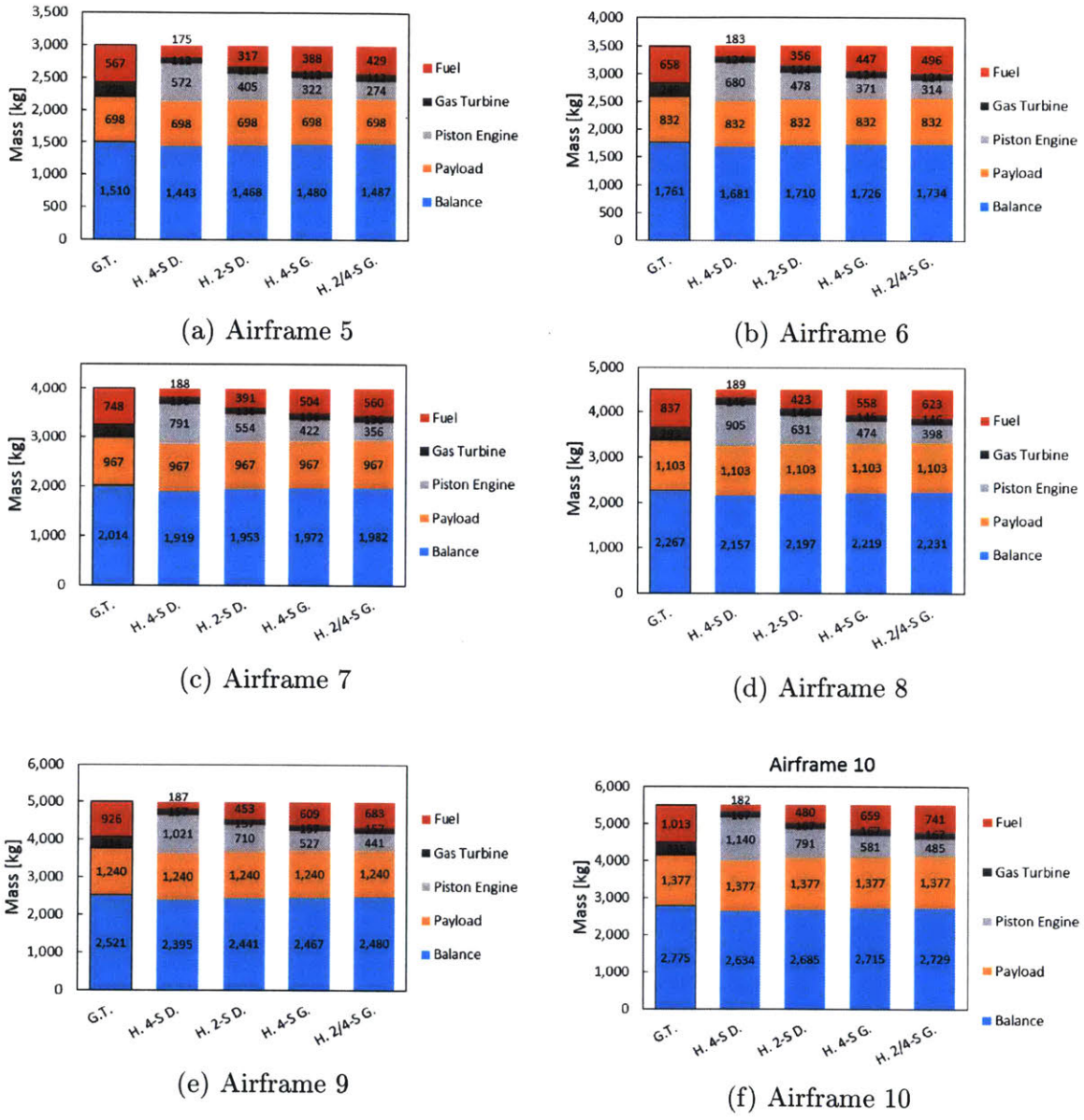


(a) Airframe 5

(b) Airframe 6

(c) Airframe 7

(d) Airframe 8

(e) Airframe 9

(f) Airframe 10

Figure D-4: The hybrid designs use one gas turbine and one piston engine to mitigate the total engine mass, as the piston engines are significantly heavier.

Table D.16: The hybrid airframes' individual engine power output

| **Airframe Number (Number of Engines)** | **Required Power Output[a](kW)** |
|---|---|
| 1 (2) | 127 |
| 2 (2) | 198 |
| 3 (2) | 273 |
| 4 (2) | 352 |
| 5 (2) | 451 |
| 6 (2) | 538 |
| 7 (2) | 627 |
| 8 (2) | 719 |
| 9 (2) | 812 |
| 10 (2) | 907 |

[a] The engine power output is for a single engine, and corresponds to both the gas turbine and piston engines.

### D.3.3 Auxiliary Engine Configurations

Finally, an auxiliary gas turbine was added to each standard piston and gas turbine configuration, with a similar goal as the hybrid designs; the auxiliary engine is used during takeoff and OEI conditions, while the main engines provide the remainder of the required power throughout the flight profile. Figures D-5 and D-6 provide the resulting mass allocation for the airframes, where the vertical axes plot the mass of each specific component, and the following abbreviations are used: gas turbine (GT, Std. for standard implementation, Aux. for the auxiliary configuration), four-stroke diesel main engine(s) and auxiliary gas turbine (Aux. 4-S D.), two-stroke diesel main engine(s) and auxiliary gas turbine (Aux. 2-S D.), four-stroke gasoline main engine(s)

and auxiliary gas turbine (Aux. 4-S G.), and two/four-stroke gasoline main engine(s) and auxiliary gas turbine (Aux. 2/4-S G.). Furthermore, Tables D.17 through D.21 contain each airframes' power required for the main and auxiliary engines. Note that the power requirements converged to common values for the majority of configurations due to the imposed limits on the acceptable ranges of power allocation caused by the hot and high and OEI considerations. These ranges, as well as the required powers, are calculated using the procedure provided in Appendix E.

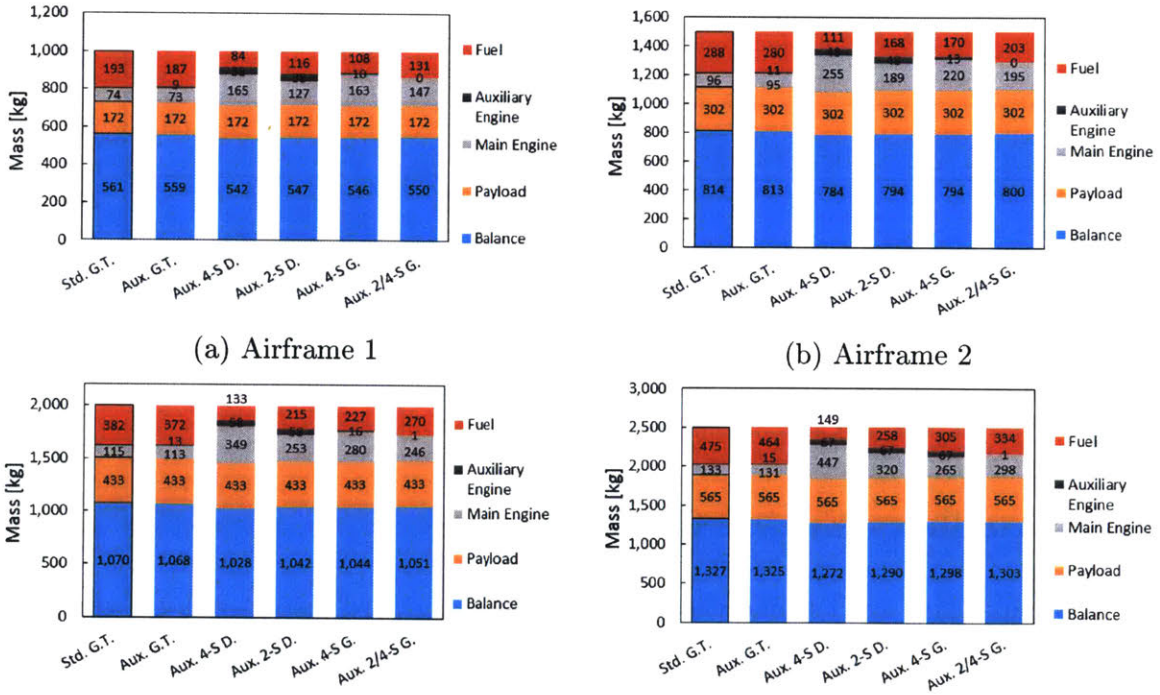


(a) Airframe 1

(b) Airframe 2

(c) Airframe 3

(d) Airframe 4

Figure D-5: The standard configurations are altered by introducing an auxiliary gas turbine, requiring changes in the mass allocation of each airframe.

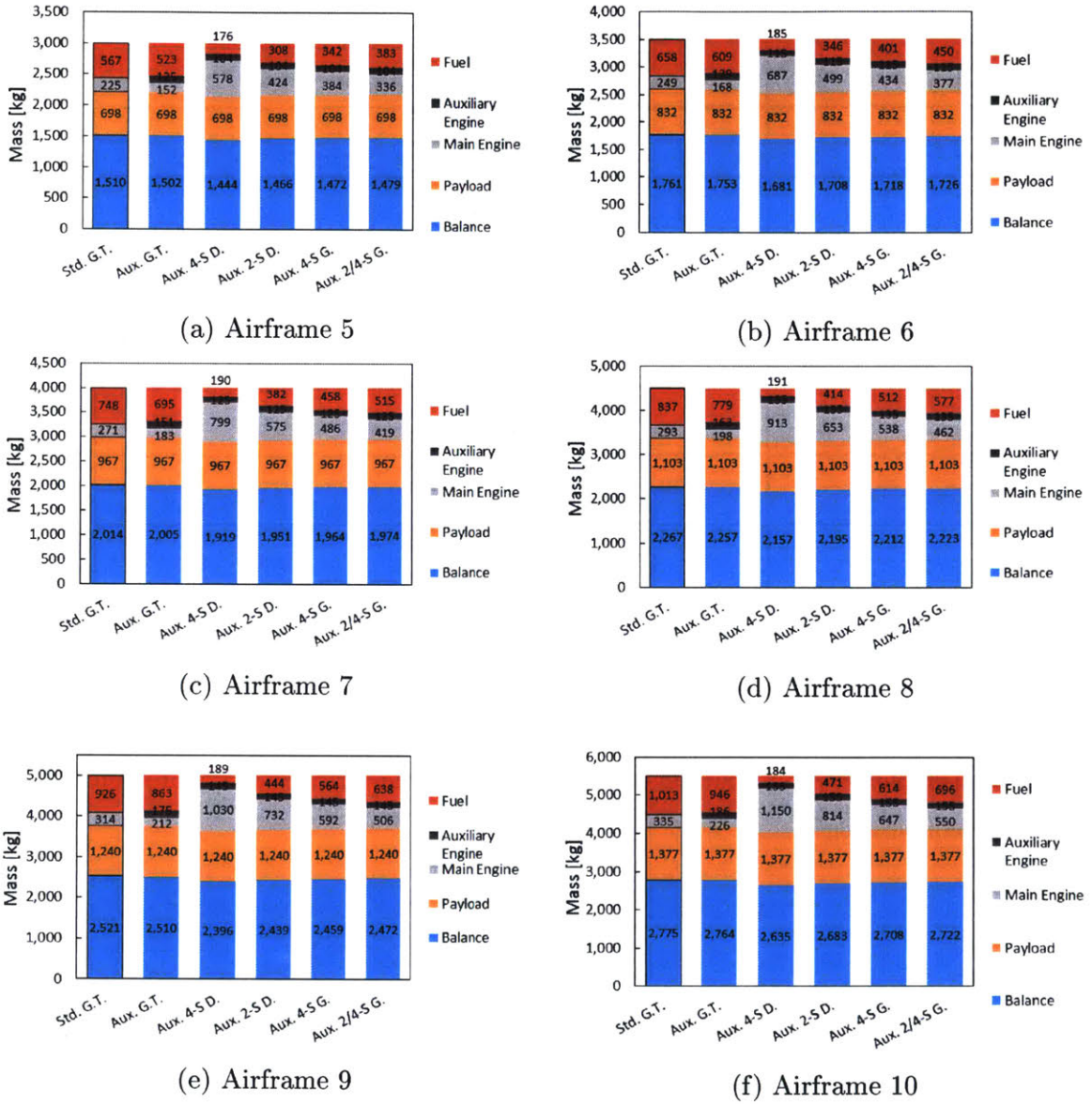


(a) Airframe 5

(b) Airframe 6

(c) Airframe 7

(d) Airframe 8

(e) Airframe 9

(f) Airframe 10

Figure D-6: The dual-main-engines are paired with an auxiliary gas turbine, requiring changes to the airframe mass allocation.

Table D.17: The auxiliary gas turbine airframes' power outputs

| **Airframe Number (Number of Engines)** | **Main Gas Turbine(s)[a] (kW)** | **Auxiliary Gas Turbine (kW)** |
|---|---|---|
| 1 (2) | 213 | 5 |
| 2 (2) | 332 | 7 |
| 3 (2) | 458 | 10 |
| 4 (2) | 590 | 13 |
| 5 (2) | 451 | 322 |
| 6 (2) | 538 | 384 |
| 7 (2) | 627 | 448 |
| 8 (2) | 719 | 513 |
| 9 (2) | 812 | 580 |
| 10 (2) | 907 | 648 |

[a] The main engine power output includes both engines if the airframe is a dual main engine configuration.

Table D.18: The auxiliary diesel four-stroke airframes' power outputs

| **Airframe Number (Number of Engines)** | **Main Diesel Engine(s)[a] (kW)** | **Auxiliary Gas Turbine (kW)** |
|---|---|---|
| 1 (2) | 127 | 65 |
| 2 (2) | 198 | 102 |
| 3 (2) | 273 | 141 |
| 4 (2) | 352 | 181 |
| 5 (2) | 451 | 232 |
| 6 (2) | 538 | 277 |
| 7 (2) | 627 | 323 |
| 8 (2) | 719 | 370 |
| 9 (2) | 812 | 418 |
| 10 (2) | 907 | 467 |

[a] The main engine power output includes both engines if the airframe is a dual main engine configuration.

Table D.19: The auxiliary diesel two-stroke airframes' power outputs

| **Airframe Number (Number of Engines)** | **Main Diesel Engine(s)[a] (kW)** | **Auxiliary Gas Turbine (kW)** |
|---|---|---|
| 1 (2) | 127 | 65 |
| 2 (2) | 198 | 102 |
| 3 (2) | 273 | 141 |
| 4 (2) | 352 | 181 |
| 5 (2) | 451 | 232 |
| 6 (2) | 538 | 277 |
| 7 (2) | 627 | 323 |
| 8 (2) | 719 | 370 |
| 9 (2) | 812 | 418 |
| 10 (2) | 907 | 467 |

[a] The main engine power output includes both engines if the airframe is a dual main engine configuration.

Table D.20: The auxiliary gasoline four-stroke airframes' power outputs

| **Airframe Number (Number of Engines)** | **Main Gasoline Engine(s)[a](kW)** | **Auxiliary Gas Turbine (kW)** |
|---|---|---|
| 1 (2) | 176 | 7 |
| 2 (2) | 274 | 11 |
| 3 (2) | 378 | 15 |
| 4 (2) | 352 | 181 |
| 5 (2) | 451 | 232 |
| 6 (2) | 538 | 277 |
| 7 (2) | 627 | 323 |
| 8 (2) | 719 | 370 |
| 9 (2) | 812 | 418 |
| 10 (2) | 907 | 467 |

[a] The main engine power output includes both engines if the airframe is a dual main engine configuration.

Table D.21: The auxiliary gasoline two/four-stroke airframes' power outputs

| **Airframe Number (Number of Engines)** | **Main Gasoline Engine(s)[a](kW)** | **Auxiliary Gas Turbine (kW)** |
|---|---|---|
| 1 (2) | 182 | 0 |
| 2 (2) | 283 | 0 |
| 3 (2) | 390 | 0 |
| 4 (2) | 502 | 0 |
| 5 (2) | 451 | 232 |
| 6 (2) | 538 | 277 |
| 7 (2) | 627 | 323 |
| 8 (2) | 719 | 370 |
| 9 (2) | 812 | 418 |
| 10 (2) | 907 | 467 |

[a] The main engine power output includes both engines if the airframe is a dual main engine configuration.

# Appendix E

# Engine Sizing

For each configuration, the engine sizing process took into account the OEI and hot and high conditions and their influences on the airframe power requirements and engine power ratings. In the calculations used to estimate the engine sizes, $P_{engine}$ is the total required power output of an individual engine in kilowatts, $P_{hover,\ H\&H}$ represents the airframe's power requirement when hovering at hot and high conditions in kilowatts, $x_{H\&H}$ is the hot and high derating for the specified engine type (i.e. gas turbine or piston), $x_{GT,\ OEI}$ is the OEI power increase for the gas turbines, and $x_{main\ frac}$ is fraction of the total airframe power allocated to the main engine(s) for the auxiliary configurations.

As discussed in Section 2.3, gas turbines are estimated to have a hot and high derating of 25%, due to the lower air density and negative effects of higher air temperature [10, 92]. Similarly, as identified in Section 3.6.1, the piston engine hot and high derating is approximated as 10%, with the negative effects being limited by the excess boosting capabilities that are achieved through proper design. Furthermore, per the data and discussion provided in Section 2.3, gas turbines are estimated to provide a 20% increase in power output during OEI operation. On the other hand, as piston engine data is based on maximum possible performance, it is assumed that attempting to gain further power output would result in rapid engine failure, due to higher speeds (and thus greater stresses) causing the rotating and reciprocating components to fail, or higher peak pressures damaging the cylinders and cylinder

heads while causing the onset of knock. Thus, the piston engine configurations were not rated for increased performance in OEI conditions. Additionally, for the OEI calculations, the constant 0.7 accounts for the engine performance requirements in this scenario. Per the analysis provided in Section 1.3, an engine must provide 70% of the takeoff decision point (TDP) power output during OEI conditions, resulting in the 0.7 factor used to calculate the power requirement at this flight profile stage. Each of these factors and parameters are used to estimate the required engine sizing for the following configurations.

## E.1 Standard and Hybrid Implementation

Using the previously outline parameters, the engine power requirements for the standard and hybrid configurations were completed using the following equations.

### E.1.1 Single-Engine Configurations

In single-engine configurations, no OEI considerations are require, and thus the engine is sized based on the power requirement of the airframe in hot and high conditions, accounting for the engine's hot and high derating.

#### Gas Turbines: Single-Engine Configurations

$$\begin{aligned} P_{\text{engine}} * x_{\text{GT, H\&H}} &= P_{\text{hover, H\&H}} \\ P_{\text{engine}} &= \frac{P_{\text{hover, H\&H}}}{x_{\text{GT, H\&H}}} \\ &= \frac{P_{\text{hover, H\&H}}}{0.75}, \end{aligned}$$

$$P_{\text{engine}} = 1.33 P_{\text{hover, H\&H}} \quad (kW). \tag{E.1}$$

**Piston Engines: Single-Engine Configurations**

$$
\begin{aligned}
P_{\text{engine}} * x_{\text{Pist, H\&H}} &= P_{\text{hover, H\&H}} \\
P_{\text{engine}} &= \frac{P_{\text{hover, H\&H}}}{x_{\text{Pist, H\&H}}} \\
&= \frac{P_{\text{hover, H\&H}}}{0.9},
\end{aligned}
$$

$$
P_{\text{engine}} = 1.11 P_{\text{hover, H\&H}} \quad (kW). \tag{E.2}
$$

### E.1.2 Dual-Engine Configurations

For dual-engine configurations, the OEI condition requires that the operable engine produces 70% of the airframe's required power at the TDP in hot and high operation, while accounting for the engine's derating in the adverse ambient conditions.

**Gas Turbines: Dual-Engine Configurations**

$$
\begin{aligned}
P_{\text{engine}} * x_{\text{GT, H\&H}} * x_{\text{GT, OEI}} &= 0.7 P_{\text{hover, H\&H}} \\
P_{\text{engine}} &= \frac{0.7 P_{\text{hover, H\&H}}}{x_{\text{GT, OEI}} * x_{\text{GT, H\&H}}} \\
&= \frac{0.7 P_{\text{hover, H\&H}}}{1.2 * 0.75},
\end{aligned}
$$

$$
P_{\text{engine}} = 0.78 P_{\text{hover, H\&H}} \quad (kW). \tag{E.3}
$$

**Piston Engines: Dual-Engine Configurations**

$$\begin{aligned} P_{\text{engine}} * x_{\text{Pist, H\&H}} &= 0.7 P_{\text{hover, H\&H}} \\ P_{\text{engine}} &= \frac{0.7 P_{\text{hover, H\&H}}}{x_{\text{Pist, H\&H}}} \\ &= \frac{0.7 P_{\text{hover, H\&H}}}{0.9}, \end{aligned}$$

$$P_{\text{engine}} = 0.78 P_{\text{hover, H\&H}} \quad (kW). \tag{E.4}$$

## E.2 Auxiliary Engine Configurations

First, for each gas turbine and piston engine configuration, the airframe's total power requirement was determined based on hot and high conditions. Subsequently, the range of allowable auxiliary engine power allocation was calculated to ensure that the airframe could produce 70% of the power required at the TDP, per the discussion provided in Section 1.3.

### E.2.1 Power Requirements

The engine configuration's total power capability is sized based on the airframe's power requirement for takeoff in hot and high conditions, accounting each engine design's hot and high derating.

**Main Engine: Gas Turbine**

$$P_{\text{main engine(s)}} + P_{\text{aux engine}} = P_{\text{hover, H\&H}}, \tag{E.5}$$

$$\begin{aligned} P_{\text{main engine(s)}} &= x_{\text{main frac}} * P_{\text{total}} * x_{\text{GT, H\&H}} \\ &= x_{\text{main frac}} * P_{\text{total}} * 0.75, \end{aligned} \tag{E.6}$$

$$\begin{aligned} P_{\text{aux engine}} &= (1 - x_{\text{main frac}}) * P_{\text{total}} * x_{\text{GT, H\&H}} \\ &= (1 - x_{\text{main frac}}) * P_{\text{total}} * x_{\text{GT, H\&H}} \\ &= (1 - x_{\text{main frac}}) * P_{\text{total}} * 0.75. \end{aligned} \tag{E.7}$$

Substituting Equations E.6 and E.7 into Equation E.5,

$$\begin{aligned} x_{\text{main frac}} * P_{\text{total}} * 0.75 + (1 - x_{\text{main frac}}) * P_{\text{total}} * 0.75 &= P_{\text{hover, H\&H}} \\ 0.75 x_{\text{main frac}} * P_{\text{total}} &= P_{\text{hover, H\&H}} \\ P_{\text{total}} &= \frac{P_{\text{hover, H\&H}}}{0.75}, \end{aligned}$$

$$P_{\text{total}} = 1.33 P_{\text{hover, H\&H}}. \tag{E.8}$$

**Main Engine: Piston Engine**

$$P_{\text{main engine(s)}} + P_{\text{aux engine}} = P_{\text{hover, H\&H}}, \tag{E.9}$$

$$\begin{aligned} P_{\text{main engine(s)}} &= x_{\text{main frac}} * P_{\text{total}} * x_{\text{pist, H\&H}} \\ &= x_{\text{main frac}} * P_{\text{total}} * 0.9, \end{aligned} \tag{E.10}$$

$$\begin{aligned} P_{\text{aux engine}} &= (1 - x_{\text{main frac}}) * P_{\text{total}} * x_{\text{GT, H\&H}} \\ &= (1 - x_{\text{main frac}}) * P_{\text{total}} * x_{\text{GT, H\&H}} \\ &= (1 - x_{\text{main frac}}) * P_{\text{total}} * 0.75. \end{aligned} \tag{E.11}$$

Substituting Equations E.10 and E.11 into Equation E.9,

$$x_{\text{main frac}} * P_{\text{total}} * 0.9 + (1 - x_{\text{main frac}}) * P_{\text{total}} * 0.75 = P_{\text{hover, H\&H}}$$

$$P_{\text{total}}(0.75 + x_{\text{main frac}}(0.9 - 0.75)) = P_{\text{hover, H\&H}},$$

$$P_{\text{total}} = \frac{P_{\text{hover, H\&H}}}{0.75 + 0.15x_{\text{main frac}}}. \tag{E.12}$$

### E.2.2 Main Engine Power Allocation Limits

The calculated limits to the main engine power allocation were based on situations when either the auxiliary engine or, for dual main engine configurations, one of the main engines fail. In the former scenario, the main engine(s) must have sufficient power to produce the requisite 70% of the power requirement at the takeoff decision point in hot and high operation, while accounting for the engine derating in this condition. Thus, this failure mode corresponds to the lower limit for the main engine sizing. As seen in Equations E.16 and E.25, the calculation of this limit is independent of the number of main engines, resulting in the single and dual main engine analyses being restricted by the same main engine lower limit.

On the other hand, when one of the main engines fail in the dual main engine configurations, only half of the power allocated to the main engines is available. Thus, as increasing the main engine power allocation would decrease the airframe's capabilities, this scenario provides the upper limit for the dual main engine sizing. For single main engine configurations, the analysis assumed that the design must only ensure OEI capabilities for the main engine, as this provides the same likelihood of catastrophic failure when compared to the standard design (i.e. the standard single engine is as likely to fail as the main engine). Thus, the upper limit for the percent of total power provided by the single main engine was determined to be 100%. The remaining lower and upper limits were calculated using the following equations, where $P_{hover,\ H\&H}$ is substituted based on Equations E.1 through E.12 for the applicable

configuration.

### Gas Turbine Lower Limit

$$P_{\text{main engine(s)}} \geq 0.7 P_{\text{hover, H\&H}}, \tag{E.13}$$

$$\begin{aligned} P_{\text{main engine(s)}} &= x_{\text{main frac}} * P_{\text{total}} * x_{\text{GT, H\&H}} * x_{\text{GT, OEI}} \\ &= x_{\text{main frac}} * P_{\text{total}} * 0.75 * 1.2 \\ &= x_{\text{main frac}} * P_{\text{total}} * 0.9, \end{aligned} \tag{E.14}$$

$$\begin{aligned} 0.7 P_{\text{hover, H\&H}} &= 0.7 * 0.75 P_{\text{total}} \\ &= 0.525 P_{\text{total}}. \end{aligned} \tag{E.15}$$

Substituting Equations E.14 and E.15 into Equation E.13,

$$\begin{aligned} 0.9 x_{\text{main frac}} * P_{\text{total}} &\geq 0.525 P_{\text{total}}, \\ x_{\text{main frac}} &\geq 0.583. \end{aligned} \tag{E.16}$$

### Gas Turbine Dual Main Engine Upper Limit

$$P_{\text{main engine}} + P_{\text{aux engine}} \geq 0.7 P_{\text{hover, H\&H}}, \tag{E.17}$$

$$\begin{aligned} P_{\text{main engine}} &= \frac{1}{2} x_{\text{main frac}} * P_{\text{total}} * x_{\text{GT, H\&H}} * x_{\text{GT, OEI}} \\ &= \frac{1}{2} x_{\text{main frac}} * P_{\text{total}} * 0.75 * 1.2 \\ &= 0.45 x_{\text{main frac}} * P_{\text{total}}, \end{aligned} \tag{E.18}$$

$$\begin{aligned} P_{\text{aux engine}} &= (1 - x_{\text{main frac}}) P_{\text{total}} * x_{\text{GT, H\&H}} * x_{\text{GT, OEI}} \\ &= (1 - x_{\text{main frac}}) P_{\text{total}} * 0.75 * 1.2 \\ &= (1 - x_{\text{main frac}}) P_{\text{total}} * 0.9, \end{aligned} \tag{E.19}$$

$$\begin{aligned} 0.7 P_{\text{hover, H\&H}} &= 0.7 * 0.75 P_{\text{total}} \\ &= 0.525 P_{\text{total}}. \end{aligned} \tag{E.20}$$

Substituting equations E.18, E.19, and E.20 into Equation E.17,

$$\begin{aligned} 0.45 x_{\text{main frac}} * P_{\text{total}} + (1 - x_{\text{main frac}}) P_{\text{total}} * 0.9 &\geq 0.525 P_{\text{total}} \\ x_{\text{main frac}}(0.45 - 0.9) &\geq 0.525 - 0.9, \end{aligned}$$

$$x_{\text{main frac}} \leq 0.833. \tag{E.21}$$

**Piston Engine Lower Limit**

$$P_{\text{main engine(s)}} \geq 0.7 P_{\text{hover, H\&H}}, \tag{E.22}$$

$$P_{\text{main engine(s)}} = x_{\text{main frac}} * P_{\text{total}} * x_{\text{Pist, H\&H}}$$
$$= x_{\text{main frac}} * P_{\text{total}} * 0.9, \tag{E.23}$$

$$0.7P_{\text{hover, H\&H}} = 0.7P_{\text{total}}(0.75 + 0.15x_{\text{main frac}})$$
$$= P_{\text{total}}(0.525 + 0.105x_{\text{main frac}}). \tag{E.24}$$

Substituting Equations E.23 and E.24 into Equation E.22,

$$0.9x_{\text{main frac}} * P_{\text{total}} \geq P_{\text{total}}(0.525 + 0.105x_{\text{main frac}})$$
$$x_{\text{main frac}}(0.9 - 0.105) \geq 0.525,$$

$$x_{\text{main frac}} \geq 0.660. \tag{E.25}$$

**Dual Main Piston Engine Upper Limit**

$$P_{\text{main engine}} + P_{\text{aux engine}} \geq 0.7P_{\text{hover, H\&H}}, \tag{E.26}$$

$$\begin{aligned} P_{\text{main engine}} &= \frac{1}{2} x_{\text{main frac}} * P_{\text{total}} * x_{\text{Pist, H\&H}} \\ &= \frac{1}{2} x_{\text{main frac}} * P_{\text{total}} * 0.9 \\ &= 0.45 x_{\text{main frac}} * P_{\text{total}}, \end{aligned} \tag{E.27}$$

$$\begin{aligned} P_{\text{aux engine}} &= (1 - x_{\text{main frac}}) P_{\text{total}} * x_{\text{GT, H\&H}} * x_{\text{GT, OEI}} \\ &= (1 - x_{\text{main frac}}) P_{\text{total}} * 0.75 * 1.2 \\ &= (1 - x_{\text{main frac}}) P_{\text{total}} * 0.9, \end{aligned} \tag{E.28}$$

$$\begin{aligned} 0.7 P_{\text{hover, H\&H}} &= 0.7 P_{\text{total}} (0.75 + 0.15 x_{\text{main frac}}) \\ &= P_{\text{total}} (0.525 + 0.105 x_{\text{main frac}}). \end{aligned} \tag{E.29}$$

Substituting Equations E.27, E.28, and E.29 into Equation E.26,

$$0.45 x_{\text{main frac}} * P_{\text{total}} + (1 - x_{\text{main frac}}) P_{\text{total}} * 0.9 \geq P_{\text{total}} (0.525 + 0.105 x_{\text{main frac}})$$

$$x_{\text{main frac}} (0.45 - 0.9 - 0.105) \geq 0.525 - 0.9$$

$$x_{\text{main frac}} \leq 0.676. \tag{E.30}$$

# Bibliography


[1] "H120." *Airbus Helicopters*, https://www.airbushelicopters.com/website/docs_wsw/RUB_26/tile_2581/H120-2016.pdf. Accessed 15 June 2016. PDF.

[2] "Bell Boeing V22 Data Brochure." *Bell Helicopter*, http://www.bellhelicopter.com/military/bell-boeing-v-22. Accessed 2 December 2016. PDF.

[3] Leishman, J. Gordon. *Principles of Helicopter Aerodynamics.* 2nd ed. Cambridge University Press, 2006.

[4] "R44 Raven II & Clipper II." *Robinson Helicopter Company*, http://www.robinsonheli.com/brochures/r44_raven_2_brochure.pdf. Accessed 31 December 2016.

[5] "Airbus Helicopters starts flight tests with high-compression engine for cleaner, more efficient and higher-performance rotorcraft." *Airbus Helicopters*, https://www.airbushelicopters.com/website/docs_wsw/RUB_151/press_1859/2015-11-10_Airbus_Helicopters_Clean-Sky_Flight-tests-with-high-compression-engine_EN.pdf. Accessed 2 February 2016.

[6] Seddon, John and Simon Newman. *Basic Helicopter Aerodynamics.* John Wiley & Sons, Ltd, 2011.

[7] Boyce, Meherwan P. *Gas Turbine Engineering Handbook.* Elsevier Inc. 2012. Internet resource.

[8] "Commission Regulation (EU) No 965/2012." European Aviation Safety Agency. OJ L 296. 5 October 2012.

[9] Soares, Claire. *Gas Turbines: A Handbook Of Air, Land And Sea Applications.* n.p.: Amsterdam: Butterworth-Heinemann, [2015], 2015. MIT Barton Catalog. Web. 18 Jan. 2017.

[10] Greatrix, David R. *Powered Flight The Engineering of Aerospace Propulsion.* Springer-Verlag London Limited. 2012.

[11] *IHS Jane's Aero-Engines.* n.p.: Coulsdon, Surrey, UK : IHS Jane's, IHS Global Limited, 2015. MIT Barton Catalog. Web. 27 Jan. 2017.

[12] *2009 Helicopter Annual.* Helicopter Association International. 2009. `http://helicopterannual.org/portals/27/pdf/ann_p3c3.pdf`. Web. 7 Dec. 2016.

[13] Taylor, Michael J. H. *Brassey's World Aircraft and Systems Directory, 1999-2000.* Herndon, VA: Brassey's Inc, 1999.

[14] Heywood, John B. *Internal Combustion Engine Fundamentals.* McGraw-Hill, Inc. 1988.

[15] Wasselin, T., et al., "Potential of Several Alternative Propulsion Systems for Light Rotorcrafts Applications." SAE Int. J. Aerosp. 6(2):2013, doi:10.4271/2013-01-2230.

[16] Kurz, Rainer, "GAS TURBINE PERFORMANCE." Proceedings of the Thirty-Fourth Turbomachinery Symposium, 2005.

[17] Kundu, Pijush K, and Ira M. Cohen. *Fluid Mechanics.* Amsterdam: Academic Press, 2008. Internet resource.

[18] Walsh, Philip P. and Paul Fletcher. *Gas Turbine Performance.* Second edition. Blackwell Science Ltd. 2004

[19] Lord, W. K., et al., "Engine Architecture for High Efficiency at Small Core Size." American Institute of Aeronautics and Astronautics Inc. 53rd AIAA Aerospace Sciences Meeting, 2015. Web. 9 Jan. 2015.

[20] Hill, Philip G., and Carl R. Peterson. *Mechanics And Thermodynamics Of Propulsion.* Second edition. n.p.: Reading, Mass. : Addison-Wesley, 1992.

[21] Dixon, S. L., and C. A. Hall. *Fluid Mechanics And Thermodynamics Of Turbomachinery.* Fourth edition. n.p.: Amsterdam : Boston : Butterworth-Heinemann/Elsevier, 2014.

[22] Hoag, Kevin and Brian Dondlinger. *Vehicular Engine Design.* Second edition. Springer Vienna, 2016.

[23] Moin, Shaik. "Petrol Engine." *Shaik Moin,* `https://shaikmoin.wordpress.com/page/6/`. Accessed 7 March 2017.

[24] "ExxonMobil Avgas." *ExonnMobile,* `https://www.exxonmobil.com/english-US/Commercial-Fuel/pds/GLXXAvgas-Series`. Accessed 19 March 2017.

[25] Sucheski, Pete. "The Physics of: Engine Cylinder Bank-Angles." *Car and Driver,* `http://www.caranddriver.com/features/the-physics-of-engine-cylinder-bank-angles-feature`. Accessed 22 March 2017.

[26] "Inline-four engine." *Wikipedia*, https://en.wikipedia.org/wiki/Inline-four_engine. Accessed 22 March 2017.

[27] "Inside The Radial Engine." *The Aviation History Online Museum*, http://www.aviation-history.com/engines/radial.htm. Accessed 22 March 2017.

[28] Jo, Y., et al., "Performance Maps of Turbocharged SI Engines with Gasoline-Ethanol Blends: Torque, Efficiency, Compression Ratio, Knock Limits, and Octane." SAE Technical Paper 2014- 01-1206, 2014, doi:10.4271/2014-01-1206.

[29] Jo, Y., et al., "Octane Requirement of a Turbocharged Spark Ignition Engine in Various Driving Cycles." SAE Technical Paper 2016-01-0831, 2016, doi:10.4271/2016-01-0831.

[30] Stein, R., et al., "Optimal Use of E85 in a Turbocharged Direct Injection Engine." SAE Int. J. Fuels Lubr. 2(1):670-682, 2009, doi:10.4271/2009-01-1490.

[31] "What about GDI (Gasoline Direct Injection) Vehicles?" *DK Auto*, http://dkautodbq.com/ourservices/fuelinjectionservice/. Accessed 29 March 2017.

[32] Nguyen-Schäfer, Hung, *Rotordynamics of Automotive Turbochargers.* 2nd ed. Springer International Publishing, 2015.

[33] Hiereth, Hermann and Peter Prenninger, *Charging the Internal Combustion Engine Powertrain.* Edited by Helmut List, Translated by Klaus Drexl, Springer-Verlag, Wien, 2007.

[34] Klein, Sanford and Gregory Nellis, *Thermodynamics.* Cambridge University Press, 2012.

[35] "Piston (Reciprocating) Engine Power Plants." *Woodbank Communications*, http://www.mpoweruk.com/piston_engines.htm. Accessed 4 April 2017.

[36] "SR305." Safran, https://www.smaengines.com/sites/snecma_sma/files/fiche_sma_sr_305_engine_bat_0.pdf. Accessed 5 November 2017. PDF.

[37] R. J. Osborne, et al., "Development of a Two-Stroke/Four-Stroke Switching Gasoline Engine - The 2/4SIGHT Concept." SAE International Technical Paper 2005-01-1137, 2005, doi:10.4271/2005-01-1137.

[38] Zhang, Y., et al., "Experiment and Analysis of a Direct Injection Gasoline Engine Operating with 2-stroke and 4-stroke Cycles of Spark Ignition and Controlled Auto-Ignition Combustion." SAE International Technical Paper 2011-01-1774, 2011, doi:10.4271/2011-01-1774.

[39] Pugnali, Lucas D., and Rui Chen, "Feasibility Study of Operating 2-Stroke Miller Cycles on a 4-Stroke Platform through Variable Valve Train." SAE International Technical Paper 2015-01-1974, 2015, doi:10.4271/2015-01-1974.

[40] Kasseris, E. and J. Heywood, "Charge Cooling Effects on Knock Limits in SI DI Engines Using Gasoline/Ethanol Blends: Part 1-Quantifying Charge Cooling." SAE International Technical Paper 2012-01-1275, 2012, doi:10.4271/2012-01-1275.

[41] Kasseris, E. and J. Heywood, "Charge Cooling Effects on Knock Limits in SI DI Engines Using Gasoline/Ethanol Blends: Part 2-Effective Octane Numbers." SAE International J. Fuels Lubr. 5(2):2012, doi:10.4271/2012-01-1284.

[42] Sun, A. and T. Kuo, "Transient Control of Electro-Hydraulic Fully Flexible Engine Valve Actuation System." IEEE Transactions on Control Systems Technology, Vol. 18 No. 3, May 2010., doi:10.1109/TCST.2009.2025188.

[43] Pournazeri, M., et. al., "An Efficient Lift Control Technique in Electrohydraulic Camless Valvetrain Using Variable Speed Hydraulic Pump." SAE International Technical Paper 2011-01-0940, 2011, doi:10.4271/2011-01-0940.

[44] Postrioti, L., et. al., "Application of a Fully Flexible Electro-Hydraulic Camless System to a Research Engine." SAE International Technical Paper 2009-24-0076, 2009, doi:10.4271/2009-24-0076.

[45] Kreuter, P., et. al., "Variable Valve Actuation - Switchable and Continuously Variable Valve Lifts." SAE International Technical Paper 2003-01-0026, 2003, doi:10.4271/2003-01-0026.

[46] Hannibal, W., et. al., "Overview of Current Continuously Variable Valve Lift Systems and Four-Stroke Spark-Ignition Engines and the Criteria for their Design Ratings." SAE International Technical Paper 2004-01-1263, 2004, doi:10.4271/2004-01-1263.

[47] Flierl, R., and M. Kluting, "The Third Generation of Valvetrains - New Fully Variable Valvetrains for Throttle-Free Load Control." SAE International Technical Paper 2000-01-1227, 20000, doi:10.4271/2000-01-1227.

[48] Setright, L., "Some Unusual Engines." London, 1979.

[49] "Something Up Its Sleeve." Flight, 7 October 1937.

[50] "GT-POWER Engine Simulation Software." *Gamma Technologies*, `https://www.gtisoft.com/gt-suite-applications/propulsion-systems/gt-power-engine-simulation-software/`. Accessed 9 April 2017.

[51] "Diesel Supercharger." *Eaton*, `http://www.eaton.com/Eaton/ProductsServices/Vehicle/Superchargers/diesel-supercharger/index.htm#tabs-3`. Accessed 25 April 2017.

[52] "TVS Supercharger." *Eaton*, `http://www.eaton.com/Eaton/ProductsServices/Vehicle/Superchargers/TVSSupercharger/index.htm`. Accessed 25 April 2017.

[53] "V-24 XB-105 Supercharger." *VORTECH SUPERCHARGERS*, https://vortechsuperchargers.com/collections/supercharger-units/products/v-24-xb-105-supercharger?variant=34797078602. Accessed 25 April 2017.

[54] "Automotive Superchargers." *ProCharger Superchargers*, https://www.procharger.com/auto-superchargers/models. Accessed 27 April 2017.

[55] "AVGAS Facts and Future." *Shell Global*, http://www.shell.com/business-customers/aviation/aeroshell/knowledge-centre/technical-talk/techart12-30071515.html. Accessed 11 April 2017.

[56] Livengood, J. C., and Wu, P. C., "Correlation of Autoignition Phenomenon in Internal Combustion Engines and Rapid Compression Machines." Proceedings of Fifth International Symposium on Combustion, p. 347, Reinhold, 1955.

[57] Bromberg, Leslie. Personal interview. 1 July 2016.

[58] Douaud, A. M., and Eyzat, P.: "Four-Octane-Number Method for Predicting the Anti-Knock Behavior of Fuels and Engines." SAE paper 780080, SAE Trans., vol. 87, 1978.

[59] Cheng, Wai. Personal interview. 21 January 2017.

[60] "U.S. DEPARTMENT OF TRANSPORTATION FEDERAL AVIATION ADMINISTRATION TYPE CERTIFICATE DATA SHEET E00052EN." Federal Aviation Administration, type certificate data sheet E00052EN, 12-21-1995.

[61] "EASA TYPE-CERTIFICATE DATA SHEET." European Aviation Safety Agency, type-certificate data sheet No. E.084, Issue 2, 03-21-2016.

[62] "Limbach Flugmotoren Operating Manual L 2400 EF/DF/ET/DT/DX." Limbach Flugmotoren GmbH & Co. KG 250.253.501.000, Translated from P/N 250.253.500.000, 02-19-2016.

[63] "LIMBACH L 2400 DX - turbocharged." Limbach Flugmotoren GmbH & Co.KG, http://www.limflug.de/en/support/downloads.php?type=datasheets&id=L2400-DX-datasheet-en.pdf&action=download. 10-25-2016. Accessed 6 November 2016. PDF.

[64] "U.S. DEPARTMENT OF TRANSPORTATION FEDERAL AVIATION ADMINISTRATION TYPE CERTIFICATE DATA SHEET E00051EN." Federal Aviation Administration, type certificate data sheet E00051EN, Rev. 5, 11-25-2015.

[65] "OPERATORS MANUAL FOR ROTAX ENGINE TYPE 912 i SERIES." BRP-Powertrain GmbH & Co KG, http://docusearch.flyrotax.com/files/pdf/d06231.pdf. Ed. 1, Rev. 3, 11-12-2015. Accessed 5 November 2015. PDF.

[66] "RotorWay RI-162F HELICOPTER POWERPLANT OPERATION AND MAINTENANCE." RotorWay International, www.rotorway.com.au/_literature_113876/RI162F_Engine_Manual. Rev. 1, 12-99. Accessed 9 April 2016. PDF.

[67] "DEPARTMENT OF TRANSPORTATION FEDERAL AVIATION ADMINISTRATION TYPE CERTIFICATE DATA SHEET NO. E4SO." Federal Aviation Administration, type certificate data sheet E4So, Rev. 1, 8-20-1997.

[68] "500 SERIES." Continental Motors, Inc., http://www.continentalmotors.aero/uploadedFiles/Content/xHome/Billboards/500series_032012.pdf. 3-2012. Accessed 6 February 2016. PDF.

[69] "SERVICE INFORMATION DIRECTIVE." Continental Motors, http://lancair.com/aircraft_documents/ES-ESP/SID97-3E.pdf. SID97-3F, 05-10-2013. Accessed 12 July 2016. PDF.

[70] "U.S DEPARTMENT OF TRANSPORTATION FEDERAL AVIATION ADMINISTRATION TYPE CERTIFICATE DATA SHEET E00060EN." Federal Aviation Administration, type certificate data sheet E00060EN, Rev. 7, 01-28-2015.

[71] "UL520i UL 520iS UL520iSA Operating Manual." ULPower Aero Engines, http://ulpower.com/content/downloads/UL520-operating-manual.pdf. MO 520A01, Rev. 2, 09-15-2014.

[72] "2011-2012 MUSTANG SVT 750 HP SUPERCHARGER UPGRADE KIT POLISHED FINISH." *Ford Performance*, https://performanceparts.ford.com/part/M-6066-MSVT29PD. Accessed 3 May 2017.

[73] "CHEVROLET CAMARO SS LT1 6.2L V8 HEARTBEAT SUPERCHARGER SYSTEM (NO CALIBRATION)." *Magnuson Superchargers*, http://www.magnusonproducts.com/. Accessed 3 May 2017.

[74] "Chevy Complete Supercharger Package." *The Blower Shop*, http://www.theblowershop.com/product/street-blower-package/. Accessed 3 May 2017.

[75] "LS Complete Supercharger Package." *The Blower Shop*, http://www.theblowershop.com/product/ls-complete-blower-package/. Accessed 3 May 2017.

[76] "TBS BilletCharger âĂIJUnder the HoodâĂİ Complete Supercharger Package." *The Blower Shop*, http://www.theblowershop.com/product/250-billet-charger-blower-kit/. Accessed 3 May 2017.

[77] "250 Blower W/O Snout." *The Blower Shop*, http://www.theblowershop.com/product/250-blower-wo-snout/. Accessed 3 May 2017.

[78] Remmert, S., et al., "Octane Response in a Downsized, Highly Boosted Direct Injection Spark Ignition Engine." SAE Int. J. Fuels Lubr. 7(1):2014, doi:10.4271/2014-01-1397.

[79] Turner, J., Popplewell, et al., "Ultra Boost for Economy: Extending the Limits of Extreme Engine Downsizing." SAE Int. J. Engines 7(1):2014, doi:10.4271/2014-01-1185.

[80] "H145." *Airbus Helicopters*, http://www.airbushelicopters.com/website/docs_wsw/RUB_32/tile_2645/H145-1_2016.pdf. Accessed 9 June 2016. PDF.

[81] "EUROCOPTER EC145 Technical Data." *Airbus Helicopters*, http://airbushelicoptersinc.com/images/products/EC145/EC145-tech_data.pdf. Accessed 13 June 2016. PDF.

[82] "eurocopter EC155 B1 Corporate Technical Data." *Airbus Helicopters*, http://airbushelicoptersinc.com/images/products/EC155/EC155_Tech_Data_B1_Corporate_2009.pdf. Accessed 13 December 2016. PDF.

[83] "SCHWEIZER 333 HELICOPTER TECHNICAL INFORMATION." *Sikorsky Aircraft*, http://www.wfhelicopters.com/images/pdf/333_techdata.pdf. Accessed 30 December 2016. PDF.

[84] "Sikorsky S-76D Executive Transport Helicopter." *Sikorsky Aircraft*, http://lockheedmartin.com/content/dam/lockheed/data/ms2/photo/Sikorsky/S-76/Sikorsky-S76D-VIP-Brochure.pdf. Accessed 19 April 2017. PDF.

[85] "Civil Range." *Airbus Helicopters*, http://www.airbushelicopters.com/website/docs_wsw/img/x300/RUB_25/tile_2651/CIVILRange-02-2016_Page_1.jpg. Accessed 19 February 2016. PDF.

[86] "H130." *Airbus Helicopters*, http://www.airbushelicopters.com/website/docs_wsw/img/x300/RUB_25/tile_2651/Broch_H130-2015.jpg. Accessed 13 December 2016. PDF.

[87] "EC135 T2e/P2e." *Airbus Helicopters*, https://www.airbushelicopters.ca/wp-content/uploads/2011/11/EC135-T2e.pdf. Accessed 5 April 2016. PDF.

[88] "AS365 N3+ Technical Data 2016." *Airbus Helicopters*, http://airbushelicoptersinc.com/images/products/AS365/365_N3_16.101.01_E_Ipad.pdf. Accessed 5 April 2016. PDF.

[89] Filippone, Antonio, "Data and performances of selected aircraft and rotorcraft." Progress in Aerospace Sciences 36 (2000) 629-654, 2000.

[90] "14 CFR 91.167 - Fuel requirements for flight in IFR conditions." *Cornell University Law School*, https://www.law.cornell.edu/cfr/text/14/91.167. Accessed 26 April 2017.

[91] Cavcar, Mustaga, "The International Standard Atmosphere (ISA)." *Anadolu University*, http://home.anadolu.edu.tr/~mcavcar/common/ISAweb.pdf. Accessed 26 April 2017. PDF.

[92] Brooks, Frank, "GE Gas Turbine Performance Characteristics." GE Power Systems, http://ncad.net/Advo/CinerNo/ge6581b.pdf GER-3567H, October 2000. Accessed 25 April 2017. PDF.

[93] "Mercedes-Benz DB 600 aircraft engine." *Mercedes-Benz*, https://www.mercedes-benz.com/en/mercedes-benz/classic/museum/mercedes-benz-db-600-aircraft-engine/. Accessed 15 April 2017.

[94] "Mercedes-Benz DB 603 E aircraft engine." *Mercedes-Benz*, https://www.mercedes-benz.com/en/mercedes-benz/classic/museum/mercedes-benz-603-e-aircraft-engine/. Accessed 15 April 2017.

[95] Chetwynd-Chatwin, Jason, "Rolls-Royce Merlin." *Spitfire Art*, http://www.spitfireart.com/merlin_engines.html. Accessed 15 April 2017.

[96] "The Griffon." Rolls-Royce, http://www.spitfireperformance.com/RR-Griffon.pdf. Accessed 15 April 2017.

[97] "CD-100 Series." Continental Motors, http://www.continentalmotors.aero/uploadedFiles/Content/Engines/Diesel_Engines/CD100-SpecSheet.pdf. Accessed 16 April 2017.

[98] Kotelnikov, Vladimir, *Russian Piston Aero Engines.* Marlborough, Wiltshire: Crowood Press, 2005.

[99] Lumsden, Alec, *British Piston Engines and their Aircraft.* Marlborough, Wiltshire: Airlife Publishing, 2003.

[100] *Jane's Fighting Aircraft of World War II.* Studio Editions Ltd, 1989.

[101] "Junkers Jumo 207 D-V2 In-Line 6 Diesel Engine." Smithsonian National Air and Space Museum, https://airandspace.si.edu/collection-objects/junkers-jumo-207-d-v2-line-6-diesel-engine. Accessed 16 April 2017.

[102] "DELTAHAWK DH180A4." DeltaHawk, http://www.deltahawk.com/content/deltahawk-dh180a4. Accessed 16 April 2017.

[103] "WAM 4 CYLINDER ENGINE." Wilksch Airmotive, http://www.wilksch.co.uk/products/wam-4-cylinder. Accessed 16 April 2017.

[104] "2010 ACURA MDX 3.7L 6-cyl Engine Code J37A1." AMSOIL, http://www.amsoil.com/mygarage/vehiclelookup.aspx?url2=2010+ACURA+MDX+7&metric=True&celsius=True. Accessed 16 April 2017.

[105] Sutton, Mike, "2010 Acura MDX." CAR AND DRIVER, http://www.caranddriver.com/reviews/2010-acura-mdx-review. Accessed 16 April 2017.

[106] "2010 ACURA RDX 2.3L 4-cyl Engine Code K23A1 Turbo." AMSOIL, http://www.amsoil.com/mygarage/vehiclelookup.aspx?url2=2010+ACURA+RDX+L&metric=True&celsius=True. Accessed 16 April 2017.

[107] "2011 Acura RDX." MOTORTREND, http://www.motortrend.com/cars/acura/rdx/2011/. Accessed 16 April 2017.

[108] "2010 AUDI A3 2.0L 4-cyl Engine Code CCTA Turbo." AMSOIL, http://www.amsoil.com/mygarage/vehiclelookup.aspx?url2=2010+AUDI+A3+K&metric=True&celsius=True. Accessed 16 April 2017.

[109] "2010 Audi A3 4dr HB S tronic quattro 2.0T Premium Plus Specs." U.S. News & Report, https://cars.usnews.com/cars-trucks/audi/a3/2010/specs/a3-4dr-hb-s-tronic-quattro-2.0t-premium-plus-310409. Accessed 16 April 2017.

[110] "2010 AUDI A4 QUATTRO 2.0L 4-cyl Engine Code CAEB Turbo." AMSOIL, http://www.amsoil.com/mygarage/vehiclelookup.aspx?url2=2010+AUDI+A4%20QUATTRO+C&metric=True&celsius=True. Accessed 16 April 2017.

[111] "Used 2010 Audi A4 Features & Specs." Edmunds, https://www.edmunds.com/audi/a4/2010/features-specs/. Accessed 16 April 2017.

[112] "2010 AUDI A5 QUATTRO 2.0L 4-cyl Engine Code CAEB Turbo." AMSOIL, http://www.amsoil.com/mygarage/vehiclelookup.aspx?url2=2010+AUDI+A5%20QUATTRO+C&metric=True&celsius=True. Accessed 16 April 2017.

[113] "Used 2010 Audi A5 Features & Specs." Edmunds, https://www.edmunds.com/audi/a5/2010/features-specs/. Accessed 16 April 2017.

[114] "2010 AUDI TT QUATTRO 2.0L 4-cyl Engine Code CDMA Turbo." AMSOIL, http://www.amsoil.com/mygarage/vehiclelookup.aspx?url2=2010+AUDI+TT%20QUATTRO+E&metric=True&celsius=True. Accessed 16 April 2017.

[115] "Used 2010 Audi TT Features & Specs." Edmunds, https://www.edmunds.com/audi/tt/2010/features-specs/. Accessed 16 April 2017.

[116] "2010 BMW 335xi 3.0L 6-cyl Engine Code N54 B30A Turbo." AMSOIL, http://www.amsoil.com/mygarage/vehiclelookup.aspx?url2=2010+BMW+335xi+G&metric=True&celsius=True. Accessed 16 April 2017.

[117] "Used 2010 BMW 3 Series Features & Specs." Edmunds, https://www.edmunds.com/bmw/3-series/2010/features-specs/. Accessed 16 April 2017.

[118] "2010 BMW X6 4.4L 8-cyl Engine Code S63B44A Turbo." AMSOIL, http://www.amsoil.com/mygarage/vehiclelookup.aspx?url2=2010+BMW+X6+S&metric=True&celsius=True. Accessed 16 April 2017.

[119] "Used 2010 BMW X6 Features & Specs." Edmunds, https://www.edmunds.com/bmw/x6/2010/features-specs/. Accessed 16 April 2017.

[120] "2010 LAND ROVER RANGE ROVER 5.0L 8-cyl Engine Code [D]." AMSOIL, http://www.amsoil.com/mygarage/vehiclelookup.aspx?url2=2010+LAND%20ROVER+RANGE%20ROVER+D&metric=True&celsius=True. Accessed 16 April 2017.

[121] "Used 2010 Land Rover Range Rover Sport Features & Specs." Edmunds, https://www.edmunds.com/land-rover/range-rover-sport/2010/features-specs/. Accessed 16 April 2017.

[122] "LEXUS IS-F 5.0L 8-cyl Engine Code 2UR-GSE." AMSOIL, http://www.amsoil.com/mygarage/vehiclelookup.aspx?url2=2010+LEXUS+IS-F+G&metric=True&celsius=True. Accessed 16 April 2017.

[123] "Used 2010 Lexus IS F Features & Specs." Edmunds, https://www.edmunds.com/lexus/is-f/2010/features-specs/. Accessed 16 April 2017.

[124] "MERCEDES BENZ CL65 AMG 6.0L 12-cyl Engine Code 275.982 Turbo." AMSOIL, http://www.amsoil.com/mygarage/vehiclelookup.aspx?url2=2010+MERCEDES%20BENZ+CL65%20AMG+5&metric=True&celsius=True. Accessed 16 April 2017.

[125] "Used 2010 Mercedes-Benz CL-Class CL65 AMG Features & Specs." Edmunds, https://www.edmunds.com/mercedes-benz/cl-class/2010/cl65-amg/features-specs/?style=101243560. Accessed 16 April 2017.

[126] "Supercharger Cfm." *High Performance Math*, http://www.hipermath.com/engines/super_charger_cfm. Accessed 15 April 2017.

[127] "MISHIMOTO UNIVERSAL RACE EDITION INTERCOOLER J-LINE." *MISHIMOTO*, https://www.mishimoto.com/mishimoto-universal-intercooler-j-line.html. Accessed 15 April 2017.

[128] "MOUNTUNE INTERCOOLER UPGRADE (BLACK) FOCUS ST 2013-16." *mountune*, https://www.mountuneusa.com/mountune-2013-16-Focus-ST-Intercooler-upgrade-p/2363-ic-ba2.htm. Accessed 15 April 2017.

[129] "Racing Fuel Comparison." *Smith Wholesalers, Inc - SWI Motorsports*, http://www.smithtex.com/racing/fuelcomp.html. Accessed 4 17 2017.

[130] Castor, Jere, "Compound Cycle Engine for Helicopter Application - Executive Summary." Garrett Turbine Engine Co., NASA Technical Report CR-175110. 25 April 1986.